



23rd

ABAF

BRNO 2022

Advanced Batteries, Accumulators
and Fuel Cells

INTERNATIONAL CONFERENCE

August 21st - August 24th 2022

Organised by:

Department of Electrical and Electronic Technology,
Faculty of Electrical Engineering and Communication,
Brno University of Technology

Organizing committee:

Marie Sedlaříková
Tomáš Kazda

Honourary Scientific Committee:

- Petr Vanýsek, *Northern Illinois University, DeKalb, Illinois, USA*
- Arnaldo Visintin, *INIFTA, La Plata, Argentina*
- Günter Fafilek, *TU Wien, Vienna, Austria*
- Elena Shembel, *USCTU, Dnipro, Ukraine*
- Vito Di Noto, *University of Padova, Padova, Italy*
- Alexei Kornyshev, *Imperial College, London, UK*
- Boris Markovsky, *Bar-Ilan University, Tel Aviv, Israel*
- Philipp Adelhelm, *Friedrich Schiller University, Jena, Germany*
- Laurence Hardwick, *University of Liverpool, Liverpool, UK*
- Renata Oriňáková, *UPJŠ, Košice, Slovakia*
- Grzegorz Lota, *Poznan University of Technology, Poznan, Poland*
- Mariusz Walkowiak, *Institute of Non-Ferrous Metals, Poznan, Poland*

Organisation Committee:

- Marie Sedlaříková, *FEEC BUT, Brno, Czech Republic*
- Tomáš Kazda, *FEEC BUT, Brno, Czech Republic*
- František Klein, *Brno, Czech Republic*
- Vítězslav Novák, *FEEC BUT, Brno, Czech Republic*
- Miroslav Zatloukal, *FEEC BUT, Brno, Czech Republic*
- Jiří Libich, *FEEC BUT, Brno, Czech Republic*
- Josef Máca, *FEEC BUT, Brno, Czech Republic*
- Tomáš Binar, *FEEC BUT, Brno, Czech Republic*
- Jiří Švarc, *University of Defence, Brno, Czech Republic*
- Pavlína Sedlaříková, *Brno, Czech Republic*

Program Committee:

- Marie Sedlaříková, *FEEC BUT, Brno, Czech Republic*
- Mariusz Walkowiak, *Institute of Non-Ferrous Metals, Poznan, Poland*
- Arnaldo Visintin, *INIFTA, La Plata, Argentina*
- Petr Vanýsek, *Northern Illinois University, DeKalb, Illinois, USA*
- Günter Fafilek, *TU Wien, Vienna, Austria*
- Boris Markovsky, *Bar-Ilan University, Tel Aviv, Israel*
- Alexei Kornyshev, *Imperial College, London, UK*
- Philipp Adelhelm, *Friedrich Schiller University, Jena, Germany*
- Laurence Hardwick, *University of Liverpool, Liverpool, UK*
- Josef Máca, *FEEC BUT, Brno, Czech Republic*
- Vítězslav Novák, *FEEC BUT, Brno, Czech Republic*
- Petr Bača, *FEEC BUT, Brno, Czech Republic*
- Tomáš Kazda, *FEEC BUT, Brno, Czech Republic*
- Helena Polsterová, *FEEC BUT, Brno, Czech Republic*
- Miroslav Zatloukal, *FEEC BUT, Brno, Czech Republic*
- Kristýna Jandová, *FEEC BUT, Brno, Czech Republic*
- Andrea Fedorková-Straková, *UPJŠ, Košice, Slovakia*
- Jiří Libich, *FEEC BUT, Brno, Czech Republic*
- Tomáš Binar, *FEEC BUT, Brno, Czech Republic*
- Jiří Švarc, *University of Defence, Brno, Czech Republic*

Main sponsors:



Other sponsors:



co-sponsored by



We would like to express our thanks to the Brno University of Technology, Faculty of Electrical Engineering and Communication for support and help with organising 23rd ABAF conference.



Contents

Lithium batteries and related systems

<i>J. Amici, C. A. Calderón, D. Versaci, D. Dessantis, G. Luque, D. Barracco, E. Leiva, C. Francia and S. Bodoardo</i> Polymer in ceramic approach towards safer electrolytes for Lithium-metal cels	9
<i>M. Kasprzyk, L. Niedzicki, A. Pajkowska, A. Zalewska, W. Wieczorek</i> Influence of Anion Shape on Non-crystallizing Region of an Electrolyte	12
<i>A. Kowaluk, J. Tańska, M. Kasprzyk, M. Broszkiewicz, K. Rogala and L. Niedzicki</i> Solid Hybrid Polymer Electrolyte for All-Solid-State Li-ion Battery Based on Novel Salts	14
<i>D. Versaci, J. Amici, P. Marquez, D. Dessantis, M. J. Aguirre, S. Ronchetti, B. Onida, C. Francia, and S. Bodoardo</i> Ultrasmall SnO₂ directly grown on commercial carbon black: a versatile composite material for Li-based energy storage	16
<i>A. Rodriguez, M. Ortiz, J. Thomas and A. Visintin</i> New approach in lithium battery from South America	19
<i>R.D. Apostolova, S.P. Kuksenko</i> Electrochemical Behavior of SiO₂-Containing Electrodes in Lithium Battery Systems: Effect of the SiO₂ Production Methods	20
<i>M. Broszkiewicz, K. Rogala, L. Niedzicki</i> Electrochemical characterisation of LiPCP and its performance with different electrodes	24
<i>D. Csík, D. Zalka, K. Saksl, A. Straková Fedorková, D. Capková</i> High entropy spinel oxide with excellent cycle stability	25
<i>P. Guricová, T. Kazda</i> The study of NMC cathodes regenerated with relithiation process	28
<i>J. Kříž, J. Černý, T. Syrový</i> An all-organic battery based on poly(9-vinylcarbazole) cathode	32
<i>C. Limachi, L. Niedzicki, W. Wieczorek, M. Armand and K. Rogala</i> Designing Batteries For Recycling: Fluorine-Free Lithium-Ion Batteries	35
<i>J. Maca, J. Libich, T. Kazda and K. Jasso</i> Influence of Negative Temperature on Negative Electrode	38
<i>Seyed Saeed Madani, Erik Schaltz, Søren Knudsen Kær, Carlos Ziebert</i> A Comprehensive Heat Generation Study of Lithium Titanate Oxide-based Lithium-ion Batteries	40
<i>I. Maksyuta, E. Shembel, V. Kyrychenko, V. Redko, T. Pastushkin, N. Zaderey</i> Melanin as Biological Organic Polymer with Semiconductor Properties is Unique Effective Modifier for MnO₂ Cathode and Increases the Energy of Li-MnO₂ Battery	43
<i>A. M Rodríguez, M. G. Ortiz, J. E. Thomas, A. Visintin</i> Electrochemical performance of Li_{1.2}Ni_{0.2}Mn_{0.6}O₂ Disordered Rock-Salt Cathode Material	46
<i>A. Pražanová, M. Havlík, M. Mika, V. Knap</i> Lithium-Ion Battery Module-to-Cell: Disassembly and Material Analysis	48
<i>M. Sedlaříková, M. Zatloukal, E. Doleželová, J. Kuchařík, P. Čudek, G. Fafílek</i> Corrosion Processes of Sintered Materials Based on Fe	52

<i>Y. Pustovalov, E. Shembel, D. Kaszuba, V. Redko, T. Pastushkin, N. Zaderey, A. Markevich, Yu. Polishchuk, I. Sagirov</i>	
Nanostructured Innovative Carbon-Based Materials Modify Electrodes and Dramatically Improve the Efficiency of Thin, Flexible Lithium Batteries	56
<i>Yu. V. Shmatok, N. I. Globa, T. V. Lisnycha, S. A. Kirillov</i>	
Cobalt and Nickel Titanates as Effective Anode Materials for Lithium-Ion and Sodium-Ion Batteries	59
<i>T. Syrový, L. Syrová, R. Jambor</i>	
Electrolytes modified with boron-based additives for high-voltage batteries	61
<i>M. Šedina and T. Kazda</i>	
How can pressure help in EV	64
<i>Z. Štubianová, O. Klvač, P. Guricová, T. Kazda, T. Zikmund, and J. Kaiser</i>	
Multiscale 3D analysis of flat Lithium-Ion batteries by X-ray computed tomography	67
<i>D. Zalka, L. S. Shankar, R. Kun, W. Mamrilla, A. Straková Fedorková, and K. Saksl</i>	
Ag₂S as an alternative electrode material for Li-ion batteries	70
<i>J. Kočí, M. Míka Havlík, N. Klusoňová</i>	
The Mullite Nanofibers for Electrotechnical Applications	74
<i>M. Mikolášek, M. Kemény, and P. Ondrejka</i>	
Analysis of Li-ion battery degradation mechanism by EIS, GITT and ICA and their possible utilization for SOH monitoring	77

Supercapacitors

<i>G. Lota, S. Znanięcki, K. Szwabińska, J. Wojciechowski, M. Baraniak and A. Skrzypczak</i>	
Capacitor lifetime prolonged by addition of organic ammonium salt	80
<i>J. Wojciechowski, K. Szwabińska, K. Fic and G. Lota</i>	
Electrochemical Capacitor with Variable Polarization	82
<i>J. Libich, M. Sedlářikova, J. Máca, P. Čudek, A. Chekannikov and G. Fafílek</i>	
Supercapacitors vs. Lithium-ion Batteries: Properties and Applications	84
<i>L. Soserov, B. Mladenova, S. Veleva, B. Karamanova, A. Stoyanova</i>	
Hybrid Supercapacitors Based of MnO₂-Carbon Xerogels Operating in Aqueous Electrolyte	86

Fuel Cells

<i>M. O. Danilov, G. I. Dovbeshko, I. A. Rusetskyi, O. P. Gnatyuk, S. S. Fomanyuk, V. O. Smilyk, G. Ya. Kolbasov</i>	
Hybrid Composite Based on g C₃N₄ with PUMWCNTs - Promising Electrode Material for the Oxygen Electrode of Fuel Cells	87
<i>M. Paidar, K. Denk, F. Zenith, L. Polák, J. Sochor</i>	
Renewable Hydrogen Sources for Fuel Cell Powered Trains in Czech Republic	91
<i>D. Budáč, V. Miloš, M. Carda, M. Paidar, K. Bouzek</i>	
Numerical Prediction of Electrical Conductivity of Porous Composite Materials: LSM-YSZ Case Study	93

Aqueous Batteries

<i>P. Kędzior, W. Rzeszutek, J. Wojciechowski, A. Skrzypczak, G. Lota</i> New starter lead–acid battery with modified electrolyte by ionic liquid	96
<i>P. Mazúr, M. Mikešová, J. Charvát, J. Pociď, M. Klikar, F. Bureš, J. Akrman, L. Kubáč</i> Organic redox compounds for cheaper and greener flow batteries – a critical view	98
<i>R. Płowens, M. Bajsert, M. Baraniak, G. Lota</i> Impact of the Carbon Additives for the Performance of the Lead-acid Battery	99
<i>L. A. Azpeitia, M. G. Ortiz, A. Visintin, C. A. Gervasi, A. E. Bolzán</i> Anodes for Li-ion Batteries based on electrodeposited Tin in Deep Eutectic Solvents	101
<i>J. Smejkal and L. Chladil</i> Influence of Different Cycling Speed on the Life-span of the Negative Electrode for Lead-acid Batteries	103
<i>L. Chladil, J. Smejkal and O. Čech</i> The Effect of Additives Suppressing Dendritic Growth on the Recrystallization of ZnO Particles in the Alkaline Environment of Batteries	106

New systems of Batteries

<i>D. Capkova, T. Kazda, M. Almasi, J. Macko, N. Kiraly, O. Petrus, A. Strakova Fedorkova, V. Knap</i> Metal-Organic Frameworks as Suitable Matrices for Sulfur in Next-Generation Batteries	109
<i>M. Zupalová, M. Vinarčíková, B. Pitňa Lásková and L. Kavan</i> Engineering of the Composite Cathode for Li-sulfur Battery	112
<i>C. Calderón, J. Amici, D. Versaci, M.L. Para, E. Leiva, C. Francia, S. Bodoardo and A. Visintin</i> Gel Polymer Electrolyte With Nanoparticles And 2D Materials As Fillers For Lithium Sulfur Batteries	114
<i>O. Čech, T. Kazda, L. Chladil, P. Čudek</i> Promising Anode Materials for Sodium-ion Batteries – Sodium Titanates	116
<i>N. I. Globa, V. A. Sirosh, Yu. V. Shmatok, T. V. Lisnycha, S. A. Kirillov</i> Effect of Structure and Morphology of Titanium Dioxide on Electrochemical Characteristics of Lithium-Sulfur Batteries	121
<i>V. Nišćáková, A.S. Fedorková</i> Sulfur/Polypyrrole Cathode Material For Lithium Sulfur Battery	123
<i>N. Hoffmann, M. G. Ortiz, J. E. Thomas, A. Visintin</i> Different Carbon Processes for Lithium-Sulfur Batteries	125
<i>R. A. Panteleimonov, O. V. Boichuk, K. D. Pershina, Yu. V. Shmatok</i> Impact of the Graphene Synthesis on Electrochemical Properties of Graphene — Graphite Systems	127
<i>Yu. Polishchuk, S. Dubinevych, V. Zinin, E. Shembel</i> Graphene-Modified Sulfur Cathode Ensuring High Stability of Li-S Batteries Parameters	130
<i>K. M. Rogala, L. Niedzicki, M. Bedecka, D. Jamroz, T. Trzeciak, A. Zalewska</i> Synthesis of a new fluorine-free ionic liquids containing an anion PCP- to use in solid state batteries	134

<i>Shiva Shankar Lakshmi, Dóra Zalka, Robert Kun</i> Supercritical carbon dioxide assisted synthesis of ultra-stable sulfur/carbon composite cathodes for Li- S batteries	135
<i>M. Zajcev, P. Richtr, J. Hnát, P. Mazúr, M. Zejmon, M. Paidar, J. Pociď</i> Development of oxygen reduction and oxygen evolution electrodes for alkaline zinc-air flow battery	138
<i>V. Procházka, M. Havlík Mika, J. Kočí</i> Characterization Of Precursor Sols For Preparation Of Silica Based Nanofibers	140

Photovoltaics

<i>S. V. Chivikov, I. A. Rusetskyi, S. S. Fomanyuk, M. O. Danilov, V. O. Smilyk, G. Ya. Kolbasov</i> Reversible photoelectrochemical cell produced by using 3D print for the accumulation "solar" hydrogen	142
<i>K. Jandova, R. Stranak</i> Design and Optimization of Solar-Powered Irrigation System	146
<i>K. Mairhofer, S. Larisegger, G. Fafílek</i> Photoelectrochemical Method for the Investigation of Wide-Bandgap Semiconductors	149
<i>J. Vaněk, P. Maule and F. Šmatlo</i> Comparison of Modelling Tools of the Photovoltaic Power Plants	151

Corrosion, applications and simulations

<i>J. Appell</i> Electrochemical Impedance Spectroscopy and quality indicators	156
<i>O. Klvač, L. Novák, Petr Glajc, T. Kazda</i> Batteries in SEM: in situ battery materials synthesis and electrical testing	159
<i>A. Kolouchová</i> Characterization of Materials for Conversion and Energy Storage – Presentation of Pragolab Company	162
<i>M. Mačák, K. Jaššo, P. Mezera, T. Kazda, P. Vyroubal</i> Experimentally Based Modelling of Li-S Batteries	164
<i>E. Shembel, K. Sukhyy, V. Redko, T. Pastushkin, Y.Pustovalov, J Kaszuba, B.Kutnick, V. Kyrychenko, D.Kaszuba, A.Fedorková, A. Markevich, Yu. Polishchuk, I. Maksyuta, N. Zaderey</i> Unconventional Hybrid Energy Systems Based on Innovative PV Modules and Electrochemical Batteries Provide High Energy Creator and Storage	167
<i>L. Varain, G. Fafílek, M. Nelhiebel, S. Larisegger</i> Electrochemical Investigation and Modeling of Ion- and Water Transport Through Polymer Membranes	170
<i>J. Viliš, Z. Pokorný, J. Zouhar, R. Vitek, and J. Procházka</i> Evaluation of ballistic resistance of thermoplastic and thermoset composite panels	171
<i>R. Bayer</i> Mathematical and Physical Analysis of Character and Position of Shock Waves During Pumping of Vacuum Chambers	172

<i>R. Cipin, M. Toman, P. Prochazka, and I. Pazdera</i> Physics Informed Neural Network and RC model of Li-Ion Battery	175
<i>P. Čudek, and K. Jaško</i> Preparation and analysis of carbon derived from biological materials for use in Li-S batteries	178
<i>L. Dobsakova and T.D. Nguyen</i> Cooling Ability of Smooth and Dimpled Surfaces	182
<i>L. Horák, J. Kazelle</i> Environmentally friendly epoxy resin	185
<i>P. Houška, K. Caisová and J. Koutský</i> The Potential of Brownfields as a Suitable Locations for Solar Panel Instalation Based on Global Radiation Measurements	187
<i>O. Klvač, T. Kazda, Y. Fam, L. Novák</i> In-situ characterization of an electrochemical cell prepared in SEM	190
<i>J. Maxa</i> Evaluation of Ballistic Coefficient for .223 rem Projectiles	193
<i>J. Maxa</i> Mathematical and Physical Analysis of Waste Heat Dissipation During Compression of Air Used as Energy Storage	196
<i>V. Redko, T. Pastushkin, E. Shembel, B. Kutnick, P. Novak. A.Fedorková, V. Khandetskyy, N. Zaderey, S.Pukha, A. Redko</i> Innovative Non-Destructive Non-Contact Methods Testing to Solve for the Bridge the Gap Between Materials Limitation and Manufacturing. Answering the Requirements of High Energy Batteries	199
<i>Z. Studeny, D. Dobrocky, J. Viliš, J. Adam</i> Overview of tribological properties of UHMW polyethylene under rotation	202
<i>P. Šabacká</i> Mathematical and Physical Analysis of Thermal Conductivity at Low Pressures	203
<i>M. Tkach, Yu. Polishchuk</i> Mobile system for power sources monitoring and diagnostics based on INA 219 module	206
<i>P. Vyroubal, M. Mačák, T. Kazda</i> Numerical Modeling of Li-Ion Battery Gassing	208
<i>J. Zimakova, T. Binar, P. Šafl, P. Čudek</i> Failure Mechanism in The Pearlite Structure	212
<i>P. Šafl, J. Zimakova, T. Binar, P. Čudek</i> Evaluation of Cold Kinetic Deposition Technology	215
<i>T. Binar, J. Zimakova, P. Šafl</i> Evaluation of The Use of Non-destructive Methods of Acoustic Emission on Materials	218
<i>P. Šteffan, V. Novák</i> Resistivity and polarization resistance of special grounding materials	221
<i>P. Vorel, J. Martis</i> Battery Powered City-Bike Light with an Optimized Step-up Converter	223
<i>J. Martis, P. Vorel</i> High Current Battery Charger with a Resonant Converter	226

Polymer in ceramic approach towards safer electrolytes for Lithium-metal cels

J. Amici^a, C. A. Calderón^b, D. Versaci^a, D. Dessantis^a, G. Luque^c, D. Barracco^b, E. Leiva^c,
C. Francia^a and S. Bodoardo^a

^a Electrochemistry Group, Department of Applied Science and Technology (DISAT), Politecnico di Torino, Corso Duca degli Abruzzi, 24, 10129 Torino, Italia

^b Instituto de Física Enrique Gaviola, Facultad de Matemática, Astronomía, Física y Computación, Universidad Nacional de Córdoba, Av. Medina Allende s/n, ciudad universitaria, Córdoba, Argentina

^c Instituto de Investigaciones en Fisicoquímica de Córdoba, Facultad de Ciencias Químicas, Universidad Nacional de Córdoba, Haya de la Torre esq. Medina Allende, ciudad universitaria, Córdoba, Argentina

Composite polymer electrolytes (CPE) are a very promising strategy for using lithium metal anodes safely. These electrolytes are formed by polymeric matrices in which ceramic nanoparticles are incorporated to modify their mechanical and conduction properties. In this work a methacrylate-based polymer matrix containing 63 wt% of ZrO₂ nanoparticles (NPs) was prepared and tested as electrolyte for lithium metal batteries. The prepared CPE shows a higher ionic conductivity than the polymer matrix without ZrO₂ NPs and a higher lithium transport number than Celgard with liquid electrolyte and stabilizes the processes of deposition-dissolution of lithium with respect to the reference cell, thus prolonging the cycling time without short circuits. Finally, the compatibility of the CPE with a LiFePO₄ cathode was verified, achieving a stable cycling at 1.0 C and at ambient temperature, with an impressive capacity of 140.18 mAh g⁻¹ even after 250 cycles.

Nowadays, electrical energy storage is one of the most critical issues to answer global warming by effectively replacing fossil energies by renewable ones. The Li-ion technology, widely studied and available on the market for multiple application is now reaching its limits and does not represent alone a viable option toward energetic transition. Therefore, one option currently under study is the use of metallic lithium as anode both in Li-ion cells and in the so-called “post Li-ion technologies”. In this perspective, lithium metal anode represents the “holy grail” of battery research for its extremely high theoretical specific capacity (3860 mA h g⁻¹), the lowest redox potential (-3.040 V vs the standard hydrogen electrode) and a low gravimetric density (0.534 g cm⁻³).

However, metallic Li also presents many challenges derived primarily from dendrite formation upon cycling causing both safety issues and poor cycling performance. In addition, liquid electrolytes contain combustible organic solvents that can cause leakage and fire risks during overcharge or abused operations, especially in large-scale operation. Therefore, replacement of liquid electrolytes with a solid electrolyte has been recognized as a fundamental approach to effectively address the above problems. Generally, all solid-state electrolytes can be classified into 3 categories: solid polymer electrolytes (SPE), inorganic ceramic electrolytes (ICE) and solid composite electrolytes (SCE). While SPEs suffer from poor ionic conductivity at room temperature and low thermal and electrochemical stability, and ICEs from poor interfacial contact with electrodes, SCEs solve these

issues and benefit from both their advantages such as good ionic conductivity, good flexibility, and intimate contact with the electrodes.

In this work a methacrylate-based polymer matrix containing 63 wt% of ZrO_2 nanoparticles (NPs) was prepared and tested as electrolyte for lithium metal batteries. The prepared SCE shows a higher ionic conductivity than the polymer matrix without ZrO_2 NPs and a higher lithium transport number than Celgard with liquid electrolyte. It stabilizes the processes of deposition-dissolution of lithium with respect to the reference cell, thus prolonging the cycling time without short circuits.

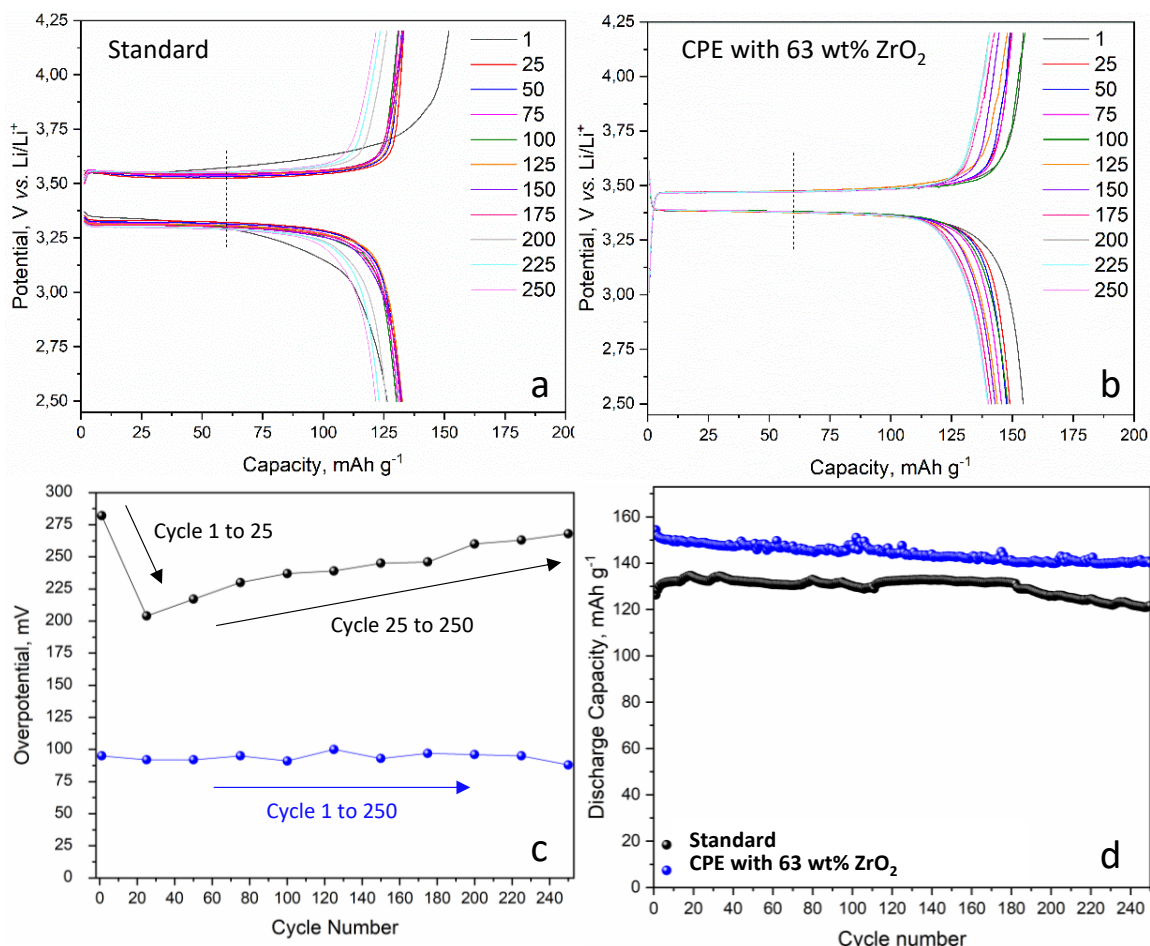


Figure 1. Voltage profiles of LFP-Li cells with Celgard2500 (Standard) (a) and CPE with 63 wt% ZrO_2 (b). Overvoltage evolution (measured at the fixed capacity of $60\ mAh\ g^{-1}$) vs. cycle number for the standard cell (black) and the CPE cell (blue). Discharge capacities of the standard cell and the CPE cell. All these results are obtained at 1 C, at room temperature.

Finally, the cycling performance of the CPE in a complete cell was tested with LFP cathodes at 1C and room temperature. As can be seen on Figure 1, the overpotential for the cell assembled with the CPE is significantly smaller than for Celgard2500 (Standard cell). As a direct consequence, after 250 cycles at 1C, the capacity of the first one is still $140.18\ mAh\ g^{-1}$ while the capacity of the second one is only $121.61\ mAh\ g^{-1}$ (Figure 1 d). To further assess this difference, the voltage hysteresis of both cells is calculated, at the fixed capacity of $60\ mAh\ g^{-1}$, and reported in Figure 1 c. The value of the overvoltage between charge and discharge is much lower, from the first cycle on, in the CPE cell, and remains smaller than half of the overvoltage of the standard cell, up to the 250th cycle. Moreover, observing the values of the Celgard2500 cell, we can note that the overvoltage initially decreases

between the 1st and the 25th cycles but successively increases constantly from the 25th to the 250th cycle.

These results confirm that the Standard cell, containing Celgard2500, cannot form a stable interface between the electrolyte and the Lithium anode, dendrites are formed and successively broken thus forming dead Li and progressively increasing the resistance of the interface and therefore the cell polarization. On the contrary, in the CPE cell the overvoltage remains low and quite constant over 250 cycles demonstrating a reduced polarization and confirming the influence of the higher t_{Li^+} number with an improved Li^+ transfer kinetics [1].

Acknowledgments

Authors kindly acknowledge Polar project (progetto per l'internazionalizzazione della ricerca tra Politecnico di Torino e Argentina, prof Silvia Bodoardo) and ENEA: Piano Triennale Di Realizzazione 2019-2021 Della Ricerca Di Sistema Elettrico Nazionale [Accordo di programma ministero dello sviluppo economico- ENEA] (Prof. Silvia Bodoardo), for the research funding.

References

1. J. Amici, C. A. Calderón, D. Versaci, G. Luque, D. Barraco, E. Leiva, C. Francia, S. Bodoardo, *Electrochimica Acta* 404 (2022)139772.

Influence of Anion Shape on Non-crystallizing Region of an Electrolyte

M. Kasprzyk^{a,*}, L. Niedzicki^a, A. Pajkowska^a, A. Zalewska^a, W. Wieczorek^a

^a Faculty of Chemistry, Warsaw University of Technology, Noakowskiego 3, 00-664 Warsaw, Poland

Lithium-ion battery technology is still in need of electrolytes development due to the continuous progress of both cathode and anode materials technologies. Non-crystallizing electrolytes could be the key to the preservation of electrodes at the extremely low temperatures. In this investigation the mixtures of EC (ethylene carbonate) and PEGs (poly(ethylene glycol)s) will be presented. The influence of the anion shape on the non-crystallizing region in the electrolyte will be discussed.

Introduction

Development of lithium-ion batteries is still possible due to fast progress in electrode materials technologies. With new electrode materials, very often the composition of electrolyte could be tailored for certain application.

Most of electrolytes used nowadays undergo crystallization even at temperatures close to 0°C. When temperature of the battery drops below the freezing point, the liquid becomes crystal. The transition into crystal indicates not only sudden drop in the conductivity but also significant damage to the electrodes. It may happen that after reheating battery to the room temperature, the permanent drop in capacity will be observed or the fatal failure of the cell could take place. Among various capabilities of the electrolytes, the non-crystallizing electrolytes could be the answer to some issues with low temperature applications. The electrolytes based on mixtures of EC and PEG's may not show the crystallization point at all (including partial formation of crystal domains). Only glass transition is observed in these systems in the whole range of temperatures, and at the quite low temperatures to that (below -80°C). During glass transition all parameters of the system are changing smoothly, unlike the situation when melting or crystallization occurs, when parameters change abruptly. Additionally, the non-crystallizing electrolytes show quite high conductivity even much below -40°C.

The main aim of the presented work is to define whether the shape of anion in salt used for electrolyte preparation has influence on the non-crystallizing region in these systems. Are there any similarities in behavior in systems with similar size of anion and is it possible to better tailor the properties of electrolytes.

Experimental and results

Various systems of salts will be presented: LiTDI (lithium 4,5-dicyano-2-(trifluoromethylene)imidazolate), LiPDI (lithium 4,5-dicyano-2-(pentafluoroethylene)imidazolate), LiI (lithium iodide), LiClO₄ (lithium perchlorate) and LiPF₆ (lithium hexafluorophosphate). The two systems of EC:PEG electrolytes will be presented for comparison.

The conductivity, cyclic voltammetry, lithium cation transference number and other electrochemical measurements will be presented.

These electrolytes exhibit conductivity above 1 mS cm^{-1} at 20°C , which is set as the minimum value required by lithium-ion battery systems. The conductivity of these systems at extremely low temperatures is quite high in comparison to other known electrolytes (0.014 mS cm^{-1} at -60°C). The high electrochemical stability window of these electrolytes is also observed, up to 4.7 V vs. Li .

Acknowledgments

This work was financially supported by Faculty of Chemistry, Warsaw University of Technology.

References

1. M.C. Smart, B.V. Ratnakumar, S. Surampudi, *J. Electrochem. Soc.*, **149(4)**, A361 (2002).
2. M. Kasprzyk, A. Zalewska, L. Niedzicki, A. Bitner, M. Marcinek, W. Wieczorek, *Solid State Ionics*, **308**, 22 (2017).
3. M. Kasprzyk, A. Zalewska, W. Wieczorek, *J. Phys. Chem. C.*, **124(9)**, 5046 (2020).

Solid Hybrid Polymer Electrolyte for All-Solid-State Li-ion Battery Based on Novel Salts

A. Kowaluk^a, J. Tańska^a, M. Kasprzyk^a, M. Broszkiewicz^a, K. Rogala^a and L. Niedzicki^{a,*}

^a Faculty of Chemistry, Warsaw University of Technology,
Noakowskiego 3, 00-664 Warszawa, Polska

leszek.niedzicki@pw.edu.pl

Solid hybrid polymer electrolyte is investigated as potential solution for safe, all-solid-state lithium-ion batteries for electric vehicles application. Optimization of composition to achieve high ionic conductivity is presented. Ionic conductivity of $\sim 0.3 \text{ mS cm}^{-1}$ at 20°C is achieved for optimized composition and lithium cation transference number of ~ 0.3 is measured for such composition.

Introduction

Electric vehicles are powered by Li-ion batteries. Those are containing predominantly liquid electrolytes, which are potentially unsafe, as they are flammable, can leak if cells are pierced and are usually quite toxic. The potential solution is use of solid electrolytes, but those are either too rigid and have poor contact with active materials of electrodes (ceramic electrolytes) and/or have too low ionic conductivity (solid polymer electrolytes and large part of ceramic electrolytes). One of the solutions is use of solid hybrid electrolytes consisting of polymer matrix providing flexibility of a bulk, lithium salt as a source of lithium cations, ionic liquid as plasticizer improving flexibility and amorphousness as well as improve conductivity and, if needed, ceramic additive made of ceramic electrolyte, which provides additional conducting channels. Selected materials for each of the components has been made in-house or provided by the Project Partners. Matrix is made of a fluorinated polymer, salt is a WUT proprietary lithium salt, ionic liquid (IL) is based on pyrrolidine cation and anion of the proprietary lithium salt (weakly coordinating anion) and the ceramic additive was an experimental garnet-type ceramic electrolyte.

Results and Discussion

The optimization of wide range of compositions (ratios between salt, IL, polymer and ceramic additive) as well as selection of the components included few candidates for IL (plasticizer), three different salts and use or lack of ceramic additive. Concentration ranges were very wide, as depending on the salt relative solubility in IL, as well as level of plasticization (in terms of crystal domains content), which was also depending on used IL, has influenced range of possible IL concentrations. Particularly, it has influenced range of concentrations that would allow to form solid electrolyte, which would be flexible (not brittle, so low crystal domains content) and not undergo liquid sweating after certain time. Due to multi-dimensional optimization, it may not have been possible to be sure about global conductivity maximum, but few local maxima were found, which were close to each other in terms of ionic conductivity value. Thus, multiple compositions achieving $0.15\text{-}0.28 \text{ mS cm}^{-1}$ ionic conductivity at 20°C have been found ($0.55\text{-}0.87 \text{ mS cm}^{-1}$ at 50°C). Selected compositions were investigated more thoroughly, showing compatibility with

lithium metal anode, relatively high lithium cation transference number (0.28) - compared to solid polymer electrolyte based on PEO-based SPEs. Electrochemical stability depends on the lithium salt used and is similar to the stability of salt. Thermal stability is wide enough for typical applications.

Conclusions

It is possible to obtain solid (hybrid) polymer electrolyte that would conduct at the minimum ionic conductivity required level at 20°C (industrial requirement for SPEs) by careful and patient optimization of composition. High conductivity and quite high (as per solid electrolyte) lithium cation transference number provide potential for application in future all-solid-state batteries.

Acknowledgments

This work has received funding from the European Union's Horizon 2020 research and innovation programme under grant agreement N°875029.

Ultrasmall SnO₂ directly grown on commercial carbon black: a versatile composite material for Li-based energy storage

D. Versaci^a, J. Amici^a, P. Marquez^b, D. Dessantis^a, M. J. Aguirre^c, S. Ronchetti^a, B. Onida^a, C. Francia^a, and S. Bodoardo^a

^a Department of Applied Science and Technology (DISAT), Politecnico di Torino, C.so Duca degli Abruzzi 24, 10129 Torino, Italy

^b Escuela de Ingeniería, Universidad Central de Chile, 8330601 Santiago, Chile

^c Departamento de Química de los Materiales, Facultad de Química y Biología, Universidad de Santiago de Chile (USACH), Av. B. O'Higgins 3363, Estación Central, Santiago, Chile

Among metal oxides, tin dioxide (SnO₂) is a very versatile low-cost raw material for energy storage, for example in lithium-ion batteries, exhibiting a high lithium storage capacity and an excellent cycling performance. Recently, SnO₂ has also been reported as a promoter catalyst for oxygen reduction reaction (ORR) for Li-O₂ batteries. Therefore, this work reports a simple, fully sustainable, and economic synthesis process to obtain SnO₂ nanoparticles (in average 5 nm diameter) finely dispersed on a commercial carbon black and tested both as anode material in Li-ion cells and ORR catalyst at the cathode of Li-O₂ cells.

Herein, we propose a hassle-free approach to prepare SnO₂/C composite using a simple, fully sustainable, and economic synthesis process, in which tin oxide is *in situ* nucleated on commercial carbon black C-ENERGYTM Super C45 (Imerys Graphite & Carbon) in form of homogeneously distributed nanoparticles. The synthesis is carried out by wet impregnation without any acid treatment or high temperature process. We focused on the presence of the existing oxygen species on the carbon surface that are accessible for tin and promote Sn–O–C interactions, suggesting synergies between the two components, with an active role of the carbon support in the SnO₂ conversion reaction.

On one hand, in Li-ion technology, development of high-performance SnO₂ anodes is hampered by its peculiar electrochemical behavior, characterized by two processes: conversion and alloying reactions. The conversion reaction being irreversible leads to specific capacities lower than theoretical, however rational design of nanosized SnO₂ can mitigate this issue, though SnO₂ low conductivity and electrode pulverization justify the need of carbon matrices. Some carbon structures proved to be strongly effective at laboratory-scale, but most are too expensive or complicated to obtain for scaling-up. Presence of oxygen species on C45 surface, accessible to tin, prevent fast formation of Li₂O, allowing to achieve high capacity and extreme electrode stability. The assembled cells with SnO₂ /C45 exhibit for more than 400 cycles the reversible capacity of 560 mA h g⁻¹ per pure SnO₂ (after subtracting C45 contribution) at 1C, demonstrating prolonged cycling operation thus providing an interesting opportunity for scalable production of stable and high-capacity battery anodes alternatively to graphite [1].

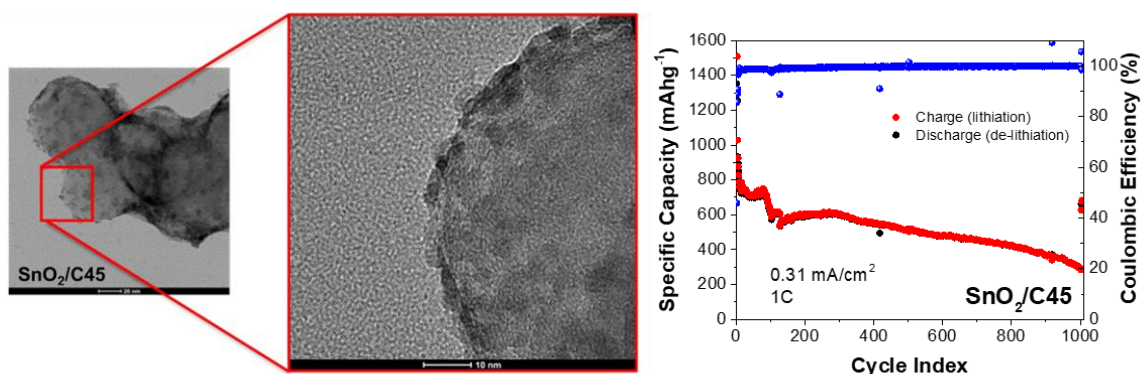


Figure 1. TEM micrograph of SnO₂/C45 (on the left), galvanostatic charge/discharge capacities of the SnO₂/C45 electrode at 1C (on the right)

On the other hand, developing efficient and low cost electrocatalysts for ORR is fundamental to bring the Li-O₂ technology closer to practical applications. The obtained composite material shows an optimal ORR activity with a final reduction mechanism following the 4 electrons pathway. This is confirmed in Li-O₂ cells, indeed compared to pure C45 air-cathodes, the composite cathodes lead to the formation of much more reversible film-like discharge products, allowing for reduced overvoltage and therefore improved cycling performances both at the high current density of 0.5 mA cm⁻² with more than 70 cycles and in prolonged discharge/charge conditions with over 1250 h of operation at the fixed capacity of 2.5 mAh cm⁻² [2].

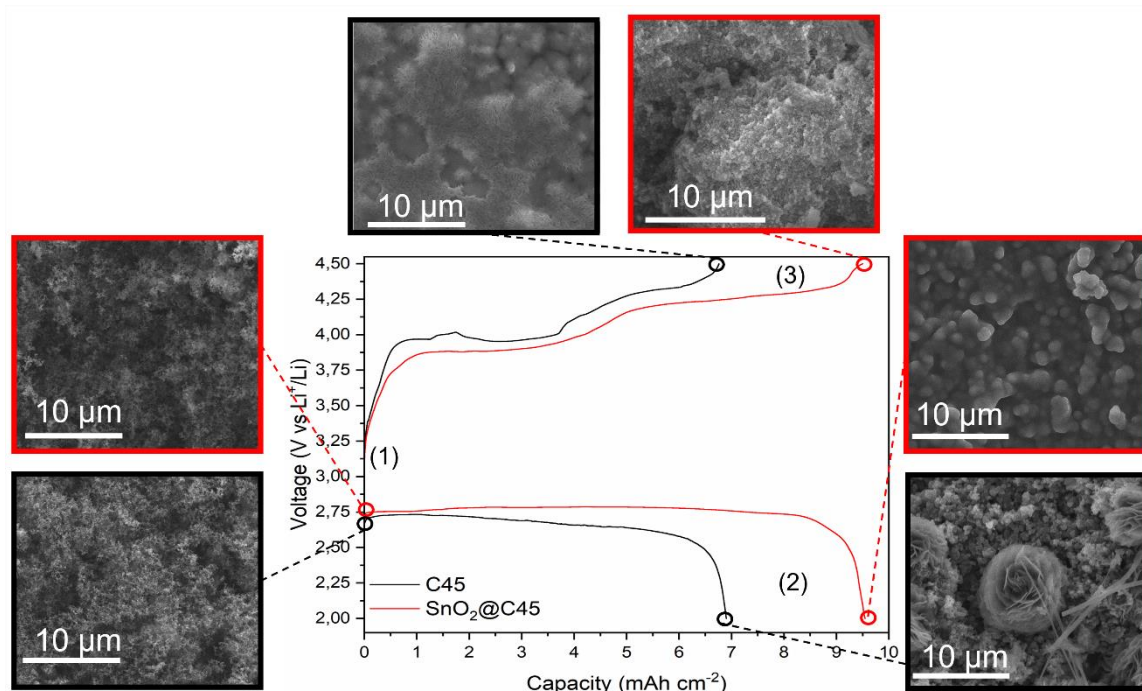


Figure 2. FESEM micrographs of C45 (black border) and SnO₂@C45 (red border) cathodes surface in different steps: pristine (1), after full discharge at current density of 0.1 mA cm⁻² (2), after full recharge at the same current density (3).

Considering the fast and inexpensive method used to prepare SnO₂/C45, these results, in terms of reversible capacities and long cycling stability, are competitive among others obtained for SnO₂-based materials synthesized by other methods such as hydrothermal, sonochemical, solvothermal, etc.

All these considerations make the synthetic route reported a suitable and interesting approach for large scale production.

References

1. D. Versaci et al., *Electrochim. Acta*, **367**, 137489 (2020).
2. J. Amici et al.. *J. Power. Sources*, in press (2022).

New approach in lithium battery from South America

Augusto Rodriguez¹, Mariela Ortiz^{1,2}, Jorge Thomas³ and Arnaldo Visintin¹

¹Instituto de Investigaciones Fisicoquímicas Teóricas y Aplicadas (INIFTA), Facultad de Ciencias Exactas, UNLP, CCT La Plata-CONICET, C.C. 16, Suc. 4, CP 1900, La Plata, Argentina.

²Centro de Investigación y Desarrollo en Ciencia y Tecnología de Materiales (CITEMA), Universidad Tecnológica Nacional - CICPBA, 60 y 124, 1923, Berisso, Argentina.

³YPF Tecnología S.A., Av. del Petróleo Argentino S/N (entre 129 y 143), B1923 Berisso, Buenos Aires, Argentina.

e-mail: visintinarnaldo2@gmail.com

Lithium-ion batteries are the most promising devices for energy storage, from low-power mobile applications to megaprojects. Moreover, some types of lithium-ion batteries have good performance for high current consumption in a cyclic way, which makes them suitable for power storage applications basically in two fields: electric vehicles and alternative energies.

This presentation shows a brief description of the advances of the technologies of lithium in South America and the state of the art of this type of battery at the level of basic research and industrial developments in Argentina and the world. In addition, some results of the development of materials for high performance electrodes for lithium-ion batteries are presented. In our laboratories we focus on the area of lithium-sulfur batteries (S/C materials cathodes) and lithium-ion batteries (materials cathodes: the spinels of LiMn_2O_4 , $\text{LiMn}_{2-x}\text{Ni}_x\text{O}_4$, $\text{LiNi}_{0.5}\text{Mn}_{1.49}\text{Ti}_{0.01}\text{O}_4$, and layered lithium-rich oxides ($\text{Li}_{1.2}\text{Ni}_{0.2}\text{Mn}_{0.6}\text{O}_2$) which are the most promising systems in this particular field), and on the synthesis and physical and electrochemical characterization of these materials using different techniques such as cyclic voltammetry, charge-discharge cycling, electrochemical impedance spectroscopy, SEM, TEM, XRD, and EDS. The synthesized cathodic materials will be used to develop lithium-ion battery prototypes. With this setup it is now possible to characterize different anodic and cathodic active materials by X-ray spectroscopy techniques such as XANES and EXAFS at different working conditions i.e., different states of charge (SOC) or during a potentiodynamic run, and also under normal operation conditions such as charge-discharge cycles.

Electrochemical Behavior of SiO₂-Containing Electrodes in Lithium Battery Systems: Effect of the SiO₂ Production Methods

R.D. Apostolova¹, S.P. Kuksenko²

¹ Ukrainian State University of Chemical Technology, Dnipro, 49005 Ukraine, e-mail apostolova.rd@gmail.com¹

² Chuiko Institute of Surface Chemistry, National Academy of Sciences of Ukraine, General Naumov str. 17, Kyiv, 03164 Ukraine

SiO₂ dioxide with a high theoretical capacity (1784 mAh g⁻¹) belongs to a series of materials being developed to replace the less energy consuming graphite (372 mAh g⁻¹) in the negative electrodes of commercial lithium-ion batteries (LIBs). The actual capacity of SiO₂ dioxide is less than the theoretical one, since it depends on a number of reasons that restrain the expanded industrial production of LIBs based on it. There are 16 SiO₂ polymorphs, the electrochemical properties of which are largely determined by the manufacturing process. This presentation shows different electrochemical behavior SiO₂-containing electrodes prepared using different technologies, with an emphasis on the need to identify the true mechanisms of effective electrode processes, excluding harmful side effects.

Electrodes with "nano-Si/SiO₂" and "nano-Si@SiO₂" powders

The electrochemical behavior of the two types of electrodes have been studied (Fig. 1): from a silicon nanopowder with a natural layer of silicon oxide on its surface (is marked as "nano-Si/SiO₂") and micropowder of silicon clusters embedded into a matrix of silicon dioxide (is marked as "nano-Si@SiO₂"), which was obtained by heat treatment SiO at 1100 °C in the stream of Ar. When the silicon nanopowder is stored in air, its surface oxidizes to give a natural oxide layer with a thickness of ~6 nm. The "nano-Si/SiO₂" powder is constituted by highly structured aggregates of ~30 nm particles with the specific surface area of 70–80 m²/g and bulk density (weight divided by geometric volume) of approximately 0.08 g/cm³. The broadening of the peaks for (111) and (220) faces in the X-ray diffraction pattern indicates that the size of single-crystal regions does not exceed 19–20 nm (the crystallite size was calculated by the Scherrer equation). The "nano-Si@SiO₂" powder is constituted by amorphous ~5 nm silicon clusters distributed in volume of SiO₂. Electrodes were fabricated from "nano-Si/SiO₂" and "nano-Si@SiO₂" powders using synthetic graphite KS6 (TIMCAL, Switzerland) with isometric particles 6.5 μm in size (D₉₀) and a specific surface area of 20.0 m²/g as electrochemically active and electrically conductive additive: 4KS6+1nano-Si/SiO₂ (with 15 wt.% PVDF) and 2KS6+1nano-Si@SiO₂ (with 8 wt.% PVDF). The electrode paste suspensions were uniformly deposited as viscous substances (as a 100–110 μm thick layer) onto a 20 μm thick Cu-foil serving as a current collector. The electrode layers were then compacted by rolling to a working thickness of ~80 μm. The electrode cycling parameters were studied with half-cells of R2016 size, in which lithium metal acted simultaneously as counter and reference electrode. As electrolyte served 1M solution of LiPF₆ in a mixture of FEC+EMC (30:70 vol.%) with addition of VC (3 wt.%) and ES (2 wt.%) [1–3]. The half-cells cycling was performed at 25°C (Fig. 1, *a*) and 50°C (Fig. 1, *b*) in the *cc/cv* (charge) and *cc* (discharge) modes: 250 mA/g,

10 mV, 25 mA/g and 250 mA/g, 1.0 V (Fig. 1, *a*); 60 mA/g, 10 mV, 6 mA/g and 60 mA/g, 1.0 V (Fig. 1, *b*).

The charge-discharge curves of both electrodes are identical except for some voltage plateau on the charging curve Fig. 1, *a*, which becomes more pronounced in subsequent cycles after the first one [4]. Its appearance is explained by the formation of intermetallic $\text{Li}_{15}\text{Si}_4$, which is impossible in the case of amorphous silicon (Fig. 1, *b*). The using of "nano-Si@SiO₂" in the electrode contributes to its stable cycling (charge-discharge curves are practically superimposed on each other after the first cycle). In the case of "nano-Si@SiO₂" is observed characteristic only of a-Si and graphite the course of charge-discharge curves.

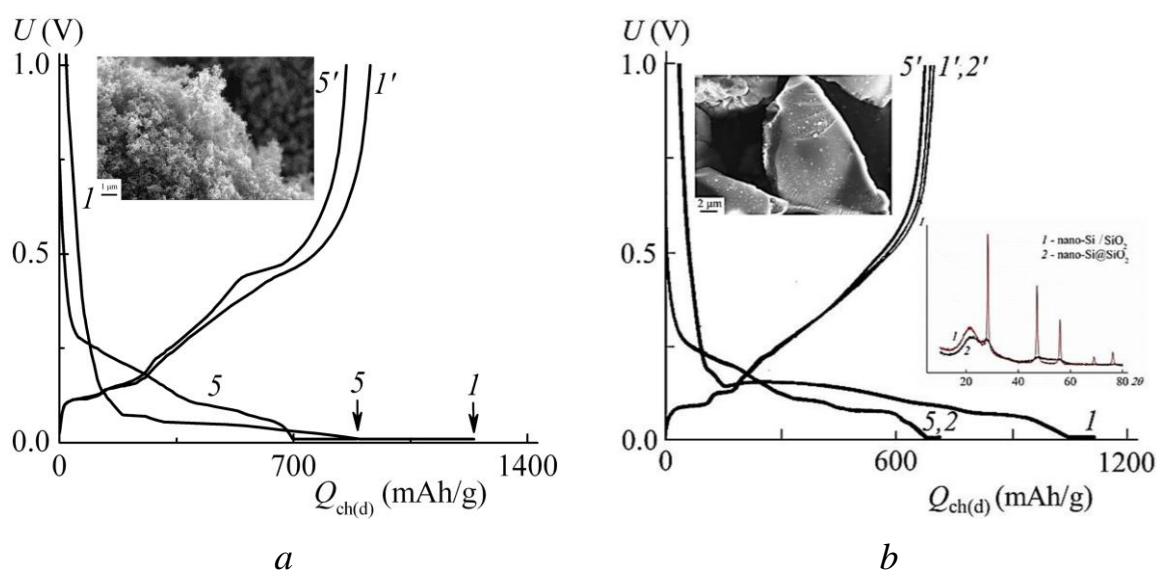


Figure 1. Charge-discharge curves of the half-cells with "nano-Si/SiO₂"- (*a*) and "nano-Si@SiO₂"-based electrodes in cc/cv (charge) and cc (discharge) modes. Inserts: micrographs of "nano-Si/SiO₂" (*a*), "nano-Si@SiO₂" (*b*) powders and their X-ray diffraction spectrums (*b*).

In the case of both electrodes, we found no evidence of direct electrochemical reduction of SiO₂.

Galvanic synthesis method and the advantages of synthesized product electrochemical characteristics

It was proposed an electrochemical synthesis of a thin-layer SiO₂/Ni composite and demonstrates the features of its electrochemical interaction with lithium. Silicon dioxide was obtained by sulfuric-acid-driven precipitation from a solution of sodium-based liquid glass $\text{Na}_2\text{SiO}_3 \cdot m\text{H}_2\text{O}$ with a density of 1.08 g/cm³. The SiO₂ precipitate was used for galvanic preparation of the SiO₂/Ni composite [5]. The thin-layer composite was deposited on a cathode made of nickel foil in an electrolytic cell with a nickel anode. The cathode was positioned horizontally, and the suspension of SiO₂ in an electrolyte for nickel-plating was poured into the electrolytic cell. At the first, the precipitation of SiO₂ particles onto the nickel electrode occurred in the absence of current. Then, the current was switched for galvanic fixing of SiO₂ particles onto the nickel electrode. The electrolyte composition for deposition of the composite (in g/L) was as follows: NiSO₄·7H₂O, 150; Na₂SO₄·5H₂O, 25; H₃BO₃, 15; KCl, 10; SiO₂, 2; pH = 5–6.: $S_{\text{cathode}} : S_{\text{anode}} = 1 : 20$; $i_{\text{cathode}} = 1.5\text{--}2.0 \text{ mA/cm}^2$. Heat treatment of SiO₂/Ni composite: 105°C for 6–7 h. Here $S_{\text{cathode}} : S_{\text{anode}}$ are the cathode and anode surface area, respectively, cm². The electrochemical characteristics of SiO₂ were

studied with galvanostatic charge–discharge cycling using a prototyping LIB with 2016 dimensions, on a test bench equipped with computer software. The prototyping battery was filled with an electrolyte with the following composition: dimethoxyethane (Merck), dioxolane (Acros), and 1 mol/L LiBF₄ (Advanced Research Chemicals).

On the XRD data, synthesized oxide belongs to an amorphous modification (Fig. 2a). The synthesized silicon dioxide has the following parameters: the mass part of moisture is 6.2%, the specific surface area is 202 m²/g, and the bulk density is 220 g/dm³. In accordance with the size distribution histogram for SiO₂ particles, their maximum size does not exceed 22 nm and reaches 12–16 nm in the main fraction (Fig. 2b). The reversible performance of SiO₂ occurrences at current density of 30 μA/cm² (Fig. 2c, the part of the charge curve 1 without the fluctuations). At the 80 μA/cm² the fluctuations arise as the result of the volume of expansion of the active electrode component, and the second horizontal voltage area with a slope appears below 0.1 V. The advantage of the synthesized material is the possibility of obtaining stable cycling at an almost fixed voltage. This is facilitated by the encapsulation of the oxide with a homogeneous distribution in a rigid nickel matrix. This effect is not achieved in an electrode with synthesized SiO₂ in a composition with graphite filler and a binder in the presence of domains and aggregates of active material particles (Fig. 2d).

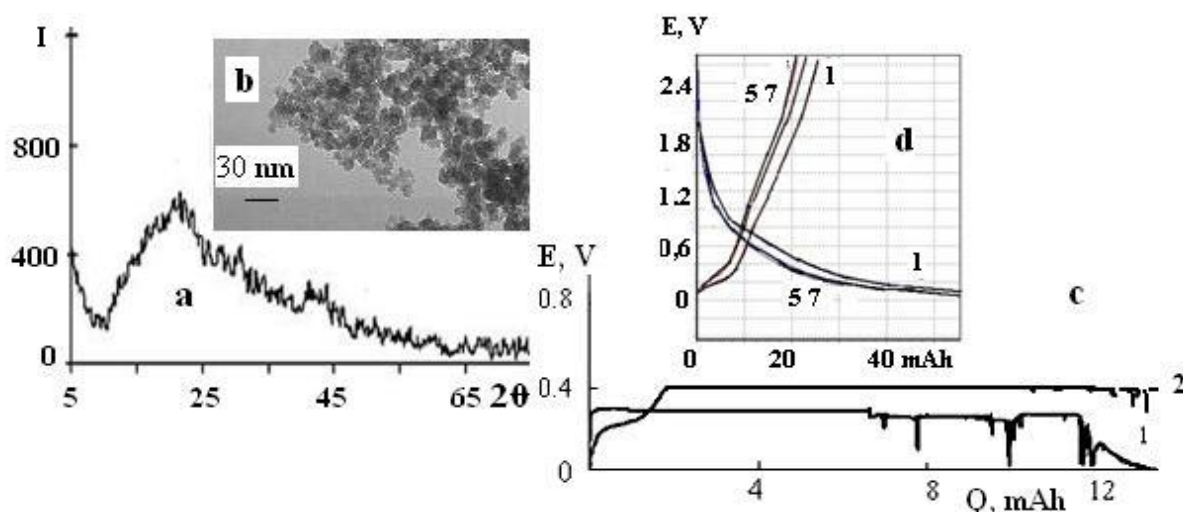


Figure 2. The investigation data of SiO₂/Ni composite (a, c) and SiO₂ (b, d): a – XRD pattern, b – the image in CEM, c, d – charge-discharge curves.

Conclusion

Thus, we did not find confirmation of SiO₂ electrochemical reduction in electrodes with "nano-Si/SiO₂" and "nano-Si@SiO₂" powders and also with synthesized domains and aggregates SiO₂ in a composition with graphite filler and a binder. The advantage of the SiO₂/Ni composite is the possibility of obtaining stable cycling at an almost fixed voltage.

References

1. Kuksenko S.P., Kovalenko I.O. Synthesis of a Silicon–Graphite Composite for the Hybrid Electrode of Lithium-Ion Batteries. *Russ. J. Appl. Chem.* 2010. **83**(10): 1811.
2. Kuksenko S.P., Kovalenko I.O. Silicon Nanopowder as Active Material for Hybrid Electrodes of Lithium-Ion Batteries. *Russ. J. Appl. Chem.* 2011. **84**(7): 1179.
3. Kuksenko S.P. Aluminum Foil as Anode Material for Lithium–Ion Batteries: Effect of Electrolyte Compositions on Cycling Parameters. *Russ. J. Electrochem.* 2013. **49**(1): 67.
4. Kuksenko S.P., Kaleniuk H.O., Tarasenko Yu.O., Kartel M.T. Stable silicon electrodes with polyvinilidenfluoride-binder for lithium-ion batteries. *Him. Fiz. Tehnol. Poverhn.* 2020. **11**(1): 58 [in Ukrainian].
5. Pat. UA118820. Apostolova R.D., Matsiyevsky M.A., Gladun V.A., Savchenko M.O.. Method of electrochemical obtaining of thin-layer SiO₂/Ni composite electrodes for lithium-ion batteries. Publ. 2019.

Electrochemical characterisation of LiPCP and its performance with different electrodes

M. Broszkiewicz^{a,*}, K. Rogala^a, L. Niedzicki^a

^a Faculty of Chemistry, Warsaw University of Technology,
Noakowskiego 3, 00-664 Warszawa, Polska

marek.broszkiewicz.dokt@pw.edu.pl

Lithium 1,1,2,3,3-pentacyanopropenide (LiPCP) is a fluorine-free lithium salt for application in electrolytes for Li-ion batteries. The salt provides high conductivity of $6.1 \text{ mS}\cdot\text{cm}^{-1}$ in standard EC:2DMC solution at 20°C with a lithium cation transference number over 0.7. It also has electrochemical stability up to 4.3 V vs. Li/Li⁺. Thus, this salt is predisposed for investigation of compatibility with different electrode materials.

Results and Discussion

The investigation includes cycling voltammetry, galvanostatic cycling, and impedance spectroscopy techniques. The investigation takes into account optimised solutions of LiPCP in EC:2DMC both with and without FEC and VC as solid electrolyte interface stabilizing additives. The electrolyte was investigated with anodes containing graphite or lithium titanate (Li₄Ti₅O₁₂) active materials as well as cathodes using active materials made of LiFePO₄, LiCoO₂, LiMn₂O₄, or LiNi_{0.5}Mn_{0.3}Co_{0.2}O₂. Binder used was mostly poly(vinylidene difluoride) and acetylene black was mainly used as a conductivity additive. It was found that with such electrode paste compositions LiPCP is compatible with graphite, LiFePO₄, and LiNi_{0.5}Mn_{0.3}Co_{0.2}O₂. However, the performance of cells with LiCoO₂ and LiMn₂O₄ was significantly worse and titanate was found to be incompatible with this salt.

Acknowledgments

This work has received funding from the European Union's Horizon 2020 research and innovation programme under grant agreement N°875029.

High entropy spinel oxide with excellent cycle stability

D. Csík^{a,b}, D. Zalka^{a,c}, K. Saksl^{a,b}, A. Straková Fedorková^c, D. Capková^c

^a Department of Materials Science, Faculty of Materials, Metallurgy and Recycling, Technical University of Košice, Letná 9, 042 00, Košice, Slovak Republic

^b Institute of Materials Research, Slovak Academy of Sciences, Watsonova 47, 040 01, Košice, Slovak Republic

^c Department of Physical Chemistry, Faculty of Sciences, Pavol Jozef Šafárik University in Košice, Moyzesova 11, 041 54, Košice, Slovak Republic

Lithium-ion batteries enable a prospective way to store energy. Moreover, they ensure high working potential at high energy density. These characteristics predetermine their usage in demanding applications, such as transport. Recently, high entropy oxides (HEO) have been introduced as anode active materials in lithium-ion batteries with superior electrochemical performance. Among the various types of high entropy oxides, spinel-structured HEOs are the most studied because they ensure three-dimensional transport of lithium ions. In this work, a novel spinel-structured high entropy oxide is presented with excellent cyclic stability at medium current density.

Introduction

The development of society depends a lot on the development of the power industry [1]. Since the 20th century, the main sources of energy are based on fossil fuels, which have many disadvantages, especially environmental problems. Utilization of green energy, such as wind power, solar and geothermal energy, could alleviate the damage caused by fossil fuel combustion. However, due to their irregular operation, the exploitation of these types of energy requires major development of electrical energy storage. Among the existing electrochemical batteries, lithium-ion batteries have been evaluated as the best choice so far, because they possess the highest energy density compared to other types of batteries [2].

Currently, the most used anode active material in lithium-ion batteries is graphite, which has a low theoretical capacity (372 mAh.g^{-1}) [3]. Higher theoretical capacities have the so-called conversion type metal oxides. Unfortunately, they are limited by the significantly volume changes during the cycling process, which leads to pulverization of the electrode material and capacity drop [2]. It has been proven that multicomponent oxides, referred to as high entropy oxides, exhibit excellent cycling stability due to the entropy stabilization of the structure [4-7]. Moreover, high entropy spinel oxides enable high rate capability because they ensure three-dimensional transport of lithium ions [5-7].

In alloys and rock-salt structured oxides four metal components are not sufficient for the entropy stabilization of the structure [4], but in spinel oxides due to the two lattice sites for the cations, their entropy is increased, thus four component spinel oxides can be described as high entropy oxides [8]. In this work, a high entropy oxide is prepared based on four transition metals and its electrochemical performance is examined.

Experimental

Medium entropy alloy CoFeCrNi was prepared by arc melting of pure elements (>99.9%) under argon atmosphere in a Mini Arc Melter (Edmund Buhler). The melt was cast into a form of small loaf of 3 g. The loaves were milled by a vibration mill at a frequency of 50 Hz. The powder particles of the alloy were oxidized in oxygen atmosphere at 1000 °C for 6 h. The sintered material was milled by a vibration mill at a frequency of 50 Hz. The final milling process was performed in a ball mill at 500 rpm for 30 min using WC balls (Ø 10 mm). The phase analysis of the alloy and the oxide was performed by XRD measurement supplemented by Rietveld refinement.

Electrochemical properties of the oxide were examined in electrochemical cells (CR2032, El-Cell, Swagelok Cell). The working electrode based on the prepared oxide was prepared in the following way. PVDF was dissolved in NMP, then a mixture of the oxide and carbon black Super P was added. The weight ratio of the oxide, Super P and PVDF was 8:1:1. The mixing of the slurry was performed in a vortex mixer at 2000 rpm for 30 min. The slurry was cast onto a Cu foil, the thickness of the wet film was 180 µm. The drying process was carried out in a vacuum dryer at 120 °C overnight. The mass load of the electrode was approx. 2.9 mg.cm⁻². The half cells were assembled in an argon filled glovebox (O₂, H₂O <1 ppm) using Li as counter electrode, Whatman GF/A as separator and 1 M LiPF₆ in a mixture of EC/DEC 50/50 as electrolyte. The charge and discharge properties were evaluated using a Landt Battery Cycler at 25 °C. Cyclic voltammetry and EIS measurements were performed using a Biologic SP-150 potentiostat.

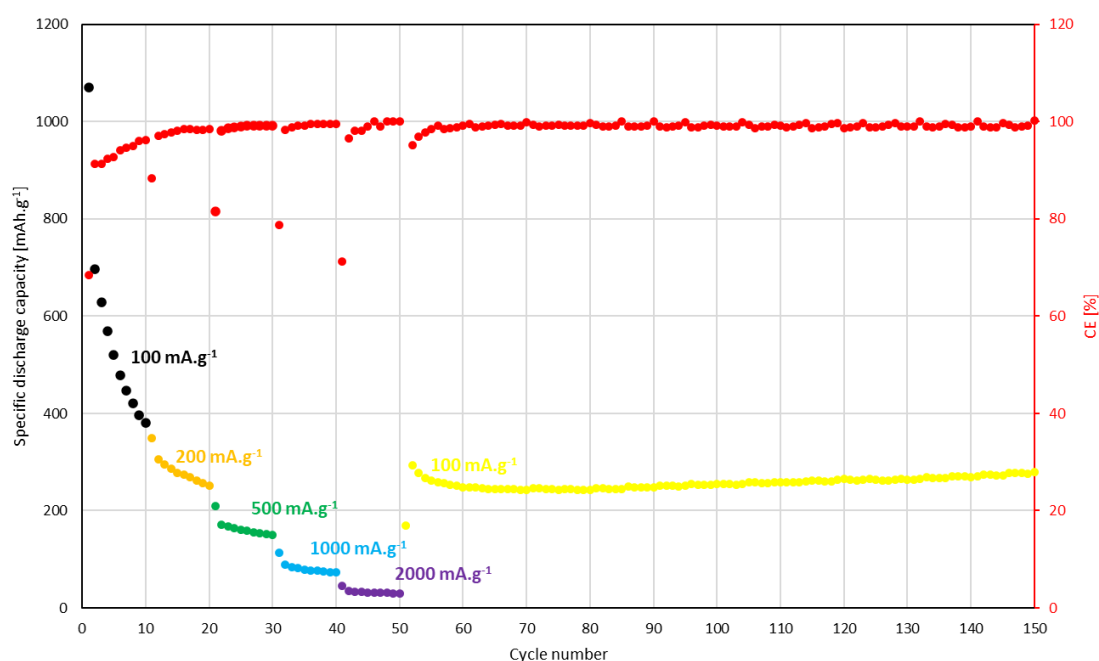


Figure 1. Rate capability of high entropy spinel oxide (CoFeCrNi)₃O₄

The medium entropy alloy CoFeCrNi has a face centred cubic structure of the Fm-3m space group ($a=3.598(9)$ Å). After heat treatment of the alloy at 1000 °C in O₂ atmosphere, an oxide system was obtained. The major phase (95 wt.%) has a spinel structure of Fd-3m space group ($a=8.319(1)$ Å), while the minor phase has a cubic structure of Fm-3m space group ($a=4.199(7)$ Å). The initial discharge capacity of the oxide was 1011 mAh.g⁻¹. The discharge capacity in the stabilized region was 253 mAh.g⁻¹. For rate performance, the prepared oxide delivered discharge capacities of 380, 251, 149, 73, 29 mAh.g⁻¹ at current densities of 100, 200, 500, 1000, 2000 mA.g⁻¹,

respectively. In the regeneration process at low current density of 100 mA.g⁻¹ a discharge capacity of 268 mAh.g⁻¹ was obtained.

Conclusion

In this work a simple preparation method of high entropy oxide is described. The prepared medium entropy alloy powder was used to prepare high entropy oxide. Despite the dual phase structure of the oxide, an incredibly stable discharge capacity of 253 mAh.g⁻¹. Increasing the current density, the discharge capacity was dropped, but due to the entropy stabilization of the structure, the capacity was regenerated (268 mAh.g⁻¹) decreasing the current density. Further optimization of preparation methods is required to obtain high capacity and cyclability of the analysed material. This work emphasizes the prospective possibility of utilization of high entropy oxides in lithium-ion batteries.

Acknowledgments

This work was realized within the frame of the project „Research centre for progressive materials and technologies for present and future applications „PROMATECH“, ITMS 26220220186; by the projects of Slovak Research and Development Agency APVV-20-0138, APVV-20-0205, APVV-21-0274 and of Slovak Grant Agency VEGA 2/0039/22.

References

1. B. Xiao *et al.*, “High entropy oxides (FeNiCrMnX)₃O₄ (X=Zn, Mg) as anode materials for lithium ion batteries,” *Ceramics International*, vol. 47, no. 24, pp. 33972–33977, Dec. 2021
2. Ali Eftekhari, “*Future Lithium-ion Batteries*”, Royal Society of Chemistry, 2019
3. H. Chen, N. Qiu, B. Wu, Z. Yang, S. Sun, and Y. Wang, “A new spinel high-entropy oxide (Mg_{0.2}Ti_{0.2}Zn_{0.2}Cu_{0.2}Fe_{0.2})₃O₄ with fast reaction kinetics and excellent stability as an anode material for lithium ion batteries,” *RSC Advances*, vol. 10, no. 16, pp. 9736–9744, Mar. 2020
4. A. Sarkar *et al.*, “High entropy oxides for reversible energy storage,” *Nature Communications*, vol. 9, no. 1, Dec. 2018
5. D. Wang *et al.*, “Spinel-structured high entropy oxide (FeCoNiCrMn)₃O₄ as anode towards superior lithium storage performance,” *Journal of Alloys and Compounds*, vol. 844, Dec. 2020
6. T. X. Nguyen, J. Patra, J. K. Chang, and J. M. Ting, “High entropy spinel oxide nanoparticles for superior lithiation-delithiation performance,” *Journal of Materials Chemistry A*, vol. 8, no. 36, pp. 18963–18973, Sep. 2020
7. C. Q. Duan *et al.*, “New spinel high-entropy oxides (FeCoNiCrMnXLi)₃O₄ (X = Cu, Mg, Zn) as the anode material for lithium-ion batteries,” *Ceramics International*, vol. 47, no. 22, pp. 32025–32032, Nov. 2021
8. O. F. Dippo and K. S. Vecchio, “A universal configurational entropy metric for high-entropy materials,” *Scripta Materialia*, vol. 201, Aug. 2021

The study of NMC cathodes regenerated with relithiation process

P. Guricová¹, T. Kazda¹

¹ Department of Electrical and Electronic Technology, Faculty of Electrical Engineering and Communication, BUT, Technická 10, 616 00 Brno, Czech Republic

Electrodes with cathode material regenerated with relithiation process were prepared. Properties of $\text{LiNi}_x\text{Mn}_y\text{Co}_{1-x-y}\text{O}_2$ (NMC) relithiated materials, extracted from Samsung INR 18650-20R aged cell were studied. NMC electrodes regenerated with different amounts of Li_2CO_3 (3w%, 5w%) were prepared and studied using electrochemical measurements. Comparison between unmodified material and materials with extra lithium is shown and discussed.

Introduction

Direct recycling is one the approaches for recycling spent Li-ion batteries. It has been discussed more and more as the production of batteries is increasing, and access to material is needed to fulfil the high demand. Electrode materials vary in chemical composition and preparation of cathodes can be later problematic due to lack of resources. For the fast production of Li-ion cells it is important to find quick and easy way how to restore such material, so they are able to work as properly as fresh materials. In this study we are discussing the relithiation approach of regenerating the used material after end of life of the battery. The main purpose is in renew the capacity in the cell by restoring the Li ions in the cathode structure, specifically by adding Li_2CO_3 .

Experimental

For the experimental part the Samsung INR 18650-20R cell was chosen. This type of battery is currently one of the most used type of battery. The capacity of this cell is 2 Ah and the cathode material has NMC chemistry, containing nickel, manganese and cobalt in particular ratio, with the formula $\text{LiNi}_x\text{Mn}_y\text{Co}_{1-x-y}\text{O}_2$. The cell was firstly aged, with aging parameters set to 500 cycles and 1C rate. After aging process the battery was disassembled and the cathode was separated for further operations. Cathode substance was extracted using dimethylsulfoxide (DMSO) heated up to 50°C and extraction time was set to 2 hours, in accordance with previous experiments [1].

Three types of electrodes were studied during this experiment. Pure material extracted from aged cell was compared with samples modified with Li_2CO_3 . Samples contained 3w% and 5w% of Li_2CO_3 . Cells were prepared in a glove box with argon atmosphere. As counter electrode, lithium metal was used, glass fibre as a separator and 1M LiPF_6 EC:DMC (1:1) as electrolyte.

For the electrochemical measurements, cyclic voltammetry and galvanostatic cycling at different C-rates, potentiostat Biologic WMP3 was used.

Discussion

Figure shows comparison of cyclic voltametries for all samples. The active area for the anodic part starts at approximately 4 V, peaks at 3,6 V and further the activity slows down. For the nonmodified material, at 4 V the current is 535 mA/g, for the sample with 3w% Li_2CO_3 at the voltage 3,95 V the current is 298 mA/g, and lastly for the sample modified with 5w% Li_2CO_3 the current at 4,2 V is 245 mA/g. From the comparison it is visible that the peak for the unmodified sample is higher which refers to highest capacity.

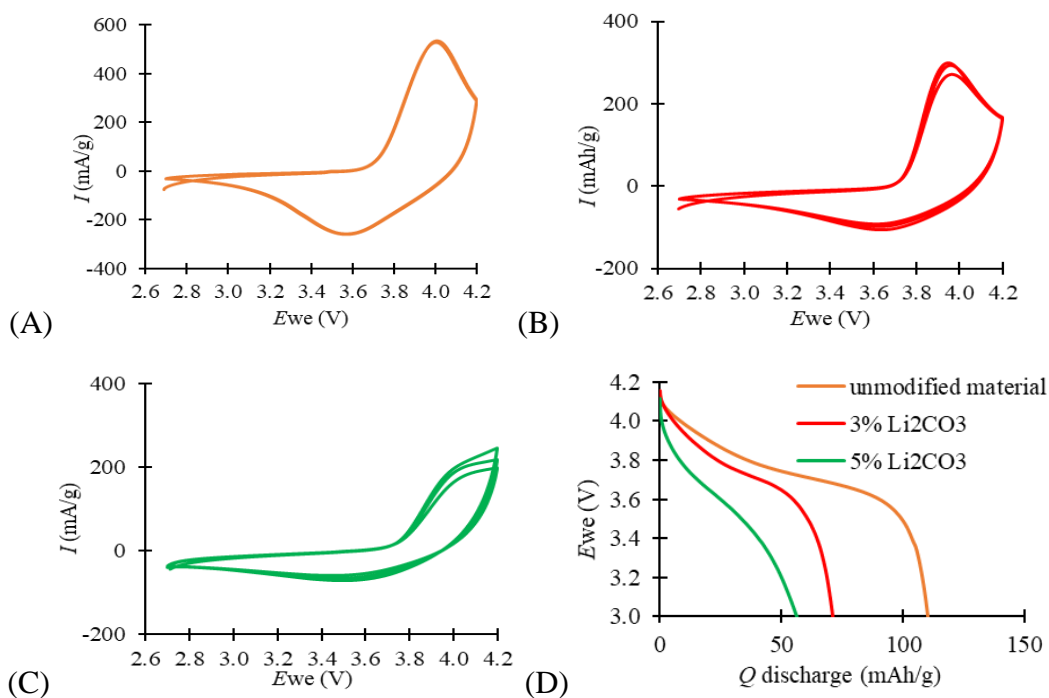


Figure 1. (A) CV for unmodified material, (B) CV for material modified with 3w% Li_2CO_3 , (C) CV for material modified with 5w% Li_2CO_3 , (D) discharging plateaus for the samples

Figure 1 (D) displays discharge plateau for all the samples. It is shown how the capacity decreases with higher amount of Li_2CO_3 . The energy that is stored in the battery also drops, because of decrease in the voltage. The fastest decrease in the capacity can be spotted in the sample with 5w% Li_2CO_3 .

Figure 2-4 shows evolution of cycling at different C-rates. Results demonstrates decrease in capacity with higher current. The unmodified electrode was working as expected but at the second 0.2C short circuit appeared at the beginning of the measurement. Although from the first values it is visible that the capacity was able to get back to its original value. In the Figure 3 is shown cycling for the 3w% sample, here the capacity decreased more over the C-rates and the last measurement had capacity less than half of its original value. The sample with 5w% Li had the biggest decrease in the capacity over cycling and resulted in minimal values of capacity in the second 0.5C cycling.

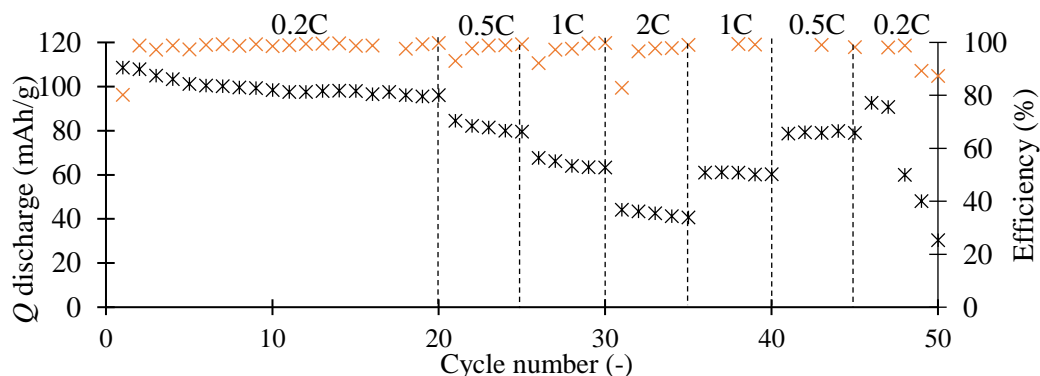


Figure 2. Cycling at different C-rates: unmodified material

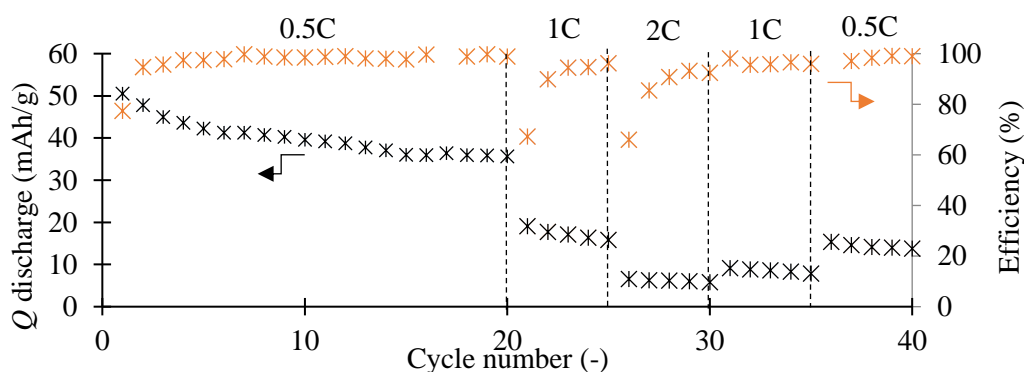


Figure 3. Cycling at different C-rates: 3w% Li_2CO_3

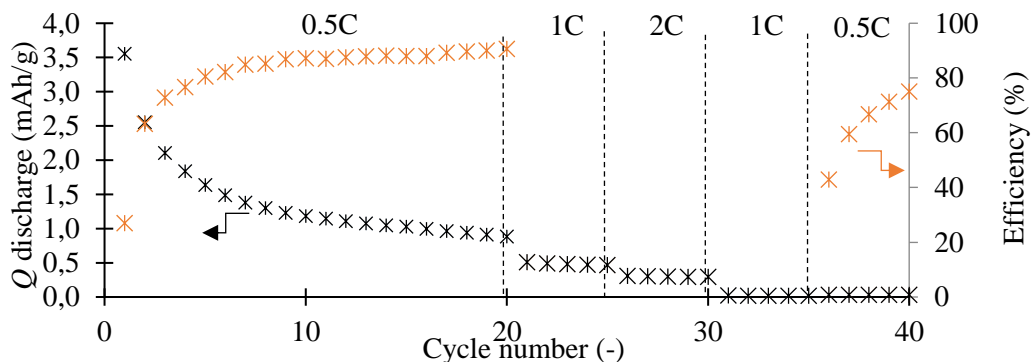


Figure 4. Cycling at different C-rates: 5w% Li_2CO_3

Conclusion

A comparison between unmodified electrodes and electrodes modified with different amounts of Li_2CO_3 was discussed. Modified electrodes prepared from aged material extracted from battery showed ability to work properly. Over the cycling the capacity was decreasing faster than for the unmodified material. The decrease in capacity over cycling for the 5w% sample was significant. We conclude that could have been due to the ongoing processes during cycling in the prepared cell. In further study we would like to test electrodes with less than 3w% Li_2CO_3 .

Acknowledgement

This work was supported by the specific graduate research of the Brno University of Technology No. FEKT-S-20-6206.

References

1. GURICOVÁ, P.; KAZDA, T. RECYKLÁCIA LI-ION BATÉRIÍ METÓDOU PRIAMEJ RECYKLÁCIE. 42. Nekonvenční zdroje elektrické energie. 1. 2021. s. 11-14. ISBN: 978-80-02-02936-6

An all-organic battery based on poly(9-vinylcarbazole) cathode

J. Kříž^a, J. Černý^b, T. Syrový^a

^a Department of Graphic Arts and Photophysics, University of Pardubice, 533 53 Pardubice, Czech Republic

^b Centre for Organic Chemistry Ltd., 53354 Rybitví, Czech Republic

All-organic batteries could provide a cheaper and more sustainable alternative to contemporary inorganic batteries. Here, we used electropolymerized poly(9-vinylcarbazole) (PVCz) as cathode and reduced tetralithium perylene-3,4,9,10-tetracarboxylate (PER) as anode. The battery was able to provide maximum discharge capacity of 61.9 mA.h.g⁻¹ and an open circuit voltage of 3.35 V. Capacity retention was 84% after 100 cycles at a cycling rate of 0.2 C. Thus, this work demonstrates the possibility of making an all-organic battery with a voltage above 2 V.

Introduction

Today's modern world is largely dependent on usable compact energy storage devices, i.e. batteries. Nowadays, lithium batteries with high energy density can be found everywhere, from small electronic devices to electric cars. In the future, interest in lithium batteries will continue to dominate, which will necessarily lead to pressure on the raw materials they are made of, especially lithium and cobalt [1]. A possible alternative is batteries based on materials other than traditional metal oxides.

Organic molecules such as carboxylates, quinones, carbazoles, and others are capable of redox reactions and thus are candidates for battery electrode materials. These molecules can be further modified to improve certain properties, such as the addition of side groups to adjust potential [2] or polymerization to achieve a lower solubility in electrolytes [3]. In some cases, these organic molecules can also be obtained from biomass or coal tar. Organic electrode materials can also work with cations other than lithium such as sodium [4], potassium [4], magnesium [5], or even a proton [6]. Although non-metallic batteries are currently in the early stages of research, some organic sodium batteries provide even better properties than lithium batteries [4]. In the future, organic batteries will compete with traditional lithium batteries in areas that are less demanding in life expectancy and energy density, due to a lower price or easier recyclability.

In this work, an all-organic battery based on PVCz cathode and PER anode was made. The PVCz cathode is a p-type material that is doped with an electrolyte anion (PF₆⁻ in this case) during charge/oxidation and dedoped during discharge/reduction. The PER anode is then an n-type material that uptakes electrolyte cations, i.e. Li⁺, during charge/reduction and releases cations during discharge/oxidation.

Experimental

The cathode material was made by mixing PVCz, carbon black conductive additive SUPER C65 and polyvinylidene difluoride binder (PVDF) in a weight ratio of 10:2.5:1 with the addition of N-methyl-2-pyrrolidone (NMP) as a solvent. The anode material was made similarly by mixing PER, SUPER C65 and water compatible binder in a weight ratio of 10:2.5:1 with water as solvent. Both

electrode slurries were coated onto aluminium foil, dried for 30 and 10 minutes at 80 and 110°C, respectively. The active material loading was 1.1 mg.cm⁻¹ and 4.2 mg.cm⁻¹ for PER and PVCz electrode, respectively. The electrodes were punched into 16 mm diameter disks. For initial doping and dedoping of PVCz and initial reduction of PER, their CR2025 half cells were assembled in an Ar-filled glovebox with lithium disk as the anode, a glass fiber separator and electrolyte of 1 M lithium hexafluorophosphate (LiPF₆) salt in a carbonates solvents. The coin cells were crimped at 800 PSI and after 2 hours the PVCz half cell was charged and discharged at 0.05 C in the range of 2.5–4.5 V and PER half cell was discharged at 0.25 C in the range of 1.0–2.0 V. Then, both cells were disassembled in a glovebox and an all-organic PVCz/PER battery was made. The specific capacity of the PVCz/PER battery was calculated using the mass of the PVCz material.

Results

The initial charge of the PVCz electrode showed a large capacity of 740 mA.h.g⁻¹, which was due to electropolymerization [7], and the discharge cycle with a mean potential of 3.8 V had a capacity of 61.5 mA.h.g⁻¹. The discharge capacity of the PER electrode was 133.9 mA.h.g⁻¹ with a mean potential of 1.1 V. The capacity of the PVCz and PER electrodes was 0.31 and 1.00 mA.h, respectively.

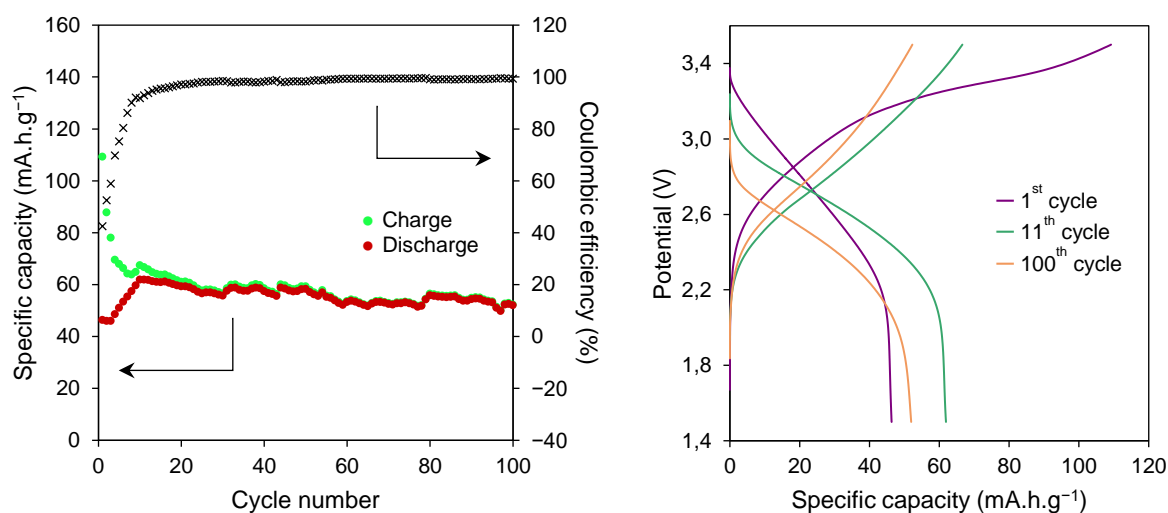


Figure 1. (a) Cycling performance and (b) charge and discharge curves of PVCz/PER battery at 0.2 C rate in 1 M LiPF₆ electrolyte.

As shown in Fig. 1a, the maximum discharge capacity of the PVCz/PER battery was 61.9 mA.h.g⁻¹ in the 11th cycle and after 100 cycles the discharge capacity decreased to 51.9 mA.h.g⁻¹ at a cycle rate of 0.2 C. Coulombic efficiency (CE) after 20 cycles reached a value of 97% and up to the 100th cycle CE oscillated around 99%. The average voltage of the PVCz/PER cell was in the 11th cycle approximately 2.6 V, and over 100 cycles, the voltage decreased to 2.4 V (Fig. 1b).

Conclusion

In this work, an all-organic battery based on poly(9-vinylcarbazole) cathode and tetra-lithium perylene-3,4,9,10-tetracarboxylate anode was assembled. The battery provided a moderate peak energy density of 161 Wh.kg⁻¹. In the future, the energy density could be improved by using an anode with a lower potential or by using a cathode with a larger specific capacity and a higher potential.

Acknowledgments

The work was supported from European Regional development Fund-Project "Organic redox couple based batteries for energetics of traditional and renewable resources (ORGBAT)" No.CZ.02.1.01/0.0/0.0/16_025/0007445 and by UPCE specific research programme (project No. SGS_2022_005).

References

1. Vaalma, C., Buchholz, D., Weil, M. et al. A cost and resource analysis of sodium-ion batteries. *Nat Rev Mater* 3, 18013 (2018). <https://doi.org/10.1038/natrevmats.2018.13>
2. L. Miao, L. Liu, K. Zhang, J. Chen, *ChemSusChem* 2020, 13, 2337.
3. Song, Z., Qian, Y., Gordin, M.L., Tang, D., Xu, T., Otani, M., Zhan, H., Zhou, H. and Wang, D. (2015), Polyanthraquinone as a Reliable Organic Electrode for Stable and Fast Lithium Storage. *Angew. Chem. Int. Ed.*, 54: 13947-13951. <https://doi.org/10.1002/anie.201506673>
4. Y. Hu, Q. Yu, W. Tang, M. Cheng, X. Wang, S. Liu, J. Gao, M. Wang, M. Xiong, J. Hu, C. Liu, T. Zou, C. Fan, Ultra-stable, ultra-long-lifespan and ultra-high-rate Na-ion batteries using small-molecule organic cathodes, *Energy Storage Mater.*, 41 (2021), pp. 738-747, [10.1016/j.ensm.2021.07.008](https://doi.org/10.1016/j.ensm.2021.07.008)
5. A.B. Ikhe, J.Y. Seo, W.B. Park, J.-W. Lee, K.-S. Sohn, M. Pyo, 3-V class Mg-based dual-ion battery with astonishingly high energy/power densities in common electrolytes, *J. Power Sources*, 506 (2021), p. 230261
6. Huan Wang, Rikard Emanuelsson, Christoffer Karlsson, Patric Jannasch, Maria Strømme, and Martin Sjödin, *ACS Applied Materials & Interfaces* 2021 13 (16), 19099-19108, DOI: [10.1021/acsami.1c01353](https://doi.org/10.1021/acsami.1c01353)
7. W. Tang, H. He, J. Shi, B. Cao, C. Yang, C. Fan, Poly(N-vinylcarbazole) (PVK) as a high-potential organic polymer cathode for dual-intercalation Na-ion batteries, *Org. Electron.*, 75 (2019), Article 105386, [10.1016/j.orgel.2019.105386](https://doi.org/10.1016/j.orgel.2019.105386)

Designing Batteries For Recycling: Fluorine-Free Lithium-Ion Batteries

C. Limachi ^a, L. Niedzicki ^a, W. Wiczorek ^a, M. Armand ^b and K. Rogala ^a

^a Department of Chemistry, Warsaw University of Technology, Noakowskiego 3, 00-664 Warsaw, Poland

^b CIC EnergiGune, Parque Tecnológico de Álava, Albert Einstein 48, 01510 Vitoria-Gasteiz, Spain

Aqueous anodes and cathodes in fluorine-free electrolytes were prepared and assembled in the laboratory. The effect of the electrolyte additive and the aqueous binder composition on the electrode slurry was investigated by cyclic voltammetry to further understand the electrolyte-electrode compatibility at room temperature. It was found that lower content of aqueous binder should be considered for future experiments. On the other hand, the additive electrolyte concentration will depend on the anode and cathode composition. Fluorine-free electrolyte conductivity was measured giving a result of $10.4 \text{ mS}\cdot\text{cm}^{-1}$ at room temperature. Finally, the initial results show compatibility between these aqueous electrodes and the fluorine-free electrolyte.

Introduction

The increasing large-scale production of lithium-ion batteries amplifies significant environmental problems [1]. Production in the automotive industry is of particular interest in this context. The most popular lithium salt used in batteries is the meta-stable LiPF_6 , which acts as an initiator of electrolyte decomposition. Therefore, this electrolyte is sensitive to impurities like moisture or acids as well as changes in temperature, which lead to the formation of toxic and bioaccumulating byproducts, like POF_3 and HF [2]. Additionally, the electrode processing is based on the use of fluorine-containing polymer, poly(vinylidene difluoride) (PVdF), as the binder, and teratogenic and toxic N-methyl-2-pyrrolidone (NMP) as a solvent/dispersant for the slurry preparation [3]. Furthermore, natural graphite and cobalt are considered critical materials nowadays.

As a consequence, key characteristics must be considered for the new generation of lithium-ion batteries such as the environmental impact, raw material availability, battery safety, and performance of the battery, all these at a reasonable cost [4].

However, finding a suitable fluorine-free electrolyte-electrode, which can fulfill the electrochemical and mechanical stability is challenging.

In this project, we target to investigate the most important developments in the field of green batteries, such as low costs, high battery performance, and environmental impact.

Experimental

Free-fluorine electrolyte conductivity at different solvent carbonates mixtures (based on ethylene carbonate and dimethyl carbonate, diethyl carbonate, or ethyl methyl carbonate), salt concentrations (0.1 to 1.2 mol kg^{-1}), and temperatures (0 to $50 \text{ }^\circ\text{C}$) were measured.

Fluorine-free lithium salt was synthesized in the laboratory (lithium 1,1,2,3,3-pentacyanopropenide) and carbonate solvents were considered for the electrolyte preparation. Additionally, after some cycling voltammetry tests, vinylene carbonate was employed as the electrolyte additive for solid electrolyte interface formation stabilization.

Active materials (lithium iron phosphate – LiFePO₄, and lithium manganese oxide – LiMn₂O₄ for the cathode; artificial graphite and silicon oxide composite for the anode), a conductive material (carbon black, Super P Conductive), and an aqueous binder were mixed at room temperature; followed by a coating of the slurry on a current collector, and subsequent drying and calendaring of the coated electrode. Finally, cyclic voltammetry (CV) was employed to further understand the fluorine-free electrolyte-electrode compatibility.

Results

Ethylene carbonate and dimethyl carbonate have shown higher conductivity, and the highest conductivity at room temperature had composition at 0.8 mol kg⁻¹. CV was performed in order to investigate the effect of the electrolyte additive and the aqueous binder on the electrochemical properties of the LiFePO₄ and artificial graphite or silicon oxide composite anodes at 0.1 mV·s⁻¹.

The anodic/cathodic signals of the LiFePO₄ cathode with 3 wt% of VC were more symmetrical and sharper, indicating its higher reversibility and better contact with the electrolyte, including SEI formation. Moreover, the redox pairs of the LiFePO₄ cathode with 3 wt% of VC exhibited a potential separation of 0.42 V when non-calendered and 0.36 V when calendered.

The anodic/cathodic signals of the artificial graphite anode CV with 5 wt% of VC content in the electrolyte have shown 88% increase of peak current over electrolyte with only 1 wt% of VC content.

The anodic/cathodic signals of the silicon oxide composite anode CV with similarly have shown 60% increase of peak current for 3 wt% VC content in the electrolyte over cycling with 1wt% of VC. However, increase of VC content to 5 wt% gained 82% increase of peak current in total over cycling with 1wt% of VC.

Therefore, with well-defined signals and small peak potential separation, at a certain electrolyte additive and aqueous binder concentration, these electrodes could achieve good electrochemical performance.

Acknowledgments

This project has received funding from the European Union's Horizon 2020 research and innovation programme under the Marie Skłodowska-Curie grant agreement No 945357.

References

1. He, X., et al., Fluorine-free water-in-ionomer electrolytes for sustainable lithium-ion batteries. *Nat Commun.* **9**(1): p. 5320, (2018).
2. Scheers, J., et al., All fluorine-free lithium battery electrolytes. *Journal of Power Sources.* **251**: p. 451-458, (2014).

3. Bresser, D., et al., Alternative binders for sustainable electrochemical energy storage – the transition to aqueous electrode processing and bio-derived polymers. *Energy & Environmental Science*. **11**(11): p. 3096-3127, (2018).
4. Dühren, S., et al., Toward Green Battery Cells: Perspective on Materials and Technologies. *Small Methods*. **4**(7), (2020).

Influence of Negative Temperature on Negative Electrode

J. Maca^{1,2}, J. Libich^{1,2}, T. Kazda^{1,2} and K. Jasso^{1,2}

¹Centre for Research and Utilization of Renewable Energy, Technicka 10, Brno, 616 00, Czech Republic

²Brno University of Technology, Technicka 10, Brno, 616 00, Czech Republic

The lithium ion batteries are present all around us. Not just in small portable electronic devices but also in more and more developed electric car area. The large battery storage for network frequency stabilization or power energy storage from renewable energy storages are more common in these days. The future trend is promising to even increase of lithium ion battery usage. Both stationary and mobile applications are influenced by temperature. The temperature has a significant influence on batteries performance. The area of temperature is highly investigating topic. This paper is showing the influence of low temperature on two main used negative electrode materials. The natural carbon 280H and lithium titan oxide (LTO) were tested at room and low, negative temperature. There is a big effort to operating temperature window extension and battery capacity stabilization.

Introduction

For determining of temperature influence on negative electrode for lithium ion batteries, two sets of negative electrodes were made. The galvanostatic cycling was made at two temperatures the room temperature in the laboratory 27 °C and low temperature – 25 °C in freezer. The capacity change in first 10 cycles was evaluated and the both electrode materials were compared. The electrode material was made from 10 weight% of binder PVDF, 10 weight% of conductivity increase part Super P and 80 weight% of active material dissolved in NMC. Two active material were used and that natural carbon 280H and ceramic lithium titan-based material $\text{Li}_4\text{Ti}_5\text{O}_{12}$ (LTO). Both materials were placed on copper current collector and the thickness of negative electrode was 150 μm . Electrodes were dried in vacuum oven at 60°C for one day. The electrodes were measured in EL-cell cells as half-cell against metal lithium. The load for both electrodes was 0.2C charging discharging rate. The capacity of electrodes is shown in Figure 1. From the results it is visible that the LTO material is more stable and have better performance in low temperature than carbon 280H. The capacity drop of LTO was 20 %. The capacity drop for carbon was in first 5 cycles 74 %. The capacity drop at room temperature after fifth cycle can be due a local shortcut inside the cell.

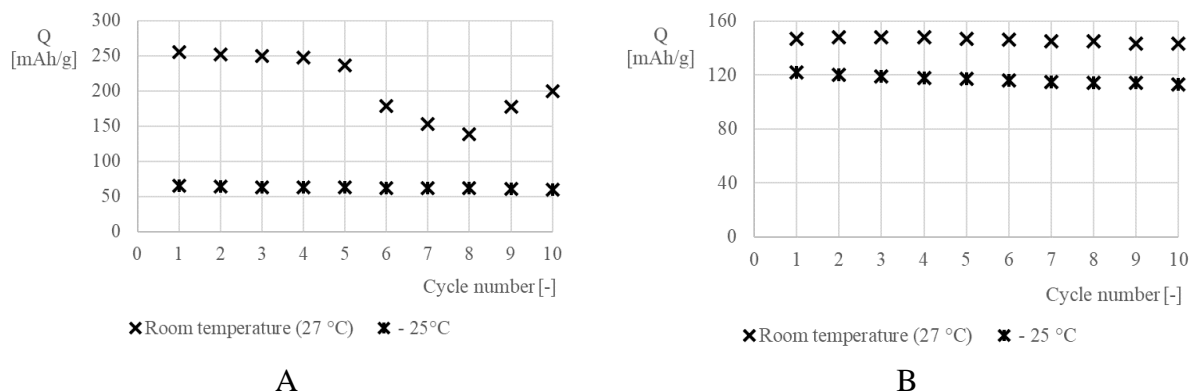


Figure 1. Capacity of negative electrodes A) carbon 280H, B) LTO based electrode

Acknowledgement

Authors gratefully acknowledge the financial support from the Ministry of Education, Youth and Sports of the Czech Republic under project No. LTT19001 and BUT specific research programme (project No. FEKT-S-20-6206)

References

1. ZHANG, Dan, Chao TAN, Ting OU, Shengrui ZHANG, Le LI, Xiaohui JI a Feng LI, 2022. Constructing advanced electrode materials for low-temperature lithium-ion batteries: A review. *Energy Reports*. 8.
2. PIAO, Nan, Xuning GAO, Huicong YANG, Zhenqiang GUO, Guangjian HU, Hui-Ming CHENG a Feng LI, 2022. Challenges and development of lithium-ion batteries for low temperature environments. *ETransportation*. 11.
3. ZHU, Caijian, Weixia LV, Jun CHEN, et al., 2020. Butyl acrylate (BA) and ethylene carbonate (EC) electrolyte additives for low-temperature performance of lithium ion batteries: A review. *Journal of Power Sources*. 476
4. JIANG, Jiuchun, Haijun RUAN, Bingxiang SUN, et al., 2018. A low-temperature internal heating strategy without lifetime reduction for large-size automotive lithium-ion battery pack: A review. *Applied Energy*. 230, 257-266. ISSN 03062619.

A Comprehensive Heat Generation Study of Lithium Titanate Oxide-based Lithium-ion Batteries

Seyed Saeed Madani¹ *, Erik Schaltz², Søren Knudsen Kær³, Carlos Ziebert⁴

^{2,3} Department of Energy Technology, Aalborg University, DK-9220 Aalborg, Denmark;

^{1,4} Institute of Applied Materials-Applied Materials Physics, Karlsruhe Institute of Technology, 76344 Eggenstein-Leopoldshafen, Germany;

A precise interpretation of lithium-ion battery (LIB) heat generation is indispensable for different applications including electric vehicles. The internal resistance of a lithium titanate oxide-based LIB was determined at different state of charge (SOC) levels and current rates to understand the relationship between internal resistance and heat generation. Random and different pulse discharge current step durations were applied to consider the effect of different SOC interval levels on the heat generation. The total generated heat was measured for different discharge rates and operating temperatures in a Netzsch IBC 284 calorimeter. It was seen that a 6.7% SOC decrease at high SOC levels corresponds to 0.38Wh, 0.73Wh, and 1.00Wh heat generation for 26A, 52A, and 78A step discharge both at 20°C and 30°C. However, a 1.85% SOC decrease at medium SOC levels, corresponds already to 0.57Wh, 0.76Wh, and 0.62Wh heat generation.

Introduction

LTO-based LIB have several features, including lifetime and safety properties, making them an appreciable and promising technology for different applications such as e-mobility and grid storage (1-3). Measuring heat generation of LIB is a challenging task because of the complex electrochemical reactions occurring and their dependence on many different parameters. Previous investigations (4-6) were limited to heat generation measurement of LIB during constant current charge and discharge full cycles. To our knowledge, thermal characterizations of LTO-based lithium-ion batteries focused on random and periodic charge-discharge pulses have not been investigated. Therefore they are in the focus of this work.

Experimental

The lithium-ion battery cells employed in this study are 13 Ah high-power lithium titanate oxide-based lithium-ion battery cells with $\text{LiNi}_x\text{Mn}_y\text{Co}_z\text{O}_2$ (NMC) on the cathode side and $\text{Li}_4\text{Ti}_5\text{O}_{12}$ (LTO) on the anode side. The minimum and maximum voltage are 1.5V and 2.9V, respectively. This research employed the isothermal IBC284 calorimeter (Netzsch) to characterize the heat loss related to constant current discharge (CCD) and constant current charge (CCC) procedures. Four different current profiles were applied both with random and periodic current pulses. Therefore, ten different step time duration was considered for SOC determination. The thermal analysis was accomplished, using Proteus Analysis Software (Netzsch) and MATLAB to analyze the data from the temperature and heat flux sensors after calibration. Dissimilar and independent loading were exerted on the cell and heat flux and surface temperatures were quantified. It took about six hours to reach thermal

equilibrium. Afterwards the specified current is applied to the cell with a Maccor battery cycler and then another six hours are needed for the temperature of the system to equilibrate.

Results and discussions

Discharge from 74.92% to 46.07% SOC demonstrated quasi-linear voltage decrease concerning SOC. With the intention of understanding the internal resistance impact as one of the principal sources of irreversible heat generation, it was determined at different SOC levels using hybrid pulse cycle experiments. It was almost constant with around 3 ohms at a SOC > 40% and to increase up to a factor of three at lower SOC levels. Open-circuit voltage (OCV) is one of the main sources of reversible heat generation. Consistent with the majority of the LTO-based cell parameters, the OCV is completely dependent on the working states, including the SOC. Different SOC levels were selected so that the cell demonstrated a quasi-linear voltage decrease concerning the SOC.

The heat generation curves of the cell that have been determined using the isothermal calorimeter are illustrated in Figure 1a) and the derived total generated heat is shown in Figure 1b). An overall increasing pattern was seen for the heat generation during discharging and an overall decreasing pattern was seen for the heat generation during the rest period for each discharge pulse. At 20°C, discharging from 74.92% to 68.23% state of charge, the heat generation was 0.377Wh, 0.728Wh, and 1.002 Wh for 26A, 52A, and 78A step discharge rates, respectively.

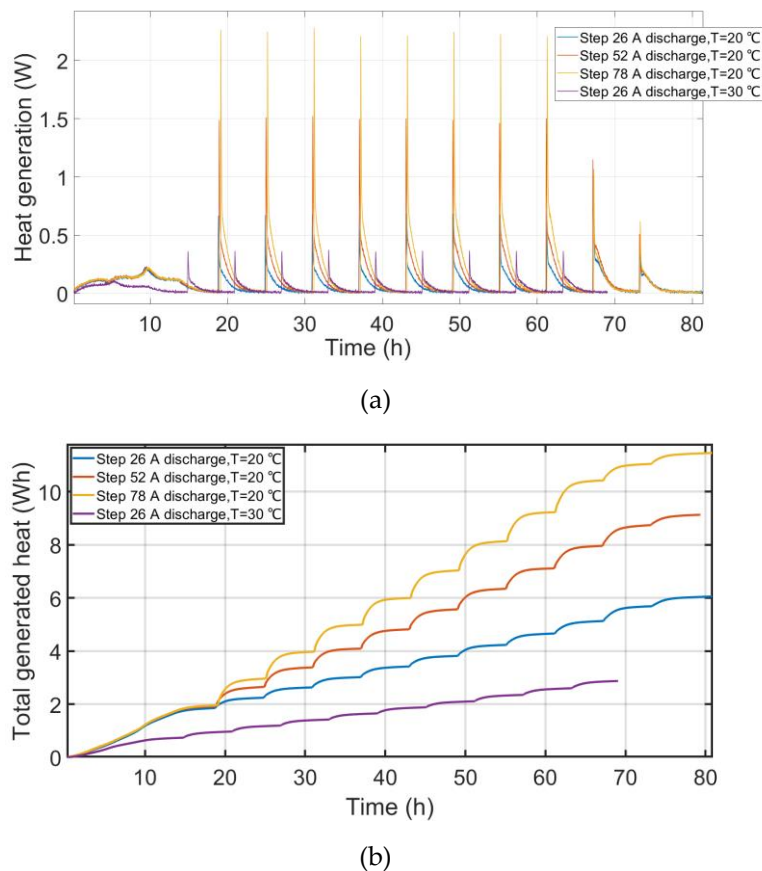


Figure 1. Isothermal calorimeter measurements on a lithium titanate oxide-based cell: (a) Heat generation curves for different current rates (b) Evolution of total generated heat as derived from (a).

Until a SOC of 74.92%, the total generated heat curves for the 26A, 52A, and 78A current rates approximately overlap each other. As the cell is more discharged, the three curves start to deviating from each other. In the SOC range of 74.92% to 46.07%, the average heat generation rate during 78 A step discharge cycles was more significant by 0.25Wh and 0.85Wh than that observed for the 26 A and 52 A step discharge. A decrease of 2% in SOC level causes an increase of 0.4Wh, 0.776Wh, 1.064Wh, and 0.229Wh in heat generation for Step 26A, 52A, 78A discharge at 20°C and step 26 A discharge at 30°C correspondingly. From the aforementioned experimental data can be inferred that the SOC level change at different SOC points has a different influence on the heat generation rate.

The rise in irreversible heat generation at bigger current rates might be attributable to elevated overpotential. Overpotential resistance decreases with increasing state of charge level towards the termination of discharge. The quantity of total generated heat declines significantly at 30 °C in comparison with the working temperature of 20 °C. It can be inferred that the cell working temperature is the most crucial factor affecting heat generation. Notwithstanding, SOC level change could be important in some SOC points, nonetheless the impact of irreversible heat and internal resistance is not insignificant. OCV demonstrated an increasing pattern towards a larger SOC and conversely, internal resistance showed approximately an overall decreasing pattern towards a larger SOC. Considering the changing pattern of heat generation at different SOC levels and total generated heat it can be concluded that internal resistance has a larger influence on heat generation of the LTO-based cell in comparison with OCV. The evolution of heat loss and efficiency as a subordinate of the current charge/discharge cycles was determined. This heat flux quantification could be employed for judging the heat transmission of the inner portion of the lithium-ion battery cell. The results of this investigation can be used as supporting benchmark data for correlation to simulation outcomes, accompanied by lithium-ion battery heat generation characteristics to assist in the design and analysis of an efficient thermal management system. When the operating temperature is 50 °C, the heat generation amount is approximately the same as at 20 °C at the lower current rates and increases comparatively towards large current rates. With the increase of charge and discharge current rates, the heat generation level increases. It is very appealing that there is a heat generation boundary for the investigated cell with individual compounds and materials, a function of operating temperature. Besides, it varies for different current rates.

References

1. M. Swierczynski, D.-I. Stroe, A.-I. Stan, R. Teodorescu, and D. U. Sauer, *IEEE Trans. Sust. Energy*, **5**(1), 90 (2014).
2. A. F. Tie and C. W. Tan, *Renewable and Sustainable Energy Reviews*, **20**, 82 (2013).
3. A. Farmann, W. Waag, and D. U. Sauer, *Energy*, **112**, 294 (2016).
4. F. Hall, J. Touzri, S. Wußler, H. Buqa, and W. G. Bessler, *J. Energy Storage*, **17**, 109 (2018).
5. Y. Abdul-Quadir T. Laurila, J. Karppinen, K. Jalkanen, K. Vuorilehto, L. Skogström and M. Paulasto-Kröckel, *Int. J. Energy Res.*, **38** (11), 1424 (2014).
6. A. Awarke, M. Jaeger, O. Oezdemir, and S. Pischinger, *Int. J. Energy Res.*, **15** (16), 1099 (2012).

Melanin as Biological Organic Polymer with Semiconductor Properties is Unique Effective Modifier for MnO₂ Cathode and Increases the Energy of Li-MnO₂ Battery.

I. Maksyuta,^a E. Shembel^{a,b}, V. Kyrychenko^c, V. Redko^b, T. Pastushkin^b, N. Zaderey^a

^a Scientific Research Laboratory of Chemical Power Sources of Ukrainian State University of Chemical Technology, Dnipro, 49005, Ukraine

^b Enerize Corporation, Coral Springs, FL, 33067, USA

^c Sunoil-Agro, Pavlograd, 51400, Ukraine

In this manuscript two important lines are presented: Melanin and MnO₂. Melanin has the unique natural as a biological organic polymer and semiconductor. This makes it is possible to successfully modify the electrodes of lithium batteries [1]. MnO₂ is used as a cathode material, which is synthesized on the basis of Ukrainian manganese ores. [2] In terms of reserves of manganese ores, Ukraine is in second place after South Africa.

Introduction

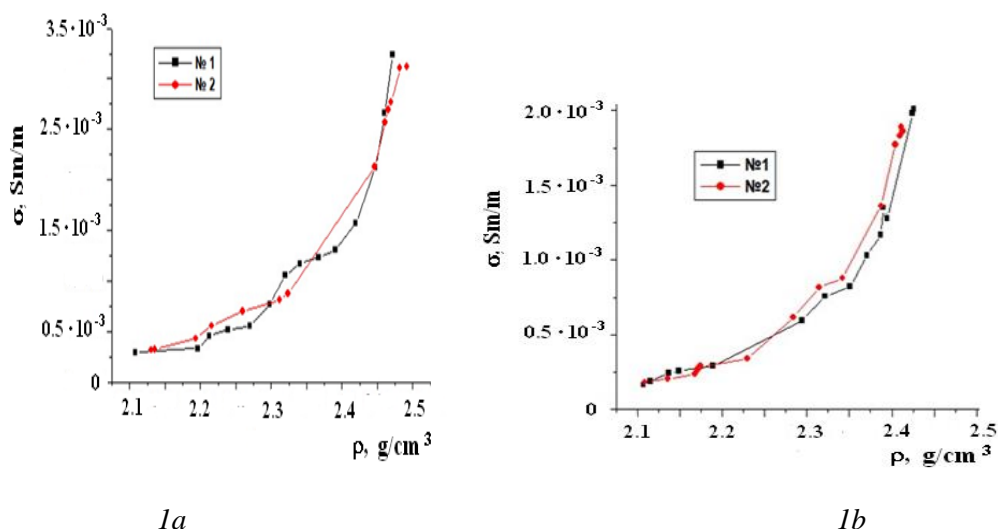
The cathode based on MnO₂ in Li- MnO₂ batteries has a number of advantages: high energy, high operative potential, low cost, and low toxicity. Improvement and modernization of existing Li – MnO₂ batteries are aimed at increasing their energy intensity, reliability and safety. We are realizing this using the modification of the MnO₂ by Melanin. Melanin, which is used for modification of the cathode based on MnO₂, is produced on the basis of innovative technologies developed by Sunoil-Agro Company. Principal common structure of Melanin is C₁₈H₁₀N₂O₄; density is 1.6 to 1.8 g/cm³; molecular weight is 318 g/mol. The innovative technologies for synthesizing and producing the MnO₂ by a chemical method is based on Ukrainian manganese ores, and are developed by Enerize Corporation company [2].

Description the Experimental

Compositions of the active mass of the cathode were as follows: 1. MnO₂ -85%, graphite (EUSM) - 5%, acetylene black - 5%, fluoroplastic binder brand 4FD- 5%. 2. MnO₂ - 64%, Melanin - 16%, graphite (EUSM) -7.5%, acetylene black - 7.5%, and fluoroplastic binder brand 4FD - 5%. The influence of melanin on the characteristics of MnO₂ in the process of multiple cycling was assessed in prototypes of lithium batteries of a disk design, size 2325. The discharge current was 0.1 mA/cm², the charge current was 0.05 mA/cm². Electrolyte: 1 M LiClO₄ in a mixture of EC and DMC (1:1), (Merck). Continuous galvanostatic cycling methods were used and cyclic voltammetry with voltage sweep. The auxiliary electrode is metallic lithium. The cells were tested at temperature +25°, and +60°C. The charge-discharge curves in the galvanostatic mode in the potential range of 2÷3.6 V were recorded on an automated stand.

Results of Investigations

On the Fig. 1 the results of investigation of the conductivity of two types of MnO_2 , which are synthesized by chemical and by electrochemical methods, are presented. The measurement of the conductivity of these powders is realized using an innovative non-contact non-destructive electromagnetic method, which developed by Enerize Corporation [3,4]. Dependence of the conductivity of the powder on its density are presented in these figures. Powder compaction is carried out by vibration,



1a

1b

Figure 1. Comparison of the conductivities of powders of MnO_2 , which is synthesized by various methods: chemical and electrochemical. Figure 1a presents the conductivity of the chemically synthesized MnO_2 by Enerize Corporation on the basis of Ukrainian manganese ores; Figure 1b presents the conductivity of the electrochemically synthesized MnO_2 from the market

Results, presented on the Figure 1, confirmed that the conductivity of the powder MnO_2 , which the chemically synthesized powder of MnO_2 from Ukrainian manganese ores, is higher than the conductivity of MnO_2 powder, which is from market. Investigation, which are presented below, have been provided with powder of MnO_2 that were chemically synthesized on the basis of Ukrainian manganese ores.

Li- MnO_2

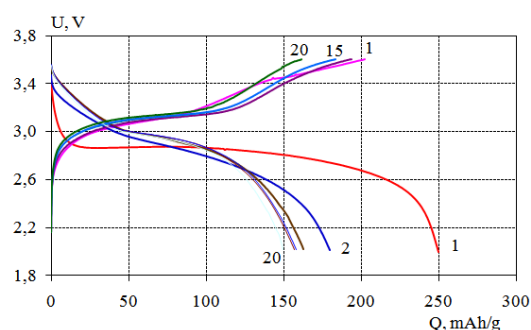


Figure 2

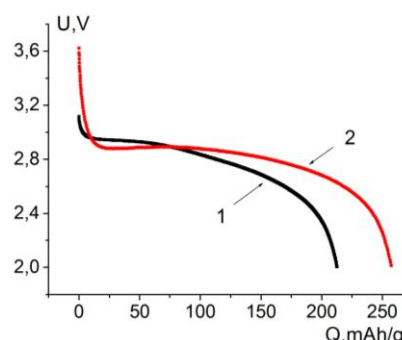


Figure 3

Figure 2. Discharge - charge the curves of electrode based on MnO_2 , which modified with melanin. Current of discharge $0,1\text{mA}/\text{cm}^2$, current of charge $0,05\text{ mA}/\text{cm}^2$.

Figures 3. First discharge curves of cathoder based on MnO_2 not modified by melanin (curve 1), and modified by melanin (curve 2). The discharge capacity of the cathode not modified with melanin is $220\text{ mAh}/\text{g}$. The discharge capacity of the melanin-modified cathode is $258\text{ mAh}/\text{g}$.

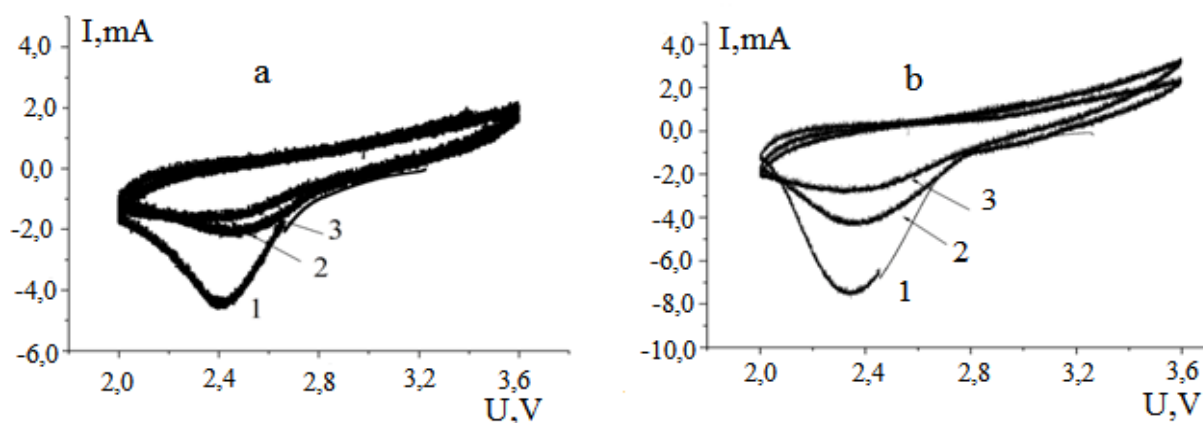


Figure 4. Cyclic voltammetry curves of the Li-MnO₂ system. Potential sweep rate is 0.5 mV/s. The numbers next to the curves are the number of the cycle. a) Electrode based on MnO₂, which is not modified with melanin. The maximum current on the first cycle is 4.56 mA. b) Electrode based on this MnO₂, which is modified with melanin. The maximum current on the first cycle is 7.56 mA.

The results presented on the Fig. 2 show that the first discharge curve has a high performance. Subsequent cycling has stable parameters. This shows that the primary current source Li-MnO₂, when using MnO₂, which modified by melanin, can be repeatedly cycled. Results, which presented on the Figures 3 and 4, confirm that the process modification of cathode based on MnO₂ significantly improves the energy and power performance of cathode, based on the MnO₂, and batteries Li-MnO₂

References

1. E. Shembel, V. Kyrychenko, I. Maksyuta, V. Redko, N. Zaderey. Melanin as Semiconductor with Polymer Structure is Effective Modifier for Electrodes of High Energy Li - Ion Batteries. *ECS Transactions*. – 2020. – Vol. 99, № 1. – P.47-56
2. E. Shembel, V. Pisniy, N. Globa, N. Zaderey, P. Novak. Manganese Dioxide for Lithium Battery Cathode. *US Patent Application 10/583,886*
3. V. Redko, E. Shembel, T. Pastushkin, etc. *Method and Device for Rapid Non - Destructive Quality Control of Powdered Materials*. US Patent No. 8,102,181
4. V. Redko, E. Shembel E., etc. *Method and Apparatus for Measuring Conductivity of Powder Materials Using Eddy Currents*. US Patent No. 7,288,941

Electrochemical performance of $\text{Li}_{1.2}\text{Ni}_{0.2}\text{Mn}_{0.6}\text{O}_2$ Disordered Rock - Salt Cathode Material

A. M Rodríguez^a, M. G. Ortiz^{a,b}, J. E. Thomas^c, A. Visintin^a

^a Instituto de Investigaciones Físicoquímicas Teóricas y Aplicadas (INIFTA), Facultad de Ciencias Exactas (UNLP), CONICET, Diag. 113 y 64, La Plata, Argentina

^b Centro de Investigación y Desarrollo en Ciencia y Tecnología de Materiales (CITEMA), Universidad Tecnológica Nacional - CICPBA, 60 y 124, 1923, Berisso, Argentina

^c YPF Tecnología S.A., Av. del Petróleo Argentino S/N (entre 129 y 143), B1923 Berisso, Buenos Aires, Argentina

In this work, lithium rich cathode materials, for Li-ion batteries, were synthesized via a solid-state reaction routine. The prepared materials were used as a cathode material for lithium-ion batteries and the electrochemical performance was studied by galvanostatic charge-discharge cycling, cyclic voltammetry, electrochemical impedance spectroscopy and rate capability, in which as electrolyte, 1M and 1.5M LiPF₆ in a mixture of ethylene carbonate and dimethyl carbonate (EC:DMC- 1:1 w/w) were employed.

Introduction

The fast and continuous development of portable electronic devices; such as laptops and cell phones, keeps increasing the demand for a new generation of high energy and high capacity cathode materials for the construction of Lithium-ion batteries [1]. The Lithium-Rich mixed oxides represent a promising family of compounds that could reach the energy and capacity requirements of, however there are some issues that must be solved like their rapid voltage and capacity fade. In this work, we synthesized and studied the electrochemical performance of a common Lithium-Rich material.

Experimental

We synthesized and studied the electrochemical performance of Lithium-Rich material ($\text{Li}_{1.2}\text{Ni}_{0.2}\text{Mn}_{0.6}\text{O}_2$) obtained through a solid-state reaction [2]; DRX analysis showed that the resulting compound has a high degree of cation disorder according to the I (003)/I (104) relation (figure 1.a); due to this phenomenon, cyclic voltammetry under normal cycling condition (2.0-4.8V), 1 M LiPF₆, exhibited and incomplete Li_2MnO_3 phase activation (figure 1.b) according to a moderate discharge capacity (144 mAh g^{-1}) at galvanostatic charge/discharge cycling, with a capacity fade of 5.64% (figure 1.e). After evaluating the stability of the electrolytes under an extended potential window (2.0-5.2V) (figure 1.d), a new potential range (2.0-5.0V) and a new electrolyte (1.5 M, EC:DMC) were selected; resulting in a better activation of the Li_2MnO_3 phase (figure 1.c) and an increase in the discharge capacity to 178 mAh g^{-1} , with a voltage fade of only 2.19% (figure 1.f). The cycling stability over 100 cycles was improved in around 20%.

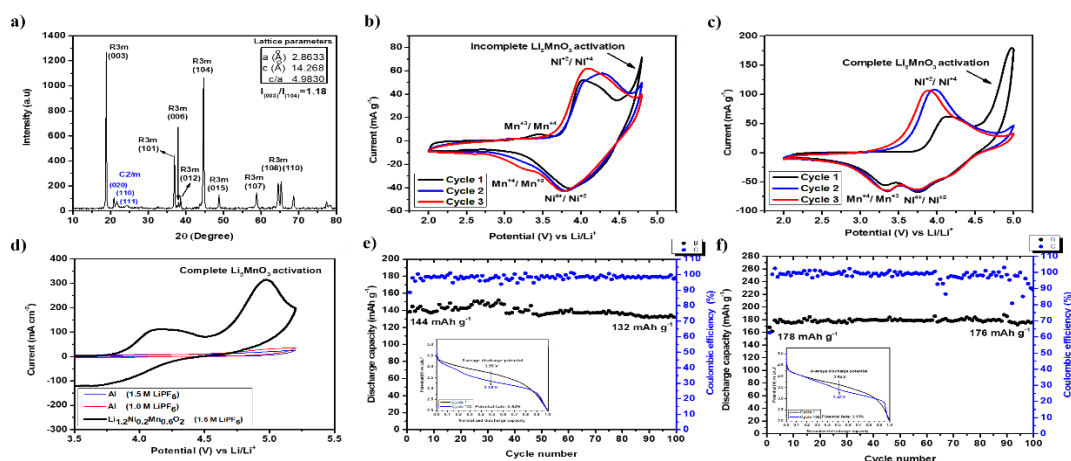


Figure 1. a) X-Ray diffraction pattern, cyclic voltammety performed under b) (2.0-4.8V) 1.0 M, EC: DMC 1:1 c) (2.0-5.0V) 1.5 M, EC: DMC 1:2, d) cyclic voltammety performed(2.0-5.2V), galvanostatic charge-discharge cycling e) (2.0-4.8V) 1.0 M, EC: DMC 1:1 f) (2.0-5.0V) 1.5 M, EC: DMC 1:2.

Acknowledgments

This work was supported by the CONICET (Consejo Nacional de Investigaciones Científicas y Tecnológicas) and ANPCyT (Agencia Nacional de Promoción Científica y Tecnológica).

References

1. P. Rozier, J. M. Tarascon. *J. Electrochem. Soc.*, **162**, A2490 (2015).
2. J. Xu, M. Sun, R. Qiao, S. E. Renfrew, L. M., T. Wu, S. Hwang, D. Nordlund, D. Su, K. Amine, J. Lu, B. D. McCloskey, W. Yang, W. Tong. *Nat. Commun.*, **9**, 947 (2018).

Lithium-Ion Battery Module-to-Cell: Disassembly and Material Analysis

A. Pražanová^a, M. Havlík Míka^b, V. Knap^a

^a Department of Electrotechnology, Faculty of Electrical Engineering,

Czech Technical University in Prague, Czech Republic

^b Department of Glass and Ceramics, University of Chemistry and Technology, Prague,
Czech Republic

Lithium-ion batteries (LIBs) are one of the most popular types of energy storage systems. Due to their excellent performance, they are widely used in portable consumer electronics and even electric vehicles (EVs). The ever-increasing requirements for emission reductions inhibit the production of new combustion vehicles. Thus, the demand for EVs increases, as well as the number of spent LIBs. Recycling is one of the most promising waste-management options in the end-of-life treatment of spent LIBs. It recovers selected materials with high efficiency and purity; therefore, economic, and environmental impacts of raw material production are lowered. This work describes the first step in the recycling processing of LIBs nickel-manganese-cobalt (NMC) based module from the Modular electric drive matrix (MEB) platform. This paper is devoted to the module-to-cell disassembly and material analysis of its individual components.

Introduction

Lithium-ion batteries (LIBs) currently represent one of the most promising electrochemical energy storage systems. They have found their place in a broad range of applications, from powering small consumer electric devices such as smartphones or laptops to integrating into electric transport systems considering electric bikes, scooters, and vehicles, as well as part of stationary energy storage systems.

At the same time, the ever-increasing requirements for the reduction of emissions decrease the production of new combustion vehicles and increase the demand for electric ones [1]. This growth in the electric vehicles market leads to the ever-increasing number of spent LIBs and brings numerous waste-management challenges in end-of-life processing [2].

The electric vehicle LIBs are typically based on valuable metals such as cobalt (Co), manganese (Mn), nickel (Ni), and lithium (Li) in the cathode, other elements such as graphite (C) in the anode, and other essential materials such as aluminum (Al), copper (Cu), and iron (Fe) in packaging and electronic components [3], [4]. Thus, recycling processing offers a very effective solution for waste treatment. Proper recycling technique recovers selected materials with high efficiency and purity reaching more than 90 % [5]; moreover, it increases the raw materials saving and reduces the energy and environmental impacts of mining [2].

This work focuses to the material analysis of the LIB's module and its NMC-based cells as the first step of recycling processing. The short-circuited module was disassembled into individual cells that were tested to characterize their condition, using the electrochemical impedance spectroscopy (EIS) and cyclic voltammetry (CV). The detailed analysis of material composition

was carried out. The content of valuable metals Ni:Mn:Co was different from the NMC (721) values of 7:2:1 which were specified by the manufacturer. Using the x-ray fluorescence (XRF) the valuable metals ratio was determined; it was closer to 7:3:3 ratio, which indicates a higher content of Mn and Co.

Experimental

In this work a material analysis and dismantling treatment on the scale of the battery module to its cells was performed. The LIB module typically used in the Modular electric drive matrix (MEB) platform was used for laboratory testing. The module consists of 24 NMC (712) pouch cells in a 3P8S connection, each of 3.65 V and 78 Ah capacity.

Firstly, the module was discharged and short-circuited. Secondly, the Al cover was milled off, and other plastics covering materials were manually removed from the module. In the next step, the rest of the insulating and thermo-insulating materials were removed, and individual cells were separated. Finally, the cell has undertaken a series of characterization measurements, including the EIS and CV; after its opening, captured in Figure 1 (a), the electrolyte and material composition proportions were analyzed using the XRF of solid thin layers.

Impedance Measurement: the complex impedance Z^* was recorded with an Autolab PGSTAT30 potentiostat using a harmonic AC field from 1MHz to 1 mHz at an amplitude of 1 mV. The absolute value of impedance $|Z|$ and its phase angle φ were plotted in a Bode plot as functions of frequency as is shown in Figure 1 (b). For the spectra analysis, the negative imaginary part $-Z_{Im}$ was plotted vs. the real part Z_{Re} , thereby forming a Nyquist plot on which frequency is a function parameter. Based on the plot shape, a design of an equivalent circuit model (ECM) with electric components whose parameters quantify the physicochemical processes inside the cell under the electric field was estimated. Using the non-least-squares complex method, the impedance data were fitted to the equivalent circuit and the corresponding parameters calculated.

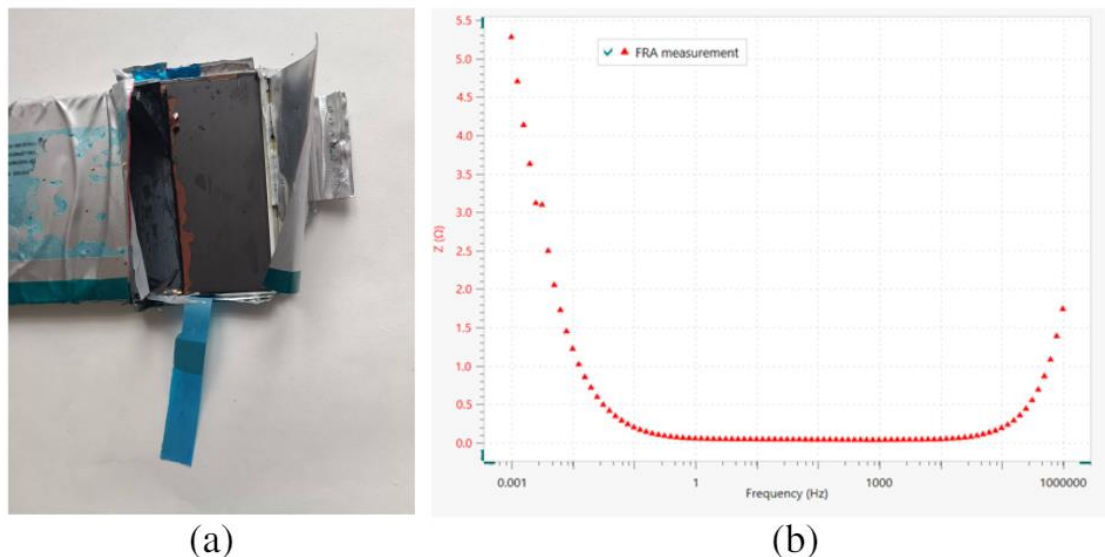


Figure 1. Example of (a) the opened cell, (b) Bode plot of $|Z|$.

Cyclic Voltammetry Measurement:

the cyclic voltammetry measuring the current as a function voltage was also recorded with an Autolab PGSTAT30 potentiostat in the staircase mode from 0 V to the potential when the current reached the value of 1 A; the potential step was 2.44 mV with scan rate 2 mV/s. The plots of current vs. voltage indicate the resistance change during the potential cycles.

Material Analysis Measurements:

the battery cell was opened and disassembled to individual layers of electrode materials soaked with electrolyte. The material was coated on thin Cu or Al metal sheets or on a separator. The XRF spectra of these solid layers were recorded using the Philips PANalytical spectrometer. The composition of cathode, anode and electrolyte materials was determined.

Results

According to this work, in the frequency range of 2 kHz to 10 Hz the impedance exhibited ohmic character with φ close to zero. For the frequencies above 2 kHz, the character was inductive ($\varphi > 0$), and below 10 Hz the character was capacitive ($\varphi < 0$). The inductive behaviour can be described by the ECM including resistance $R_1=38 \text{ m}\Omega$ in series with the parallel circuit of resistance $R_2= 8.2 \text{ }\Omega$ and inductance $L= 0.29 \text{ }\mu\text{H}$.

Moreover, this work provides a material analysis and dismantling treatment on the scale of the LIB MEB module to its cells. The determined ratio of Ni:Mn:Co in the cathode material was closest to the values of 7.00:3.09:2.57. The anode material contained about 90 wt% of C. The electrode materials were soaked with liquid electrolyte which contained F and P. For different layers, the concentration of P varied from 1 to 6 wt%, F from 2 to 10 wt% and P:F ratio from 1:1 to 1:15. The performed material composition analysis will be used in future work to implement the recycling technique and choose optimal processes, leading to the output products' highest possible efficiency and purity.

Acknowledgments

This research was supported by ŠKODA AUTO, a.s., and undertaken as part of SGC grant CTU, number SGS22/058/OHK3/1T/13.

References

1. L. Lander *et al.*, “Financial viability of electric vehicle lithium-ion battery recycling,” *iScience*, vol. 24, no. 7, Jul. 2021, doi: 10.1016/J.ISCI.2021.102787.
2. G. Harper *et al.*, “Recycling lithium-ion batteries from electric vehicles,” *Nat. 2019 5757781*, vol. 575, no. 7781, Nov. 2019, doi: 10.1038/s41586-019-1682-5.
3. C. Xu, Q. Dai, L. Gaines, M. Hu, A. Tukker, and B. Steubing, “Future material demand for automotive lithium-based batteries,” *Commun. Mater.*, vol. 1, no. 1, Dec. 2020, doi: 10.1038/S43246-020-00095-X.
4. Dai, Spangenberg, Ahmed, Gaines, Kelly, and Wang, “EverBatt: A Closed-loop Battery Recycling Cost and Environmental Impacts Model Energy Systems Division,” 2019, Accessed: Mar. 09, 2022. [Online]. Available: www.anl.gov.
5. A. Pražanová, V. Knap, and D.-I. Stroe, “Literature Review, Recycling of Lithium-Ion Batteries from Electric Vehicles, Part I: Recycling Technology,” *Energies 2022, Vol. 15, Page 1086*, no. 3, Feb. 2022, doi: 10.3390/EN15031086.

Corrosion Processes of Sintered Materials Based on Fe

M. Sedlaříková^a, M. Zatloukal^a, E. Doleželová^a, J. Kuchařík^a, P. Čudek^a, G. Fafílek^b

^a) Department of Electrical and Electronic Technology, FEEC, Brno University of Technology, Technická 10, 616 00 Brno, Czech Republic

^b) Institute of Chemical Technologies and Analytic, TU Wien, Getreidemarkt 9, 1060 Wien

Introduction

Bone injuries such as fractures often result in permanent bone damage such as weakness and structural or volumetric changes in fused bones. Treatment of such injuries can be long and expensive. Biodegradable materials may offer an improvement to such treatment, as they could provide the necessary short-term fixation and support for the fractured bone to be fused together. Biodegradable bone support will be gradually absorbed by corrosion processes and safely removed from the patient's body. Various compositions of such materials and manufacturing processes are investigated in different corrosion environments to evaluate a number of properties such as corrosion rate and corrosion potential. Key parameters for biodegradable materials are mechanical strength, flexibility, tissue compatibility, and rapid degradability.

Corrosion is a spontaneous, gradual transformation of metals or non-metallic organic and inorganic materials. It occurs as a result of a chemical or electrochemical reaction of the base material with the external environment. Electrochemical corrosion is a case of metal corrosion in electrolytes (conductive environments). It consists of two partial reactions – an anode reaction and a cathode reaction. Both the anode and cathode reactions are interrelated and cannot occur without each other unless an external electric current passes through the corroding metal. Anode reaction represents the oxidation of the metal and is therefore its own type of corrosion. The depolarizing cathode reaction represents the reduction of oxygen dissolved in the electrolyte or the discharging of the hydrogen ion [1].

Preparation and Description of Samples

Manufacturing of biodegradable bone implant samples can be described in the following steps: The first step is to prepare the material for sintering and the next step is sintering. In the first step, one of the batches is prepared by mixing the powdered metal material with the organic polymer carrier that forms the basic structure. The mixture is poured into a mold, the solvent is evaporated and dried. The carrier polymer is then removed by annealing. Another batch uses polyurethane (PUR) foam that is soaked into the mixture of powdered metals and demineralized water. Drying is applied to remove all water and annealing is used to remove the polymer matrix carrier. The second step is sintering using a defined temperature and time. The temperature of 450 degrees Celsius is maintained for 2 hours. The temperature is then increased to 1120 degrees Celsius and maintained for one hour. This is done in a protective non-corrosive atmosphere of nitrogen or argon. The resulting material from both batches is hard and free of any polymer matrix carrier and is ready for examination and exposure to a corrosive environment. The samples were subjected to two different corrosion solutions. The first solution is sodium chloride and water, the second is simulated body liquid (SBL). Samples number 3 and 15 were soaked in salt solution and samples 4 and 14 were exposed to simulated body liquid (SBL). Samples 14 and 15 were made by soaking polyurethane foam in a mixture of powdered metal

and water. The organic polymer matrix carrier method was used for samples number 3 and 4. The samples are made of pure iron powder.

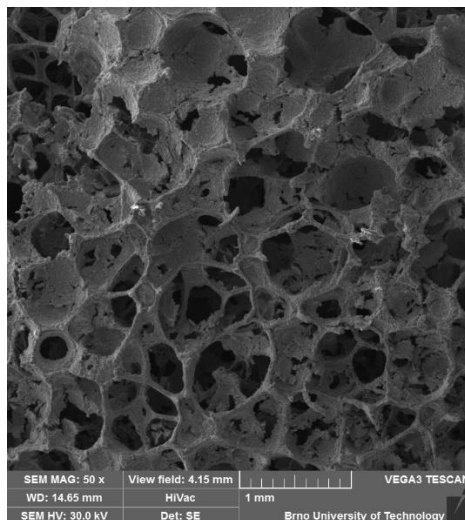


Figure 1. Environmental scanning electron microscope image of internal structure of sample prepared by PUR method [2]

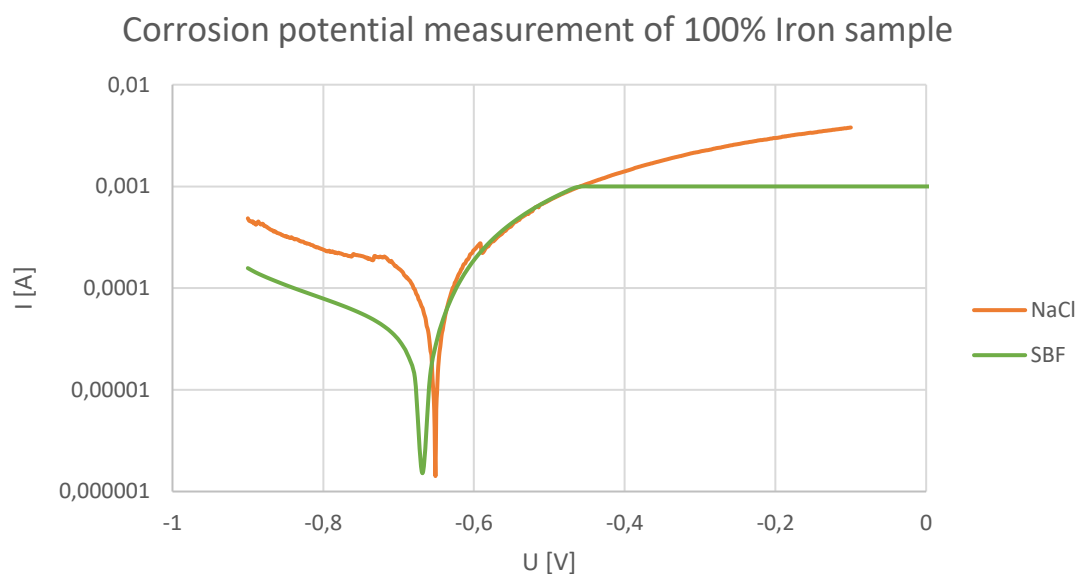


Figure 2. Difference in corrosion potential of 100 % iron sample in NaCl and SBF [3]

The device which was used for measuring corrosion potential was potentiostat α AUTOLAB mode, type II.

Table 1. Changes of corrosion conductivity of the samples

Sample	Solution	Matrix	γ [mS/cm]			
3	NaCl	PS	34.35	34.89	37.50	39.42
4	SBL	PS	44.57	48.40	49.47	49.85
14	SBL	PUR	42.03	45.02	53.43	54.73
15	NaCl	PUR	33.77	37.67	38.88	36.89
Number of days			32	61	88	119

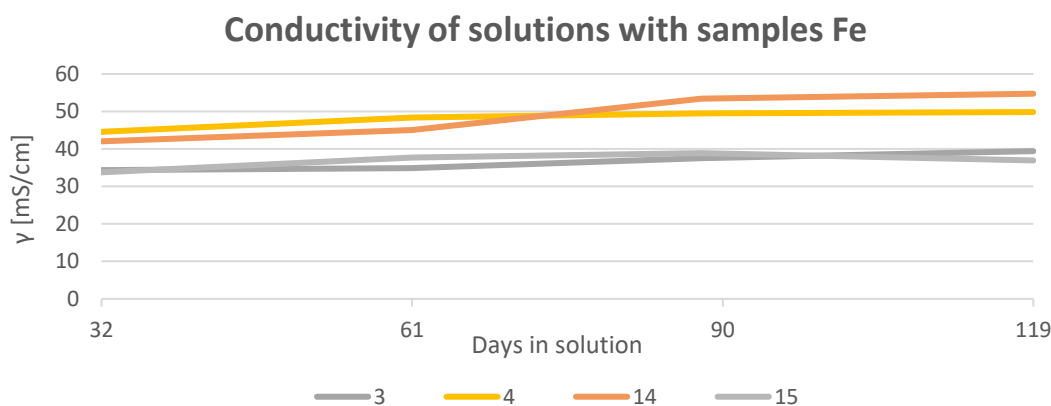


Figure 3. Difference in conductivity of solution with samples Fe

Conclusion

Four samples of pure iron biodegradable bone implants produced by the two methods described above (one method using PUR sponge as a matrix carrier and the other method using a polymer-solvent as a matrix carrier) were subjected to long-term immersion in two different corrosion solutions (sodium chloride dissolved in water and SBL solution). The conductivity of the soaking solutions was periodically measured. Samples 4 and 14 soaked in SBL showed a lower (more negative) corrosion potential than samples 3 and 15 soaked in sodium chloride solution. The subsequently measured corrosion potentials (day 61, 88 and 119) in SBL were higher than in NaCl solution. Samples exposed to NaCl solution did not show significant change and the values fluctuated around the initial value. The sample produced by the PUR method in SBL solution showed a lower corrosion potential than the sample produced by the polymer-solvent method. Samples made by different manufacturing methods soaked in NaCl solution did not show significant difference in corrosion potential. This is due to chloride ions disrupting the forming of the passivation layer; new material is exposed and corrosion continues. On the other hand, the SBL solution showed more variance, a lower corrosion potential at the beginning (PUR sample) and the polymer-solvent sample a higher potential. The difference persisted the whole time. The PUR sample was more porous, the larger surface area made the passivation layer more permeable and the corrosion rate was high. The polymer-solvent sample was less porous and the passivation layer protected the fresh metal from further corrosion, so the corrosion potential was higher. The presence of phosphorus ions in the SBL helped to form a stable passivation layer.

References

1. DOLEŽELOVÁ, Eva. Determination of the corrosion potential of powdered materials, Second laboratory task. Brno, 2022 [cit. 2022-07-11]. Vysoké učení technické v Brně, Fakulta elektrotechniky a komunikačních technologií, Ústav elektrotechnologie.
2. TKÁČOVÁ, Tereza. *Biodegradabilní kostní implantáty na bázi železa* [online]. Brno, 2020 [cit. 2020-06-02]. Dostupné z: <https://www.vutbr.cz/studenti/zav-prace/detail/127492>. Diplomová práce. Vysoké učení technické v Brně, Fakulta elektrotechniky a komunikačních technologií, Ústav elektrotechnologie. Vedoucí práce Marie Sedlářková.
3. GALANOVÁ, Z. Biodegradable bone implants. Brno: Vysoké učení technické v Brně, Fakulta elektrotechniky a komunikačních technologií. Ústav elektrotechnologie, 2017. 102 s., 4 s. příloh. Diplomová práce. Vedoucí práce: doc. Ing. Marie Sedlářková, CSc.

Nanostructured Innovative Carbon-Based Materials Modify Electrodes and Dramatically Improve the Efficiency of Thin, Flexible Lithium Batteries

Y. Pustovalov^a, E. Shembel^{b,c}, D. Kaszuba^a, V. Redko^b, T. Pastushkin^b, N. Zaderey^c,
A. Markevich^c, Yu. Polishchuk^c, I. Sagirov^a

^a INT sp z o.o., Ul Pilsudskiego 17/4, 34-074 Rztyszów, Polska

^b Enerize Corporation, Coral Springs, FL, 33067, USA

^c Scientific Research Laboratory of Chemical Power Sources of Ukrainian State University of Chemical Technology, Dnipro, 49005, Ukraine

The developed innovative carbon-based nanostructured materials have high electronic conductivity, have magnetic properties, could be pressed without a binder, have a low density, effectively modify electrodes and affect the mechanism of redox electrochemical processes, increase the energy, power and stability of the parameters of thin flexible lithium batteries.

Introduction

Carbon nanomaterials are at the forefront of the emerging technologies of the third millennium and represent a vast area of required knowledge for the design of tomorrow's devices. Innovative carbon nanomaterials are being developed by INT sp. z o.o. Poland on the basis of many years of research by its employees of similar materials for various applications, including those used in the field of high-energy current sources, in order to increase the energy, power stable parameters of Li-batteries [1], in the field of polymer materials [2], for fuel catalysts elements [3], and also promising for Mg-ion, Li-S, lead and other batteries.

Thin flexible battery market will grow from US\$98 million in 2020 to US\$296 million by 2025. This means that the market will grow by an average of 24.7% per year from 2020 to 2025. [4,5]. These abstracts are devoted to the project of INT Sp z o.o., the purpose of which is to develop a technology for manufacturing thin flexible high-energy lithium-ion current sources based on nanostructured carbon materials. In the current source being developed, the anode is based on thin-layer graphite plates, the cathode is based on lithiated metal oxides, which is deposited on a thin-layer of nanostructure carbon materials plate.

Structural Characteristics of Nanostructured Carbon Materials for Modification of Electrodes of Lithium – Ion Batteries

The parameters of the structure the nanomaterials affect the micro- and macrostructural characteristics of the modified electrodes, increase the efficiency of current distribution over the volume of the electrodes, and increase the energy and power of the lithium batteries

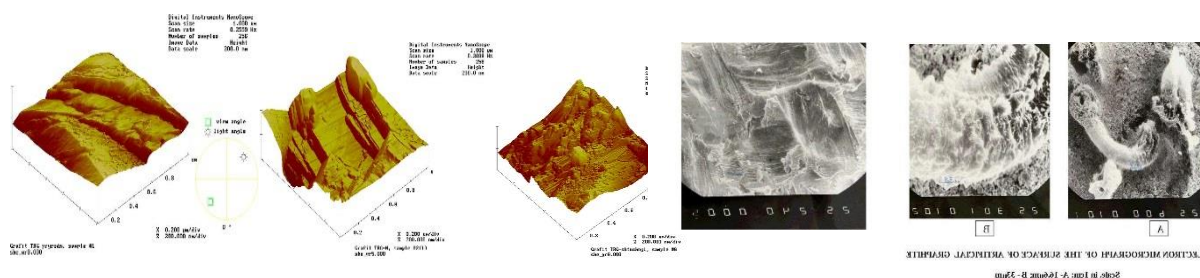


Figure 1. AFM and ESM structural characteristics of nanostructured carbon materials, which are synthesized by various methods.

Electronic Conductivity of Nanostructured Carbon Powders as a Function of Magnetic Field Frequency and Powder Density

The data presented in Fig. 2 and 3 illustrate the dependence of the conductivity of graphite powders on their density and magnetic field frequency. Two types of powders of graphite are presented

- synthesized nanostructured graphite and
- natural graphite, which is widely used in Li-ion batteries.

The numbers on the curves show the magnetic field frequencies at which the measurements were made. The conductivity of carbon powders over a wide range of magnetic field frequencies was measured by an innovative non-contact, non-destructive electromagnetic method developed by Enerize Corporation. [7, 8, 9, 10]

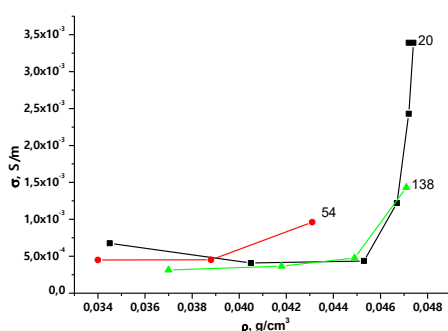


Figure 2

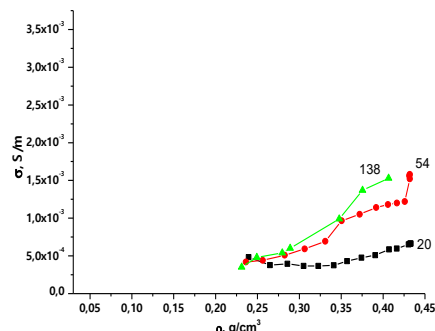


Figure 3

Figure 4

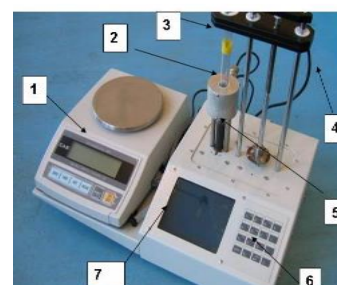


Figure 2. Results of testing innovative nanostructured carbon powders

Figure 3. Results of testing graphite, which is widely used for cathodes and anodes of Li-ion batteries.

Figure 4. Device for non-destructive non-contact electromagnetic test of the electrical conductivity of powdered materials. Description of the front side of the device: 1. Electronic scales; 2 Removable resonator chamber; 3. Glass containers; 4. Optical-mechanical device for measuring volume of powder; 5- Radial vibro seal; 6. Keyboard for control and data entry; 7. Graphic display

The data, which presented, illustrate the high electronic conductivity and low density of the synthesized innovative nanostructured carbon materials compared to the carbon material commonly used in Li-ion batteries. An important factor is that the conductivity of the synthesized nanomaterials depends on the frequency of the magnetic field. These parameters affect the mechanisms of

electrochemical redox reactions of modified anodes and cathodes. The low density of the nanostructured carbon powders ensures its uniform distribution in the volume of the electrode mass

Li-ion batteries, which anodes and cathode are modified with nanostructured carbon powders, have low impedance parameters, high reversibility of discharge and charging processes, stability of characteristics during numerous charge-discharge cycles, and high energy in a wide range of currents and temperatures.

During the 23ST International Conference ABAF 23 and in a publication in the Journal of Physics: Conference Series we will present the results of a study of the influence of structural characteristics, electrical conductive and magnetic properties of innovative nanostructured carbon materials on the parameters of Li-ion batteries.

References

1. J. Gómez, M. V. Sulleiro, D. Mantione. and N. Alegret. *A State of the Art. Polymers (Basel)*. 2021 Mar; 13(5): 745.
2. S.G. Peera, R. Koutavarapu, S. Akula. *A Review. Energy Fuels* 2021, 35, 15, 11761–11799. Publication Date: July 20, 2021
3. <https://thebatteries.tech/product/>
4. <https://www.marketsandmarkets.com/Market-Reports/flexible-battery-market-190884508.html>
5. Y. Pustovalov, E. Shembel, V. Redko, T. Pastushkin, etc. *PS Global. Word Science*. №2 (42) VoI.1. February 2019.
6. V. Redko, E. Shembel, T. Pastushkin, etc. *Method and Device for Rapid Non - Destructive Quality Control of Powdered Materials*. US Patent No. 8,102,181
7. V. Redko, E. Shembel E., etc. *Method and Apparatus for Measuring Conductivity of Powder Materials Using Eddy Currents*. US Patent No. 7,288,941
8. Y. Pustovalov, E. Shembel, L. Vishnyakov, etc. *Carbon material for electrodes of lithium-ion power sources and method of production thereof*. US Patent application No. 10/898631
9. V.Redko, E. Shembel, etc. *Methods and Systems for Non-Destructive Determination of Fluorination of Carbon Powders*. US Patent application No. 10/898631

Cobalt and Nickel Titanates as Effective Anode Materials for Lithium-Ion and Sodium-Ion Batteries

Yu. V. Shmatok^a, N. I. Globa^a, T. V. Lisnycha^a, S. A. Kirillov^a

^a Joint Department of Electrochemical Energy Systems,
38A Vernadsky Ave., Kyiv 03680, Ukraine

Compounds with a perovskite structure are considered as promise anode materials for lithium-ion and sodium-ion batteries [1, 2]. This is due to their excellent chemical stability and high theoretical specific capacity of 500 mAh/g. This work is focused on the synthesis, physico-chemical and electrochemical investigation of CoTiO₃ and NiTiO₃ bimetallic oxides with the perovskite structure.

Equimolar oxide mixtures of TiO₂-CoO and TiO₂-NiO were synthesized by co-precipitation from solutions of titanium chloride (TiCl₄) and nitrate salts of cobalt or nickel. A solution of lithium hydroxide (LiOH) as a source of template ions was used. The resulting oxide mixtures were thermally treated at temperatures of 400-800 °C for obtaining perovskite-type compounds. Phase transitions and physico-chemical characteristics of oxides obtained were determined by the thermogravimetric analysis (TGA), X-ray diffraction (XRD), scanning electron microscopy and porosimetry methods.

Based on the thermograms, it was established that the main mass losses occur in the temperature range of 120-250 °C and are related to water removal. The complete transition of precipitated TiO₂-CoO and TiO₂-NiO oxides into compounds with the perovskite structure occurs in the temperature range of 600-700 °C, which corresponds to small exothermic peaks. The results of TGA correlate well with XRD data, which show that the crystal structure of perovskite begins to form at the temperature of 500 °C. The raising of the annealing temperature to 600, 700 and 800°C leads to a significant increase in crystallinity and particle size of materials, as well as a significant decrease in specific surface area and porosity. Samples annealed at a temperature of 800°C are practically non-porous and have submicron particle size.

The specific and kinetic characteristics of CoTiO₃ and NiTiO₃ oxides in lithium and sodium cells have been determined by galvanostatic cycling and impedance spectroscopy methods. The oxides annealed at the temperatures of 600, 700 and 800 °C were taken for electrochemical tests. This made it possible to determine the optimal annealing temperature providing a high specific capacity and its stability during long-term cycling and discharge at high current densities.

The dependences of specific capacity on cycle number and discharge current density are shown in Figure 1 and 2 in lithium and sodium cells, respectively. It is shown that annealed at the temperature of 800 °C CoTiO₃ and NiTiO₃ samples have high specific capacity, better cyclability and rate capability both in lithium and sodium electrochemical cells. In lithium cells CoTiO₃ and NiTiO₃ demonstrate stable specific capacity of ~200 and ~150 mAh/g, respectively, at the cycling current density of 0.1 A/g and good capacity retention at the discharge currents up to 5 A/g. In sodium cells, the specific capacity of CoTiO₃ sample is lower being ~95 mAh/g at the same cycling current and the maximum discharge currents reach 1 A/g.

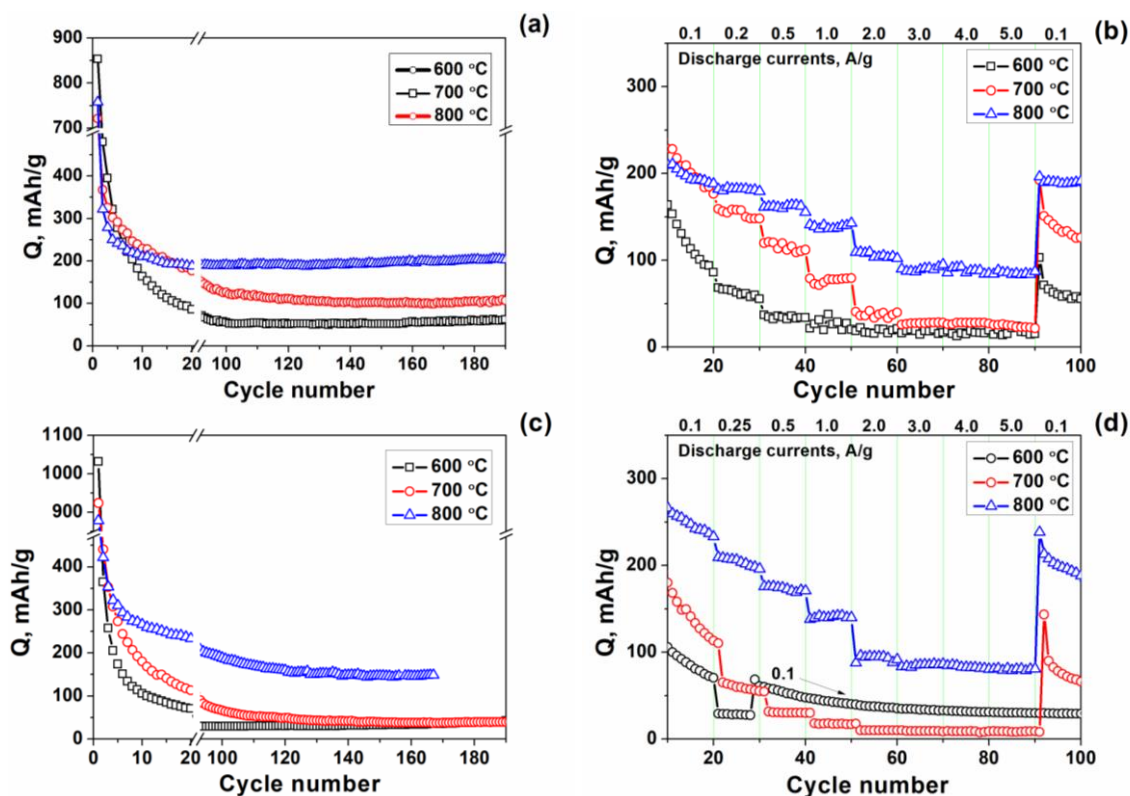


Figure 1. Cycling performance of CoTiO_3 (a, b) and NiTiO_3 (c, d) in lithium cells. (a, c) At constant cycling current density of 0.1 A/g. (b, d) At different discharge currents and constant charge current of 0.1 A/g. Electrolyte – 1M solution of LiTFSI in EC:DMC:FEC (4:5:1 volume ratio).

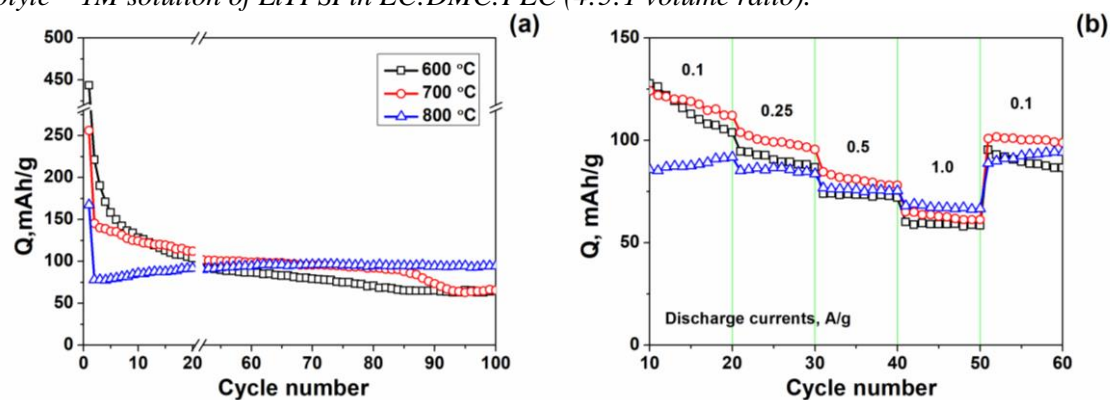


Figure 2. Cycling performance of CoTiO_3 in sodium cells (a) at constant cycling current density of 0.1 A/g and (b) at different discharge currents and constant charge current of 0.1 A/g. Electrolyte – 1M solution of NaClO_4 in EC:DMC:FEC (4:5:1 volume ratio).

References

1. J. Li, D. Wang, J. Zhou, L. Hou, F. Gao, *J. Alloys Compd.*, **793**, 247 (2019).
2. Z.-D. Huang, T.-T. Zhang, H. Lu, T. Masese, K. Yamamoto, R.-Q. Liu, X.-J. Lin, X.-M. Feng, X.-M. Liu, D. Wang, Y. Uchimoto, Y.-W. Ma, *Energy Storage Mater.*, **13**, 329 (2018).

Electrolytes modified with boron-based additives for high-voltage batteries

T. Syrový^a, L. Syrová^a, R. Jambor^b

^a Department of Graphic Arts and Photophysics, University of Pardubice, 533 53 Pardubice, Czech Republic

^b Department of General and Inorganic Chemistry, University of Pardubice, 532 10 Pardubice, Czech Republic

The presented study focuses on the improvement of battery performance by optimizing electrolytes by adding boron-based additives. Half-cells based on cathode (LMNO) and lithium anode were used as electrodes. The best performing cells showed a specific capacity of up to 137.1 mAh/g at a current load of 0.15 C and a gravimetric energy density of 610 Wh/kg calculated to the cathode.

Introduction

The wide range of LIBs powered applications and the continuously decreasing availability of raw materials create strong pressure to increase the energy density of batteries. From this perspective, in the case of LIBs, alongside the anodes, the focus is on cathode materials providing high energy density, such as $\text{LiNi}_x\text{Mn}_x\text{Co}_x\text{O}_2$ (NMC) allowing energy densities up to values of 550 Wh/kg [1]. Even higher energy densities with a theoretical range of up to 700 Wh/kg [2-3] are achieved by $\text{LiNi}_{0.5}\text{Mn}_{1.5}\text{O}_4$ (LMNO) or lithium cobalt phosphate (LCP) with 800 Wh/kg [4] and operating voltages > 4.8 V. LMNO is also attractive because of its well-developed flat discharge plateau, and the absence of Co is also valuable from a material point of view. However, there are also drawbacks such as the low stability of LMNO cells, which are mainly caused by electrolyte instability at high operating voltage and secondly by the dissolution of manganese ions from the structure of the electrode material. Therefore, in the context of solving the given problem, our study focuses on increasing the stability of electrolytes and LMNO-based cells using additives based on boron compounds, which could lead to higher electrolyte stability or forming protective SEI layer, also. The study presented here introduces newly synthesized boron compounds as additives to obtain high-voltage electrolytes that will increase the stability of LMNO cells.

Experimental

In the experiment, a half cell was prepared with a Li metal chip as the anode, and the cathode was LMNO-based with PVDF as the binder. A Timcal Super C45 was used as conductive additives for the LMNO electrode. The ratio of LMNO to PVDF in the ink formulation was set at ration 8:1. The electrode layers were first dried at 80 ° C and then at 120 ° C for 1 h. The electrode was cut by die (area 2 cm²), then encapsulated together with the lithium anode and the glass fiber separator in a CR2025 coin cell housing under an atmosphere of argon (Jacomex glove box). As electrolyte, 1.5 M LiPF_6 dissolved in carbonate solvents, or with additives (BOR0 – BOR8) at a amount of 2.5 mol % was used. Galvanostatic cycling was carried out in the range of 3.5 –4.9 V at a current load of 0.15 C to monitor cell degradation during galvanostatic cycling. Cyclic voltammetry and EIS analysis of cells was performed before and after galvanostatic cycling.

Results

Half cells consisting of an LMNO cathode and Li anodes were fabricated with six various electrolytes in CR2025 coin cell enclosures. From the galvanostatic measurements performed, the highest initial capacity was obtained for cells with BOR0-based electrolyte, where 137.1 mA.h/g was achieved for the seventh cycle at a current load of 0.15 C. From Figure 1B it is obvious that the highest retention of capacity delivered cells with electrolyte based on BOR2. It is clear from the data that cells with various electrolytes differed in the initial cycles, in terms of coulombic efficiency (Figure 1C), energy efficiency (Figure 1D), etc. The low coulombic efficiency at initial cycles could be caused by formation processes within the cells.

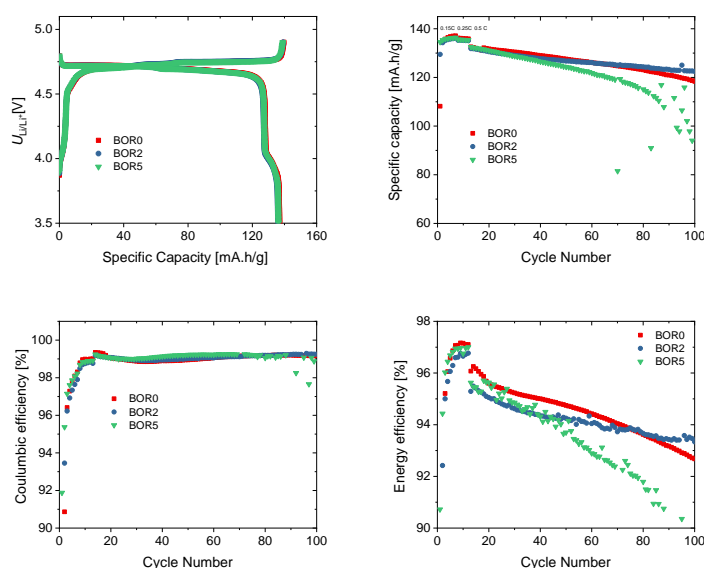


Figure 1 (A) Charging/discharging curves for initial cycle for cells with LMNO cathode and Li anode and electrolytes modified by boron based compounds, (B) Galvanostatic cycling of LMNO/Li cells at various C rates, (C) Coulombic efficiency for LMNO/Li cells at various C rates, (D) Energy efficiency for LMNO/Li cells at various C rates.

Conclusion

In the presented study, the investigation of influence of various boron-based compounds in electrolyte to the LMNO/Li half cell performance was performed. From various characteristics such as galvanostatic cycling stability, coulombic efficiency, energy efficiency, etc. It is obvious that the BOR2 additives allowed the best cells performance.

Acknowledgments

The financial support of the Technological Agency of the Czech Republic (TK04030083) and UPCE specific research programme (project No. VA390012) are gratefully acknowledged.

References

1. Zhao J., Kuai X., Dong X., Wang H., Zhao W., Gao L., Wang Y. A Huang R. Phase transitions and related electrochemical performances of Li-Rich layered cathode materials for high-energy lithium ion batteries. *Journal of Alloys and Compounds*. 2018, **732**(1), 385-395. doi:10.1016/j.jallcom.2017.10.179
2. Kazda T., Vondrák J., Di Noto V., Sedlaříková M., Čudek P., Omelka L., Šafaříková L., Kašpárek V. Study of electrochemical properties and thermal stability of the high-voltage spinel cathode material for lithium-ion accumulators. *Journal of Solid State Electrochemistry*. 2015, **19**(6), 1579-1590. doi:10.1007/s10008-015-2772-4
3. Amin R., Muralidharan N., Petla Ramesh K., Yahia H. B., Al-Hail S. A. J., Essehli R., Daniel C., Khaleel M. A., Belharouak I., Research advances on cobalt-free cathodes for Li-ion batteries - The high voltage LiMn_{1.5}Ni_{0.5}O₄ as an example, *Journal of Power Sources*, 2020, 467, doi: 10.1016/j.jpowsour.2020.228318.
4. Ludwig J., Nilges T., Recent progress and developments in lithium cobalt phosphate chemistry- Syntheses, polymorphism and properties, *Journal of Power Sources*, 2018, 382, 101-115, doi: 10.1016/j.jpowsour.2018.02.038

How can pressure help in EV

M. Šedina^a and T. Kazda^a

^a Department of Electrotechnology, Brno university of technology, Brno 61600, Czech Republic

This article briefly describes the prediction of its market growth and the drivers of change. There is mention of how a battery in the electric vehicle works and which parts are included in it. The last part is focused on research on how external force affects batteries.

Introduction

There were many types of vehicles, which served as personal transportation in history. The last type of these vehicle is a car which was powered by an engine. It started with steam-powered cars, thru electric cars powered by lead-acid batteries to cars powered by internal combustion engines (ICE). ICEs are a major powertrain since the 20s of the 20th century. [1] At the end of the last century, governments started pushing environmental rules for the car industry which should make road transportation more environmentally friendly. In Europe, it is a EURO emission standard. The actual version is EURO 6d-ISC-FCM, which came into power in 2021. [2]

Electromobility

Modern electromobility starts as an easier way how to achieve flotilla emissions, which are set by the European Union. Development in the field of electric vehicles (EVs) started to speed up and now is clear that EVs will be one of the most used types of cars on the market. It is possible to see this from the prediction of car sales in Figure 1. This prediction will probably change with the banning of sales of new ICEs in 2035.

Expansion of the EVs speeds up the research in many sectors of industry to achieve better user comfort with the usage of EVs. Most of the research is focused on the battery and its charging. The goals are faster charging, greater range, cheaper battery, safer chemistry, etc.

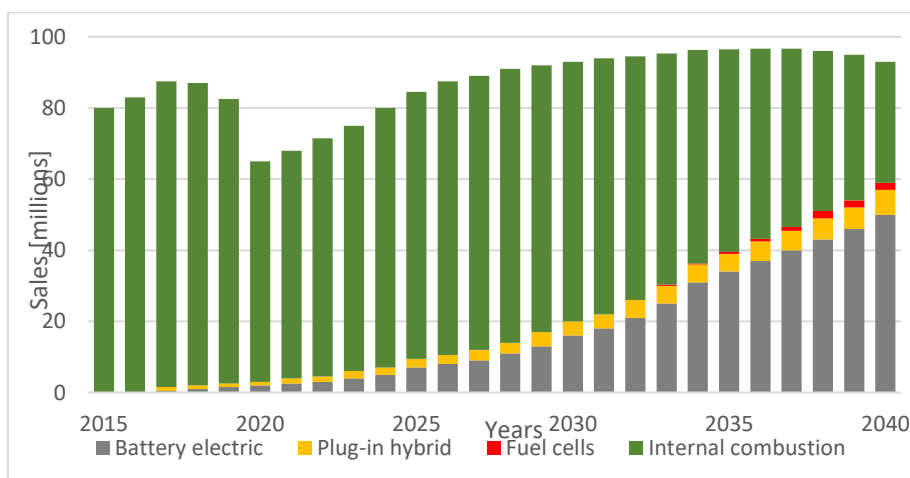


Figure 1. Global annual passenger vehicle sales by drivetrain [3]

EV battery

The battery pack of an electric car is made up of different elements including a control unit, fuses, a battery management system (BMS), and several battery modules. The pack is designed to maximize space usage and to fit as many batteries as possible. The pack is placed under the floor of the driver's compartment, which strengthens the entire vehicle. One of the parameters that determine the maturity of the manufacturer is the gravimetric capacity of the whole pack. Battery modules contain individual battery cells and may contain cooling and heating elements, temperature sensors, or secondary control. **Figure 2.** Battery module Audi e-tron [4]Figure 2 illustrates a battery module with pouch cells. [3]

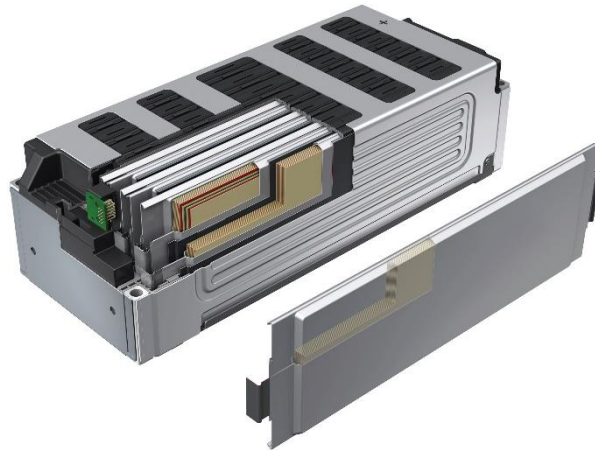


Figure 2. Battery module Audi e-tron [4]

Nowadays EVs are using Li-ion batteries with liquid electrolytes and a graphite anode. There is a trend to use silicone/graphite composite in the anode and improve its capacity. Another trend is the development of the solid-state electrolyte, solid electrolytes are safer than liquid ones because they don't include organic solvents. Both trends relate to great volume changes of the battery. And these volume changes could have some effect on the condition of the battery inside the module because there could be some pressure effect on the battery cell. [5][6]

Measure battery under external mechanic load

My research is focused on measuring batteries under constant mechanical load. The goal of the research is to find how external load affects the battery or how can this load improve battery parameters. For this experiment are used batteries from EV Škoda Enyaq. It is an LG Chem E78 battery with a capacity of 78 Ah and it is a pouch cell.

For the moderating force is used clamp with eight springs with a maximal load of 50 kg on each spring (see Figure 3). In the experiment are used loads of 5, 10, and 20 kg were developed on each spring.

At this moment I am using four pouch cells, one is used for uncompressed measurement and one for each force. The battery is compressed during the cycling and measuring electrochemical impedance spectroscopy and then is uncompressed and run the parametric test.

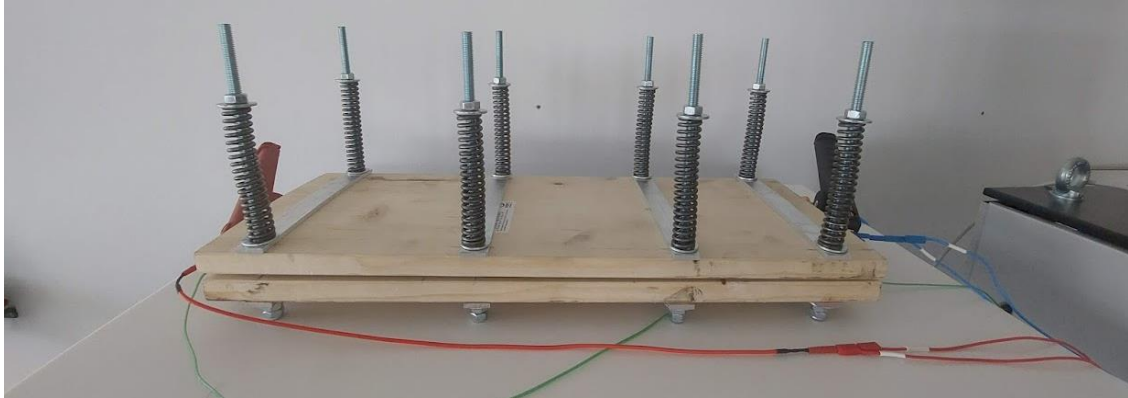


Figure 3. Battery during the measurement

Acknowledgments

This work was supported by the specific graduate research of the Brno University of Technology No. FEKT-S-20-6206. This work was supported by Škoda Auto a.s.

References

1. “Worth the Watt: A Brief History of the Electric Car, 1830 to Present”, *Car and Driver*, 02018.
2. *Nářízení Komise (EU) 2018/1832*, vol. 2018, no. 2018/1832. 2018.
3. *Intelligence in Mobile Battery Applications (D5.1 Desk Research & Data Analysis IMBA – Release 1)*. 2019.
4. “Audi e-tron quattro concept”, *Audi MediaCentral*, 02015.
5. W. Zhang et al., “(Electro)chemical expansion during cycling: monitoring the pressure changes in operating solid-state lithium batteries”, *Journal of Materials Chemistry A*, vol. 5, no. 20, pp. 9929-9936, 2017.
6. V. Müller et al., “Effects of Mechanical Compression on the Aging and the Expansion Behavior of Si/C-Composite/NMC811 in Different Lithium-Ion Battery Cell Formats”, *Journal of The Electrochemical Society*, vol. 166, no. 15, pp. A3796-A3805, Nov. 2019.

Multiscale 3D analysis of flat Lithium-Ion batteries by X-ray computed tomography

Z. Štubianová^a, O. Klvač^b, P. Guricová^b, T. Kazda^b, T. Zikmund^a, O. Čech^b and J. Kaiser^a

^a Central European Institute of Technology, Brno University of Technology, Brno, Czech Republic

^b Department of Electrical and Electronic Technology, Faculty of Electrical Engineering and Communication, BUT, Technická 10, 616 00 Brno, Czech Republic

X-ray computed tomography is a non-destructive 3D imaging technique allowing research on the whole cell level and microstructure level of the battery cell. This paper describes the advantages and challenges of using CT analysis for multiscale 3D analysis of various types of batteries. Subsequently, analyzed CT data of flat batteries are presented, and the next steps are proposed to analyze inner defects.

Introduction

Lithium-ion batteries (LIBs) are secondary power sources with high energy density, low self-discharge rate and long lifetime. Currently, two Li-ion cells are widely used - cylindrical and flat (pouch and prismatic). Although cylindrical cells have more outstanding durability, their shape cannot efficiently fill the available space due to their dimensions. Therefore, flat cells are increasingly finding their way into this application. [1] Battery research focuses on improving battery performance, higher energy density, and longer life; it can be complemented by techniques such as X-ray computed tomography (CT). CT analysis is a non-destructive technique allowing research at the whole cell level, measuring the thickness of the anode and cathode and the arrangement in the assembled cells. At the microstructure level, the electrode structure can be analyzed quantitatively (investigation of inhomogeneity of particle distribution, changes during cycling). [2]

When it comes to commercial cylindrical cells, CT analysis is used to describe the ageing mechanism. Common are, for example, deformation of the electrodes during cycling, delamination of the active material and subsequent loss of capacitance. For these purposes, a 20 μm /voxel resolution is sufficient. [3] For grain-level analysis, however, a higher resolution is needed. During the investigation of cylindrical cells at CEITEC BUT, a resolution of 8 μm was achieved. It was possible to analyze the defects and perform a correlative analysis, which confirmed the theory of "void spots" - manufacturing defects. [4] Currently, a similar resolution is not achieved for flat cells, which are typically disassembled during CT analysis. Smaller parts are examined or polished, and the section is imaged using SEM. [5] This work focuses on applying the existing methodology and achieving the needed resolution on flat cells while their non-symmetrical shape is challenging for CT analysis.

Materials and methods

The first sample analyzed is a commercial pouch-type cell KOKAM with a capacity of 4.8 Ah. The cathode is based on NMC ($\text{LiNi}_x\text{Mn}_y\text{Co}_z\text{O}_2$), and the anode is made of graphite. In the first phase of the research, an experiment was performed on a GE phoenix v|tome|x L240 CT system using a 240kV microfocus tube and circular trajectory. A resolution of 38 μm was achieved through

multiscan (the samples were scanned in halves and reconstructed). The resulting data can be seen in Fig. 1. Afterwards, the achieved resolution was 15 μm by scanning the section of the battery (Region of interest) with dimensions of 20 x 10 mm (Fig. 2).

Secondly, a commercial prismatic-type cell Cellevia battery L402025 was analyzed with a capacity of 0.15 Ah. Firstly the same procedure as for pouch-type cell KOKAM was applied to the selected region of interest (15 x 5 mm) with a resolution of 6 μm (Fig. 3). Subsequently, an overview battery scan was performed using HeliScan microCT (Thermofisher Scientific) with 140 kV tube voltage, 4.5 s exposure time, space-filling helical trajectory, and resolution of 15 μm (Fig. 4).

Experiment results

Fig. 1 shows achieved data with a resolution of 38 μm , and irregular alignment of cathode sheets can be seen. The anode layers always protrude above the edge of the cathode layers. For the assessment of the structure at the individual electrode/grain level (deposition of active material on the current collectors, its delamination and manufacturing defects), the achieved resolution of 38 μm is insufficient. Fig. 2 shows data with a resolution of 15 μm ; it is possible to distinguish collectors based on contrast; however, defects on the level of individual electrodes cannot be observed.

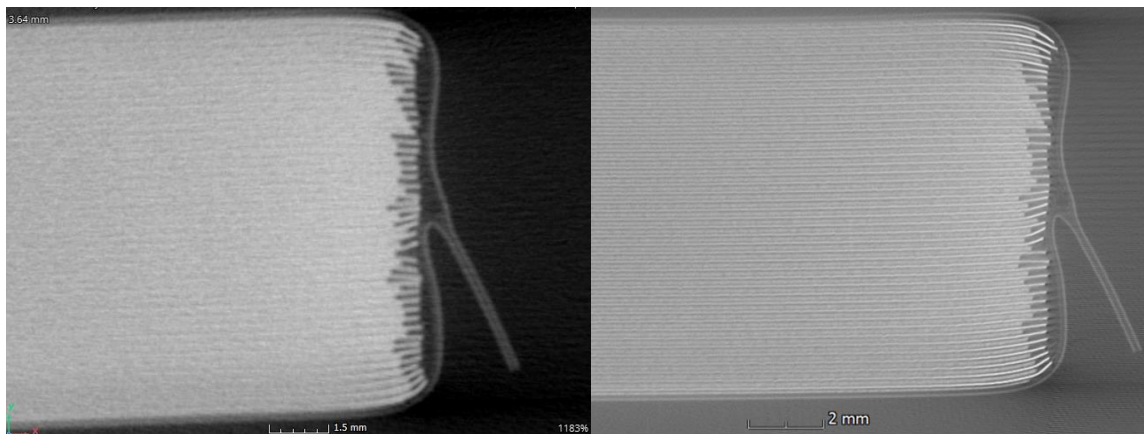


Figure 1. (left) KOKAM battery, 38 μm

Figure 2. (right) KOKAM battery, 15 μm

Fig. 3 presents the results of the second experiment resulting in a resolution of 6 μm . Current collectors are visible. Possible defects at the level of individual electrodes can be observed. Overview scan (Fig. 4) with the resolution of 15 μm of the sample enabled the detection of critical regions, which can be further scanned with higher resolution as presented in Fig. 3.

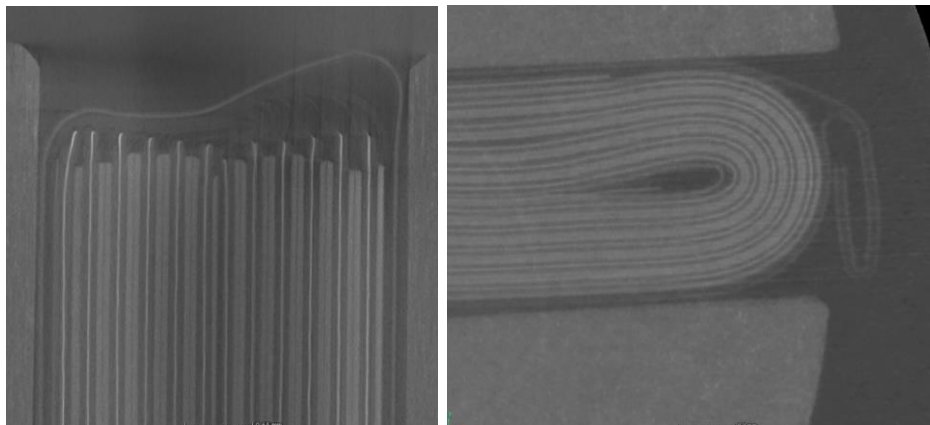


Figure 3. (left) Cellevia battery 6 μm

Figure 4. (right) Cellevia battery 15 μm

Conclusion

In the first research stage, we applied methodology for CT analysis of cylindrical cells on flat cells. We achieved desired resolution in which all components (electrodes, current collectors, separators) can be distinguished. We will continue with the cycling of Cellevia battery L402025 with 500 cycles. Afterwards, the battery will be scanned, and defects on the electrode levels will be analyzed.

Acknowledgments

This work was supported by the specific graduate research of the Brno University of Technology No CEITEC VUT/FEKT-J-22-7899 and FEKT-S-20-6206. The work was developed in cooperation with Thermo Fisher scientific Brno.

References

1. R. Xiong et al., Applied Energy, 279 (2020)
2. P. Pietsch and V. Wood, Annual Review of Materials Research, 47, 451-479 (2017)
3. T. Waldmann et al., Journal of The Electrochemical Society, 161, A1742-A1747 (2014)
4. P. Blažek et al., ECS Transactions, 105, 69-76 (2021)
5. Kovachev et al., Batteries, 5 (2019)

Ag₂S as an alternative electrode material for Li-ion batteries

D. Zalka^{a,b,c}, L. S. Shankar^c, R. Kun^c, W. Mamrilla^{d,b}, A. Straková Fedorková^a, and K. Saks^{l,b,e}

^a Faculty of Sciences, Pavol Jozef Šafárik University in Košice, Moyzesova 11, 04154, Košice, Slovak Republic

^b Slovak Academy of Sciences, Institute of Materials Research, Watsonova 47, 04001 Košice, Slovak Republic

^c Research Centre for Natural Sciences, Hungary, 1117, Budapest, Magyar Tudósok körútja, 2.

^d The Faculty of Mechanical Engineering at the Technical University of Košice, Letná 9, 042 00 Košice, Slovak Republic

^e The Faculty of Materials, Metallurgy and Recycling at the Technical University of Košice, Letná 9, 042 00 Košice, Slovak Republic

Li-ion batteries are a unique combination of high energy and power density which approves these electrochemical systems to be applied in portable electronic devices, power tools and hybrid/full electric vehicles. However, the maximum capacity of commercial Li-ion anode materials like graphite is 372 mAh·g⁻¹, for which this value is insufficient in order to meet with the increasing demand for higher electrochemical performance. In recent years, the application of Ag and S-based materials has created a new research area that aims to increase the capacity of Li-ion batteries. The theoretical capacity of an Ag₂S and Li₂S containing system is 1310 mAh·g⁻¹ which is several times higher capacity compared to that of the transition-metal oxides (positive electrode materials in Li-ion batteries).

Theoretical background

Silver sulfide, (Ag₂S) is a well-known inorganic compound because it used as a photosensitizer in the classical photography. Recently Ag₂S nanoparticles has received increasing attention, because they can be applied as e.g. ion selective electrodes [1], CO₂ reduction catalyst [2], photodetector [3], in different antibacterial applications [4,5]. However, it has been discovered not long ago that it is also possible to use silver sulfide in Li-ion batteries [6]. It can be assumed that the problems encountered when using sulfur as positive electrode (i.e. polysulfide shuttle) could be eliminated with the usage of Ag₂S.

On the basis of ex situ XRD measurements, the proposed electrochemical reaction mechanism during discharge of this type of battery is the following [6]:



It can be assumed that γ -Li₉Ag₄ phase also formed as intermediate-product, but this phase also turning to Ag in the final step of the discharge. During the charge the Li₂S progressively develops back to Ag₂S, of course some amount of Ag and S also remain back in this process.

It can be interesting how the doping agent like Se can influence this reaction, maybe with the suppression of polysulfide formation, elevate the electronic properties of the Ag_2S . For the best of our knowledge Se doped Ag_2S never have been applied in Li-ion batteries yet.

Experimental

The Ag_2S and $\text{Ag}_2\text{Se}_x\text{S}_{1-x}$ samples were prepared with a conventional solid synthesis route. The Ag, S (and Se in the case of doped samples) powders weighted on electronic scale with an accuracy of 10^{-4} g. Then the powders have been manually mixed in appropriate proportions, placed in a stainless-steel tube, and kept at 160°C for 10 hours under an argon atmosphere. The heating rate of the furnace has been set up to $5^\circ\text{C}/\text{min}$. After the samples had cooled back to room temperature, the resulted in powders have been grounded by an agate mortar and sieved with a $45\ \mu\text{m}$ mesh test sieve.

The Ag_2S or Se doped Ag_2S powders were mixed with Carbon Black and PVDF in 8:1:1 ratio. The mixture was homogenized in planetary ball mill (Fritsch planetary micromill pulverisette 7) for 45 minutes. After the milling, the powder was solved in N-Methyl-2-pyrrolidone (NMP), and the obtained slurry was spread to a copper foil with an automatic film applicator (BYK-Gardner 2105). The copper tape with the coating was room dried and later placed into a vacuum oven for 60°C for 24 h. Then 14 mm disks were cut out from the tape to obtain electrodes. CR2032 type button cells were assembled in a glovebox (MBraun) under an argon atmosphere. To ensure reproducibility of the experiments, the same volume of $150\ \mu\text{l}$ of electrolyte was introduced into the cell in each case. Metal lithium was used as the negative electrode (Lithium ribbon, thickness 0.75 mm, 99.9 % Sigma-Aldrich).

In order to study the milled samples scanning electron microscopy (SEM) was used. The SEM observations were done by Quanta 3D FEG dual beam SEM-FIB equipment at different magnifications. 20 kV accelerating voltage, $40\ \mu\text{m}$ aperture, $1\ \mu\text{s}$ acquisition time and 12 mm working distance was applied for the measurements. The beam current was 4 nA and 8 nA respectively.

Results and discussion

During the SEM examination of the samples, it was observed that not only the formation of silver outcrops takes place, but depending on the current density applied, these outcrops can be erased from the substrate surface, or more precisely, the silver protrusions can be retracted into the silver sulfide matrix.

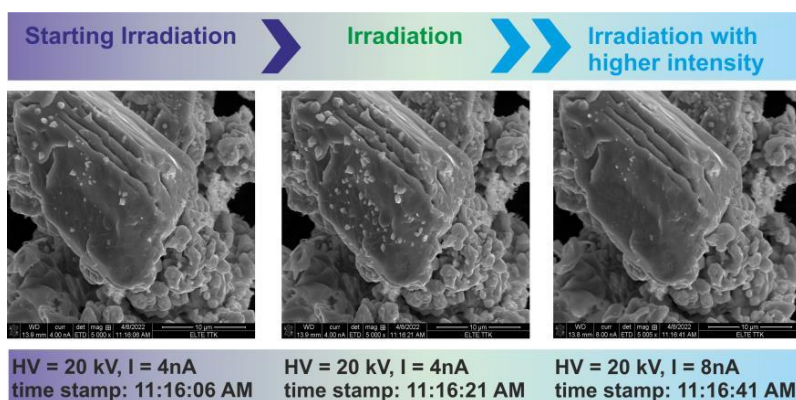


Figure 1. Formation and retraction of Ag particles on an Ag_2S crystal.

The nano-dots formation on silver sulfide surface using electron beam irradiation is a well-known phenomenon [7–9]. The rapid development of silver protrusions by irradiation was clearly observed on the silver sulfide crystals. By not changing the accelerator voltage, focusing, or working distance, and only increasing the current to 8 nA, the silver precipitates that developed under the influence of the current disappeared completely from the surface in 20 seconds (Figure 1). Samples containing Se as a doping component showed the same effect. The combined interaction of primary, back- and forward-scattered and secondary electrons generated by the SEM can displace silver ions and create silver atoms instead. However, by further increasing the intensity of the radiation, the silver can re-ionize into silver ions, and this explains why the metallic silver disappears. A more interesting problem is that this silver formation and re-ionization also occurs when the battery, which is made of this material, is charged and discharged. This, however, puts a huge volumetric stress on the electrode and is a possible explanation for the unstable electrochemical performance of this electrode material (doped samples also behave irreversibly).

Cyclic voltammetry measurements have been recorded at scanning rate of $0.1 \text{ mV}\cdot\text{s}^{-1}$ in a potential range of 0.0–2.5 V. In the case of Ag_2S electrode polysulfide formation can be observed during the first cycle. The double peak at 2.2 V can be observed only in the case of the Ag_2S electrode, while in the case of the doped samples it seems to be that the polysulfide formation is suppressed.

The initial capacity values for Ag_2S and Se-doped samples are shown in Table 1.

Table 1. Resulted in specific charge-discharge capacities of Ag_2S and Se-doped Ag_2S samples in different electrolytes.

	<i>Electrolyte</i>	Ag_2S	$\text{Ag}_2\text{Se}_{0.05}\text{S}_{0.95}$	$\text{Ag}_2\text{Se}_{0.1}\text{S}_{0.9}$	$\text{Ag}_2\text{Se}_{0.2}\text{S}_{0.8}$	$\text{Ag}_2\text{Se}_{0.3}\text{S}_{0.7}$	$\text{Ag}_2\text{Se}_{0.4}\text{S}_{0.6}$
QDCH (mAh g ⁻¹) ¹⁾	1 M LiPF ₆ in EC/DEC	153.4	267.1	168.8	336.2	261.9	250.8
QCH (mAh g ⁻¹)	1 M LiPF ₆ in EC/DEC	285.6	130.5	130.7	195.8	293.7	124.1
QDCH (mAh g ⁻¹) ¹⁾	2:1 DME:DOL+ 0.7 M LiTFSi + 0.25 LiNO ₃	1120.5	-	-	-	790.7	-
QCH (mAh g ⁻¹)	2:1 DME:DOL+ 0.7 M LiTFSi + 0.25 LiNO ₃	903.8	-	-	-	784.5	-

The electrochemical stability of the system was not sufficient, the capacity decreased to more than 80% after 10 cycles. Therefore, this system can be used only as primary Li-ion battery (non-rechargeable).

References

1. V. Horváth, G. Horvai, Ion-Selective Electrodes| Solid-State, in: P. Worsfold, A. Townshend, C. Poole (Eds.), *Encycl. Anal. Sci.* (Second Ed., Second Edition, Elsevier, Oxford, 2005: pp. 502–508.
2. L. Zeng, J. Shi, J. Luo, H. Chen, Silver sulfide anchored on reduced graphene oxide as a high-performance catalyst for CO₂ electroreduction, *J. Power Sources.* 398 (2018) 83–90.
3. H. Roshan, F. Ravanan, M.H. Sheikhi, A. Mirzaei, High-detectivity near-infrared photodetector based on Ag_2S nanocrystals, *J. Alloys Compd.* 852 (2021) 156948.
4. A.M. Awwad, N.M. Salem, M.M. Aqarbeh, F.M. Abdulaziz, Green synthesis, characterization of silver sulfide nanoparticles and antibacterial activity evaluation, *Chem. Int.* 6 (2020) 42–48.

5. Y. Delgado-Beleño, C.E. Martínez-Nuñez, M. Cortez-Valadez, N.S. Flores-López, M. Flores-Acosta, Optical properties of silver, silver sulfide and silver selenide nanoparticles and antibacterial applications, *Mater. Res. Bull.* 99 (2018) 385–392.
6. Y. Hwa, C.M. Park, H.J. Sohn, The electrochemical characteristics of Ag₂S and its nanocomposite anodes for Li-ion batteries, *J. Electroanal. Chem.* 667 (2012) 24–29.
7. H. Sone, T. Tamura, K. Miyazaki, S. Hosaka, Nano-dots formation on silver sulphide surface using electron beam irradiation, *Microelectron. Eng.* 83 (2006) 1487–1490.
8. S. V. Rempel, Y. V. Kuznetsova, E.Y. Gerasimov, A.A. Rempel', The irradiation influence on the properties of silver sulfide (Ag₂S) colloidal nanoparticles, *Phys. Solid State.* 59 (2017) 1629–1636.
9. L. Motte, J. Urban, Silver clusters on silver sulfide nanocrystals: Synthesis and behavior after electron beam irradiation, *J. Phys. Chem. B.* 109 (2005) 21499–21501.

The Mullite Nanofibers for Electrotechnical Applications

J. Kočí^a, M. Míka Havlík^a, N. Klusoňová^a

^a Department of Glass and Ceramics, University of Chemistry and Technology Prague, Technická 5, 166 28, Prague

Our research is focused on the development and modification of inorganic refractory nanofibers for advanced applications, made from the most available ceramic raw materials (Al_2O_3 and SiO_2) in the right proportions for crystallization of Mullite, commonly used high-temperature material. The intention is to create a modifiable refractory material for use in electrotechnical applications as electrodes, separators or a solid electrolyte in a new type of safe solid-state batteries. For these reasons, the nanofibers are modified with different conductive materials, for example different types of spinels. Spinel with the formula AB_2O_4 , specifically CuCr_2O_4 , have been studied due to their significant electrical and magnetic properties, that are suitable for their intended purposes.

Composite modifiable nanofibers

The development and modification of inorganic refractory nanofibers for advanced applications is highly desirable at a time of growing economic and environmental demands. The intention is to create a modifiable material for use in electrotechnical applications as electrodes, separators or solid electrolyte for the new types of safe solid-state batteries and many other applications. The most studied system are composite nanofibers made from the most available ceramic raw materials (Al_2O_3 and SiO_2) in the right proportions for crystallization of Mullite, commonly used high-temperature material (1).

Mullite nanofibers

The presented work is focused on the preparation of Mullite nanofibers from Boehmite (AlOOH) nanoparticles, tetraethyl orthosilicate (TEOS) with a silica component and PVP polymer, which together with colloidal TEOS form fibrous templates for different types of nanoparticles. The high-voltage electrospinning method was successfully used to produce mullite nanofibers with a diameter in the range of hundreds of nanometers by the sol-gel technique. Mullite is one of the best and cheapest thermal insulation materials, e.g., in industrial, due to its refractory properties, high melting point (1840 °C) and economic availability. Nanofibers created from mullite have constant properties even above 1000 °C (2).

New possibilities of filling organic templates with inorganic nanoparticles and sintering into a fibrous structure are not yet as effective as older and more expensive methods, but they give the possibility to produce nanofibers from any material that can be grind to the required small fractions. One of the main modifiers are different types of spinels, due to their extraordinary properties.

Crystalline spinels

One of the main modifiers are different types of spinels, due to their extraordinary properties. Spinel with the formula AB_2O_4 and their various properties have taken significant roles in many applications such as electronics, laser and sensors. The structure of $CuCr_2O_4$ is normal spinel structure where Cu occupies the centers of tetrahedrally coordinated positions, Cr occupies the centers of octahedrally coordinated positions, and the anion sits at the polyhedral vertexes. Due to their magnetic and electrical properties, $CuCr_2O_4$ spinels show potential as suitable materials for the intended applications in batteries (conduction and storage of electrical energy) (3).

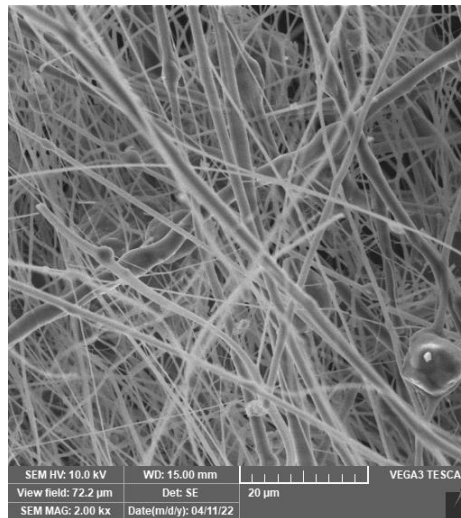


Figure 1. SEM image of ultra-thin nanofibers, where mullite crystallizes from precursors.

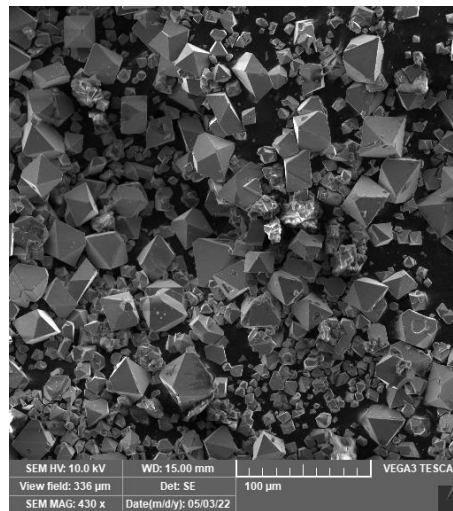


Figure 2. SEM image of spinels crystallized in molten glass with the correct composition.

References

1. G.L. Lecomte-Nana and A. Hammas, *Mullite: Structure and Properties*, M. Pomeroy, Editor, Encyclopedia of Materials: Technical Ceramics and Glasses, Elsevier: Oxford (2021)
2. Takei, T., et al., *Crystallization Kinetics of Mullite in Alumina–Silica Glass Fibers*. Journal of the American Ceramic Society (1999)
3. M. Míka and P. Hrna, *Rheology of spinel sludge in molten glass*. Ceramics - Silikáty. **44** (1999)

Analysis of Li-ion battery degradation mechanism by EIS, GITT and ICA and their possible utilization for SOH monitoring

M. Mikolášek^a, M. Kemény^a, and P. Ondrejka^a

^aInstitute of Electronics and Photonics, Slovak University of Technology, Ilkovičova 3, 812 19 Bratislava, Slovakia, email: miroslav.mikolasek@stuba.sk

The aim of this paper is to introduce the electrical characterization techniques EIS, GITT, and ICA as powerful non-destructive tools for the investigation of degradation mechanisms in Lithium-ion batteries. For this purpose, NCA-based batteries Panasonic NCA18650B were degraded by various stress conditions including High-Current, Over-Charging, and Under-Charging. The possible utilization of ICA peaks monitoring is proposed for advanced battery management focused on the accurate monitoring of the battery SOH.

Introduction

Li-ion batteries are attracting strong attention due to the increasing number of their application, such as electromobility, consumer electronics and stationary storage systems. The capacity and lifetime are strongly determined by the condition under which the battery operates [1]. The understanding of the degradation mechanism allows to focus the battery management systems on a weak part of the battery and adjust the operating conditions to prolong the battery's lifetime. For this purpose, new diagnostic approaches with the ability to analyze these degradation mechanisms are demanded [2]. The aim of this paper is to utilize advanced electrical characterization techniques, electrochemical impedance spectroscopy (EIS), galvanostatic intermittent titration technique (GITT) and incremental capacitance analysis (ICA) for characterization and identification of degradation mechanisms in Li-ion batteries. The possibility for utilization of these analysis tools for State-of-health (SOH) monitoring is discussed.

Experimental set-up

All experiments were carried out on cylindrical Li-ion battery NCR18650B (LiNiCoAlO₂ cathode and a graphite anode) from Panasonic, which is popular for electromobility applications. The capacity of the battery is 3400 mAh, the recommended charge rate is 0.5C (1.625 A), maximum allowed C-rate is 0.7C (2.38 A). The Maximum and minimum voltages of the battery are 4.2 V and 2.5 V, respectively. All electrical characterizations were carried out by Gamry Interface 5000P potentiostat/galvanostat. Three different scenarios of cyclic degradation were studied, specifically High-Current (1C current rate), Over-Charge (charge to 4.3V), and Under-Charge (discharge to 2.3V) cycling. The results were compared with the Reference cycling conditions with the maximum allowed charging-discharging parameters for the studied battery. GITT and ICA analysis is provided by 0.1C rate. The provided results are plotted as a function of the state of the charge (SOC) or voltage.

Results and discussion

Figure 1 shows the battery degradation for different stress conditions. Strong capacity fading is observed for High-Current and Over-Charge cycling. Due to the limited space, only selected results for High-Current scenario are shown in this abstract.

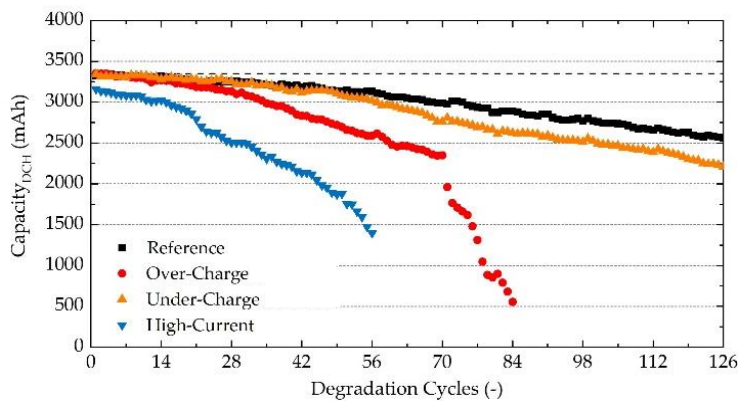


Figure 1. Discharge capacity of the studied NCA18650B batteries for an increasing number of degradation cycles under different stress scenario.

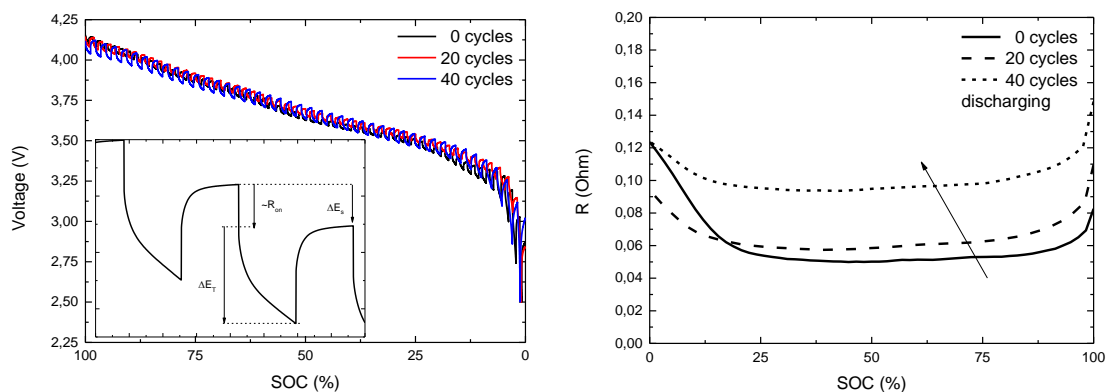


Figure 2. GITT curves taken during High-Current cycling before degradation and after 20 and 40 cycles and extracted battery internal resistance, R as a function of SOC.

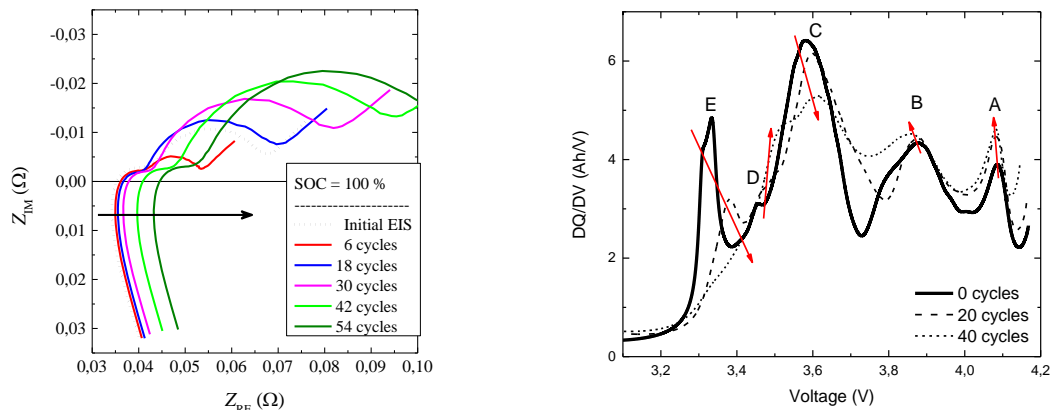


Figure 3. EIS at 100% SOC and ICA curves for different degradation rates under High-Current cycling.

Figure 2 revealed a strong increase of internal resistance, R upon the cycling degradation, which results in increased power fading and increased thermal losses in the battery. The internal resistance change is one of the main indicators of the battery SOH. However, R needs to be correlated with the battery SOC to achieve good SOH reliability. The reliability of SOH will be thus strongly connected with reliable determined SOC. The increase of the battery serial and dynamic resistance upon the degradation is observed also in EIS data presented in Figure 3 (left). Detailed analysis of these data will be shown elsewhere [3].

Figure 3 (right) shows ICA calculated as a function of voltage under different degradation rates during High-Current cycling. The ICA analysis revealed the presence of 5 peaks labeled by the letters A-E. These peaks are associated with active material phase transformations at the cathode and anode sides of the battery. The change of ICA peak position or magnitude during the cycling degradation can indicate the dominant degradation mechanism responsible for the capacity fade of the battery. By considering the detailed ICA study and simulation presented in [4], the observed pattern of low magnitude changes of the A and B peaks and higher shifts for D and G peaks suggest a dominant degradation mechanism at the cathode side of the battery.

While the ICA peaks follow the specific phase transformation of the active material in the battery, their position can be used as SOC indicator. Under such an assumption, the shift between ICA peaks upon the degradation can provide information about the SOH. The main advantage of such an approach is, that SOH can be determined without the knowledge of SOC. The possible utilization of ICA for SOH determination will be discussed in detail in the forthcoming publication.

Acknowledgments

This work was supported by Grants VEGA 1/0529/20 supported by the Ministry of Education, Science, Research and Sport of Slovakia and by the Slovak Research, and Development Agency under contract APVV-20-0111.

References

1. Birkl .R., et al., *Journal of Power Sources*, 341, 373-386, (2017)
2. Hu X., et al., *Joule*, 4(2), 310-346, (2020)
3. Kemeny M., Ondrejka P., Mikolasek M., *Batteries*, submitted
4. Devie A., et al., *Batteries*, 2(3), p.28, (2016)

Capacitor lifetime prolonged by addition of organic ammonium salt

G. Lota^{a,b}, S. Znaniecki^a, K. Szwabińska^a, J. Wojciechowski^a, M. Baraniak^a and A. Skrzypczak^a

^aInstitute of Chemistry and Technical Electrochemistry, Poznan University of Technology, Berdychowo 4, 60–965 Poznan, Poland

^bŁukasiewicz Research Network – Institute of Non-Ferrous Metals Division in Poznan, Central Laboratory of Batteries and Cells, Forteczna 12, 61-362 Poznan, Poland

It is well known that electrochemical corrosion negatively affects the functional properties of metal and steel materials that constitute a part of systems conducting an electric charge. On the other hand, corrosion is rarely associated with the degradation of chemical power sources and energy storage devices. This work is aimed to fill this gap by describing the effect demonstrated by a substituted ammonium salt with cyclohexyl substituent and 2,5-dihydroxybenzenesulfonate anion used as a corrosion inhibitor in symmetrical electrochemical capacitor system. The accelerated ageing test of capacitor systems has shown that the addition of substituted ammonium salt to capacitor electrolyte allows to extend the service lifetime of the entire system by inhibiting the corrosion of 316L stainless steel current collectors.

Introduction

An electrochemical capacitor (EC) as a type of capacitor is a device able to store electrical energy. Its working principle is based on the electric double layer phenomenon occurring in the electrode/electrolyte interphase. This phenomenon involves charge separation as charges of one sign are accumulated in an electrode material while the charges of the opposite sign concentrate in the electrolyte close to the interface, forming a layer of adsorbed ions. An electrochemical capacitor consists of two electrodes with an electrolyte-soaked separator placed in between. In such an arrangement, electric double layers are formed on both electrodes, although in both cases, their structures look slightly different as the electrodes have opposite polarities [1–4]. An additional component of an electrochemical capacitor, commonly used in the construction of commercial devices, is a metal or steel current collector. It can be considered as a part of an electrode, serving as a support for the electrode active mass to be deposited on. It also provides low-resistance electron transport from a capacitor active mass, through an active mass/current collector interphase, the collector itself, down to capacitor leads. In the case of stainless steel current collectors, the control of corrosion processes in the electrolyte environment becomes a crucial issue. As it has been shown so far by Znaniecki et al. [3] and Wojciechowski et al. [4], the corrosion of stainless steel current collectors can be correlated with such parameters of EC performance as its capacitance, maximum voltage, charge transfer resistance and lifetime (so the factors affecting the specific energy of the system). It should be noted, however, that the phenomenon of capacitor current collector corrosion and its influence on a device operation are still relatively poorly understood and described in the literature [5, 6].

Materials and methods

This work presents the results of the study on corrosion inhibition properties of substituted ammonium salts (SAS) with cyclohexyl substituents and 2,5-dihydroxybenzenesulfonic anion. The influence of 5 different SASs on the anti-corrosive properties of 316L stainless steel in the aqueous electrolyte solution (1 M Na₂SO₄) was estimated by means of electrochemical DC and AC techniques. Furthermore, one of these SASs was examined as an additive to the electrolyte solution of a model symmetrical electrochemical capacitor system. Its influence on the corrosion of current collectors (316L stainless steel) and, thus, on the device performance was assessed using electrochemical measurements and physicochemical analysis.

Results and discussion

Substituted ammonium salts with a 2,5-dihydroxybenzenesulfonate anion act as an anodic corrosion inhibitor of 316L stainless steel. The addition (0.1 wt%) of these compounds to the aqueous electrolyte solution inhibits the phenomenon of electrochemical corrosion by inhibiting only one reaction, i.e. oxidation of steel components (anodic inhibitor). The use of substituted ammonium salts in the electrochemical capacitor cell system allowed to inhibit the phenomenon of electrochemical corrosion of the current collectors (316L stainless steel), especially the collector of the positive electrode, which is polarized anodically during the capacitor charging mode. Therefore, inhibiting the degradation of the steel surface allowed to extend the life of the electrochemical capacitor cell by retarding the transfer of steel corrosion products to the porous space of the carbon electrode material.

Acknowledgements

This work was supported by the National Science Centre, Poland (Grant No. 2018/31/B/ST8/01619 and the Ministry of Education and Science, 2022 (Poland).

References

1. B.E. Conway, *Electrochemical Supercapacitors. Scientific Fundamentals and Technological Applications*, Springer, New York (1999).
2. A. Burke, *J. Power Sources*, **91**, 37 (2000).
3. S. Znaniecki, K. Szwabińska, J. Wojciechowski, A. Skrzypczak, G. Lota, *ChemElectroChem*, **8**, 3685 (2021).
4. J. Wojciechowski, Ł. Kolanowski, M. Graś, K. Szubert, A. Bund, K. Fic, G. Lota, *Electrochim. Acta*, **372**, 137840 (2021).
5. J. Wojciechowski, Ł. Kolanowski, A. Bund, G. Lota, *J. Power Sources*, **368**, 18 (2017).
6. Q. Abbas, P. Ratajczak, F. Béguin, *Faraday Discuss.*, **172**, 199 (2014).

Electrochemical Capacitor with Variable Polarization

J. Wojciechowski^a, K. Szwabińska^a, K. Fic^a and G. Lota^{a,b}

^aInstitute of Chemistry and Technical Electrochemistry, Poznan University of Technology, Berdychowo 4, 60–965 Poznan, Poland

^bŁukasiewicz Research Network – Institute of Non-Ferrous Metals Division in Poznan, Central Laboratory of Batteries and Cells, Forteczna 12, 61-362 Poznan, Poland

This paper discusses the effect of corrosion of steel current collectors on the performance of an electrochemical capacitor and a possible way of protecting these collectors from the destructive phenomena, through the application of a variable polarization protocol. The presented results of electrochemical techniques, mainly the potentiostatic technique (voltage-holding tests) confirm the fact that the current collector, being one of the elements of positive electrode, on which during charging, oxidation reactions occur, after 60 hours in the charged state undergoes tremendous degradation. In the case of the application of variable polarization protocol, electrochemical capacitor worked flawlessly, being fully charged for the next 140 hours.

Introduction

The energy storage phenomena in the electrochemical capacitors is performed on the basis of the formation of the electrical double layer at the electrode/electrolyte interface. These systems are built of two activated carbon electrodes separated by a separator. Both, electrodes and separator are soaked with organic or aqueous electrolyte. Active electrode material is applied on the metal or steel current collector surface. Those current collectors are exposed to corrosive electrolytes [1]. Thus, they are subjected to corrosion processes [2-5]. As it has been shown so far by Znaniecki et al. [6] and Wojciechowski et al. [7], the corrosion of stainless steel current collectors can be correlated with such parameters of electrochemical capacitor performance as its capacitance, maximum voltage, charge transfer resistance and lifetime (so the factors affecting the specific energy of system). It should be noted, however, that the phenomenon of capacitor current collector corrosion and its influence on a device operation are still relatively poorly understood and described in the literature [1, 8].

Materials and methods

In this study we present a novel path of electrochemical capacitor utilization, which leads to the inhibition of the corrosion phenomenon of the current collector of the positive electrode, and thus extending the service life of the entire device. Electrochemical measurements of symmetrical electrochemical capacitors (EC) were conducted in a two-electrode Swagelok® cells. Two systems of ECs were used in the electrochemical tests. Both of these systems were built of current collectors (316L stainless steel), activated carbon (active material, i.e. electrode material), separator and aqueous electrolyte (1 M Na₂SO₄). They have been subjected to the long-term procedure consist of a recurring multiple steps test cycle until ECs systems were destroyed. A single cycle was performed in the following sequence: (i) charging the system by the galvanostatic method (1 A/g)

(1.6 V); (ii) floating, i.e. keeping the capacitor charged for 5 hours (potentiostatic mode 1.6 V); (iii) galvanostatic charge/discharge (2 A/g); (iv) cyclic voltammetry tests (10 mV/s); (v) open circuit condition (OCV) for 1 hour; (vi) electrochemical impedance spectroscopy (± 10 mV vs. OCV, 100 kHz–10 mHz). As mentioned earlier, the tests were carried out for two capacitor systems. In one of them, a constant polarization (CP) was used, i.e. negative and positive electrodes were established. In the case of the second system, the polarity of the electrodes was changed alternately every other cycle of the long-term test procedure, i.e. each electrode was alternately operated as negative and positive (VP, variable polarization).

Results and discussion

The use of variable polarization protocol in electrochemical capacitor cell system performance allowed to inhibit the phenomenon of electrochemical corrosion of the current collectors (316L stainless steel), which were alternately polarized anodically during the capacitor charging mode. Therefore, inhibiting the degradation of the steel surface allowed to extend the life of the electrochemical capacitor cell by retarding the transfer of steel corrosion products to the porous space of the carbon electrode material.

Acknowledgments

This work was supported by the National Science Centre, Poland (Grant No. 2018/31/B/ST8/01619).

References

1. J. Wojciechowski, L. Kolanowski, A. Bund, G. Lota, *J. Power Sources*, **368**, 18 (2017).
2. R.W. Revie, H.H. Uhlig, *Corrosion and Corrosion Control*, fourth ed., John Wiley & Sons, New Jersey (2008).
3. E. R.W. Revie, *Uhlig's Corrosion Handbook*, third ed., John Wiley & Sons, New Jersey (2011).
4. E. McCafferty, *Introduction to Corrosion Science*, Springer, New York (2010).
5. A. Groysman, *Corrosion for Everybody*, Springer, New York (2010).
6. S. Znaniecki, K. Szwabińska, J. Wojciechowski, A. Skrzypczak, G. Lota, *ChemElectroChem*, **8**, 3685 (2021).
7. J. Wojciechowski, Ł. Kolanowski, M. Graś, K. Szubert, A. Bund, K. Fic, G. Lota, *Electrochim. Acta*, **372**, 137840 (2021).
8. Q. Abbas, P. Ratajczak, F. Béguin, *Faraday Discuss.*, **172**, 199 (2014).

Supercapacitors vs. Lithium-ion Batteries: Properties and Applications

J. Libich^a, M. Sedlaříkova^a, J. Máca^a, P. Čudek^a, A. Chekannikov^b and G. Fafilek^c

^aBrno University of Technology, Faculty of Electrical Engineering and Communication,
Department of Electrical and Electronic Technology, Technická 10, 616 00 Brno, Czech Republic

^bMoscow Institute of Physics and Technology 9 Institutskiy per., Dolgoprudny,
Moscow Region, 141701, Russian Federation

^cVienna University of Technology, Getreidemarkt 9, 1060 Vienna, Austria;

The development of human society is in close connection with the development of technology. Within last few decades, the technology advanced on the green, environmental and sustainable way. One of the main pillars of this progress is the production and utilization of electric energy. It is essential to learn, not only how to produce electric energy, but how to efficiently manipulate and store this electric energy. Nowadays, there are two main, most common devices for storing of electric energy batteries and capacitors. Both kinds of energy storage devices have their own leading, most advanced technologies, it is supercapacitors and lithium-ion batteries. Supercapacitors attract attention due to their superior values in the parameters like capacitance, discharge currents and cycle lifespan. Supercapacitors are designed and used in many applications where they partially or completely substitute conventional batteries.

Introduction

Supercapacitors and lithium-ion batteries, the right understanding of physics and operation principle of each device is crucial to ensure their correct and effective application. This paper contains summarized facts and aspects relating to both devices aiming to provides comprehensive point of view. It is necessary to realize, how important and widely spread the energy storage devices are today. There are plenty of varying applications which requires energy storages. It is not only transportation as cars, busses, forklifts and small electric vehicles and portable consumer electronic devices. But there are the other growing markets like renewable energy storage, grid and industry. Each application has got its own special requirements and operation conditions which must be taken into account if the energy should be effectively utilised.

Both devices as lithium-ion batteries and supercapacitors undergone a long development during their know existence. In case of the batterie, we can start the at the turn of the 18th and 19th century with the voltaic pile, in case of capacitors we can start in the year 1745 by discover so called Leyden jar which represents first capacitor at all. During the years there were many types of batteries and capacitors, skip the other important types of batteries and capacitors which appeared during the development period and look at the present time. Today, the lithium-ion batteries and supercapacitors

represent the most advanced, leading technology among batteries and capacitors. The development of rechargeable lithium-ion cells begins in the late 1970s with the discovery of reversible intercalation of lithium into graphite, along with the discovery of the positive electrode material LiCoO_2 (Lithium Cobalt Oxide). This was followed in the mid-1980s by the first experimental secondary cells where the negative electrode was made of graphite and the positive electrode LiCoO_2 only in 1991, SONY launched the first commercial secondary lithium-ion battery powering a portable camera. The development of supercapacitors ran in parallel with the development of lithium-ion batteries, but due to the success of these batteries, the development of supercapacitors was to some extent lagged behind. The first experiments with supercapacitors (in this time called ultracapacitors or late electrochemical capacitors) date from the 1950s to the 1970s by General Electric and Standard Oil of Ohio (SOHIO), the capacity of these supercapacitors was around 1 F. The first commercial supercapacitors named "GoldCap" from Panasonic and "Supercapacitor" from Japanese Nippon Electric Company (NEC) companies were patented and introduced to commercial market in the 1970s. These first supercapacitors differed in used electrolyte where GoldCap use aprotic electrolyte and Supercapacitor use aqueous electrolyte, unfortunately both possessed high internal resistance. In the 1980s, the first supercapacitor with low internal resistance, manufactured for militant purposes was introduced. In the early 1990s, Maxwell Laboratories launched the first commercial supercapacitor with capacitance 1 kF. This modern supercapacitor named "BoostCap" already had low internal resistance I can be considered as direct predecessor present supercapacitors. Today, supercapacitors over 3 kF are commonly available.

EDLC Supercapacitor and lithium-ion battery

To understand operation principle of each device is necessary to understand the way which each device use for storing of electric charge. First it is necessary to define the major electrical quantities which describe both devices. The supercapacitors can be characterised by the electric potential marked by symbol V or φ measured by joule per coulomb (J/C) or more common in volts (V). The difference between electric potential points, in case of supercapacitors it is between two electrodes, we call electric potential difference, commonly called as voltage that is symbolised by U or V and having the same unit volt (V). In case of lithium-ion batteries, we work with electromotive force abbreviated as *EMF* or Greek letter ε , sometimes denoted as E , to avoid confusion with energy symbolized by E and have unit joule (J) the Greek letter ε is preferred. Same as in supercapacitor, the *EMF* measured between two battery electrodes is called electromotive force difference and as in the supercapacitors, this difference is names as voltage symbolised as U or V and having the same unit volt (V). Here is very important to realise that whereas electric potential or sometimes called electrostatic potential is extensive physical quantity, i.e. in our cases depends on the amount of the charge stored, the EMF is intensive physical property linked with energy of the reaction and molecule bond i.e. does not depend on the amount of the charge stored.

Acknowledgments

This work was supported by the specific graduate research of the Brno University of Technology No. FEKT-S-20-6206.

Hybrid Supercapacitors Based of MnO₂–Carbon Xerogels Operating in Aqueous Electrolyte

L. Soserov, B. Mladenova, S. Veleva, B. Karamanova, A. Stoyanova

Institute of Electrochemistry and Energy Systems – BAS
10 Acad. G. BonchevStr., 1113 Sofia, Bulgaria

Hybrid supercapacitors systems are based on the coupling of a battery electrode with a carbon electrode, while allowing the latter to operate over the widest possible potential range and to increase the limited of conventional carbon/carbon capacitors. In this work, hybrid supercapacitors based on Activated carbon xerogels (AXs), α -MnO₂ and Aquvion E87-05S membrane soaked in 1 M Na₂SO₄ were studied. AXs are synthetic carbon materials, obtained from the polymerization reactions between a Resorcinol and a Formaldehyde in the solvent, with different pH of the precursor solution (5.97 and 6.5). They possesses high purity, surface area, porosities, and pore volume. These properties make them promising materials for supercapacitors applications. α -MnO₂ is synthesized by a simple co-precipitation technique and exhibits pseudocapacitive performances. The hybrid supercapacitors based on AXs/MnO₂ are a perspective and provide higher energy density than the symmetric systems.

Acknowledgement

Authors acknowledge the financial support of the Bulgarian Ministry of Education and Science under the National Program "European Science Networks" (grand agreement D01-286 / 07.10.2020).

Hybrid Composite Based on g C₃N₄ with PUMWCNTs - Promising Electrode Material for the Oxygen Electrode of Fuel Cells

M. O. Danilov^{1*}, G. I. Dovbeshko², I. A. Rusetskyi¹, O. P. Gnatyuk², S. S. Fomanyuk¹,
V. O. Smilyk¹, G. Ya. Kolbasov¹

¹V.I.Vernadskii Institute of General and Inorganic Chemistry of the NAS of Ukraine, 32/34 Academic Palladin Avenue, Kyiv, 03142, Ukraine.

²Institute of Physics of the National Academy of Science of Ukraine, 46 Nauky avenue, Kyiv, 03039, Ukraine.

*Corresponding Author E-mail Address: danilovmickle@rambler.ru

A new hybrid composite based on graphite-like carbon nitride and a partially unzipped multi-walled carbon nanotube has been synthesized. This composite was obtained by thermochemical synthesis of urea and melamine with a partially unzipped multi-walled carbon nanotubes obtained by electrochemical synthesis. The resulting hybrid composite based on graphite-like carbon nitride and partially unzipped multi-walled carbon nanotubes has been characterized by X-ray diffraction, selected area electron diffraction, electron transmission microscopy and Fourier-transform infrared spectroscopy. These methods have been proven the production of a hybrid composite of graphite-like carbon nitride and partially unzipped multi-walled carbon nanotubes. Electrochemical studies have established that the obtained composites are promising materials as a metal-free catalyst for oxygen electrodes of fuel cells. The obtained materials were stable in operation time for six months as an oxygen electrode in a fuel half cell.

The use of an air or oxygen electrode in devices that generate electrical energy is promising, since it doesn't create environmental problems and saves non-renewable natural resources. An air or oxygen electrode consists of a catalyst and a carrier, the interaction between them determines mainly the magnitude of the generated current. A promising line of work on the creation of efficient oxygen electrodes is the search for catalytically active and stable carriers for catalysts. Widely known from the literature is carbon. It has been shown that carbon materials doped with heteroatoms are good catalysts in the oxygen reduction reaction [1]. Such materials can be carbon nanotubes and graphenes doped with nitrogen [2, 3]. It was noted in [1] that doping with nitrogen is the most effective method for improving the electrocatalytic activity of carbon nanomaterials. It has been shown that carbon nitrides are effective electrocatalysts for oxygen electrodes [4]. It is also known that partially unzipped multiwalled carbon nanotubes (PUMWCNTs) are good catalyst carriers for oxygen electrodes [5]. Therefore, it is interest to study a composite based on PUMWCNTs and carbon nitride.

The aim of our work was to create a new hybrid composite and study obtaining material as a metal-free catalyst for the oxygen electrode of a fuel cell. To obtain layered composites based on graphite-like carbon nitride, a thermochemical synthesis method was proposed.

This method consists in heating a mixture of urea, melamine, PUMWCNTs in a crucible with a lid to temperature of 550°C, similarly to the method described in our works [4]. PUMWCNTs

were obtained by the method described in [5]. As a result of the synthesis, a finely crystalline black powder was obtained. Figure 1a and Figure 1b shows micrographs of the obtained sample at various magnifications.

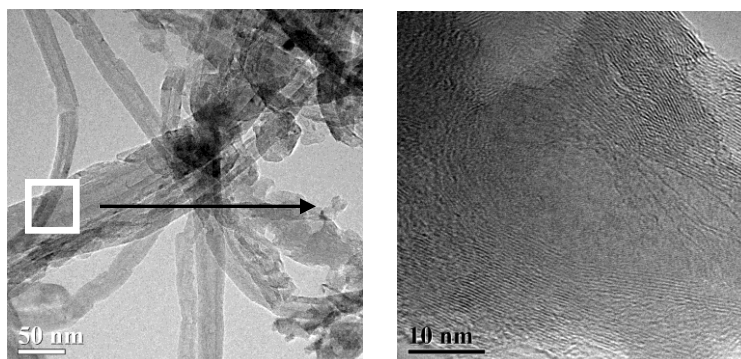


Figure 1. Micrograph of a composite of graphite-like carbon nitride and PUMWCNTs.

Figure 2 shows the X-ray of powder of the obtained composite.

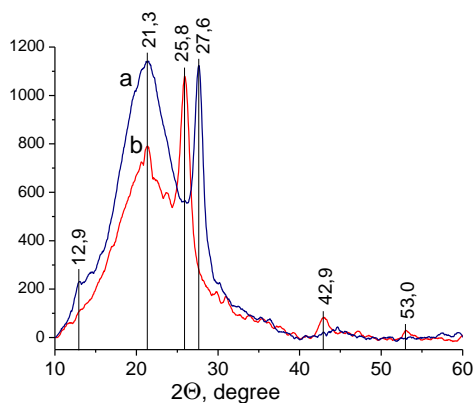


Figure 2. X-ray diffraction patterns of the hybrid nanocomposites from layered structures of graphite-like carbon nitride (a) and nanocomposites from graphite-like carbon nitride and PUMWCNTs (b).

Figure 3 shows the IR spectra of graphite-like carbon nitride and its composite with PUMWCNTs.

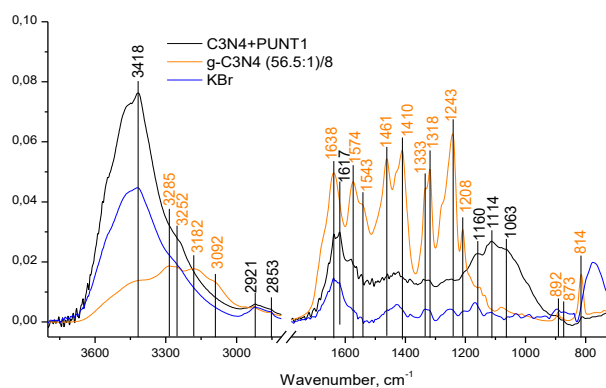


Figure 3. IR spectra of graphite-like carbon nitride and its composite with PUMWCNTs. Tablets were pressed in KBr.

The graphite-like C_3N_4 sample contains only C-N and C=N bonds, as well as vibrations of the triazine ring as a whole. The low-frequency bands in the region 814 and 892 can be attributed to the respiratory modes of triazine rings. All bands from 1208 to 1638 refer to C-N and C=N stretching vibrations in heterocycles. In particular, 1461, 1410, 1243, and 1218 can be attributed to C-N, and bands 1543, 1574, and 1638 to C=N. A number of bands in the region 3285, 3252, 3182 can be attributed to hydrogen-bonded N-H, 2921, 2853 - valence CH, 3092 - ring CH. It is possible that the appearance of CH bands is associated with the presence of defects in the structure, vacancies. In [6], an increase in the contribution of the NH region 3300 with an increase in the contribution of short fragments is noted. (5 rings each), then the appearance of end groups NH, NH_2 , CH is possible. With an increase in the polymerization temperature from 520 to 670 degrees, the number of short fragments increases [6-8]. After the formation of a composite with partially opened carbon nanotubes, the IR absorption spectrum changes radically. The absorption increases in the region of 1160, 1114, and 1063, which is not characteristic of C_3N_4 and may possibly be associated with the formation of a composite.

Based on the analysis of XRD, TEM, IR spectroscopy and Raman, it can be concluded that a new hybrid composite of g C_3N_4 with PUMWCNTs has been obtained.

The synthesized composite was investigated as a metal-free catalyst for the oxygen electrode of a fuel cell. Studies were carried out on a mock up of fuel cells, with a zinc electrode used as the anode as described in [9]. As can be seen from Figure 4, the characteristics of the resulting composite are approaching in their performance characteristics to oxygen electrodes based on platinum-containing materials. The obtained materials were stable in operation for six months.

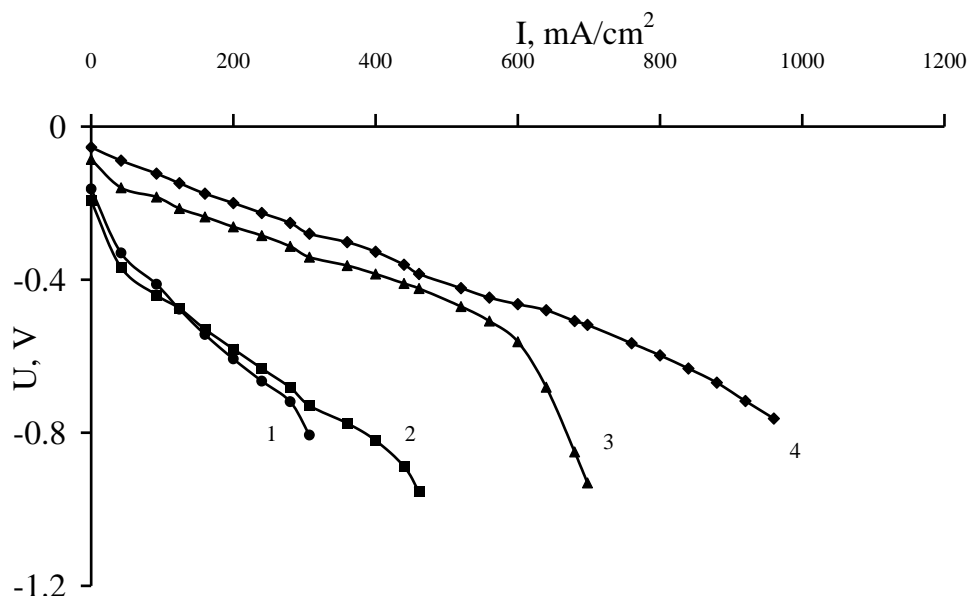


Figure 4. Volt-ampere characteristics of oxygen electrodes with an active layer of various electrode materials: 1 – PUMWCNTs; 2 – g C_3N_4 ; 3 – composite of g C_3N_4 with PUMWCNTs; 4 - MWCNT coated with platinum in the amount of 10 wt.%.

Thus, as a result of the thermochemical synthesis of melamine urea and partially unzipped multi-walled carbon nanotubes, a hybrid composite is obtained that has high electrocatalytic properties in the oxygen reduction reaction.

References

1. Wang M, Wu Z, Dai L 2015 *J. Electroanalyt. Chem.* **753** 16
2. Yu D, Zhang Q, Dai L 2010 *J. Am. Chem. Soc.* **132** 15127
3. Qu L, Liu Y, Baek J -B, Dai L 2010 *ACS Nano* **4** 1321
4. Danilov M O, Dovbeshko G I, Rusetskyi I A, Afonina U K, Bykov V N, Gnatyuk O P, Fomanyuk S S, Kolbasov G Ya 2021 *ECS Trans.*, **105** 87
5. Danilov M O, Dovbeshko G I, Rusetskyi I A, Pekhnyo V I, Nikolenko A S, Kolbasov G Ya 2020 *Applied Physics A* **126**, 764
6. Po Wu, Jiarui W, Jing Zh, Liejin G, Frank O E 2014 *J. Mater. Chem. A* **2** 20338
7. Li W, Chen Q, Zhong Q 2020 *J Mater Sci.* **55** 10712
8. Gao W, Zhao Y, Mao Z, Bi D, Chen J, Wang D -J 2018 *J Mater Sci.* **53** 9473
9. Danilov M O, Rusetskii I A, Dovbeshko G I, Nikolenko A S, Fomanyuk S S, Kolbasov G Ya 2019 *ECS Trans.* **95** 273

Renewable Hydrogen Sources for Fuel Cell Powered Trains in Czech Republic

M. Paidar¹, K. Denk¹, F. Zenith², L. Polák³, J. Sochor⁴

¹University of Chemistry and Technology, Prague, Technická 5, Prague 6, 166 28, Czech Republic

²SINTEF AG, Strindvegen 4, 7034 Trondheim, NORWAY

³ÚJV Řež, a.s, Hlavní 130, 250 68 Husinec, Czech Republic

⁴Czech Hydrogen Technology Platform, Hlavní 130, 250 68 Husinec, Czech Republic

To introduce hydrogen powered trains in Czech Republic it is necessary to evaluate its economic feasibility. The comparison of battery, fuel cell and catenary powered trains was done for selected non-electrified lines. One of the crucial conditions for fuel cell powered trains is the source of hydrogen. Thus evaluation of possible hydrogen sources under conditions of Czech Republic was realized. Water electrolysis in direct connection of photovoltaic suffers for short operation time. Additional sources of electric energy are required to improve hydrogen production economy.

Today society faces to several challenges. Frequent weather extremes in the regions without previous experience with it. Global market is paralysed by pandemic situation. Russian aggression are connected with uncertain supply of oil and natural gas. All this things raise the need for change of energy mix not only in transportation. European Union countries keep strong ambitions to decarbonise its economy including transportation. The renewable power sources like photovoltaic and wind power plants will be the important part in future energy supply. For transportation it means abatement of combustion engines and introduction of electric powered vehicles. In contrast to the car sector in railway transportation electricity is frequently used for decades. The electrified railways with overhead catenary are today most efficient solution on frequently used lines. But the electricity is generated mostly in fossil fuel combustion power plants. Production of renewable power sources are not synchronized with energy demand also in transportation. With energy supply based on fluctuating performance power source some kind of energy buffer is required anyhow. Frequently used lines represents almost stable consumption of electric energy. Significantly different situation is for less frequently used lines without installed catenary. The installation of catenary and its maintenance is costly, therefore alternative solutions have to be considered too. The “easiest” solution is to convert the railway to bicycle path and move public transportation to the roads. It suffers from several reasons. The modern trend is to reduce individual transportation and increase public transport. In Czech Republic the roads are often congested and bus capacity is lower in contrast to train. It hardly attract passengers to change their habits if travel quality is insufficient. For preservation of public transport on railway it is necessary to change train power from diesel to an alternative. Building of new catenary requires significant constructions along whole line. On the other hand battery or hydrogen powered train can be operated on lines in its current state. Only charging or refilling infrastructure have to be constructed. Benefits of battery powered train are mainly in relative simplicity and possibility for recharging if operated on partly electrified lines. But battery trains are not suitable for long distances. For long distances the hydrogen powered trains are

more suitable. Also the operating line profile, speed and number of operated trains play important role in economic evaluation of each possibility.

For hydrogen powered train it is crucial to ensure sufficient supply of hydrogen. Filling station for hydrogen trains needs locally large amount of hydrogen. One regional passenger train (Regional Multiple Units type) for daily distance 500 km needs approximately 125 kg of hydrogen. For year operation it is over 45 t of hydrogen. From it follows that for hydrogen powered train operation is necessary to find sustainable and sufficient hydrogen supply.

There are several methods of hydrogen production. To stress environmental aspect of hydrogen powered transportation it is desired to use renewable hydrogen or with low carbon pathway. Water electrolysis in combination with renewable power source is the preferred way. Photovoltaic power plants are the most accessible form of renewable energy source in Czech Republic. Required size of power plant in combination with proper size of water electrolyser must be calculated to define parameters of sufficient onsite hydrogen generation. The mathematical model was created to evaluate quantity of renewable hydrogen produced on the base of power plant performance in time and electrolyser operation parameters. For economic feasibility the CAPEX of electrolyser plays decisive role. As it was found increase of electrolyser capacity over some level brings only small increase of produced hydrogen mass but significantly increase of electrolyser price. Without possibility of electrolyser operation from electric network by use of “green electricity” certificates the electrolyser will mostly operate below 40% of its capacity. Therefore combination with other electricity source is desired. One option is hydropower or also unused electricity from locomotives recuperation to catenary. Each of it elongate electrolyser operation time and thus improves economy of water electrolysis significantly.

Beside water electrolysis there are also other alternatives for hydrogen production. In the case of gas network available it is possible to use transferred bio-methane and with onsite steam reforming to generate hydrogen. In contrast to the electricity the transfer of bio-methane via gas network on the base of “green origin” certificates is possible. Nevertheless the local emissions are produced from this hydrogen production like standard natural gas steam reforming process.

Local production of renewable or low emission hydrogen is beneficial also for other transport types like buses, trucks and passenger cars. It should be the crucial step for regional hydrogen mobility.

Acknowledgments

This project is financed by the Technology Agency of the Czech Republic under grant TO01000324, in the frame of the KAPPA programme, with funding from EEA Grants and Norway Grants.

Numerical Prediction of Electrical Conductivity of Porous Composite Materials: LSM-YSZ Case Study

D. Budáč^a, V. Miloš^b, M. Carda^a, M. Paidar^a, K. Bouzek^a

^a Department of Inorganic Technology, University of Chemistry and Technology, Prague, Czech Republic

^b Mathematical Institute, Charles University, Prague, Czech Republic

Composite of lanthanum strontium manganite and yttria-stabilized zirconia (LSM-YSZ) is the state-of-the-art oxygen electrode material in the solid oxide cells due to its excellent electro-catalytic properties and long lifespan. While the LSM is excellent electronic conductor and electro-catalyst, the content of ionically conductive YSZ increases the amount of electrochemically active sites, the triple phase boundary, thus increasing the overall electrode electro-catalytic performance. However, it also considerably lowers the total electrical conductivity. This applies for all ceramic-based composites. We developed a unique universal equivalent circuit network model for prediction of electrochemical properties of composite electrodes. A set of porous LSM-YSZ samples was prepared to attain the validation data for our model. The data included the impedance behavior of the samples with respect to their electrical conductivity and polarization resistance. The model showed good qualitative and quantitative agreement in terms of electrical conductivity prediction.

Introduction

Solid oxide cells (SOCs) represent efficient energy conversion devices. SOCs are currently commercially available mainly in the form of highly efficient μ -cogeneration units utilizing methane as fuel, in addition, they show high potential in the hydrogen economy concept as water electrolyzers and/or fuel cells. The high conversion efficiency of SOCs is predominantly due to favorable fast kinetics resulting from operation temperature of 600 to 900 °C. Furthermore, the high operation temperature enables to work without expensive Pt-based electro-catalysts. On the other hand, the elevated operation temperature poses high stability requirements of the materials used in the SOCs limiting the choice of materials mostly to ceramics and cermets.

The SOCs are composed of three key components, electrolyte and two electrodes, each component having its specific requirements. High ionic conductivity, negligible electronic conductivity and gas tightness are necessary for the electrolyte. High electro-catalytic activity, high electrical conductivity and high gas permeability is required for the materials of electrodes. Furthermore, the key components need to be compatible in terms of thermal expansion coefficient and mutual chemical inertia.

At the oxygen electrode the oxygen evolution or reduction reaction takes place depending on the SOCs operation mode. Perovskite-based materials represent an attractive group of materials for the oxygen electrode. Lanthanum strontium manganite (LSM) is the state-of-the-art perovskite electrode due to its high electro-catalytic activity and high electronic conductivity. However, its negligible ionic conductivity limits the performance of the LSM electrode exclusively to active sites,

the triple-phase-boundaries (TPB) – interfaces of the electrode, electrolyte and gaseous phase (1). Introduction of the ionically conductive phase into the volume of LSM electrode leads to the increase of TPB length, thus increasing the total electro-catalytic performance of the oxygen electrode.

The application of such composite electrodes is common practice in the SOCs field. The most-used oxygen electrode is the LSM paired with yttria-stabilized zirconia (YSZ) in a 50:50 weight ratio as reflected by the literature (2). On the other hand, at the temperature of 800 °C pure LSM has electrical conductivity of ca. 220 S cm⁻¹ (3), while pure YSZ of only 0.04 S cm⁻¹ (4), suggesting the electrical conductivity of resulting LSM-YSZ composite is considerably lower than that of pure LSM. Considering the necessary porosity of the oxygen electrode, the electrical conductivity of the composite electrode can be decreased down to 3 S cm⁻¹ at 800 °C (5). Even though it is well known LSM-YSZ provides excellent electro-catalytic properties, the effect of porosity on such electrode is not sufficiently considered in the open literature.

The model

We propose a 3D equivalent electronic circuit (EEC) network model for prediction of the electrochemical properties of composite porous electrodes. The model distinguishes between multiple material species – electron conductor, ionic conductor and non-conductive pore. The input data for the EEC model are the conductivities of the single-phase materials, composition and apparent porosity of the material. Based on the input data, multiple random 3D artificial specimen of 25x25x25 cubic voxels representing the input phases are generated. The model creates an EEC network substituting the voxels for a matrix of electrical resistors for each artificial specimen. The model can differentiate between the interfaces of LSM|LSM, YSZ|YSZ and LSM|YSZ. If the LSM|YSZ (electrical | ionic conductor) interface is detected, a parallel combination of resistor and capacitor is added as a representation of a charge-transfer reaction. Based on the EEC networks, the model allows to predict electrical conductivity and impedance behavior of composite materials. It can simulate also impedance behavior of patterned materials which is an undisputable advantage of our approach over traditional approaches. That suits present trends of microstructural optimization of composite applications perfectly. Furthermore, the EEC network model can be used to predict the electrical conductivity of any composite material if the single-phase conductivities are known making it a useful tool for broad range of scientific fields.

Multiple porous samples of various LSM:YSZ:porosity composition were prepared for the validation of the EEC network model. Electrochemical impedance spectroscopy was used to evaluate the electrochemical properties of the samples at temperatures of 400 to 800 °C.

The EEC network model shows a good agreement with the experimental data up to composite porosity of 50 %. Yet, above this threshold such electrodes are not considered for practical use in the field of SOCs. The model also qualitatively corresponds to the experimental data concerning the impedance behavior, which differs for LSM-percolated and non-LSM-percolated samples. The results clearly showed, that in materials with a low amount of LSM, the LSM particles act as bipolar electrodes influencing the overall impedance behavior of the material.

Acknowledgments

This work was supported by the Technology Agency of the Czech Republic under project no. TK04030143 and Specific university research (A2_FCHT_2022_057).

References

1. S. B. Adler, *Chemical Reviews*, **104**(10), (2004)
2. N. Mahato, *Progress in Materials Science*, **72**, (2015)
3. T. M. Huber, *Journal of The Electrochemical Society*, **165**, (2018)
4. C. Ahamer, *Journal of The Electrochemical Society*, **164**, (2017)
5. O. O. Agbede, *Materials Today Chemistry*, **16**, (2020)

New starter lead–acid battery with modified electrolyte by ionic liquid

P. Kędzior^{a,b}, W. Rzesutek^a, J. Wojciechowski^b, A. Skrzypczak^b, G. Lota^b

^a PPUH Autopart Jacek Bąk sp. z o.o., Mielec 39-300, POLAND

^b Institute of Chemistry and Technical Electrochemistry, Poznan University of Technology,
Berdychowo 4, Poznań 60-965, POLAND

pkedzior@autopart.pl

Introduction

Lead-acid batteries over the years have become cheaper in production, more reliable, maintenance-free and by reducing the mass of components, their specific energy has increased. Due to their parameters and extensive recycling system, lead-acid batteries are still the most commonly used chemical power source. However, bearing in mind the requirements of the market, the industry producing lead-acid batteries and suppliers connected with it are facing a challenge. The development of materials used for their production is a key aspect for the further development of this technology (1). The possibility of using ionic liquids (ILs) as an additive modifying electrolyte is an exciting issue (2-6). IL have become the group of the most promising chemical compounds due to their unique properties, like high conductivity, thermal and chemical stability, low volatility, low toxicity and almost endless possibilities between cations and anions combinations. They found many applications in the chemical industry, including electrochemistry (7-8).

In the presented work, it is proposed to modify the electrolyte composition by introducing ILs to improve the performance of lead-acid batteries. The main goals of the research are to inhibit the corrosion process of current collectors and to increase the stability of the electrolyte based on sulfuric acid during the charging process while maintaining the basic parameters, i.e. capacity and cranking performance.

Experimental

Eight ammonium ILs were used as additives to the electrolyte. The differences between the used compounds are based on the different types of anion in the molecule, the amine used in the synthesis, and the cation side chain length. ILs used in the research can be divided into two basic groups: alkylammonium sulfates and alkylimidazolium sulfates. The cations differ in the number of alkyl groups in the structure and the length of the main substituent. The basic long-chain alkyl group in the investigated ILs was the hexadecyl group.

Preliminary three–electrode electrochemical measurements of cells were performed at ambient conditions in 37% H₂SO₄ aqueous electrolyte with 0.0; 0.1; 0.3 or 0.5 mg L⁻¹ IL additive. PbCaSn alloy for lead–acid battery grid (current collector) manufacturing was used as a working electrode, while Pb (purity min. 99,9%) and Hg/Hg₂SO₄/1M H₂SO₄ served as a counter and reference electrode, respectively. At the beginning, hydrogen and oxygen evolution potentials were measured. Then, corrosion potential and corrosion current density values were determined by means of Tafel extrapolation method. The electrochemical parameters were assessed using the linear sweep voltammetry. All of the above tests were performed using an electrochemical workstation potentiostat/galvanostat VMP3 (Biologic, France) with impedance module.

Additionally, the corrosion resistance of the current collectors was tested on the basis of the weight loss assessment. These measurements were performed at 60°C in 37% H₂SO₄ aqueous electrolyte with the same concentrations of ILs in the electrolyte as in the preliminary tests. Real current collector using in lead–acid battery was used as a working and counter electrode. A constant current flow was set through the test cell for 10 days. After this time, the current collectors were etched and the weight loss was assessed.

In the next part of the experiment, reference batteries and batteries with electrolytes modified by selected ILs in different concentrations were made. Autopart technology and machinery were used in this case. The internal resistance of all the batteries was measured. Capacity, Cold Cranking Amps (CCA), endurance in cycling, corrosion and water consumption tests were performed according to the EN 50342-1: 2016 standard: Lead-acid starter batteries – Part 1: General requirements and methods of test. Scanning electron microscopy (SEM) analysis and X-ray diffraction (XRD) analysis of positive and negative active mass were performed. The current collectors were analyzed using the energy-dispersive x-ray spectroscopy (EDS) technique.

Results and discussion

The presented results show that the modification of the electrolyte with an IL increases the overpotential of the hydrogen and oxygen evolution reaction and have a strong influence on the corrosion intensity of PbCaSn alloy, even at low concentration. This phenomenon can be explained by the forming an organic layer at the alloy/sulfuric acid and the negative active mass/sulfuric acid interfaces.

Acknowledgments

The authors thank the Polish Ministry of Education and Science for financial support (Applied Doctorate Program, No. DWD/3/20/2019).

References

1. Pavlov D.: Lead-Acid Batteries Science and Technology, 1 Ed. 2011,
2. B. Rezaei, S. Mallakpour, M. Taki, J. Power Sources, 187 (2009) 605–612,
3. B. Rezaei, E. Havakeshian, A.R. Hajipour, J. Solid State Electrochem., 15 (2011) 421–430
4. M.A. Deyab, J. Power Sources, 390 (2018) 176–180.
5. K. Kopczyński, A. Gabryelczyk, M. Baraniak, B. Łęgosz, J. Pernak, P. Kędzior, G. Lota, Int. J. Electrochem. Sci., 13 (2018) 11058 – 11073,
6. K. Kopczyński, A. Gabryelczyk, M. Baraniak, B. Łęgosz, J. Pernak, P. Kędzior, G. Lota, Int. J. Electrochem. Sci., 13 (2018) 4390 – 4400,
7. D.R. Macfarlane, M. Forsyth, P.C. Howlett, J.M. Pringle, J. Sun, G. Annat, W. Neil and E.I. Izgorodina, Acc. Chem. Res., 40, 1165 (2007).
8. H. Liu, Y. Liu and J. Li, Phys. Chem. Chem. Phys., 12, 1685 (2010).

Organic redox compounds for cheaper and greener flow batteries – a critical view

¹P. Mazúr, ¹M. Mikešová, ²J. Charvát, ²J. Pocedič, ³M. Klikar, ³F. Bureš, ⁴J. Akrman, ⁴L. Kubáč

¹University of Chemistry and Technology Prague, Dept. of Chemical Engineering, Technická 5, 166 28 Prague, Czech Republic, mazurp@vscht.cz; +420220443244

²University of West Bohemia, New Technologies – Research Centre, Univerzitní 8, 301 00 Plzeň

³Institute of Organic Chemistry and Technology, Faculty of Chemical Technology, University of Pardubice, Studentská 573, Pardubice, Czech Republic

⁴Centre for Organic Chemistry, Rybitví 296, 533 54 Rybitví, Czech Republic

Redox flow batteries (RFB) represent safe, reliable and long-lasting energy storage technology for stationary applications. The currently most matured system based on vanadium is being commercially deployed worldwide by several companies such as CellCube (AUT), Invinity Energy Systems (GB), Sumitomo Electric (JAP), Volterion (GER) or Pinflow Energy Storage (CZE). However, the high price, limited accessibility and negative environmental aspects of use of vanadium and other metals motivates the search for alternative redox compounds, very often from organic chemistry.[1, 2]

In our contribution, we will provide the overview of currently investigated and employed organic redox couples for aqueous RFB electrolytes including own data obtained with quinone and viologen groups. The most promising organic chemistries will be compared with the benchmark inorganic RFB based on vanadium ions with respect to the technical and economical parameters using our own experimental data. The directions towards industrially suitable solutions will be outlined.

Acknowledgments:

The work was supported from European Regional development Fund-Project "Organic redox couple based batteries for energetics of traditional and renewable resources (ORGBAT)" No.CZ.02.1.01/0.0/0.0/16_025/0007445. The research leading to these results has received funding from the European Union under Grant Agreement no. 875913.



EUROPEAN UNION
European Structural and Investment Funds
Operational Programme Research,
Development and Education



References:

1. Fischer, P., P. Mazúr, and J. Krakowiak, Family Tree for Aqueous Organic Redox Couples for Redox Flow Battery Electrolytes: A Conceptual Review. *Molecules*, 2022. **27**(2): p. 560.
2. Sánchez-Díez, E., et al., Redox flow batteries: Status and perspective towards sustainable stationary energy storage. *Journal of Power Sources*, 2021. **481**: p. 228804.

Impact of the Carbon Additives for the Performance of the Lead-acid Battery

R. Płowens^{a, b}, M. Bajsert^a, M. Baraniak^b, G. Lota^b

^a Jenox Akumulatory Sp. z o.o., Notecka 33, Chodzież 64-800, Poland

^b Institute of Chemistry and Technical Electrochemistry, Poznan University of Technology, Berdychowo 4, Poznań 60-965, Poland

Electrical production is changing dramatically worldwide due to the need to reduce greenhouse gas emissions and introduce mixed energy sources. The electricity grid faces great transmission and distribution challenges to meet demand with unpredictable daily and seasonal fluctuations. An energy storage system (EES) is recognized as an essential technology with great potential to meet these challenges, whereby energy is stored in a certain state according to the technology used and converted into electricity when necessary. One of the common sources of energy storage is lead-acid batteries. Materials based on carbon additives have a wide range of properties to modify an active mass in a lead-acid battery. Presented research concerning the influence of carbon additives on the properties of the negative electrode, such as capacity, charge acceptance and cycle lifetime.

Introduction

The continuous development of civilization increases the demand for electricity, which is still obtained mostly by burning fossil fuels. This contradicts the efforts of the most developed countries to reduce CO₂ emissions and the associated greenhouse effect. For this reason, renewable energy sources (RES) such as solar energy, wind energy, geothermal energy, biogas and biomass are becoming more and more popular. One of the problems of RES is periodicity in obtaining energy, especially when the forces of nature generate energy, therefore an energy storage system is used to eliminate fluctuations in production. In large-scale storage in the order of 10's to 100's of MWh, flow batteries, compressed air energy storage, and pumped hydro storage are suitable. In small RES installations system, the most popular are wind energy and solar energy, for energy storage, usually, electrochemical batteries such as lead-acid batteries, Ni-MH batteries or Li-ion batteries are used. Li-ion batteries have the highest specific energy, but their price and recycling difficulties greatly disadvantage them. On the other hand, lead-acid batteries have lower specific energy (25-50 Wh / kg) and low capital cost (50-100 \$ / kWh) [1], and the possibility of full recycling makes them an interesting alternative, especially in small RES installations.

A frequent cause of failure is sulphation of the Pb / PbO₂ cell, which occurs during stops at a partial state of charge, which can occur on both electrodes, especially on the negative electrode. The cause of this phenomenon is the formation of coarse crystalline layers of lead sulphate, which are very difficult to remove during conventional charging of the cell. It is also closely related to the ability of the electrodes to receive a charge, especially during the initial stages of charging in the case of negative electrodes. In order to counteract this phenomenon, added additives are added to the negative active mass, called an expander, which is a mixture of lignin, barium sulphate and carbon [2-3]. Lignosulfonate prolongs the life cycle, prevents passivation and increases active mass use [4-6]. Barium sulfate (BaSO₄) acts as a nucleating agent for the formation and growth of small PbSO₄ crystals and ensures the even distribution of these crystals [7]. Carbon additives are added to the paste

mainly to improve the electrical conductivity of the active mass at the end of the discharge when the content of PbSO₄ crystals in the negative active mass (NAM) increases significantly [8-10]. Although carbon in the negative electrode increases capacity, reduces hydrogen evolution overpotential, increases conductivity, changes porosity, and reduces lead sulfate crystal growth [8-10], the beneficial effect of carbon is not fully understood. It is likely due to a combination of one or more attributes.

This work presents the effect of selected carbon additives on the operating parameters of a lead-acid battery. It has been shown that carbon additives improve charge acceptance and, to a lesser extent, increase battery cycle life.

Acknowledgements

The authors thank the Polish Ministry of Education and Science for financial support (Applied Doctorate Program, No. DWD/3/20/2019).

References

1. X. Luo, J. Wang, M. Doonner and J. Clarek, *Applied Energy*, **137**, (2015), 511-536.
2. D. Pavlov: *Lead-Acid Batteries Sciencs nad Technology*, Elsevier, Amsterdam, 2 Ed. (2017).
3. P. T. Moseley, *J. Energy Storage*, **19**, (2018), 272-290.
4. D. von Borstel, G. Hoogestraat and W. Ziechmann, *J. of Power Sources*, **50** (1994) 131–140.
5. B.O. Myrvold, *J. of Applied Electroch.*, **35** (2005) 573–579.
6. K. Sawai, T. Funato, M. Watanabe, H. Wada, K. Nakamura, M. Shiomi and S. Osumi, *J. of Power Sources*, **158** (2006) 1084–1090.
7. D. Pavlov, Additives to the Pastes for Positive and Negative Battery Plates, in: *Lead-Acid Batteries: Science and Technology*, Elsevier, Amsterdam, 2 Ed. (2017).
8. R. Marom, B. Ziv, A. Banerjee, B. Cahana, S. Luski and D. Aurbach, *J. of Power Sources*, **296** (2015) 78–85.
9. J. Lach, K. Wróbel, J. Wróbel, P. Podsadni and A. Czerwiński, *J. of Solid State Electroch.*, **23** (2019) 693–705.
10. X. Zou, Z. Kang, D. Shu, Y. Liao, Y. Gong, C. He, J. Hao and Y. Zhong, *Electroch. Acta*, **151** (2015) 89–98.

Anodes for Li-ion Batteries based on electrodeposited Tin in Deep Eutectic Solvents

L. A. Azpeitia^{a,b}, M. G. Ortiz^{a,c}, A. Visintín^a, C. A. Gervasi^{a,b}, A. E. Bolzán^a

^a Instituto de Investigaciones Fisicoquímicas Teóricas y Aplicadas (INIFTA), Universidad Nacional de La Plata - CONICET, Sucursal 4 Casilla de Correo 16 (1900) La Plata, Argentina

^b Facultad de Ingeniería; Universidad Nacional de La Plata, 1900 La Plata, Argentina

^c Centro de Investigación y Desarrollo en Ciencia y Tecnología de Materiales (CITEMA), Universidad Tecnológica Nacional - CICPBA, 60 y 124, 1923, Berisso, Argentina

In this work, Tin anodes materials are were prepared by electrodeposition in deep Eutectic Solvents on copper foil, with ERGO; and the electrochemical performances were tested.

Introduction

Considering the potential value of tin and tin compounds as materials for Li-ion batteries anodes, the simplicity of the electrodeposition techniques and the increasing interest in deep eutectic solvents as strategic green solvents, we studied the preparation of tin electrodes of different structures and composition. For this purpose, anodes based on copper foils and copper foams were used [1]. Copper foams were prepared in our laboratory by electrodeposition of copper from copper sulphate solutions under galvanostatic conditions, and heat treated to improve their mechanical characteristics. Both, foams and foils, were covered by a thin film of electroreduced graphene oxide (ERGO) formed by the drop-casting method [2]. The purpose of this highly conductive layer was to separate copper substrate from tin electrodeposit to hinder the diffusion of tin atoms into the copper lattice with the subsequent formation of intermetallics. Afterwards, tin anodes were prepared by electrodeposition in deep Eutectic Solvents and the electrochemical performances were tested.

Experimental

Tin anode materials were prepared by electrodeposition from a choline chloride + tin chloride 1:2 molar deep eutectic solvent by applying a pulse plating technique under galvanostatic conditions [3]. Four different types of electrodes were synthesised and tested: i) copper foil + ERGO + tin; ii) copper foil + ERGO + tin oxide; iii) copper foam + ERGO + tin and iv) copper foam + ERGO + tin oxide. Electrodes consisting of tin oxide were prepared by electro-oxidation in 0.05M KClO₄ applying a galvanostatic double-pulse routine by stepping from 5 mA/cm² for 1 s, to 0 mA/cm² for 1s, during t = 1200 s. Results show significant improvement on the electrodes performance after changing from a smooth to a 3D structure and from tin to tin-oxide electrode. The electrochemical performances were tested and the electrochemical behaviour during the charge-discharge cycling are shown in Figure 1.

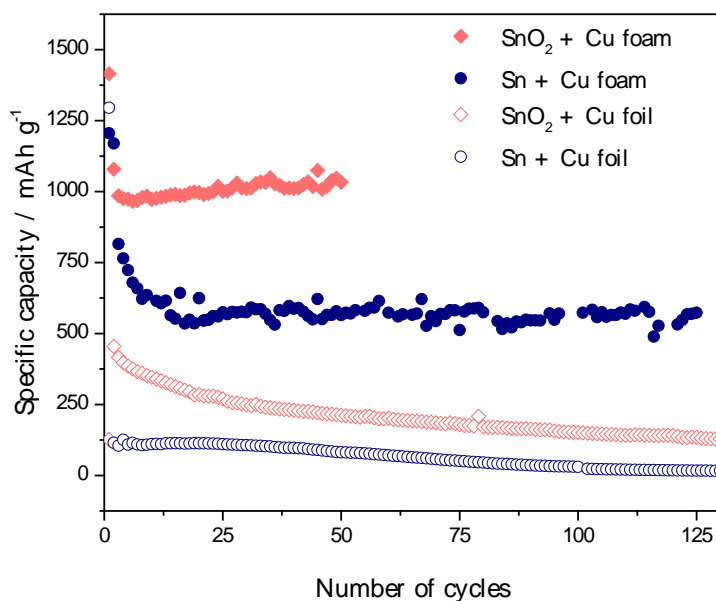


Figure 1. Specific Capacity of Discharge for the anode materials.

Acknowledgments

This work was supported by the CONICET (Consejo Nacional de Investigaciones Científicas y Tecnológicas) and ANPCyT (Agencia Nacional de Promoción Científica y Tecnológica).

References

1. H. C. Shin and M. Liu, in “Copper foam structures with highly porous nanostructured walls,” *Chem. Mater.*, **16**, 25,5460, (2004).
2. A. Ambrosi and M. Pumera, “Precise tuning of surface composition and electron-transfer properties of graphene oxide films through electroreduction,” *Chem. - A Eur. J.*, **19**, 15, 4748, (2013)
3. E. L. Smith, A. P. Abbott, and K. S. Ryder, “Deep Eutectic Solvents (DESs) and Their Applications,” *Chem. Rev.*, **114**, 21, 11060 (2014).

Influence of Different Cycling Speed on the Life-span of the Negative Electrode for Lead-acid Batteries

J. Smejkal^a and L. Chladil^{a,b}

^a Institute of Electrotechnology, Faculty of Electrical Engineering and Communication, BUT, Technická 10, 616 00 Brno, Czech Republic

^b Centre for Research and Utilization of Renewable Energy, Faculty of Electrical Engineering and Communication, BUT, Technická 10, 616 00 Brno, Czech Republic

This article is focused on studying the effect of cycling speed on the long-term life of the negative electrode in a lead-acid battery. Experiments were designed to gain a deeper understanding of the processes taking place on the surface of the negative electrode. The performed measurement focuses on the analysis of changes in the chemical composition on the surface of the negative electrode during the charging and discharging of a lead-acid battery. The measured negative electrode was cycled at rates of 0.3 C and 0.5 C. During cycling, it was measured using an X-ray diffractometer at different levels of SOC. The results of this measurement indicate uneven dissolution of lead sulfate and unstable discharge of the negative electrode during cycling, which reduced the capacity of the lead-acid battery.

Introduction

Lead-acid batteries are one type of secondary cell. Primary and secondary cells differ in that, unlike secondary cells, primary cells cannot be recharged and reused as a source of electrical energy. In the case of secondary cells, it is possible to repeat the process of recharging in the order of hundreds to thousands of cycles. Recharging is limited only by the degradation mechanisms occurring in each type of accumulator [1].

Currently, technologies based on the production of renewable electricity are increasingly being used. The growth of these technologies can significantly affect the stability of the electricity grid, and there is also an increase in the costs associated with the integration of renewable sources into the existing electricity grid. For these reasons, the storage of electrical energy is increasingly being addressed using battery systems, which offer a possible alternative to overcome some of the problems described above. Due to their properties, recycling possibilities, the high number of cycles, and low purchase price, lead-acid batteries are an interesting alternative for these energy storage from renewable sources [2].

Lead-acid batteries, like other types of batteries, are subject to a large number of degradation mechanisms that significantly reduce the capacity and lifetime of the batteries. Degradation mechanisms in accumulators are closely related to the materials used. In the case of improvement of one of the undesirable properties, there is usually a deterioration of other properties. One of the most significant degradation mechanisms are PCL phenomena (Premature Capacity Loss). Currently, the most problematic phenomenon is PCL 3. In the PCL 3 phenomenon, the negative electrode is sulfated. A fine layer of lead sulfate forms on the surface of the negative electrode, prevents the movement of ions and causes the battery capacity to decrease [3]. PCL 3 is also associated with the selective discharge of the negative electrode and reduction of lead acid battery cycles [4].

Experimental

The experiment focused on analyzing changes in the chemical composition on the surface of the negative electrode of a lead-acid battery using X-ray diffraction spectroscopy during discharge and charging at a rate of 0.3 C and 0.5 C. Lead electrodes were created for the experiment. A layer of active material was subsequently applied to the created electrodes. The composition of the active mass of the electrode with a total weight of 10 g shows Table 1. The electrode was then placed in a PEEK holder (semicrystalline thermoplastic). The electrode aged for 5 days in an environment close to 100% humidity. The total weight of the active material applied to the substrate was 0.82 g. Subsequently, the measured electrode was cycled in a sulfuric acid solution with a concentration of 27%. During charging, a current of -13.16 mA was supplied for 5 hours with a potential limitation of $E_M = -1.3$ V vs. MSRE (mercury sulfate reference electrode), during discharge, a current of 13.16 mA was supplied for 6 hours with a potential limitation of $E_M = -0.8$ V vs MSRE. A total of 20 formation cycles took place before the measurement.

Table 1. Exact composition of the active mass of the negative electrode

Ingredients	Quantity (g)
Lead powder	8.42
Demineralized water	0.92
Sulfuric acid	0.51
Borosilicate	0.02
Barium sulphate	0.13

The measurement took place in an aqueous sulfuric acid solution with a concentration of 33% in a three-electrode circuit. During the measurement, there was a gradual galvanostatic discharge of the electrode from a maximally charged state to a fully discharged state after a step of 20% SOC. The charging of the electrode also took place galvanostatically. At a rate of 0.3 C, a current of ± 31.43 mA was delivered during charging and discharging for 31 minutes with a limiting charging potential of $E_M = -1.3$ V vs. MSRE and during discharge $E_M = -0.8$ V vs. MSRE. At a rate of 0.5 C, a current of ± 47.15 mA was delivered during charging and discharging for 18 minutes with a limiting charging potential of $E_M = -1.3$ V vs. MSRE and during discharge $E_M = -0.8$ V vs. MSRE. At each of the discharge/charge states, the chemical composition on the electrode surface was measured using an X-ray diffractometer.

At a speed of 0.3 C, it was possible to observe (Figure 1. on the left) that in a fully charged and discharged state, there is a high amount of used material on the surface of the electrode, which does not change from lead to sulfate and vice versa during cycling of the negative electrode. During the discharge, it is possible to observe that the conversion of lead to sulfate occurred in the later stages of the discharge cycle. The fastest conversion of lead to lead sulfate on the electrode surface at a rate of 0.3 C was between 40% SOC and 20% SOC when the representation of metallic lead decreased by 10 mol. %. In contrast, during discharge, the decrease in the lead between 100% SOC and 80% SOC was only 3 mol. %. It can be seen from the graph that there was no significant deflection in the representation of Pb and PbSO₄ during the charging and discharging of the electrode, and the progression of the representation of individual elements on the surface of the electrode was almost linear.

At a speed of 0.5 C, it was possible to observe (Figure 1. on the right) a lower representation of the used material on the surface of the electrode, where there is no transformation from lead to lead sulfate and vice versa. Compared to the rate of 0.3 C, the used material was reduced by 5 mol. %. The increase in unused material indicates that at higher discharge and charge rates, the electrode is

not able to convert the used material quickly enough during cycling, and therefore the entire volume of the negative electrode is not effectively used. When discharging at a rate of 0.5 C, there was a more pronounced decrease in the lead between 80% and 60% SOC. Between 80 % and 60 % SOC there was a 10 mol. % decrease in the lead.

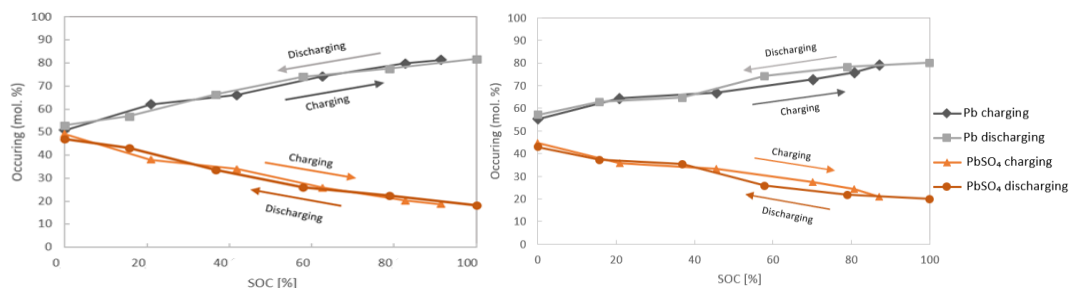


Figure 1. Chemical composition on the surface of the active mass of negative electrode at different SOC. On the left at a rate of 0.3 C and on the right at a rate of 0.5 C during cycling.

Conclusions

From the measured results, it can be observed that at a speed of 0.3 C, the amount of material that did not take part in the conversion during cycling reached almost 65 mol. %. At a speed of 0.5 C, there was a further increase of this material by another 5 mol. %. The increase in unused material indicates that at higher rates of discharge and charge, the electrode is not able to convert the used material quickly enough during cycling, and thus the entire volume of the negative electrode is not effectively used. The decrease in total capacity at increasing rates (0.3 C vs. 0.5 C) of electrode discharge was 13 percent. It follows from this behavior that with increasing discharge rates, there is a more pronounced material transformation near the collector of the negative electrode.

Acknowledgment

This work was supported by the specific graduate research of the Brno University of Technology No. FEKT-S-20-6206.

References

1. S. Jiang, A review on the state of health estimation methods of lead-acid batteries. *Journal of Power Sources* (2022)
2. Burheim, *Engineering Energy Storage. The Power Grid*. Elsevier (2017)
3. K. Nakano, *Furukawa Review*. Furukawa Electric (2007)
4. L. T. Lam, Influence of residual elements in lead on oxygen- and hydrogen-gassing rates of lead-acid batteries. *Journal of Power Sources* (2010)

The Effect of Additives Suppressing Dendritic Growth on the Recrystallization of ZnO Particles in the Alkaline Environment of Batteries

L. Chladil^a, J. Smejkal^{a,b} and O. Čech^a

^a Department of Electrotechnology, Faculty of Electrical Engineering and Communication, BUT, Technická 10, 616 00 Brno, Czech Republic

^b Central European Institute of Technology, BUT, Technická 10, 616 00 Brno, Czech Republic

Our contribution deals with a process of decomposition and recrystallization of alkaline supersaturated zincate solution (SZS) based on KOH and monitored the growth of zinc oxide crystals on a broad timescale. Decomposition of SZS is an important process taking place in the entire volume of supersaturated zincate solutions that are the mostly used electrolyte for Ni-Zn or Zinc-Air batteries. SZS is formed primarily at a short distance from the negative electrode during the fast discharging of zinc anode or an entire volume of electrolyte in the final stage of discharging. Our study pointed to important differences in recrystallization and growth process in presence of surfactants.

Introduction

An important investigation aspect in the field of Ni-Zn alkaline accumulators is the ability of effective suppression of zinc dendrite growth at charging when the dissolved tetrahedral zinc species are re-deposited from electrolyte onto the surface of the negative electrode current collector [1], [2]. Many different approaches to this challenge were investigated and most of them have begun taking the organic cationic, anionic, or nonionic surfactants that were identified to be effective in the dendrite growth inhibition. The presence of these surfactants on the one side can resolve this fractional problem but on the other side also can influence many other processes which have occurred in the Ni-Zn cells during battery operation. Whereas some of these processes as self-discharging, dendrite inhibition, or electrode passivation were studied in detail [3], the influence of these additives on the decomposition rate of supersaturated zincate solution (SZS) and also to recrystallization were neglected. The rate of the decomposition process is influenced by temperature, initial supersaturation concentration of zincate, the concentration of hydroxide (pH), and also by the presence of specific additives [4]. Concerning the last mentioned, for example, the study of SiO_3^{2-} additive effect on decomposition kinetics shows that SiO_3^{2-} causes complete inhibition of decomposition by its adsorption on the surface of ZnO. At decomposition firstly the formation of nuclei take place and follow these nuclei further grow into the final shape as the supersaturated concentration decrease. In some studies, it was concluded that the specific shape of ZnO crystal strongly influences the cyclability of negative electrodes. Also, many studies were focused on preparing specific shapes of ZnO particles by a hydrothermal synthesis method where organic additives such as CTAB, SDS, Starch, etc. were used to reach the appropriate particle shape. It would seem that the presence of dendrite inhibitors that are mostly organic ion-active substances could also influence the crystallinity of active materials of negative electrodes and thus influence also the cyclability of Ni-Zn or Zinc-air batteries. The use of any organic additives should be preceded by a study of how these additives affect the growth of ZnO crystals and how they affect the upcoming recrystallization processes.

Experimental

Supersaturated zinc solution with potassium hydroxide concentration 6 mol/l was prepared as follows – the necessary amount of potassium hydroxide was dissolved in approx. 10 ml of deionized water and then the zinc oxide was gradually dissolved and the solution was heated and mixed by a magnetic stirrer for 30 minutes. After reaching of fully clear and transparent solution with very high molality was then diluted to obtain 500 ml of supersaturated solution. The solution was dispensed to 100 ml sample containers and the surfactants were added to each container. Then the samples were placed in the climatic cell tempered to 30 °C. The concentration of solute zincate was continually measured by chelatometric titration and calculated by the following equation

$$\frac{V_{std}}{V_{titr}} * C_{chel} * M_{mZnO} = C_{ZnO} \quad (1)$$

Where V_{std} is the amount of titration standard (μ l), V_{titr} is the amount of analyzed sample (50 μ l), C_{Chel} is Chelaton III concentration (0,01 mol/l), M_{mZnO} is zinc oxide molar mass and C_{ZnO} corresponds to the final concentration of zinc oxide (g/l).

After long-term recrystallization (>2000 h), ZnO crystals were separated and undergo to SEM observation and BET analysis. Separation of ZnO crystals was performed using repeated washing with distilled water and centrifugation until the neutral pH of the washing solution was reached.

Results and discussion

Fig.1 shows the soluble ZnO concentration decrease over time. We can easily recognize the difference in concentration decrease based on the presence of different additives. Also, we can conclude, that presence of surfactant can increase or decrease the speed of decomposition rate of SZS. After 2000 h we performed the first crystal separation and undergo the ZnO particles to SEM and BET analysis.

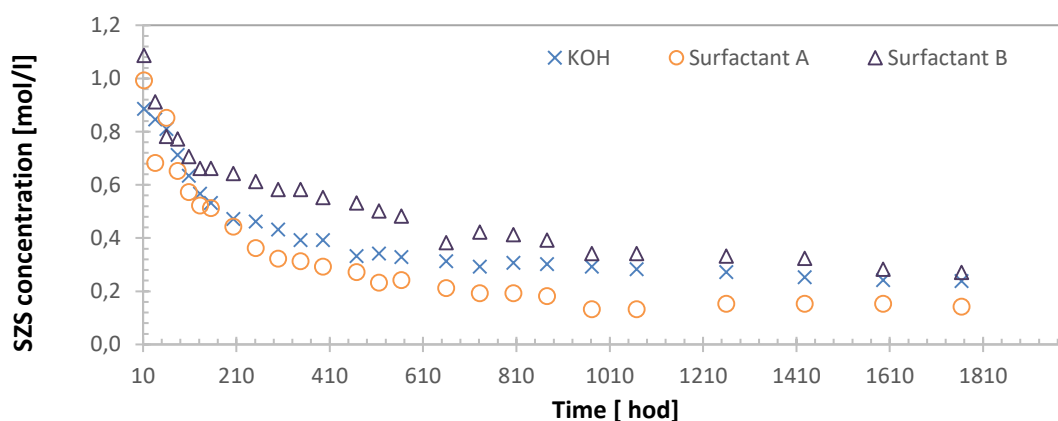


Figure 1. Evolution of supersaturated zincate concentration in the SZS during its decomposition for pure supersaturated solution ($6 \text{ mol/dm}^3 \text{ KOH} + \text{ZnO}$) and for solution with the addition of Surfactants A and B

Fig. 2 shows the obtained ZnO powder and we can see, that in the case of Surfactant A the precipitate ZnO crystals are in form of powder, and in detail, we can see the individual hexagonal ZnO particles that are the product of hexagonal wurtzite unit cell from $P6_3mc$ space group. The presence of surfactant B enabled the formation of a solid ZnO crust in which individual ZnO particles are fused into a solid layer. In this case, the particles have the shape which was determined by other crystals in the layer, and also the SEM images revealed the very low porosity of such system.

Electrochemical kinetics of high-performed electrode needs to ensure that all active mass is in good electronic contact with the current collector and also with good ionic contact with electrolyte. Solid crust form Fig. 2 b) is inconsistency with these requirements and thus we can expect the worse reaction kinetic in the system with Surfactant B, especially after a longer period of battery standing without operation.

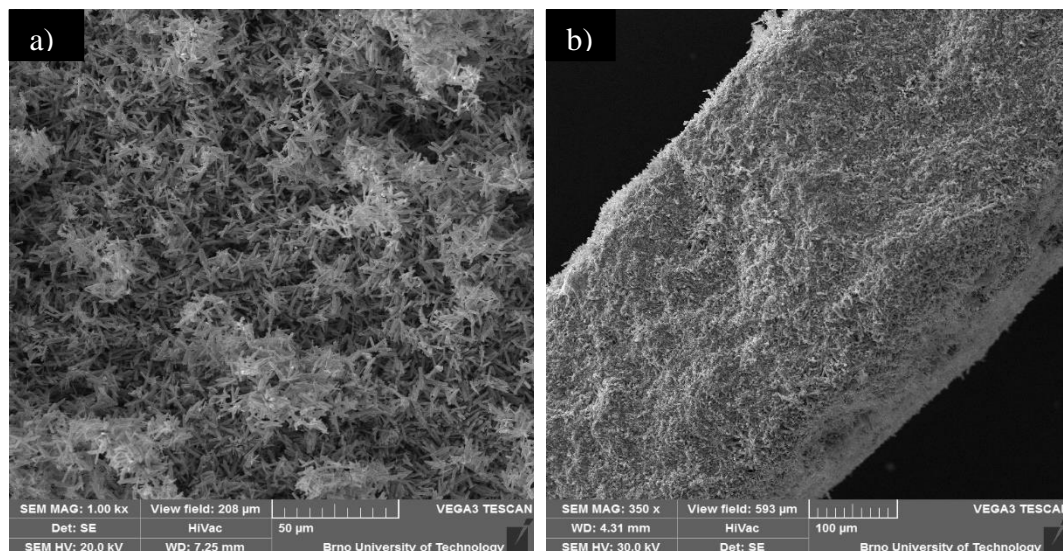


Figure 2. SEM images of precipitates of ZnO from SZS electrolyte with a) addition of Surfactant A, b) addition of Surfactant B

Conclusions

This study identifies the remarkable differences in process of decomposition and recrystallization and based on the experiment design we can conclude that these differences are affected by the presence of different organic additives. Presence of organic additives influence the decomposition rate and during the following recrystallization via Ostwald Ripening can prevent the formation of a compact electrode layer that could inhibit the electrode's kinetic and thus degrade the battery system.

Acknowledgement

This work was supported by the specific graduate research of the Brno University of Technology No. FEKT-S-20-6206.

References

1. J. Jindra, *J. Power Sources*, **66**, 15-25 (1997).
2. J. Jindra, *J. Power Sources*, **88**, 202-205 (2000).
3. L. Chladil, *J. Energy Storage*, **21**, 295-300 (2018).
4. C. Debiemme-Chouvy, *J. Electrochem. Soc.*, **138**, 9, 2538-2542 (1991).

Metal-Organic Frameworks as Suitable Matrices for Sulfur in Next-Generation Batteries

D. Capkova^a, T. Kazda^b, M. Almasi^c, J. Macko^a, N. Kiraly^c, O. Petrus^d, A. Strakova Fedorkova^a, V. Knap^e

^a Department of Physical Chemistry, Faculty of Sciences, Pavol Jozef Safarik University in Kosice, Kosice, Slovak Republic

^b Department of Electrical and Electronic Technology, Faculty of Electrical Engineering and Communication, Brno University of Technology, Brno, Czech Republic

^c Department of Inorganic Chemistry, Faculty of Sciences, Pavol Jozef Safarik University in Kosice, Kosice, Slovak Republic

^d Institute of Materials Research, Slovak Academy of Sciences, Kosice, Slovak Republic

^e Department of Electrotechnology, Faculty of Electrical Engineering, Czech Technical University in Prague, Prague, Czech Republic

As a new generation of energy storage systems, lithium-sulfur batteries are receiving significant attention due to their high theoretical capacity and energy density. The electrochemical properties of lithium-sulfur batteries may be improved by the application of appropriate conductive and porous additives to sulfur in the cathode material. Recently, materials belonging to the group of metal-organic frameworks have been widely studied as host materials for sulfur due to their unique porous structure. In this work, various types of metal-organic frameworks were applied in the cathode material. Moreover, metal-organic frameworks were carbonized in order to improve the electrochemical properties of the electrode material.

Introduction

The dynamic development of modern society has created a high energy demand, especially for portable electronic devices, the automotive industry, and aerospace. The main challenge is how to store electric energy effectively and safely (1, 2). Rechargeable lithium-ion (Li-ion) batteries have become indispensable energy storage devices due to their high safety (3). However, their specific energy density based on the intercalation process is insufficient for future applications. As an alternative, the conversion mechanism of lithium-sulfur (Li-S) batteries became the target of intensive research. Li-S batteries are considered a candidate for next-generation energy storage systems due to their high theoretical energy density (2600 Wh kg⁻¹), low sulfur cost, and environmental compatibility (4-6). However, their practical application is hindered by several issues. A volumetric expansion of sulfur during charging is up to 80 % which can cause a reduction in contact between different parts of the cathode. Another challenge is the polysulfide shuttle. The higher polysulfides (Li₂S₈, Li₂S₆, Li₂S₄) are soluble in the electrolyte and can migrate to the anode side. They can reduce to lower polysulfides (Li₂S₃, Li₂S₂) which can migrate back to the cathode, this process describes the polysulfide shuttle (7, 8). Above mentioned shortcomings lead to the loss of active material, decline in specific capacity, and decrease in Coulombic efficiency (9).

Various strategies have been proposed in order to alleviate the aforementioned issues. The reduction of shortcomings may be achieved by the application of conductive material with a large surface area and desirable pore size distribution. As cathode materials have been investigated porous carbon materials (6), carbon nanotubes (10), or graphene (11). Nevertheless, the non-polar nature of carbon materials provides a weak affinity for polysulfides, they can only operate as a physical barrier against the diffusion of polysulfides. Therefore, polar materials such as metal-organic frameworks (MOFs) are needed to arrange chemical interactions to entrap polysulfides (12).

In this work, various MOF materials are tested as support for sulfur in Li-S batteries. MOFs have different structures and organic linkers are connected via different metal ions. The structure of activated MOF-76(Gd) showed the lowest capacity fade per cycle despite 50 cycles during multi-current testing. In an effort to improve the electrochemical properties, MOFs were carbonized. It was proven, that the carbonization process of MOF enhanced its properties and the electrode material showed highly stable cycle performance. Overall, the best electrochemical properties, the highest discharge capacities, and stable cycle performance showed carbonized MOF-76(Gd).

Experimental

Two different MOFs in an activated form and a carbonized form were tested as hosts for sulfur in Li-S batteries. Microporous materials MOF GaTCCP with chemical formula $\{[\text{Ga}_2(\text{H}_2\text{TCCP})(\text{OH})_2] \cdot 5\text{DMF} \cdot 2\text{H}_2\text{O}\}_n$ and MOF-76(Gd) with an exact chemical formula $[\text{Gd}(\text{BTC})(\text{H}_2\text{O})] \cdot \text{DMF}$ were analyzed in an activated state. MOF-76(Gd) and MIL-101(Fe)-NH₂ ($\{[\text{Fe}_3(\mu_3\text{-O})(\mu_4\text{-BDC-NH}_2)_3(\text{H}_2\text{O})_2\text{Cl}] \cdot \text{G}\}_n$ (G = a guest molecule)) were studied in a carbonized form. The composition of the cathode material was 60 % of sulfur, 15 % MOF, 15 % carbon Super P, and 10 % polyvinylidene fluoride (PVDF) as a binder.

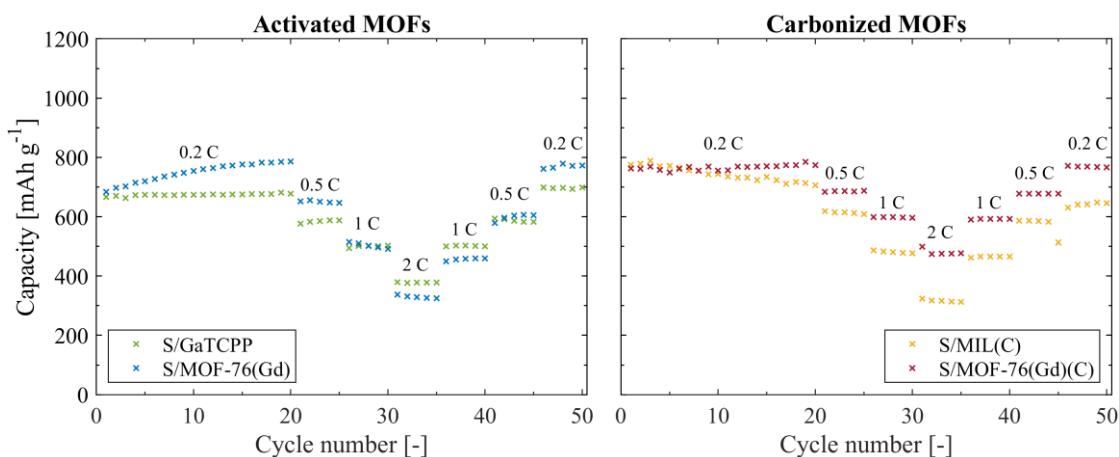


Figure 1. Galvanostatic cycling of different activated and carbonized MOFs at various C-rates.

Conclusions

Various MOF materials have been analyzed as a matrix for sulfur in Li-S batteries. Comparatively, high initial discharge capacities were observed for the MOF-76 and GaTCCP materials (684 and 667 mAh g⁻¹ at 0.2 C). After 50 cycles, the highest discharge capacity was observed for MOF-76(Gd), although the capacity at 2 C was higher for GaTCCP. Another approach

of this work is the improvement of the electrochemical properties by the carbonization process. The enhancement of the properties was demonstrated by the carbonization of MOF-76(Gd), wherein in an activated form the initial discharge capacity at 0.2 C was 684 mAh g⁻¹ and in a carbonized form the capacity increased up to 763 mAh g⁻¹. Moreover, carbonized MIL-101(Fe)-NH₂ was also applied in cathode material for Li-S batteries. The S/MIL electrode achieved a similar initial discharge capacity to S/MOF-76(Gd)(C). However, MOF-76(Gd) showed highly stable cycle performance with the highest discharge capacity after 50 cycles.

Acknowledgments

This research was sponsored by the following projects: APVV-20-0138, Development of Novel 3D Materials for Post Lithium Ion Batteries with High Energy Density; APVV-20-0111, Towards Lithium Based Batteries with Improved Lifetime; iCoTS No. 313011V334, Innovative Solutions for Propulsion, Power and Safety Components of Transport Vehicles; VEGA 1/0074/17, Nanomaterials and Nanostructured Layers with Specific Functionality, VEGA 1/0294/22, Porous Coordination Polymers for Environmental Applications, and specific graduate research of the Brno University of Technology No. FEKT-S-20-6206.

References

1. Y. Zheng, S. Zheng, H. Xue and H. Pang, *Journal of Materials Chemistry A*, **7**, 3469–3491 (2019).
2. V. Knap and D.-I. Stroe, *Journal of Power Sources*, **498**, 229913 (2021).
3. Z. Yu, H. Wang, X. Kong et al., *Nature Energy*, **5**, 526 – 533 (2020).
4. D. Capkova, T. Kazda, O. Cech et al., *Journal of Energy Storage*, **51**, 104419 (2022).
5. T. Kazda, D. Capkova, K. Jasso et al., *Materials*, **14**, 5578 (2021).
6. D. Capkova, T. Kazda, A. Strakova Fedorokova, *ECS Transactions*, **95**, 19-26 (2019).
7. D. Capkova, T. Kazda, P. Cudek and A. Strakova Fedorokova, *ECS Transactions*, **99**, 161-167 (2020).
8. D. Capkova, T. Kazda, M. Almasi et al., Proceedings of the International Astronautical Congress, C3 (2021).
9. D. Capkova, M. Almasi, T. Kazda et al., *Electrochimica Acta*, **354**, 136640 (2020).
10. G. Ma, Z. Wen, Q. Wang et al., *Journal of Power Sources*, **273**, 511 (2015).
11. M.Q. Zhao, Q. Zhang, J.Q. Huang et al., *Nature Communications*, **5**, 3410 (2014).
12. W. Yao, W. Zheng, J. Xu et al., *ACS Nano*, **15**, 7114-7130 (2021).

Engineering of the Composite Cathode for Li-sulfur Battery

M. Zukalová, M. Vinarčíková, B. Pitňa Lásková and L. Kavan

J. Heyrovský Institute of Physical Chemistry, v.v.i., CAS, Dolejškova 3, Prague 8, Czech Republic

The influence of different carbonaceous oxide additives on the performance of sulfur/composite cathode in Li-sulfur battery was studied by cyclic voltammetry. The external surface area was found to be the decisive parameter for the performance of carbonaceous additives. The additional TiO₂ top layer significantly increases the charge capacity of the corresponding Li-sulfur battery due to efficient polysulfide adsorption. TiO₂ exhibits inherent electrochemical activity for sulfur reduction at potentials negative to the flat band potential. The impregnation of a glass microfiber separator with TiO₂ further hinders the diffusion of Li polysulfides to the anode compartment of the battery and improves the electrochemical performance of sulfur composite cathode containing both kinds of activated carbon.

The rechargeable lithium-sulfur battery is regarded as a promising next-generation electrochemical energy storage device, due to the high theoretical capacity (1675 mAh/g) of sulfur, as well as the abundance, low cost, and eco-friendliness of elemental sulfur(1). Nevertheless, the electrochemical stability and commercial application of Li-S batteries are inhibited by the insulative sulfur and Li₂S/Li₂S₂, the shuttling effect in the electrolyte, and significant volume change(2). Non-conductivity of sulfur requires the incorporation of electron-conductive additive and volume changes accompanying polysulfide formation represent a challenge for cathode architecture. In particular, the use of carbonaceous materials (including carbon nanotubes(3, 4), graphene derivatives(5, 6), and calcined carbon materials) with various structural motifs has been demonstrated to enhance the performance of sulfur-based cathode composites.

In our work, we studied the effect of the morphology of the carbonaceous additive on the charge capacity and cycling stability of the Li-sulfur battery. We found that the external surface area of activated carbon represents the decisive parameter for the performance of the carbon/sulfur composite cathode(7). The presence of metal oxide slightly increases the charge capacity of the composite sulfur cathode, but this effect correlates neither with their BET surface area nor chemical composition. Additional TiO₂ top layer on the carbon/sulfur composite cathode increases substantially charge capacity and cycling stability of the Li-sulfur battery due to effective PS localization in the cathode compartment of the battery. In addition, TiO₂ exhibits inherent electrochemical activity for sulfur reduction at potentials negative to the flat band potential(8). The impregnation of a glass microfiber separator with TiO₂ further hinders the diffusion of polysulfides to the anode compartment of the battery and improves the electrochemical performance of the sulfur composite cathode. The composite cathode containing mesoporous carbon with a large external surface area, and an additional TiO₂ top layer in the Li-sulfur battery with TiO₂ modified separator provided a charge capacity of 1427 mAh/g, which represents a 75% increase as compared to the system without the top layer and modified separator.

Acknowledgment

This research was funded by the Grant Agency of the Czech Republic (contract No. 20-03564S).

References

1. R. Yan, M. Oschatz and F. Wu, *Carbon*, **161**, 162 (2020).
2. L. Zhang, W. Zhao, S. Yuan, F. Jiang, X. Chen, Y. Yang, P. Ge, W. Sun and X. Ji, *J Energy Chem*, **60**, 531 (2021).
3. S. Xin, L. Gu, N. H. Zhao, Y. X. Yin, L. J. Zhou, Y. G. Guo and L. J. Wan, *J Am Chem Soc*, **134**, 18510 (2012).
4. Y. P. Huang, X. G. Sun, J. Wang, X. Li, W. Chen, C. C. Wei, H. Hu and G. D. Liang, *J Alloy Compd*, **776**, 187 (2019).
5. J. Kim, Y. Kang, S. W. Song and J. Suk, *Electrochim Acta*, **299**, 27 (2019).
6. R. Yi, C. Liu, Y. Zhao, L. J. Hardwick, Y. Li, X. Geng, Q. Zhang, L. Yang and C. Zhao, *Electrochim Acta*, **299**, 479 (2019).
7. M. Zúkalová, M. Vinarciková, M. Bousa and L. Kavan, *Nanomaterials* **11** (2021).
8. M. Zlámalová, B. Pitňa Lásková, M. Vinarčíková, M. Zúkalová and L. Kavan, *J Solid State Electrochem*, **26**, 639 (2022).

Gel Polymer Electrolyte With Nanoparticles And 2D Materials As Fillers For Lithium Sulfur Batteries

C. Calderón^a, J. Amici^b, D. Versaci^b, M.L. Para^b, E. Leiva^c, C. Francia^b, S. Bodoardo^b and A. Visintin^d

^a Facultad de Matemática, Astronomía, Física y Computación, Universidad Nacional de Córdoba, Instituto de Física Enrique Gaviola, Córdoba 5000, Argentina

^b Politecnico di Torino, Department of Applied Science and Technology, Electrochemistry Group, Turín 10129, Italia

^c Facultad de Ciencias Químicas, Universidad Nacional de Córdoba, Instituto de Investigaciones en Fisicoquímica de Córdoba, Córdoba 5000, Argentina

^a Facultad de Matemática, Astronomía, Física y Computación, Universidad Nacional de Córdoba, Instituto de Física Enrique Gaviola, Córdoba 5000, Argentina

Gel polymer electrolytes (GPE) are a very promising strategy for using lithium metal anodes safely and avoiding shuttle effect in lithium sulfur batteries. These electrolytes are formed by liquid electrolyte embedded in a polymeric matrix. In this work a methacrylate-based polymer is used as a matrix and inorganic fillers were added to improve mechanical and conductive properties and to improve the performance as electrolyte for lithium metal and sulfur batteries.

Discussion

Lithium metal anode represents the “holy grail” of battery research for its extremely high theoretical specific capacity (3860 mA h g^{-1}), its lowest redox potential (-3.04 V vs. the standard hydrogen electrode), and low gravimetric density (0.534 g cm^{-3}). On the other hand, metallic Li being thermodynamically unstable in all liquid electrolytes immediately forms a solid-electrolyte interphase (SEI) when immersed into electrolyte [1]. An ideal SEI should inhibit the further reaction between Li and electrolytes and suppress the Li dendrite formation. However, spontaneously formed SEI is fragile and heterogeneous with variable spatial resistance, which induces uneven Li-ions flow, random Li deposition underneath and formation of high surface area lithium (HSAL) [1]. Li-S technology is expected to achieve 2-3 times higher (about 2600 Wh kg^{-1}) energy density than the actual LIBs, thanks to the particular chemistry of the system through the formation of lithium polysulfides (LiPSs) intermediates [2].

A solution to these problem is the use of a solid electrolyte with a very high Young's modulus to efficiently block HSAL formation [3] and with capability to trap LiPSs [4]. Solid polymeric electrolytes (SPE) are an alternative that is being widely investigated since their softness compared to ceramic improves the contact with the electrode surface [5]. GPE are formed from the absorption of liquid electrolyte in a polymeric matrix, they generally have higher ionic conductivity than solid polymeric electrolytes. Secondly, polymer electrolytes allow to use several additives to improve their properties. Inorganic fillers are added to different polymer-based electrolyte forming composite polymer electrolytes to improve mechanical strength and ionic conductivity [6]. Particularly 2D nanomaterials have attractive properties originating from their ultrathin structure

with a high degree of anisotropy and chemical functionality [7]. In this work we present the preparation of a methacrylate-based polymer matrix, in a solvent-free, thermally induced radical polymerization, encompassing ZrO₂ nanoparticles (NPs), g-C₃N₄ and h-BN. Polymers were activated with liquid electrolyte to form GPE with inorganic fillers and tested in lithium metal cells.

Butyl methacrylate (BMA) was used as monomer, with crosslinking agent polyethylene glycol diacrylate and high-purity monoclinic ZrO₂ NPs, g-C₃N₄ and h-BN were added as fillers, since ZrO₂ is well known for its high dielectric constant [8]; and 2D materials have proven to effectively decrease HSAL formation and to trap polysulfides. Polymer matrix were synthesized using a thermo-initiated, solvent-free, free radical polymerization. We were able to obtain crosslinked composite polymer containing up to 80 wt% of ZrO₂ NPs with optimal mechanical properties. The membrane containing the optimized content of 63 wt% of additive showed the best electrochemical properties with a high ionic conductivity and a high tLi⁺ number, confirming its ability to limit ionic concentration gradients in the electrolyte. 2D materials g-C₃N₄ and h-BN were added due their capacity to avoid HSAL formation [9] and to trap LiPSs [7].

Acknowledgments

The authors wish to thank the POLAR project (progetto per l'internazionalizzazione della ricerca tra Politecnico di Torino e Argentina, prof Silvia Bodoardo) and ARTIC project (ARgenTina-Italia Colaboration MINCYT-MAECI, prof Arnaldo Visintin) for the funding.

References

1. H. Yang, C. Guo, A. Naveed, J. Lei, J. Yang, Y. Nuli, J. Wang, *Energy Storage Mater.* **14** 199–221 (2018).
2. L. Borchardt, M. Oschatz, S. Kaskel, Carbon Materials for Lithium Sulfur Batteries - Ten Critical Questions, *Chem. - A Eur. J.* **22** (2016) 7324–7351
3. Y. Wang, E. Sahadeo, G. Rubloff, C.F. Lin, S.B. Lee, *J. Mater. Sci.* **54** 3671–3693 (2019).
4. Q. Yang, N. Deng, J. Chen, B. Cheng, W. Kang, *Chem. Eng. Journal* **413**, 127427 (2021).
5. Q. Zhang, K. Liu, F. Ding, X. Liu, *Nano Res.* **1** 1–36 (2017).
6. J. Amici, C.A. Calderón, D. Versaci, G. Luque, D. Barraco, E. Leiva, C. Francia, S. Bodoardo, *Electrochim. Acta* **404** 139772 (2022).
7. D. Versaci, M. Cozzarin, J. Amici, C. Francia, E.P.M. Leiva, A. Visintin, S. Bodoardo, *App. Mater. Today* **25** 101169 (2021).
8. P.K. Alaboina, S. Rodrigues, M. Rottmayer, S.J. Cho, *ACS Appl. Mater. Interfaces* **10** 32801–32808 (2018).
9. X. Luan, C. Wang, X. Gu, J. Yang, Y. Qian, *ACS Appl. Mater. Interfaces* **12**, 11265–11272 (2020).

Promising Anode Materials for Sodium-ion Batteries – Sodium Titanates

O. Čech^a, T. Kazda, L. Chladil^a, P. Čudek

Department of Electrical and Electronic Technology, Faculty of Electrical Engineering and Communication, BUT, Technická 10, 616 00 Brno, Czech Republic

Sodium-ion batteries are very promising complementary power sources usable in applications where cost of starting materials and battery itself is more important than its energy density. Sodium titanates with different crystallographic phases and stoichiometry ration were synthesized by hydrothermal reaction followed by high temperature treatment. Energy storage properties were investigated using common electrochemical methods. Structural characterization was performed mainly by XRD and SEM.

Introduction

The Sodium-ion batteries are very promising complementary power sources to the lithium-ion batteries because they utilize the same principles and technology. At the cost of lower energy density, they can potentially offer solid energy storage system without the need of rarer elements – mostly lithium. Sodium is abundant element, it occupies 2.6 % of the Earth's crust and which is extremely easy to obtain.

The general sodium-ion battery working principle and it same as the well-known and described lithium-ion technology, which can significantly increase interest in their research use. Main drawbacks of sodium-ion technology lies in the fact, that no sufficient anode material, cheap, durable and with high energy density. Titanates, especially the monoclinic $\text{Na}_2\text{Ti}_3\text{O}_7$ with layered structure, are promising candidates due to very low intercalation potential of Na^+ ions.

This work is focused on the synthesis and electrochemical characterization of electroactive material for sodium ion battery anode based on sodium titanates with different crystallographic phases and Na/Ti/O stoichiometry

Experiment

Sodium titanate samples were prepared by microwave assisted hydrothermal reaction. Titanium isopropoxide (CAS 546-68-9), sodium hydroxide and hydrogen peroxide were used as the starting precursors. Hydrothermally treated precipitate was washed intensively by centrifugation and then calcined at temperatures 700 °C, 800 °C and 900 °C respectively. The purity and crystallographic composition of the samples were examined by XRD and the morphology was observed by SEM. Electrochemical behavior was studied by cyclic voltammetry and galvanostatic cycling. All measurements were performed in three-electrode cells with metallic sodium as the counter and the reference electrodes. 1 mol/l NaClO_4 in the mixture of ED:DMC was used as an electrolyte.

Results and discussion

Figure 1 shows the SEM images of pristine hydrothermally treated sample and samples prepared at 700°C, 800°C and 900°C respectively. The raw material shows foamy turbostatic structure unlike the calcined materials are crystalline consisting of nanorod-shaped crystals. The size of the crystals differs significantly with temperature applied in final calcination where higher temperature gains crystals with same length but higher diameter. All the samples were cooled down naturally at the end of the calcination and the difference in crystal size can be caused by different cooling time.

XRD data depicted at Figure 4 show that calcination below the temperature of 800 °C does not produce result with purely two desired phases but residual peaks from raw hydrothermally treated powder are still present. The phase composition of samples prepared at 800°C and 900°C does not change with temperature but on the other hand, the SEM images revealed that at temperatures higher than 800 °C the thickness of the crystallites grows rapidly. Under these conditions, sample prepared at 800 °C with crystallographic composition of 42% $\text{Na}_2\text{Ti}_3\text{O}_7$ to 58% $\text{Na}_2\text{Ti}_6\text{O}_{13}$ was selected for further electrochemical characterization by electrochemical impedance spectroscopy, cyclic voltammetry and galvanostatic cycling.

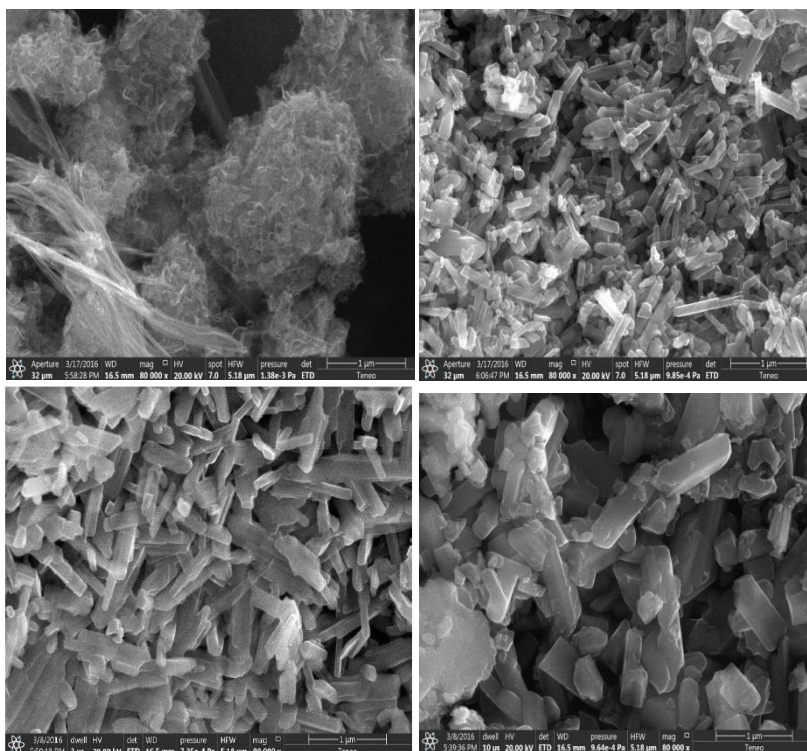


Figure 1. SEM images of hydrothermally synthesized $\text{Na}_2\text{Ti}_3\text{O}_7/\text{Na}_2\text{Ti}_6\text{O}_{13}$ mixed titanate showing a) pristine material after hydrothermal treatment b) calcination at 700 °C c) calcination at 800 °C d) calcination at 900 °C.

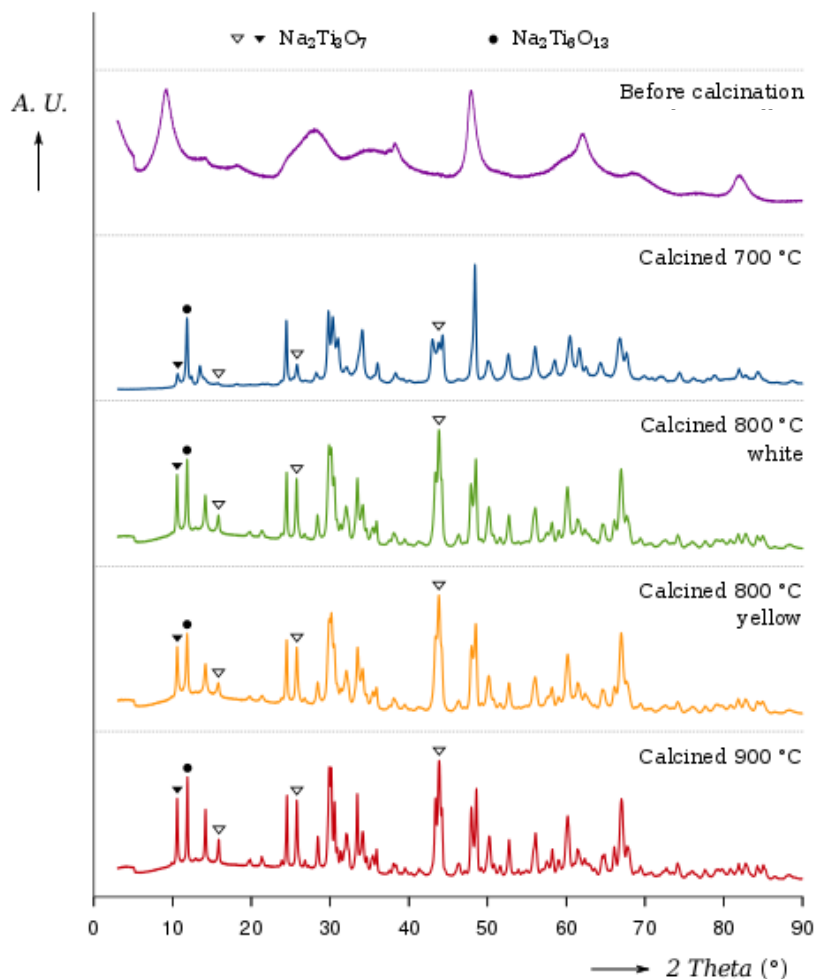


Figure 2. XRD spectra of raw and calcined hydrothermally treated titanate

Cyclic voltammetry shows two peaks at both oxidation and reduction parts. It was shown previously (2) that each peak corresponds to the intercalation into a different crystallographic phase occurring in the sample. Voltammograms captured at scan rate 2mV/s depicted on Figure 5 exhibit very good stability, it is obvious that the material undergoes formation until it reaches stable state. It is also clearly shown that there is a significant change between the first and the rest of the cycles pointing to irreversible capacity. Figure 6 shows cyclic voltammograms performed at 0.1 mV/s and there is some increase of peak currents also apparent between the first and the second cycle. The lower peak at 0.3V at anodic direction splits into two separate peaks at the lower scan rate showing possible surface activity and pseudocapacitive behaviour of the sample in this region (3).

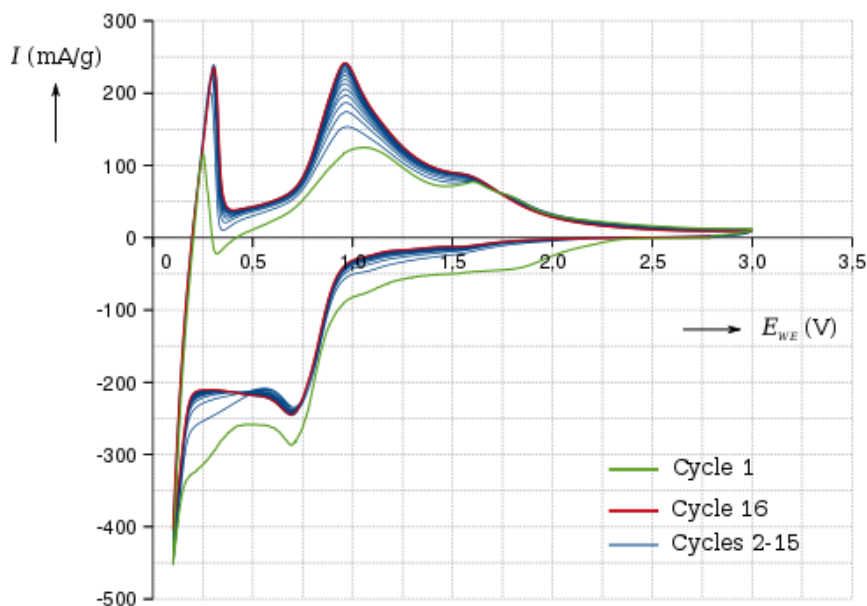


Figure 3. Cyclic voltamogram of $\text{Na}_2\text{Ti}_3\text{O}_7/\text{Na}_2\text{Ti}_6\text{O}_{13}$ mixed sample prepared at 800°C gathered at 2mV/s

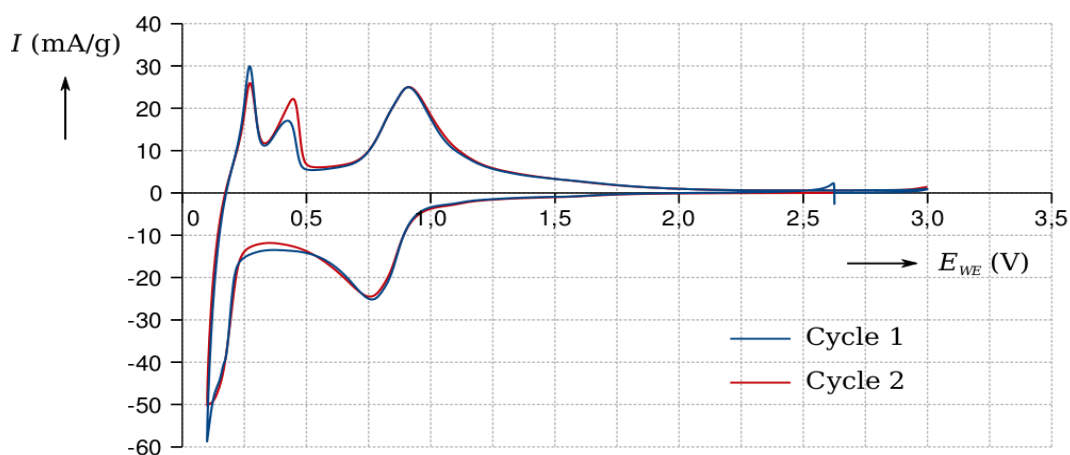


Figure 4. Cyclic voltamogram of $\text{Na}_2\text{Ti}_3\text{O}_7/\text{Na}_2\text{Ti}_6\text{O}_{13}$ mixed sample prepared at 800°C gathered at 0.1mV/s

Initial charge capacity of the sample at the rate of C/50 was 160 mAh/g with discharge capacity of 90 mAh/g . It indicates high irreversible capacity in the first cycle, as shown in Figure 7 but such result can be also given by extremely low current rate in the first cycle.

Figure 8 is a graph showing another 4 cycles obtained at the discharge rate of C/5 with stable discharge capacity of 65 mAh/g .

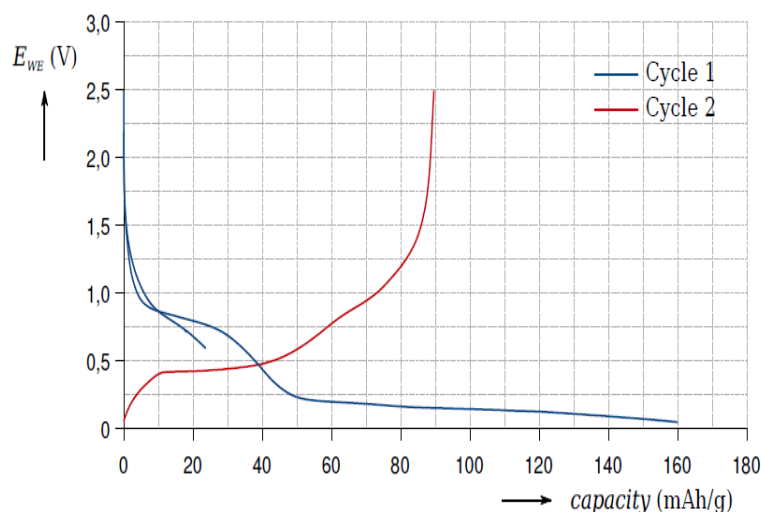


Figure 5. First charge/discharge cycle at low current rate (0.02C)

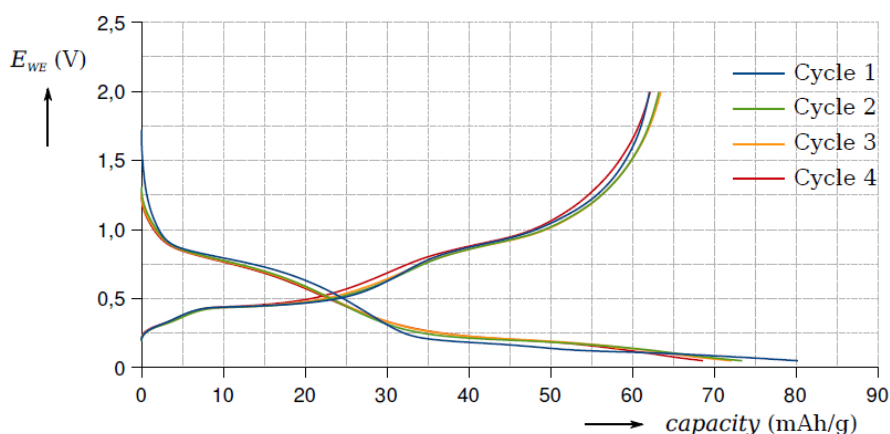


Figure 6. Four charge/discharge cycles of mixed titanate with current rate 0.2 C

Conclusion

Nanostructured sodium titanate with mixed stoichiometry was successfully synthesized by calcination of hydrothermally treated pristine titanate. Structural characterization showed that the powder calcined at 800 °C consists of nanorods less than 1 μm long with diameter less than 100 nm. Phase composition was 42 % of $\text{Na}_2\text{Ti}_3\text{O}_7$ and 58 % of $\text{Na}_2\text{Ti}_6\text{O}_{13}$ as was examined by XRD.

Electrochemical activity with respect to reversible intercalation of sodium ions was also proven. The results of the cyclic voltammetry show stable material undergoing further formation during cycling. Initial discharge capacity at the first cycle was 90 mAh/g at C/50 and at further cycling applied C/5 the material exhibit capacity 65 mAh/g .

Acknowledgments

CzechNanoLab project LM2018110 funded by MEYS CR is gratefully acknowledged for the financial support of the measurements/sample fabrication at CEITEC Nano Research Infrastructure. This work was supported by the specific graduate research of the Brno University of Technology No. FEKT-S-20-6206.

Effect of Structure and Morphology of Titanium Dioxide on Electrochemical Characteristics of Lithium-Sulfur Batteries

N. I. Globa^a, V. A. Sirosh^a, Yu. V. Shmatok^a, T. V. Lisnycha^a, S. A. Kirillov^a

^a Joint Department of Electrochemical Energy Systems,
38A Vernadsky Ave., Kyiv 03680, Ukraine

Lithium-sulfur batteries are among the most researched electrochemical systems, not least due to the high theoretical specific capacity of sulfur (1672 mAh/g). However, the problems of their practical implementation and prevention of self-discharge process continue to be in the focus of attention of researchers and developers.

One way to improve the specific electrochemical characteristics of lithium-sulfur batteries is to use synergistic effects based on the combined use of sulfur and additives of compounds containing polar groups. This allows the sulfur discharge/charge products to be retained in the electrode structure. The simultaneous combination of the effective electrolyte composition and the composite electrode makes it possible to stabilize the specific capacity during cycling, increase the sulfur utilization ratio and discharge/charge Coulombic efficiency.

It is known that LiNO₃ is one of the effective additives to electrolyte ensuring the formation of a stable solid electrolyte film (SEI) on the surface of the lithium electrode. This avoids the so-called shuttle effect and the associated decrease in specific capacity. The second important factor capable of increasing the specific capacity and its cycling stability is the nature of the composite electrode components. Traditionally used carbon additives increase the electrical conductivity of sulfur electrode, but are not able to retain polysulfides in the electrode structure due to the low polarity of their molecules. In this regard, it is proposed to use oxides of transition metals along with the addition of carbon in the composition of sulfur electrodes. Titanium dioxide (TiO₂) is considered as one of the effective additives. However, the effect of the structure, specific surface area and porosity of TiO₂ on the characteristics of sulfur electrodes in lithium batteries continues to be discussed.

In our work, we present the results of studies of sulfur-titanium dioxide (S-TiO₂) composite electrodes in electrochemical cells with a lithium anode. The influence of TiO₂ additives on the capacitive and cyclic characteristics of sulfur cathodes was determined taking into account their structure and surface properties.

TiO₂ with rutile and anatase structure have been used as additives to electrode. The selected oxides differed in structure, particle size, specific surface area, pore volume and porosity. These differences were achieved by different modes of thermal treatment and synthesis conditions. The characteristics of TiO₂ samples used are given in Table I.

TABLE I. Surface characteristics of TiO₂ powders.

Type of TiO ₂	Specific surface area, m ² /g	Pore radii, nm	Pore volume, cm ³ /g
Anatase 350	174	2.2	0.264
Anatase 470	80	2.8	0.154
Rutile 150	204	1.7	0.25
Rutile 400	82	8.2	0.33

The study of S-TiO₂ composite cathodes was carried out in 2016 coin cells. The electrodes consisted of 70 % mixture of elemental sulfur and TiO₂ (in mass ratio 8:2), 10 % Super P, 10 %

graphite and 10 % PVDF. A slurry was applied to an aluminum foil (50 μm) using a doctor blade. The mass of sulfur in cathodes was 1.8–1.9 mg/cm^2 (total electrode surface 2 cm^2). For research, two compositions of electrolytes differ in their physico-chemical characteristics were taken, namely a salt-solvate electrolyte containing 0.4 mol fractions of lithium trifluoromethanesulfonimide $\text{LiN}(\text{CF}_3\text{SO}_2)_2$ in tetraethylene glycol dimethyl ether (TG) and a diluted electrolyte comprising 1 M solution of $\text{LiN}(\text{CF}_3\text{SO}_2)_2$ in a 1:1 mixture of TG and dioxolane (DOL) with the addition of 0.3 M LiNO_3 .

The dependences of specific capacity of sulfur on cycle number in two electrolyte solutions are shown in Figure 1. In both electrolytes used, the addition of TiO_2 changes the value of the specific capacity of sulfur. The efficiency of TiO_2 addition depends on the structure of TiO_2 and electrolyte composition. As one of the reasons for the observed effect, the influence of the size and morphology of TiO_2 particles on the properties of the porous structure of composite electrodes can be considered. However, this assumption requires further research.

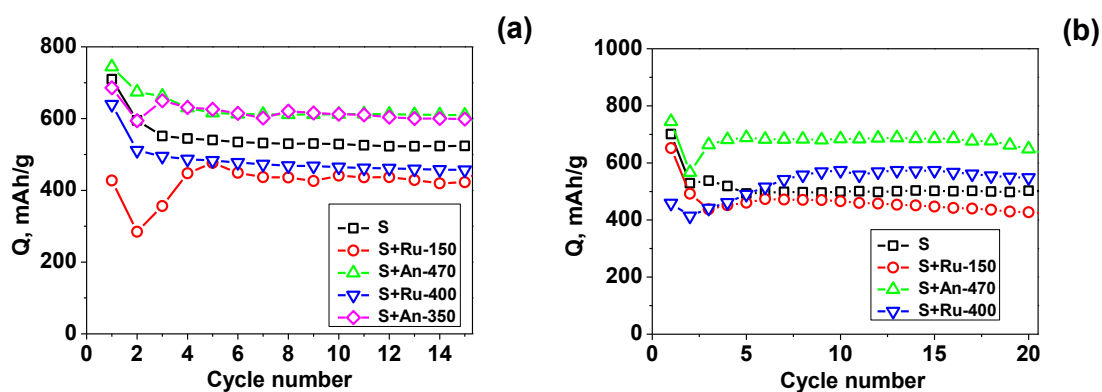


Figure 1. The dependences of specific capacity of sulfur on cycle number during cycling (a) in salt-solvate electrolyte at current density of 0.1 mA/cm^2 and (b) in diluted electrolyte solution at current density of 0.2 mA/cm^2 .

Sulfur/Polypyrrole Cathode Material For Lithium Sulfur Battery

V. Niščáková^a, A.S. Fedorková^a

^a Department of Physical Chemistry, Faculty of Science, P.J. Šafarik University in Košice, Moyzesova 11, 041 54, Košice

In recent years, there has been a huge increase in the development of modern intelligent electronic devices and the modernization of transport in the field of electromobility, which is leading to a huge demand for high-performance battery systems with high energy density [1,2]. The currently used lithium-ion batteries do not sufficiently meet the conditions required for modern equipment. Elemental sulfur as a new potential electrode material is gradually attracting more attention from researchers due to its high theoretical specific capacity of 1675 mAh g⁻¹ and theoretical energy density of 2600 Wh kg⁻¹. This new type of secondary battery has many advantages as abundant resources, nontoxicity, low cost, and environmental friendliness. However, Li-S batteries also suffer from certain shortcomings such as the insulating nature of sulfur, volume changes during charging and discharging, which exert strong pressure on the integrity of the cathode with rapid loss of active materials and the last solubility of polysulfide intermediates in the electrolyte resulting in reduced Coulomb efficiency and cycling stability [2,3].

Research to prevent these imperfections uses several methods to address these barriers to support LSB's electrochemical performance. Most research focuses on sulfur modification with various types of conductive polymers and carbon materials, such as polypyrrole (PPy), mesoporous carbon, carbon graphene nanotubes, etc. These materials can significantly improve the conductivity and cyclic stability of the sulfur electrode and reduce the high solubility of polysulfides in the electrolyte [2]. Compared to the widely reported carbon-based materials and metal compounds, conducting polymers have received little attention in the field of Li-S batteries. Conductive polymers can be used in Li-S batteries as coatings, conductive host cells, separator modifiers / functional interlayers, and binders. For example, after coating with conductive polymer layers, the conductivity of sulfur cathodes is improved, while the diffusion and shuttling of lithium polysulfides are also suppressed effectively [4].

In this work, a positive electrode containing polypyrrole was prepared for a Li-S battery having the following composition of 90% S/C/ppy composite and 10% PVDF (polyvinylidene fluoride as a binder). The prepared electrode was tested by various electrochemical procedures such as cyclic voltammetry, and galvanostatic cycling. The cycling took place in the range of potentials from 1,8 V - 2,8 V. The initial discharge capacity of the prepared electrode at 0.1 C was around 753 mAh g⁻¹. After 20 cycles at 0,2 C discharge capacity decreased from 711 mAh g⁻¹ to 694 mAh g⁻¹.

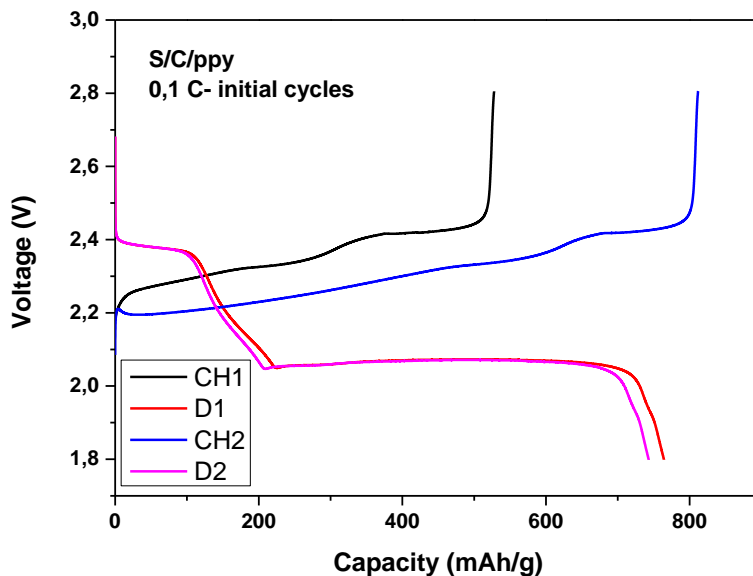


Figure 1. Initial Charge/discharge curves of S/C/ppy composite at 0,1 C

Acknowledgments

This publication was supported by the Operational program Integrated Infrastructure within the project: Innovative Solutions for Propulsion, Power and Safety Components of Transport Vehicles, 313011V334, cofinanced by the European Regional Development Fund and of the Slovak Research and Development Agency APVV-20-0138 and APVV-20-0111 and by VVGS UPJS project no. 2022-2193.

References

1. L. Huang, J. Li, B. Liu, Y. Li, S. Shen, S. Deng, C. Lu, W. Zhang, Y. Xia, G. Pan, X. Wang, Q. Xiong, X. Xia, J. Tu, *Electrode Design for Lithium–Sulfur Batteries: Problems and Solutions*, 1–30, *Adv. Funct. Mater.* 30 (2020).
2. P. Xin, B. Jin, H. Li, X. Lang, C. Yang, W. Gao, Y. Zhu, W. Zhang, S. Dou, Q. Jiang, *Facile Synthesis of Sulfur–Polypyrrole as Cathodes for Lithium–Sulfur Batteries*, 115–121, *ChemElectroChem.* 4 (2017).
3. M. Zhao, B.Q. Li, X.Q. Zhang, J.Q. Huang, Q. Zhang, *A Perspective toward Practical Lithium-Sulfur Batteries*, 1095–1104, *ACS Cent. Sci.* 6 (2020).
4. X. Hong, Y. Liu, Y. Li, X. Wang, J. Fu, X. Wang, *Application progress of polyaniline, polypyrrole and polythiophene in lithium-sulfur batteries*, *Polymers (Basel)*. 12 (2020).

Different Carbon Processes for Lithium-Sulfur Batteries

N. Hoffmann^a, M. G. Ortiz^{a,b}, J. E. Thomas^c, A. Visintin^a

^a Instituto de Investigaciones Fisicoquímicas Teóricas y Aplicadas (INIFTA), Facultad de Ciencias Exactas (UNLP), CONICET, Diag. 113 y 64, La Plata, Argentina

^b Centro de Investigación y Desarrollo en Ciencia y Tecnología de Materiales (CITEMA), Universidad Tecnológica Nacional - CICPBA, 60 y 124, 1923, Berisso, Argentina

^c YPF Tecnología S.A., Av. del Petróleo Argentino S/N (entre 129 y 143), B1923 Berisso, Buenos Aires, Argentina

In this work, different carbon modification processes have been employed and the results have been compared with the unmodified Super-P carbon. The active materials were used in respective cathodes materials for Li/S batteries. The electrochemical performance was studied by galvanostatic charge-discharge cycling, cyclic voltammetry, electrochemical impedance spectroscopy and rate capability.

Introduction

The progress on lithium-ion batteries is close to reaching its physical upper bounds, and thus different chemical systems must be used to achieve higher energy densities. Among the chemistries currently under research, the system based on the reaction between lithium and sulfur is closest to adoption, with several prototypes demonstrating its viability. Lithium-sulfur batteries are expected to reach a capacity of 600 Wh/kg, almost tripling the 200 Wh/kg that lithium-ion batteries deliver on average. However, the complex chemistry of the system requires a strategy to circumvent its disadvantages.

Experimental

In this work, three different carbon modification processes [2,3,4] have been employed and the results have been compared with the unmodified Super-P carbon (CSP). In one process, the carbon has been processed with boiling nitric acid (CSP-HNO₃). In the second process, the carbon has been ground with dissolved ammonium hydroxide (CSP-NH₃). In the third and last process, the carbon has been reacted with concentrated hydrogen peroxide (CSP-H₂O₂) at high temperature. Each of the processed carbons was employed as the sulfur host for different cathode active materials. The active materials were used in respective cathodes, and each cathode was tested in a CR2032 battery with a lithium anode.

It was found that the carbon processed with boiling nitric acid and possessed both the highest capacity for all discharge rates and the highest capacity retention after 100 cycles at C/10, though most carbons had approximately similar capacities in that test. The carbon processed with ammonia yielded the lowest capacities at C/10, and the carbon processed with peroxide yielded very low capacities at higher C-rates, with almost no recovery upon further cycling at a lower rate (Figure 1).

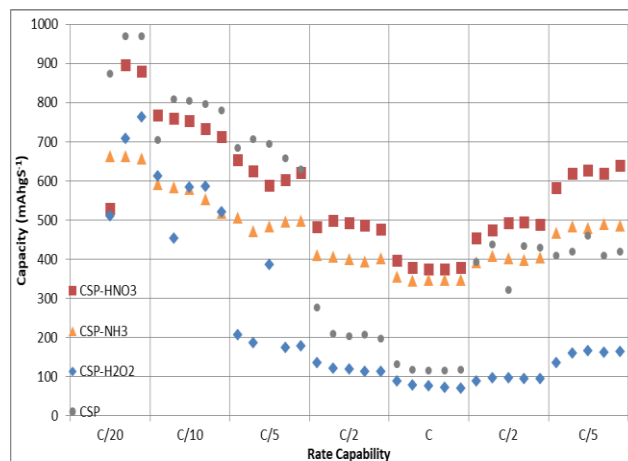


Figure 1. Rate capability of cathode materials

Acknowledgments

This work was supported by the CONICET (Consejo Nacional de Investigaciones Científicas y Tecnológicas) and ANPCyT (Agencia Nacional de Promoción Científica y Tecnológica).

References

1. M. Zhao, B-Q. Li, X-Q. Zhang, J-Q. Huang, Q. Zhang. *ACS Central Sci.* **6**, 7, 1095 (2020).
2. G. Jin, Z. Mingang, Y. Shijian, Y. Xiaoyan, W. Shiwei. *Ionics* **24**, 2219 (2017).
3. D. Leistenschneider, K. Zürbes, C. Schneidermann, S. Grätz, S. Oswald, K. Wegner, B. Klemmed, L. Giebeler, A. Eychmüller, L. Borchardt. *J. Carbon Research*, **4**, 14 (2018).
4. R. Pongilat, S. Franger, K. Nallathamby. *J. Phys. Chem. C*, **122**, 11, 5948 (2018)

Impact of the Graphene Synthesis on Electrochemical Properties of Graphene — Graphite Systems

R. A. Panteleimonov^{a,b}, O. V. Boichuk^a, K. D. Pershina^{a,b}, Yu. V. Shmatok^b

^a VI. Vernadskii Institute of General and Inorganic Chemistry NAS of Ukraine, Palladin Ave, 32/34, Kyiv 03142, Ukraine

^b Joint Department of Electrochemical Energy Systems NAS of Ukraine, Vernadskii Ave, 38, Kyiv, 03142, Ukraine

The electrochemical impedance spectroscopy and scanning electron microscopy investigated the relationship between the electrical parameters of the graphite-graphene systems with various graphite content and the structural-morphological features of graphene. The dependence between graphite-graphene ratio and electrochemical properties was found. The impact of graphite content and media of synthesis on changing the conductivity type was determined. The changing of the graphite concentration in the graphene/graphite mixture regulates the type of doping and electrical parameters of the mixture. The impact of heat treatment on the change of electrical parameters of the whole system is shown.

Introduction

Graphene-based supercapacitors are one of the most discussed topics in the scientific community today due to the ability of graphene to build such structures as graphene sheets rolled into a tube with a diameter in the range of 1 nm ÷ 100 nm (1). The mixture of the graphene materials (nanotubes and sheets) can perform a high capacitance (290 F/g and 200 F/g), in aqueous and organic electrolytes (2). These values were 20% higher than for pure graphene-based electrodes. This was explained by the fact that graphene alone can repackage with the formation of graphite and nanotubes due to Van der Vals, reducing the active surface area. A composite of these structures, on the contrary, prevents repackaging ability and the formation of beams in the entire graphene structure, thereby increasing the active surface area, which accelerates the diffusion of ions (3). The nitrogen-doped graphene/graphite mixture provides excellent electrochemical characteristics for the lithium-ion battery, such as a high specific capacity of up to 781 mAh/g, a bandwidth of 351 mAh/g, and instead stability - maintaining a capacity of 98.1% at 10 °C after a cycle of 1000 cycles (4). Therefore, our study aimed to establish the effects of graphene content and kind of synthesis on the structural changes and electrical parameters (conductivity and capacity) of graphite- graphene mixture.

Components of mixture were electrolytic graphite and graphenes. Graphenes were synthesized using two methods of plasma arc discharge from an aqueous and nitrogen medium (water and liquid nitrogen). Graphenes and graphite mixed in the mass ratio according to the table 1. The heat treatment of samples carried out during one hour with a gradual increase in temperature up to 250 °C.

TABLE I. Synthesis method, composition, and heat treatment conditions of graphite-graphene mixtures

Number of samples and synthesis method	Mass ratio graphene/ graphite	Heating temperature °C
1. The liquid nitrogen media	1/5	25
2. The liquid nitrogen media	1/3	25
3. The liquid nitrogen media	1/1	25
4. The liquid nitrogen media	1/1	250
5. The water media	1/1	25
6. The water media	1/3	25
7. The water media	1/3	250

The capacity values and the active resistance of the samples fixed the differences in these systems. The mixture with graphene from water media reduces the average values of capacity relatively to graphene from nitrogen media by 10 times, and significantly increases the active resistance at the mass ratio of graphene to graphite 1:3, and with a ratio of 1:1, they are commensurate. Such differences are based on various structural and morphological properties of samples (fig.1).

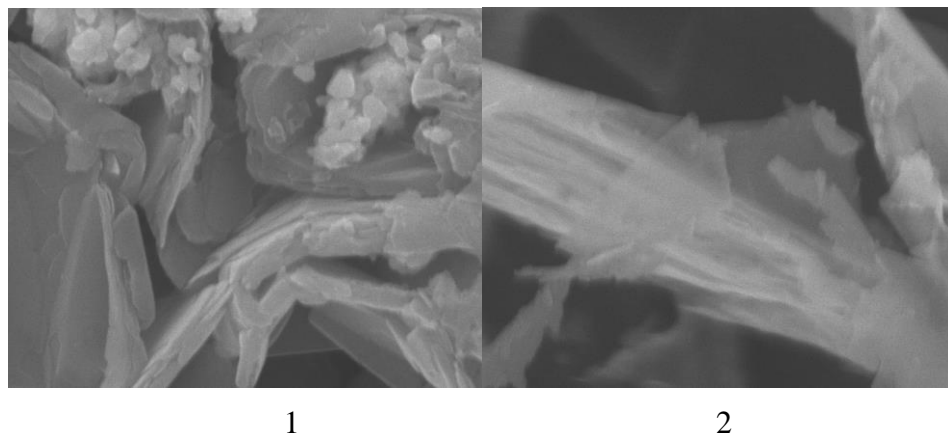


Figure 1. The SEM images of the graphene synthesized from liquid nitrogen media -1, and from water media -2.

Calculations of the average electrical conductivity data in systems with graphene synthesized in a nitrogen medium show the dependence of the increase of the electrical conductivity and an increase of the capacitance on the graphene content (fig. 2). High values of capacitance and conductivity were obtained in systems with a ratio of graphene/graphite 1: 1 (sample 3, 4). However, the maximum average values of capacity (into 2 times higher) are observed in a system with equal content of graphene and graphite, which is synthesized in nitrogen with heat treatment of the sample at 250 °C . By graphical integration of the active resistance and capacity data on the frequency plane (5, 6) was fixed the changes in the charges distribution in the samples in various frequency ranges. So, the media affect the ability of graphene to be in an open sheet stay, and regulate future interactions between graphene and graphite. Graphite regulates the main electrochemical properties of the mixture in the case of the graphene from nitrogen media. The change of the graphite concentration in the graphene/graphite mixture may regulate the type of doping and electrical parameters of the whole mixture.

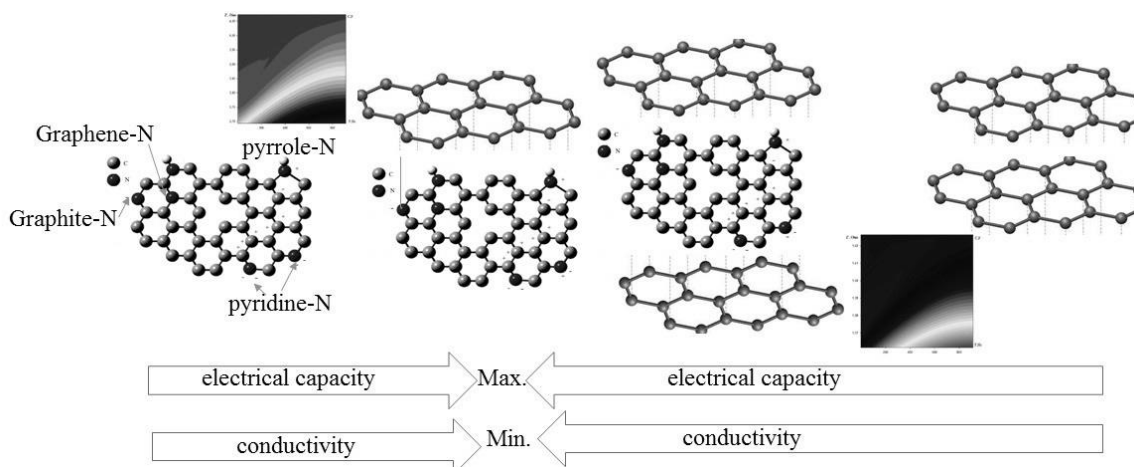


Figure 2. The scheme of changing electrochemical properties (capacitance, conductivity, and surface charge distribution) in the graphene from liquid nitrogen media according to electrochemical impedance data and Raman spectra.

Acknowledgments

Writing the article became possible due to the framework 314E "Physical-inorganic chemistry of functionally oriented nanosystems, heterostructures and composites" of the NAS of Ukraine.

References

1. Q. Cheng, J. Tang, J. Ma, H. Zhang, N. Shinya, L.C. Qin, *Physical Chemistry Chemical Physics*, **39**(13), 17615 (2011).
2. A. Ansaldo, P. Bondavalli, S. Bellani, A. E. Del Rio Castillo, M. Prato., V. Pellegrini, F. Bonaccorso, *ChemNanoMat.*, **6**(3), 436 (2017).
3. W. Guanghui, L. Ruiyi, L. Zaijun, L. Junkang, G. Zhiguo, W. Guangli, *Electrochimica Acta.*, **171**, 156 (2015).
4. M. Terrones, A.R. Botello-Méndez, J. Campos-Delgado, F. López-Urías, Y.I. Vega-Cantú, F.J. Rodríguez-Macías, H. Terrones, *Nano today*, **4**(5), 351 (2010).
5. O.L. Riabokin, A.V. Boichuk, K.D. Pershina, *Surf. Engin. Appl. Electrochem.*, **54**(6), 614 (2018).
6. O. Boichuk, K. Pershina, O. Riabokin, A. Kravchenko, R. Panteleimonov, *Ukrainian Chemistry Journal*, **86** (4), 108 (2020).

Graphene-Modified Sulfur Cathode Ensuring High Stability of Li-S Batteries Parameters

Yu. Polishchuk^a, S. Dubinevych^b, V. Zinin^b, E. Shembel^{a,c}

^aUkrainian State University of Chemical Technology, Dnipro, 49005, Ukraine

^bLLC “MaxAh” K, Kyiv, 01001, Ukraine

^cEnerize Corporation, Coral Springs, FL, 33067, USA

Dynamics of changes in the impedance spectra and electrochemical parameters of Li-S batteries with graphene in non-aqueous liquid electrolyte 0.7 M LiIm, 0.25 M LiNO₃, DME:DOL (2:1) were studied. The investigation showed a positive effect of graphene materials in the active mass of the S-based electrode. The effect of interface stabilization was expressed in a decrease in impedance spectra, an increase in discharge capacity, and more stable long-term cycling with high parameters.

Carbon materials with high electrical conductivity and variable structures are extensively used in lithium non-aqua batteries. Relatively new forms of carbon are fullerenes and graphenes. Graphene is a potent conductor of electrical and thermal energy, extremely lightweight, chemically inert, and flexible with a large surface area. Graphene, like all carbon materials, is also considered eco-friendly and sustainable.

In recent years, graphene has begun to play an important role in power sources application due to its ultra-high electrical conductivity, large surface area, and flexible two-dimensional nanostructure [1]. As a rule, graphene is used for multilayer electrode materials: as flexible self-supporting graphene / S paper [2]; as graphene / S / C layered nanocomposite [3]; as surface modification sulfur by graphene [4], etc. Earlier, we showed the possibility of increasing the electrical parameters of a Li-S battery due to the use of a special layered design of S-based cathode [5]; due to the use of graphene materials [6].

In this investigation, we used graphene materials obtained by a unique technology developed by LLC “MaxAh” K company. The positive electrodes were fabricated by slurry coating. The aluminum foil was used as the current collector. Disk electrodes based on sulfur had the following parameters: $d = 1.6$ cm, working surface – 2 cm². Cathode mass had the following composition: natural sulfur (75%); graphene materials produced by LLC “MaxAh” K or graphite/carbon black mix and PVdF (6020/1001, Solef) as a binder. The drying of the cathode was at 60°C for 6 h under vacuum and 2 h at 120°C without vacuum. The multilayer cathode was produced using acetylene black by the technology described in [5].

The negative electrodes were made of lithium foil. The microporous polypropylene Celgard® 2300 with a thickness of 25 μm was used as a separator. Electrolyte composition was 0.7M bis(tri fluoromethanesulfone)imide (LiIm), 0.25M LiNO₃, DME:DOL (2:1). All procedures were carried out in an Ar-filled glove box.

The following measurements were used: XRD spectroscopy with monochromatic Co-K α radiation. Identification of compounds (phases) was carried out by comparing the interplanar distances (d , Å) and relative intensities of the experimental curve with the data of the PCPDFWIN

electronic base. The spectra of the Stokes scattering component were recorded, excitation at a wavelength of 532 nm, power density - $0.25 \text{ mW}/\mu\text{m}^2$, spectral resolution $\approx 2 \text{ cm}^{-1}$. Impedance spectra of Li-S batteries were obtained using VoltaLab PGZ 301 analytical radiometer. The frequency range was from 100 MHz to 100 kHz. Potentiodynamic cycling was performed in the range of potentials from 1.5 to 2.9 V with a $0.5 \text{ mV}/\text{sec}$ scan rate. Galvanostatic cycling was performed in the range of potentials from 1.5 to 2.9 V at discharge current - $200 \mu\text{A}$, and charge current - $100 \mu\text{A}$. The measurements were conducted at a temperature of $25 \text{ }^\circ\text{C}$.

The characteristics of the original and processed graphene powders are shown in Fig. 1. According to X-ray diffraction analysis, both materials contain graphite. The amount of crystalline carbon in the original sample is 60%. After processing, the amount of carbon with crystalline phase decreases to 32%.

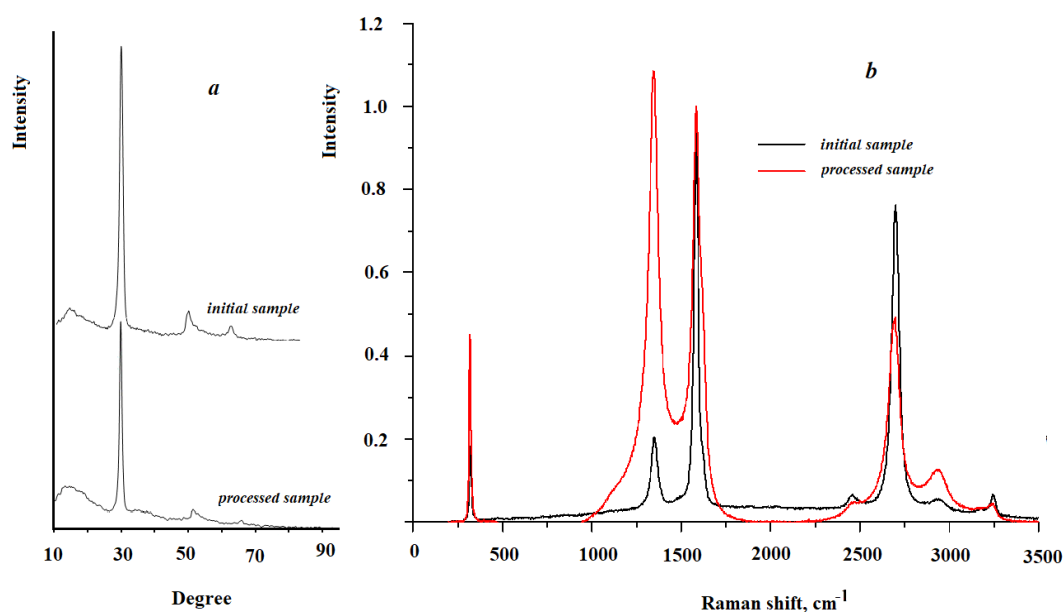


Figure 1. Characterization of the initial and processed graphene samples with (a) XRD and (b) Raman spectroscopy

The processed graphene sample is characterized by the presence of some graphene oxide, as evidenced by an intense peak at 1350 cm^{-1} on the Raman spectrum. The average size of crystallites L of the original sample is 267 \AA , and, for the processed graphene sample, L is 346 \AA . The number of layers in both types of graphene samples is two.

The hodographs of S-based electrodes with graphene in the Li-S-Li cell are several orders of magnitude lower than those of cathodes with a graphite/carbon black mix (Fig. 2). This trend has been observed for several days of storage. However, the replacement of carbon materials in the cathode mass with graphene does not lead to a significant decrease in the complex resistance of the Li-S system as a whole. We attribute this to the predominance of passive film formation on lithium.

The effect of graphene is more significant during potentiodynamic cycling. The first cathode curve of the current-voltage characteristic of the S-based electrodes with graphite/carbon black mix (Fig. 3 a) shows two clear peaks at potentials of 2.2 and 1.9 V.

In this range of potentials, the formation of various compounds is possible, for example, Li_2S and Li_2S_2 . During cycling, there is a small shift of the potential of the first cathode peak to 2.3 V, which may correspond to Li_2S_4 formation.

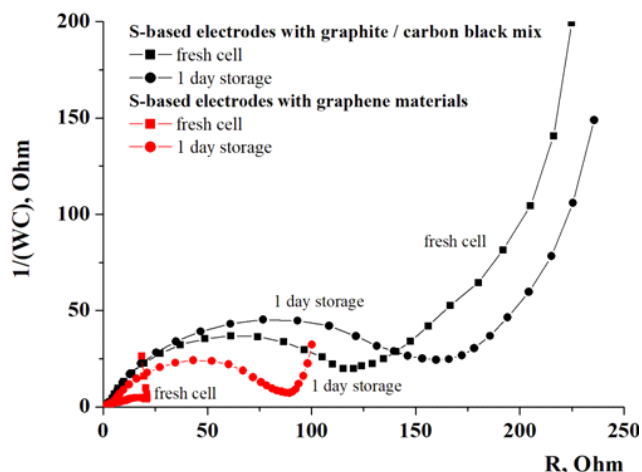


Figure 2. Impedance spectra of Li-S-Li cells

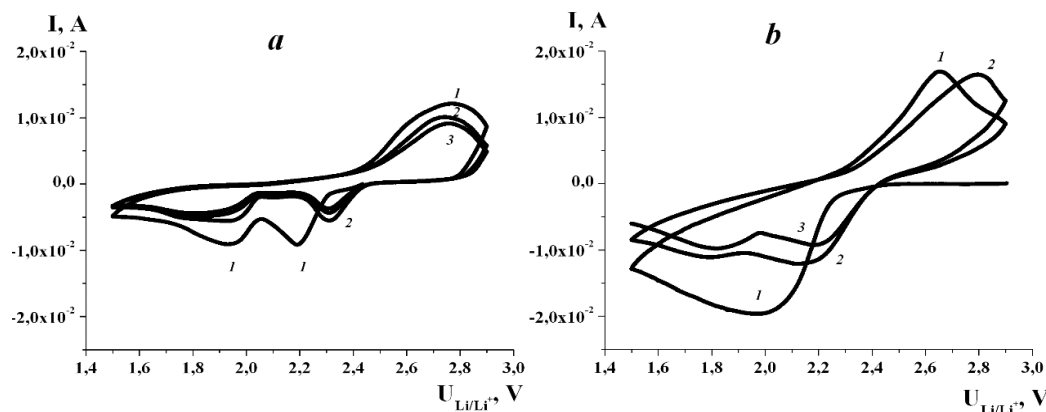


Figure 3. Change of Li-S cell volt-ampere curves. The cathode contains 75% sulfur: S-based electrodes with graphite/carbon black mix (a); S-based electrodes with graphene materials (b). The numbers on the curve are the numbers of the cycles

The anode curve has a clear peak at a potential of 2.6-2.7 V for both types of carbon materials in cathode mass. It should be noted that the use of graphene in S-based electrodes leads to a twofold increase in the current value in the cathode and anode peaks.

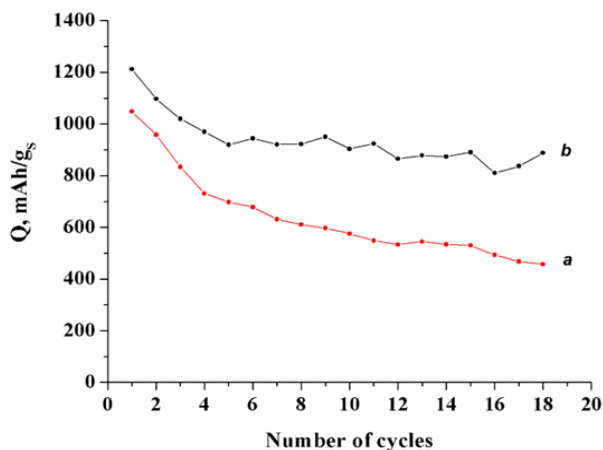


Figure 4. Dynamics of specific capacity changes in Li-S cell. The cathode contains 75% sulfur: S-based electrodes with graphite / carbon black mix (a); S-based electrodes with graphene materials (b)

The reduction in the rate of polysulfides formation and decreasing of shuttle effect due to the use of graphene materials and a special design of the cathode is confirmed by the results of galvanostatic cycling (Fig. 4).

Conclusion

A complex of investigations allows us to conclude that the unique structural features and physical parameters of graphene materials and the use of a special electrode design make it possible to reduce the resistance of sulfur-based electrodes as well as significantly stabilize the discharge capacity of lithium-sulfur batteries during cycling.

References

1. C.H. Xu, B.H. Xu, Y. Gu; Z.G. Xiong; J. Sun; X.S.Zhao. *Energy Environ. Sci.*, **6**, 1388 (2013).
2. J. Jin. Z. Wen, G. Ma, Y. Lu, Y. Cui, M. Wu, X. Liang and X. Wu. *RSC Adv.*, **3**, 2558 (2013).
3. K. Jin, X. Zhou, and Z. Liu. *Nanomaterials*, **5**, 1481 (2015).
4. M. Yu, R. Li, M. Wu, and G. Shi. *Energy Storage Materials*, **1**, 51 (2015).
5. Yu. Polishchuk, E. Shembel, and A. StrakovaFedorkova. *ECS Trans.*, **99**, 133 (2020).
6. S. Dubinevych, V .Zinin, V. Redko, B. Blyuss, E. Shembel, N. Zaderey, Yu. Polishchuk, A. Markevych, A. Strakova Fedorkova and M. Tkach. *ECS Trans.*, **105**, 247 (2021).

Synthesis of a new fluorine-free ionic liquids containing an anion PCP⁻ to use in solid state batteries

K. M. Rogala*, L. Niedzicki, M. Bedecka, D. Jamroz, T. Trzeciak, A. Zalewska

Faculty of Chemistry, Warsaw University of Technology, Noakowskiego 3, 00-664 Warsaw, Poland

klaudia.rogala@pw.edu.pl

Most electronic devices use lithium-ion batteries as their energy source. One of the biggest challenges in modern battery technology is the elimination of the fluorine salt LiPF₆ that is the dominant salt on the market. Issues related to LiPF₆ include, but are not limited to: low thermal stability (only up to 70°C), moisture sensitivity (decomposition upon contact with ppm-level moisture presence), HF formation, toxic phosphoryls formation, corrosion of electrodes, reactivity with silicon from new generation of anode and cathode active materials, etc. The answer to these problems may be the new fluorine-free salt for lithium-ion battery applications. This is why we decided to develop LiPCP (lithium 1,1,2,3,3-pentacyanopropenide) salt (Fig. 1).

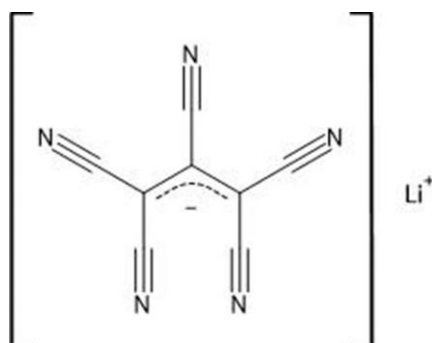


Figure 1. Structure of lithium 1,1,2,3,3-pentacyanopropenide

The salt was obtained in a two-step synthesis and its structure, as well as purity, have been confirmed by nuclear magnetic resonance (NMR) techniques, Raman spectroscopy, infrared (FTIR) spectroscopy and high resolution mass spectroscopy (ESI-HRMS). Electrochemical characterization confirmed that the LiPCP salt exhibits similar or the same electrochemical parameters as benchmark LiPF₆ one. In addition, it is more thermally stable (up to 315°C) than the LiPF₆ salt, and is stable in the presence of water. Tests performed using the galvanostatic cycling method confirmed that the salt is able to work in full Li-ion cells.

Satisfactory results obtained for salt caused a promising anion to be used as a component of new ionic liquids (ILs) to be used as potential plasticizing additives for solid electrolyte cells. As a result, a group of ILs containing PCP⁻ anion was obtained. As the cations imidazole, ammonium and pyrrolidine derivatives were used. Each of the synthesis was carried out in one step with high efficiency. Thermal stability tests of the investigated ILs were made by differential scanning calorimetry method (DSC). In the presentation results of electrochemical characterization of ionic liquids and their suitability for use in solid electrolyte batteries will be shown.

Acknowledgments

This work has received funding from the European Union's Horizon 2020 research and innovation programme under grant agreement N°875029.

Supercritical carbon dioxide assisted synthesis of ultra-stable sulfur/carbon composite cathodes for Li- S batteries

Shiva Shankar Lakshmi ^a, Dóra Zalka ^{a, b, c}, Robert Kun ^{a, d, *}

^a Institute of Materials and Environmental Chemistry, Research Centre for Natural Sciences, H-1117 Budapest, Magyar tudósok krt. 2., Budapest, Hungary

^b Institute of Materials Research, Slovak Academy of Sciences, Watsonova 47, 04001 Košice, Slovak Republic

^c Faculty of Science, Institute of Physics, Pavol Jozef Šafárik University in Košice, Košice 041 80, Slovak Republic

^d Department of Chemical and Environmental Process Engineering, Faculty of Chemical Technology and Biotechnology, Budapest University of Technology and Economics, Műegyetem rkp. 3, H-1111 Budapest, Hungary

To mitigate the shuttle effect and enhance the electrical conductivity in Li-S battery cathode, the unique characteristics of supercritical CO₂ solvent (SC-CO₂) and distinctive porous and layered microstructure of reduced graphene oxide (rGO) are exploited in the fabrication of high-performance rGO/sulfur composite cathode. Exploiting SC-CO₂ technology can realize highly efficient sulfur transfer and precise microstructure regulation of S/C composite cathodes for Li-S batteries. An important feature is that the S/C composites can be prepared at room temperature, unlike other conventional techniques which require a higher temperature. Moreover, the product mixture can be separated simply by de-pressuring SC-CO₂. Herein, the rGO/sulfur composite cathode prepared in a lab showed excellent performance (1024 mAhg⁻¹ at 0.1C) with an ultralow decay of 0.03% per cycle even after 200 charge-discharge cycles. Through this work, we believe that the synergistic effect of SC-CO₂ technology and rGO as sulfur host will open up a promising future for the synthesis of efficient S/C composite cathodes with ultra-high cycling stability.

Significance of the current research work

Li-S batteries are believed to be one of the most promising next-generation high-energy-density rechargeable battery chemistries. But the cycle life and efficiency need to be improved for them to be employed in practical applications. The preliminary and most important step to developing high-performance Li-S batteries is a suitable sulfur encapsulation technique that can enhance the utilization of the active material and limiting the loss of the active material. To date, different strategies such as mechanical mixing, heat treatment, solution-based synthesis, etc. have been exploited by the research community. This includes melt diffusion [1], solution infiltration [2], vapor phase infusion [3], mechanical infusion such as ball milling [4], wet chemical processes utilizing soluble sulfur-containing compound [5]. However, these methods involve the usage of toxic solvents like CS₂, benzene, toluene, etc., and demand high energy consumption. Moreover, a precise sulfur

content with its uniform distribution and affinity with the carbon host cannot be guaranteed. In this regard, the development of a more facile, sustainable and efficient strategy is paramount for the synthesis of the high-performance sulfur cathode in Li-S batteries.

In this work, SC-CO₂ technology, which is so far very less investigated in battery studies, is utilized in encapsulating sulfur into a porous reduced Graphene oxide host, and the feasibility of SC-CO₂ media to formulate S/C composite is evaluated. Reduced graphene oxide possesses a special kind of layered, disordered microstructure providing more interlayer space, serving as a perfect host material that can enable the facile intercalation of active sulfur particles enabling faster reaction kinetics. Concurrently, SC-CO₂, on exposure, due to the sudden pressure release process expands the interlayers of rGO rendering plenty of storage space for small sulfur allotropes in carbon matrices. This creates direct contact of sulfur with rGO interlayers, guaranteeing precise sulfur content, uniform sulfur distribution, and strong interaction between sulfur and carbon leading to enhanced electrical conductivity and sulfur utilization efficiency. Most importantly, SC-CO₂ is non-toxic, non-flammable, cost-effective, and recyclable, and the liquid waste problem can also be minimized [6]. This strategy of utilizing SC-CO₂ by eliminating the toxic solvents for sulfur dissolution makes supercritical technology a “green process”. Employing the as-prepared rGO/sulfur composite cathode can realize the highly efficient intercalation/anchoring of sulfur within the rGO host and precise microstructure regulation of S/C composite cathodes for Li-S batteries. This ultimately helps diminishing the shuttle effect of Lithium polysulfides, thereby enhancing the electrochemical stability in Li-S batteries.

Experimental section in brief

In this work, we have employed modified Hummer’s method for the preparation of GO. This modified method of synthesis involves both oxidation and exfoliation of graphite sheets due to the thermal treatment of the solution. However, GO is an electrical insulator, due to the disruption of its sp² bonding networks. Therefore, GO is reduced by heat treatment, resulting in reduced graphene oxide (rGO). In the synthesis of carbon/sulfur composite, the as-prepared rGO and elemental sulfur powder were mixed in a 2:1 ratio and transferred into the high-pressure supercritical reactor. Subsequently, CO₂ (99.9%) was pumped into the reactor and the mixture was agitated at 350 RPM for 12 hours. The temperature and pressure during the whole process were maintained at 32 °C and 100 bars respectively. After the SC-CO₂-assisted milling, the reactor was gently depressurized by releasing out CO₂ and the as-prepared rGO/sulfur composite (RGO-S-SCC) powder was then collected from the reactor. The prepared rGO/sulfur composite was mixed with conductive carbon black (Super C65, Imerys), and polyvinylidene fluoride (PVDF 99.9%, Solvay), in a weight ratio of 80:10:10. The mixture was then made into a slurry with N-methyl-2-pyrrolidone (99.9%, Sigma-Aldrich) as the solvent and spread onto the copper foil. The coated electrode tape was dried in the vacuum chamber and punched into circular discs in order to prepare CR2032-type coin cells for electrochemical performance tests.

Results and discussions

The developed cells with RGO-S-SCC cathode, Li metal anode, and 1 M LiTFSi in DME and DOL (1:1 volume ratio) electrolyte showed outstanding electrochemical performance with respect to specific capacity, Coulombic efficiency, and stable cycle life even at higher current rates for prolonged cycling. The cell showed excellent capacity retention of 92.2 % delivering an initial discharge capacity of 1024 mAh/g and a discharge capacity of 945 mAh/g after 200 charge-discharge cycles at 0.1 C rate. The developed cells showed high-rate performance with an ultralow decay of

0.04 % per cycle even after 200 charge-discharge cycles. Moreover, the highly sustained Coulombic efficiency (around 99.5%) is a scalar indicator of the good electrochemical reversibility of the battery electrode function. The above results demonstrate the synergistic effects of utilising *i*) supercritical CO₂ technology and *ii*) rGO carbon host by the design of C/S nanocomposites for highly stable Li-S rechargeable batteries.

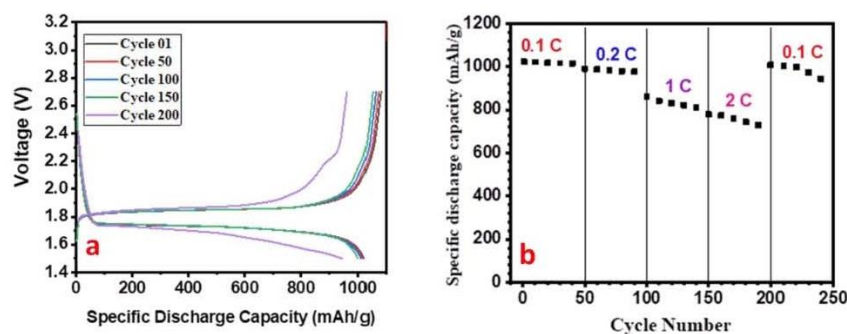


Figure 1. (a) Charge -discharge voltage profiles of RGO-S-SCC @ 0.1 C rate, (b) rate performance plot of the RGO-S-SCC electrode

Acknowledgement

The authors thank the financial support from Project no. RRF-2.3.1-21-2022-00009, titled National Laboratory for Renewable Energy that has been implemented with the support provided by the Recovery and Resilience Facility of the European Union within the framework of Programme Széchenyi Plan Plus.

References

1. R. Elazari, G. Salitra, A. Garsuch, A. Panchenko, D. Aurbach, *Adv. Mater.* **23** (2011).
2. F.F. Zhang, X.B. Zhang, Y.H. Dong, L.M. Wang, *J. Mater. Chem.* **22** (2012).
3. Z. Li, T. Huang, W. Gao, Z. Xu, D. Chang, C. Zhang, C. Gao, *ACS Nano.* **11** (2017).
4. M.-S. Song, S.-C. Han, H.-S. Kim, J.-H. Kim, K.-T. Kim, Y.-M. Kang, H.-J. Ahn, S.X. Dou, J.-Y. Lee, *J. Electrochem. Soc.* **151** (2004).
5. C. Hernández-Rentero, R. Córdoba, N. Moreno, A. Caballero, J. Morales, M. Olivares-Marín, V. Gómez-Serrano, *Nano Res.* **11** (2018).
6. M.A. Pigaleva, I. V. Elmanovich, M.N. Temnikov, M.O. Gallyamov, A.M. Muzafarov, *Polym. Sci. - Ser. B.* **58** (2016.)

Development of oxygen reduction and oxygen evolution electrodes for alkaline zinc-air flow battery

M. Zajcev^a, P. Richtr^a, J. Hnát^b, P. Mazúr^a, M. Zejmon^b, M. Paidar^b, J. Pociđič^c

^aUniversity of Chemistry and Technology Prague, Dept. of Chemical Engineering,
Technická 5, 166 28 Prague, Czech Republic

^bUniversity of Chemistry and Technology Prague, Dept. of Inorganic Technology,
Technická 5, 166 28 Prague, Czech Republic

^cNew Technologies – Research Centre, University of West Bohemia,
Univerzitní 8, 306 14 Plzeň, Czech Republic

The energy and environmental crises ongoing are speeding up the decarbonization of the energy sector further, as necessity pushes the sector towards more renewable sources less affected by the issues. Renewable sources have an inherently more fluctuating nature, however, which is stabilized by the usage of stationary energy storages, among which the most frequently used are Li-ion batteries, hydrogen technologies et cetera. However, not all these technologies are as efficient in reducing the strain on our safety and environment, and often some of them are also limited by resource availability. Zinc-air flow batteries are promising alternatives due to their high theoretical energy density, safety of exploitation and environmental friendliness. This electrochemical system, however, is in an early stage of development and advances in commercialization are limited by a few technical issues, among which dendritic growth of metal zinc, long-term instability of air electrodes and reduced efficiency of certain processes are most notable.

The aim of this work is to develop stabler and more efficient electrodes for oxygen evolution reaction (OER) and oxygen reduction reaction (ORR) for application in alkaline zinc-air flow batteries. As part of the work on OER, several 3D electrodes based on nickel foam and expanded nickel, which was catalytically activated by NiCo₂O₄ in electrochemically assisted precipitation followed by calcination, were tested. The electrodes were characterized by various techniques (SEM, EDS, XRD) and were also electrochemically tested under no-flow conditions. These electrodes were consequently tested in a modified flow cell with hydrogen evolution on a nickel plate being the counter reaction. The cell implemented a Nafion N115 membrane. The performance and mid-term stability of the OER electrode was tested under current load. It was tested by a combination of galvanostatic load, electrochemical impedance spectroscopy and load curve measurements, as well as tested under different temperatures to determine the characteristics of the reactions and the electrode stability with varying conditions.

In the second part of the work, the focus was on the development of a gas diffusion electrode, which would provide high performance and low permeability for the liquid electrolyte. Several commercial gas diffusion layers have been characterized, specifically their elemental composition, permeability for water, wettability, and inner texture. Most suitable GDL have been then selected and used for electrode fabrication. Electrodes were fabricated by spraying of Pt-based catalytic ink. The prepared electrodes were characterized in a modified flow cell using OER on nickel mesh as the counter reaction. The cell implemented a porous separator (CELGARD 5500). Electrodes with different compositions in terms of amount of PTFE in the catalytic layer have been implemented, and were tested in regards to the effect of the PTFE composition of the catalytic layer.

The optimized electrodes will be further tested in a zinc-air flow battery using three electrode configuration.

Acknowledgement

This work was supported by TAČR, program THÉTA2, project no. TK02030001.

Characterization Of Precursor Sols For Preparation Of Silica Based Nanofibers

V. Procházka^a, M. Havlík Míka^a, J. Kočí^a

^aDepartment of Glass and Ceramics, Institute of Chemical Technology, Prague, Czech Republic

Objective of this study was to prepare and characterize electrospun silica-based nanofibers. The goal of this research was to create amorphous to semicrystalline nanofiber mats, which are easily modifiable and usable in electrochemical applications such as separators or electrodes in amorphous glass solid state batteries. We investigated stability of precursor sols, and effect of sol ageing on fibre morphology. Sol-gel reaction mechanism was investigated by liquid state ²⁹Si NMR spectroscopy.

Nanofibrous structures

Nanofibrous structures shows great potential for applications in all industries such as tissue engineering, energy storage technologies, fuel cells composite materials, coating materials or filtration membranes. By definition nanofibers have diameters between 1 nm and 1 μm. Due to this, nanofibers have extremely large length to diameter ratio resulting in higher mechanical strength, flexibility, surface area to volume ratio, porosity, gas permeability, and structural stability than microfiber or bulk counterparts(1, 2). Their diameters generally range from 100 nm to 800 nm, however it is possible to mass produce fibres with diameter 36 nm and in small scale 2 nm(3, 4).

A lot of methods have been reported to prepare nanofibers, among these techniques most versatile is considered electrospinning. With this method is possible to process large number of materials, easily control fiber diameter, fabricate multicomponent configurations an even nanotubes, nanorods or nanowires. Electrospun fibers are relatively easy to align, assemble and process into application with relatively low cost(5). Electrospinning is one of few viable methods of silica-based nanofibers preparation. Other possibility is melt-blowing technique which usually results in fibers with diameters over 800 nm(4).

Resulting product is influenced by large number of factors often divided into 3 categories: 1) material properties (concentration, viscosity, conductivity, surface tension), 2) processing parameters (voltage, flow rate, collector distance, spinner configuration), and 3) ambient condition (mainly ambient temperature and humidity)(4).

Presented work is focused on preparation of amorphous silica and alumino-silica glass nanofibers via electrospinning process. Precursor sols are based on tetraethylorthosilicate (TEOS) and using polyvinylpyrrolidone (PVP) as stabilizing agent and carrier polymer.

References

1. Yang, X.-h., P. He, and Y.-y. Xia, *Preparation of mesocellular carbon foam and its application for lithium/oxygen battery*. *Electrochemistry Communications*, 2009. **11**(6): p. 1127-1130.
2. Zhang, B., et al., *Recent advances in electrospun carbon nanofibers and their application in electrochemical energy storage*. *Progress in Materials Science*, 2016. **76**: p. 319-380.
3. Soltani, I. and C.W. Macosko, *Influence of rheology and surface properties on morphology of nanofibers derived from islands-in-the-sea meltblown nonwovens*. *Polymer*, 2018. **145**: p. 21-30.
4. Zdraveva, E., et al., *Electrospun nanofibers*. 2017. p. 267-300.
5. Liu, Y., et al., *Preparation and characterization of electrospun SiO₂ nanofibers*. *Journal of nanoscience and nanotechnology*, 2008. **8 3**: p. 1528-36.

Reversible photoelectrochemical cell produced by using 3D print for the accumulation "solar" hydrogen

S V Chivikov^a, I A Rusetskyi, S S Fomanyuk, M O Danilov, V O Smilyk, G Ya Kolbasov

^aV.I.Vernadskii Institute of General and Inorganic Chemistry of the NAS of Ukraine,
32/34 Academic Palladin Avenue, Kyiv, 03142, Ukraine.

*Corresponding Author E-mail Address: s.v.chivikov@gmail.com

A reversible photoelectrochemical system using accumulated hydrogen has been developed. Reversibility is ensured by introducing a third electrode based on Cu₂S, onto which a metal hydride electrode based on MH alloys is discharged. The photoaccumulator made it possible to obtain a maximum current of 97 mA and $V_{o.c.} = 0.337$ V during the discharge by the MH electrode without illumination. A new feature of the cell design was 3D modeling. Almost all the details of the cell were printed on a 3D printer. It was found that the peak current during cell illumination was several times higher than the maximum current obtained by the 2-electrode scheme. For consumers with uneven power consumption, such a system is equivalent to a solid state system with more power.

Introduction

Electrochemical processes are widely used in science and technology. Electrochemical reactions occur on the surface of the electrodes and are associated with the process of charge transfer through the interface. For their study and improvement, electrochemical cells are used - specially designed devices with the help of which conditions are created for carrying out one or another electrochemical process. Photoelectrochemical systems, in which it is possible to use semiconductor anodes that are sensitive to the visible spectrum of sunlight, and cathodes that effectively absorb hydrogen, are one of the promising areas for creating systems for the production and accumulation of "solar" hydrogen.

At present time, additive technologies are increasingly used in industry and technology. The ability to print complex-shaped parts using a 3D printer can be used to manufacture electrochemical cells.

Results and Discussion

We have developed a layout of a fully reversible photoelectrochemical cell using stored hydrogen (Fig. 1). Reversibility is provided by the introduction of the third electrode to the anode part of the cell, on which the metal hydride electrode based on the alloys AB₅ is discharged. The necessity of introducing the third electrode is due to the fact that on photoelectrodes based on cadmium chalcogenides, the polysulfide ion reduction reaction practically does not proceed at the potential at which operated MH electrodes in the absence of illumination

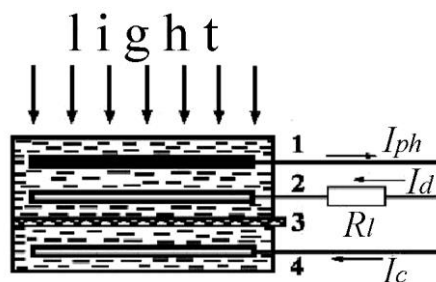


Figure 1. Scheme of a reversible photoelectrochemical system: 1-photoelectrode in a polysulfide solution, 2-counter electrode, 3- cation-exchange membrane, 4- the storage electrode in an alkaline solution. R_l - load resistance. I_{ph} - photocurrent, I_{ch} - charge current, I_{dch} - discharge current.

As a counter electrode for the polysulfide system we used electrode based on copper sulfides. Nickel, cobalt, lead, ruthenium, and molybdenum sulfides can also be used as counter electrodes. These electrodes have a low overvoltage for the $2S^{2-} + 2p^+ \rightarrow S_2^{2-}$ reaction, Copper sulfide showed the highest activity among the studied sulfides [1].

The results of some prior investigation [2] let us to develop three electrodes photo-electrochemical cell. New feature of the design of the cell was 3D modeling. Almost all details of the cell were printed on 3d printer. New additive technology make possible to change design of details of the cell according to the results of experiments. It is create fundamentals for quick improvement of electrochemical characteristic of the cell. For the printing anode and cathode cell chambers of photo-electrochemical cell we used polypropylene, material for other parts was ABS plastic.

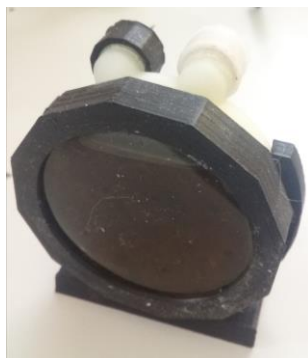


Figure 2. Reversible photoelectrochemical cell.

The TiO_2 (NT- TiO_2) nanotubes on the Ti substrate were obtained by the method of potentiostatic anodic polarization of titanium foil. The electrolyte contained 70 % glycerol, 30 % water and 1.5 wt % NH_4F . Titanium foil was previously degreased in the acetone. The process was carried out at 30 V for 1 hour, followed by annealing at 500 °C for 3 hours [3, 4]. Under laboratory conditions, it was found that the formation of a layer of TiO_2 nanotubes leads to an increase in the efficiency of charge carrier accumulation on NT- TiO_2 /CdSe electrodes. This is due to the increase in the potential of flat zones, which determines the magnitude of the electric field at the surface of the semiconductor that affects the separation rate of photogenerated carriers, thereby reducing recombination in the space charge region (SCR) [5].

CdSe films were obtained by the painting method on previous prepared Ti substrate with surface area 15,8 cm². For the deposition following suspension was prepared: to the 1 g of CdSe and 0.25 g of $CdCl_2$ was added 0.5 g of an aqueous solution of polyethylene glycol (1 % by weight). The starting CdSe powder was milled in a ball mill with agate balls for 32 hours and then treated for 2 hours with an ultrasonic disperser UD-11 (Techpan, Poland): the oscillator frequency was 22 kHz,

and the power was 100 watts. The films of CdSe were applied in 2 layers. Each layer was annealed in an air atmosphere at 535 °C for 30 minutes. After that, the surface was activated in an aqueous solution of 0.5 M CrO₃ for 45 seconds at room temperature and washed in distilled water.

As a hydrogen absorbing electrode (cathode), a commercially produced active mass MH from industrial Ni-MH batteries were used. The Cu₂S electrode was prepared by dipping copper-coated nickel foam into a polysulfide solution. Copper was deposited by the electrochemical method from a solution containing CuSO₄ 200 g/l H₂SO₄ 50 g/l by the current density 3 A/dm². Copper in a polysulfide solution gradually corrodes, forming a Cu₂S layer. When studying the parameters of a 3-electrode photoelectrochemical cell, it was found that the maximum current during illumination was several times greater than the maximum current obtained by using a 2-electrode scheme. At the same time, the photoaccumulator made it possible to obtain a maximum current of 97 mA during the discharge of the MH electrode without illumination. The value of the open-circuit voltage of such a photoaccumulator in the absence of illumination is about ~0.4V.

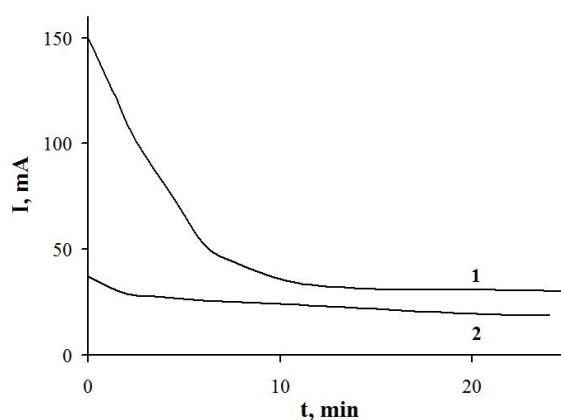


Figure 3. Current - time dependence. 3-electrode photoelectrochemical cell (1); 2-electrode cell (2).

Conclusions

We have developed a reversible photoelectrochemical system using the accumulated hydrogen. Reversibility is ensured by introducing a third electrode based on Cu₂S, onto which a metal hydride electrode based on MH alloys is discharged. The need to introduce a third electrode is due to the fact that on photoelectrodes based on cadmium chalcogenides, the reduction reaction of the polysulfide ion practically does not proceed at the potential that is established on MH electrodes in the absence of illumination. The photoaccumulator made it possible to obtain without illumination a maximum current of 97 mA and $V_{o.c.} = 0.337$ V during the discharge of the MH electrode. A new feature of the cell design is 3D modeling. Almost all the details of the cell were printed on a 3D printer. New additive technologies make it possible to change the design of cell parts based on the results of experiments. This creates the basis for rapidly improving the electrochemical performance of the cell. It was found that the maximum current during cell illumination was several times higher than the maximum current obtained by the 2-electrode scheme. For the consumers with uneven consumption of electricity, such system is equivalent to a solid state system with the more power.

References

1. Hodes G, Manassen J 1980 *J. Electrochem. Soc.* **127**(3) 544
2. Rusetskii I A, Shcherbakova L G, Danilov M O, Slobodyanyuk I A, Kolbasov G Ya, Fomanyuk S S, Solonin Yu M 2018 *ECS Trans.* **87**(1) 335
3. Rusetskyi I A, Danilov M O, Fomanyuk S S , Slobodyanyuk I A , Vorobets V S, Kolbasov G Ya 2019 *Res. Chem. Intermed.* **45**(8) 4121
4. Macak J M, Hildebrand H, Marten-Jahns U, Schmuki P 2008 *J. Electroanal. Chem.* **621**(2) 254
5. Pleskov YuV, Gurevich YuYa. *Semiconductor Photoelectrochemistry*. New York: Springer; 1986, p. 422.

Design and Optimization of Solar-Powered Irrigation System

K. Jandova^a, R. Stranak^a

^a Department of Electrotechnology, Brno University of Technology, Faculty of Electrical Engineering and Communication Technologies, Technicka 10, 616 00 Brno, Czech Republic

There are currently several commercially produced solar-powered irrigation systems that allow irrigation to be used even in areas where pressurized water is not available. However, these are mostly systems that are only basic and do not allow for further improvements.

This article describes the design and manufacture of a custom solar irrigation system that includes, for example, a liquid fertilizer reservoir for better plant growth or a moisture meter that prevents waterlogging of individual crops. It has also built-in protection against self-destruction. Features of this system reflect not only the needs of the operator, but also the needs of the plants and, thanks to the use of a solar module; the system utilizes the most environmentally friendly source of energy.

Introduction

With the advent of more efficient and affordable photovoltaic panels, a new agricultural concept called solar irrigation is emerging. This concept offers an energy-independent solution with minimal future costs. An electric pump controlled by a timer switch offers the advantage of eliminating the human factor and replacing it with a time-controlled water-saving system. Precise timing is achieved by the proportionality of the solar cells power output on the intensity of solar radiation. At high intensities, the on-board batteries take less time to charge, thus the plants receive irrigation at the exact moment when the soil beneath them is dry and needs the moisture the most. Water saving is achieved by using drip irrigation, where water is not sprayed fan-shaped onto the soil, but it drips from central holes in a hose directly to the root of the plant, thus avoiding watering unused areas and thus additionally suppressing weed growth [1] [2].

Design and Optimization of Solar-Powered Irrigation System

The actual design of the solar-powered irrigation system evolved from the the primary components of the system. The first system component considered and analyzed was a solar panel. A 12 V/10 W polycrystalline solar panel was selected. Lithium-ion batteries type 18650 with nominal voltage 3.7 V and capacity 2600 mAh were selected for energy storage. The next step considered diaphragm water pump. The FL-3308 type was chosen, with an input of 70 W at 12 V and a flow rate of 4-6 l/min. Lastly, a microcontroller was selected as the control unit, specifically the Raspberry Pi Pico [2].

The next step in the development of the whole device were calculations that reflected the volume of water that needs to be pumped to irrigate an average garden when watering repeatedly several times a day. The design continued with the creation of a block diagram, which at the top level consists of the power management, controller and output peripherals.

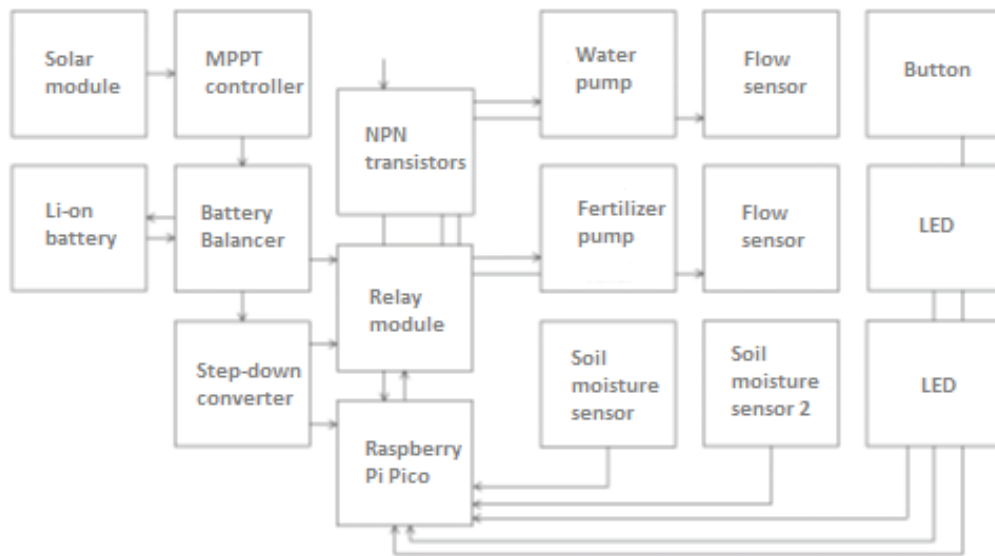


Figure 1. Solar-powered irrigation system layout block diagram [2]

From the block diagram comes the electrical design, which includes the creation of a circuit board (Figure 2). Subsequently, a 3D model of the device was created in SolidWorks and consists of an external and an internal part.

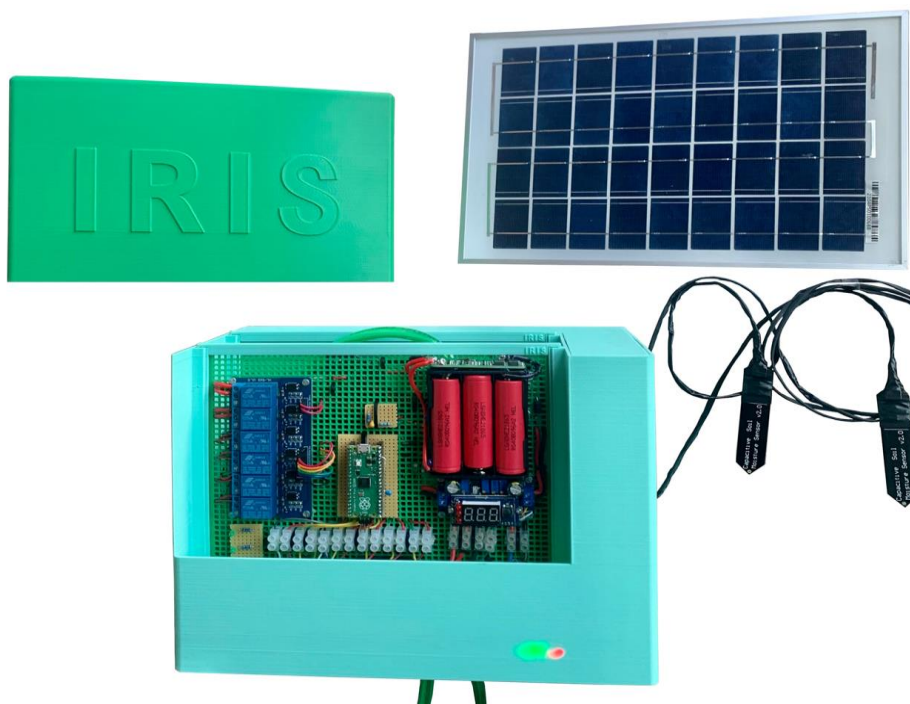


Figure 2. Designed solar-powered irrigation system [2]

The complete system has been subjected to several tests. The first test was the irrigation cycle time, where after pumping 60 liters of water, irrigation was restarted after one hour. Next, a test of the protection of the equipment was carried out, when after disconnecting the supply hose from the water, the system detected an error and switched off the equipment. And the last test, the pre-irrigation test, reliably started irrigation only when the correct soil moisture values were measured (Figure 3).

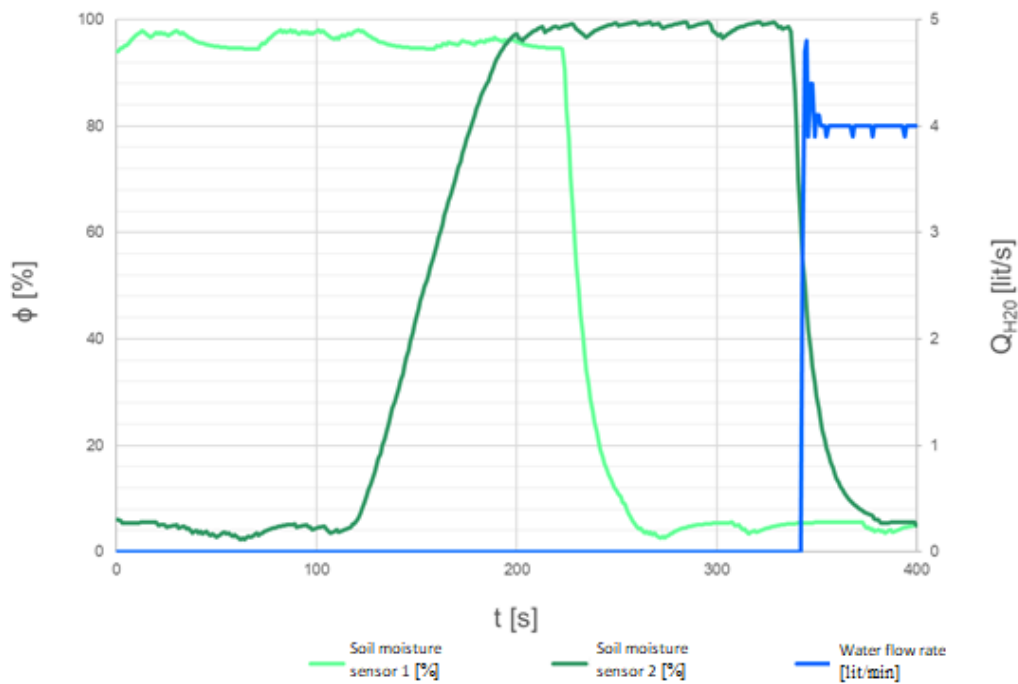


Figure 3. Soil moisture sensor tests [2]

Conclusion

The paper focuses on the description of an automatic solar-powered irrigation system that was developed addressing the identified shortcomings of commercially produced irrigation systems. Powered by a photovoltaic panel, the system is independent of a grid connection and, thanks to the built-in pumps; no source of pressurized water is required. The major benefits of this system are its environmental friendliness, water conservation and automated operation. The addition of a fertilizer tank ensures even better plant care. Similarly, the addition of protective elements ensures a longer lifetime of the entire system.

Acknowledgments

This work was supported by the specific graduate research of the Brno University of Technology No. FEKT-S-20-6206.

References

1. Solar irrigation [online]. [cit. 2021-5-9]. Available from: https://ecoproduct.cz/c/vsechno-solarni-zavlazovani-1880?gclid=CjwKCAjwkN6EBhBNEiwADVfyawnaR3AwnD8bx3I_I7AZlhqytbmz-NzKudAAGT2SO68ZSXYBvLO-DhoCqA0QAuD_BwE
2. Straňák, R. Solar Irrigation, Brno 2022, Bachelor Thesis, Brno University of Technology, Faculty of Electrical Engineering and Communication Technologies, Department of Electrotechnology, 2022-06-15, Available from: <https://www.vut.cz/en/students/final-thesis/detail/141576>.

Photoelectrochemical Method for the Investigation of Wide-Bandgap Semiconductors

Katharina Mairhofer^a, Silvia Larisegger^a, Günter Fafilek^b

^a KAI GmbH, Europastraße 8, AT-9524 Villach

^b Vienna University of Technology, Institute of Chemical Technologies and Analytics, Getreidemarkt 9, AT-1060 Vienna

A new setup for an inverted rotating disk electrode (IRDE) was developed for the investigation of photoassisted or photoelectrochemical processes involving mass transfer reactions, as in electrodeposition or etching processes. In this setup, rotation of the disk electrode is achieved by magnetic coupling between a driver magnet (i.e. a magnetic stirrer) and the follower magnet included in the sample holder. For photoelectrochemical experiments, the cell allows a homogeneous illumination and removal of gaseous reaction products, while still providing leak tightness. In this way, controlled flow conditions are provided with the possibility to simultaneously illuminate the sample surface from a distance as small as 20 mm. At the same time gases formed during the reaction can easily ascend through the electrolyte.

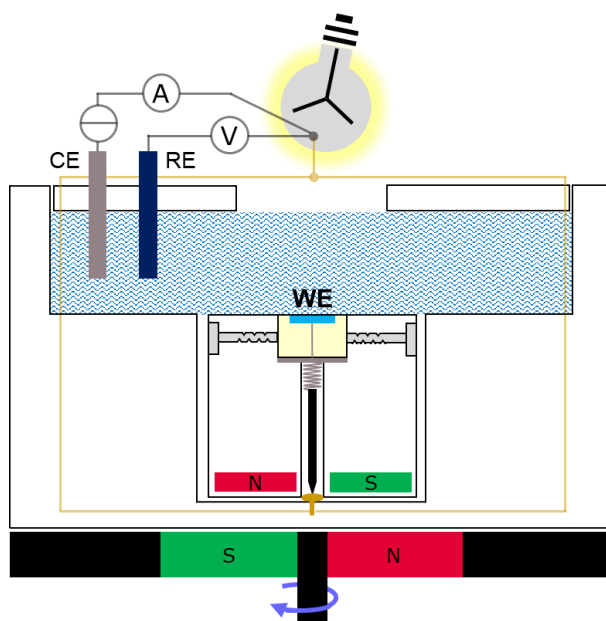


Figure 1. Schematic representation photoassisted electrochemical reactions done in the newly developed inverted rotating disk electrode setup.

The light source is placed on top of the cell and illumination is done through the electrolyte. A low liquid level (≥ 15 mm) allows a small distance between the sample and the light source and therefore a high light intensity on the sample surface. Illumination is done using a high-power LED. Due to the high power, thermal effects need to be taken into consideration and especially an effective cooling of the LED is essential.

As a wide band gap semiconductor, silicon carbide (SiC) has gained large interest due to its high chemical and physical stability. Since photoassisted anodic etching of n-type 4H silicon carbide in potassium hydroxide solutions [1] requires both UV illumination and the removal of gaseous reaction products, this reaction is investigated in the newly developed IRDE setup. Possible applications for such a process are defect decoration [2], trench etching, and dicing.

Photoassisted anodic etching of n-type SiC occurs in three steps: (1) hole generation in the material through illumination with light with an energy higher than the bandgap of the semiconductor (2) oxidation of silicon and carbon through the holes driven to the semiconductor-electrolyte interface by an external potential and (3) dissolution of the oxidation products in the electrolyte. In accordance with the three steps of the reaction, different processes can be limiting: For low light intensities (either through a large distance between the sample and the LED or through low driving currents through the LED) the number of photon-induced holes is limiting. At low electrolyte concentrations, the transport of hydroxyl ions and the dissolution of the oxidation products determine the etch rate. For high light intensities and high electrolyte concentrations, the external potential and thereby the oxidation reaction are limiting for the overall current flow. These different reaction regimes can be distinguished in cyclic voltammetry measurements in the newly developed IRDE cell.

References

1. D. H. van Dorp und J. J. Kelly, „Photoelectrochemistry of 4H–SiC in KOH solutions,“ *Journal of Electroanalytical Chemistry*, Bd. 599, Nr. 2, pp. 260-266, 2007.
2. J. L. Weyher, S. Lazar, J. Borysiuk und J. Pernot, „Defect-selective etching of SiC,“ *physica status solidi*, Bd. 202, Nr. 4, pp. 578-583, 2005.

Comparison of Modelling Tools of the Photovoltaic Power Plants

J. Vaněk^a, P. Maule^a and F. Šmatlo^b

^a Department of electrotechnology, Brno University of Technology, Brno, Czech Republic

^b Brno University of Technology, Brno, Czech Republic

Authors of this paper describe the creation of a 3D model of the PV system environment directly in the PVSOL software tool and compares it with a second 3D model created in the PIX4D photogrammetric software. The main advantage of both 3D models is the accuracy of the shading simulation. Any shadow on the PV module reduces the output power, so it is important to have an accurate model of any object that could shade the PV modules. This paper also describes the PV system design in the PVSOL design software.

General information

When designing a photovoltaic system, it is important to evaluate several aspects. These aspects include the geographical location, specific system location and orientation, system size, and shading effects. Because the shading greatly affects the output power of the photovoltaic modules, great care should be taken to avoid this effect. For this reason, it is advisable to precisely determine the degree of shading of the photovoltaic modules and adjust the system to ensure the highest efficiency and yield of the system. The PVSOL design software allows you to create 3D models of buildings on which photovoltaic modules can be installed. Creating larger and more complex 3D models in PVSOL is very laborious and time consuming. That is why the photometric software PIX4D was used in this work, which enables to create a real 3D model of larger building complexes and their surroundings and thus increase the accuracy of the screening and also to determine the influence of larger surroundings on the screening of photovoltaic modules.

Creating 3D models

PVSOL

PVSOL software allows you to create 3D building models by pulling an object from the map. Use this tool to eject a 3D object from an aerial photo of a building. The tool is sufficient to determine the degree of shading of panels and is often used for most buildings. It is very suitable for determining the degree of shielding of objects placed on the roof (chimney, satellite, sunroof). With this tool it is also possible to create distant large objects eg factory chimney. A problem may arise if a building with a photovoltaic system is surrounded by a large number of buildings that cast shadow on the photovoltaic modules. These objects can be created, but implementation would be very time consuming.



Figure 1. 3D model created in PVSOL (part of town)



Figure 2. Detail 3D model created in PVSOL (building)

PIX4D

Photometric software PIX4D is used for digitizing photographs taken from drones. However, any 3D model can be created using this software. Unlike PVSOL, where one photo and knowledge of all building dimensions is used to create 3D models, PIX4D needs a large number of photos to create a real 3D model. 103 photos from different angles were used for the 3D model (Figure 3). However, the advantage is that to determine the exact scale of the model, it is necessary to know only one exact dimension of the building, eg the length of the wall. For this work, photos taken in Google Earth were used. By combining the photographs, a 3D model of the part of the city of Brno, in which the building with the proposed photovoltaic system is located, was created.



Figure 3. 3D model created in PIX4D (part of town)



Figure 4. Detail of 3D model created in PIX4D (building)

Photovoltaic system design

After creating a 3D model, the design of the photovoltaic system is very individual. In the PVSOL software it is possible to select the type of the modules, their placement and fixing to the roof. Regarding the selection of the inverter for the designed system, PVSOL allows for automatic configuration and selection of the inverter based on the selected panels, their distribution into strings and performance. The cable connection is generated automatically and can be modified. The big advantage of PVSOL is that every photovoltaic component (inverters, modules, batteries) available on the market is cataloged and has a model with exact parameters in PVSOL. [3]

Shading simulation

The PVSOL software allows simulation of average annual shading. An important input parameter for the simulation is the geographical location of the object with a photovoltaic system. Shading simulation calculates the average annual shading of each module in the system. The result of the simulation is shown as a percentage and using a color scale. Comparing the shading simulations of the two 3D models, we can see that the models are very similar (Figure 5, 6). Both 3D models also have very similar specific annual yields. Yield differs by 4.52 kWh / kW_p, or 0.44%. Another important output value of the simulation is to reduce the yield by shading. At this value, the models differ by about 0.5% / year or 9.8% of the total yield of the photovoltaic system.



Figure 5. Shading simulation of PVSOL model

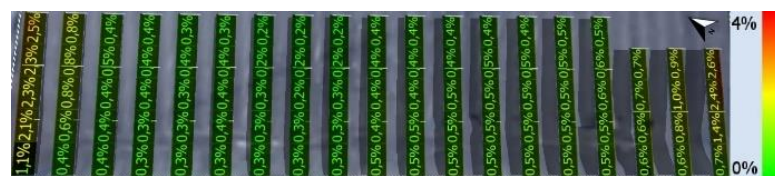


Figure 6. Shading simulation of PIX4D model

Economic simulation results

The total energy produced by the PV generator is 28 282 kWh/year. Almost all of the energy produced is consumed directly in the building (99.5%). Only 137 kWh/year will flow into the distribution network. Although almost all energy produced is consumed directly, the degree of self-sufficiency is only 15.2%.

The investment costs for the PV plant were estimated at CZK 2 064 271.62. Half of this is the cost of system components. The other half is the cost of installation and all design. The aid amounts to 65% of the investment costs. The amount of support was estimated between the amount of support for medium and large enterprises according to the subsidy program that the proposed PV system could use. Furthermore, the annual cost was estimated at CZK 25 791. This amount is used to cover the maintenance of the PV plant.

After the installation of the PV plant, the amount of energy savings is approximately CZK 133 000. If we deduct maintenance costs, we get annual savings of about 110 000 CZK. With the same savings each year, the payback is just 6.6 years. This means that in nearly 7 years the PV system will save the same amount as the initial investment with a subsidy.

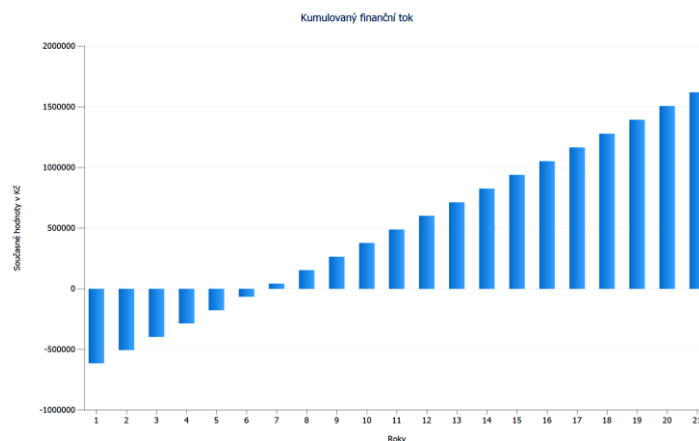


Figure 7. Economic simulation of designed PV system

Table I: Financial analysis

Total investment costs	CZK 2 064 271.62
Total return on capital	15.38%
Amortization period	6.6 Years
Own production costs of electricity	2.27 CZK / kWh

Conclusion

Shading is an important influence on the output of the photovoltaic system. By determining the exact screening rate, the system yield can be determined sufficiently accurately. The main aim of this work is to describe the creation of 3D models in PVSOL and PIX4D, accuracy of shielding simulations and their comparison. Comparing the results of the shielding simulation it was found that both models are very similar. The model created in PIX4D has a greater degree of shading. This was probably due to inequalities in the 3D model. Due to small variations in simulation results, this model can be described as sufficiently accurate. In terms of the time required to create 3D models, it depends on the complexity of the objects that can obscure the photovoltaic modules. If it

is an environment with minimal shading of surrounding objects (arrays, separate objects) it is preferable to use the 3D editor PVSOL. On the other hand, for built-up environments (cities, company premises) it is better to use the photogrammetric software PIX4D.

Acknowledgements

This work was supported by the specific graduate research of the Brno University of Technology No. FEKT-S-20-6206.

References

1. Valentine Software [online]. [cit. 2019-03-14]. WEB: <https://www.valentin-software.com/en/products/photovoltaics/57/pvsol-premium>
2. PIX4D [online]. [cit. 2019-03-14]. Dostupné z: <https://www.pix4d.com/>
3. HASELHUHN, Ralf a Petr MAULE. Fotovoltaické systémy: energetická příručka pro elektrikáře, techniky, instalatéry, projektanty, architekty, inženýry, energetiky, manažery, stavitele, studenty, učitele, ostatní odborné a profesní soukromé nebo veřejné instituce a zájemce o fotovoltaický obor a energetickou nezávislost. Plzeň: Česká fotovoltaická asociace, 2017. ISBN 978-80-906281-5-1.

Electrochemical Impedance Spectroscopy and quality indicators

J. Appell

BioLogic, Grenoble, France

There are two main types of techniques in electrochemistry: Direct Current (DC) and Alternative Current (AC). DC techniques mainly include potential or current steps, pulsed and sweep methods such as Chronopotentiometry, Chronoamperometry, Linear Scan Voltammetry or Cyclic Voltammetry. With DC techniques, the response of an electrochemical system is studied as a function of time. With AC techniques, such as Electrochemical Impedance Spectroscopy (EIS), the response of the system to a potential or current sinusoidal perturbation is studied as a function of the frequency, which is swept over a few decades. The frequency sweep enables access to all processes taking place at the electrode such as charge transfer and mass transport. Any other electrical contribution and artefacts would also be visible with EIS.

To provide high quality data three conditions are required, the system must be linear, time invariant and with a good signal to noise ratio. Three indicators (THD, NSD and NSR) calculated by the EC-Lab software from BioLogic can be used to check that these conditions are met and that data can be trusted.

Total Harmonic Distortion (THD)

Most of the electrochemical systems are non-linear but by applying an input signal of small amplitude, non-linear systems can be considered as linear as the curve under study around the operating point can be approximated by its tangent.

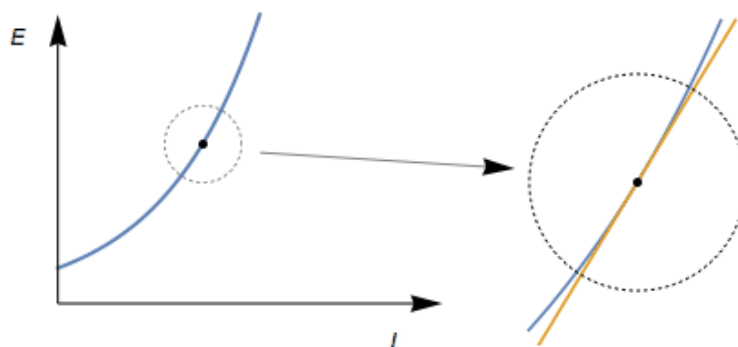


Figure 1. Non-linear steady-state E vs I curve in blue and its tangent in orange.

THD indicates if the amplitude of the current or potential modulation applied to the system is small enough to consider that it behaves linearly. If a system behaves nonlinearly the output signal will contain some harmonics. The THD quantifies the nonlinearity by evaluating the amplitudes of the N harmonics:

$$\text{THD}_N = \frac{1}{|Y_f|} \sqrt{\sum_{k=2}^N |Y_k|^2}$$

where $|Y_f|$ is the amplitude of the signal at the fundamental frequency f (or first harmonic) and $|Y_k|$ is the amplitude of the k th harmonic number.

THD is expressed as a percentage, it is generally considered that a THD below 5 % is acceptable. In EC-Lab, it is calculated on the potential and on the current and over 6 harmonics ($N = 7$).

In the example below using a test box, EIS measurements were done on the frequency range 100 kHz – 1 Hz and using increasing amplitudes of 2, 5, 10, 13, 15 and 20 mV. We see on the Nyquist diagrams from figure 2 that plots are not overlaying, meaning the system is non linear. On the THD vs $\log(f)$ plots of figure 3 we see that the higher the amplitude, the higher the THD. In this case the limit of a 5% THD is obtained for the 5 mV and 2 mV amplitudes. We can also note that frequency has an effect on the THD, this could be used in some cases as a way to avoid non linearity.

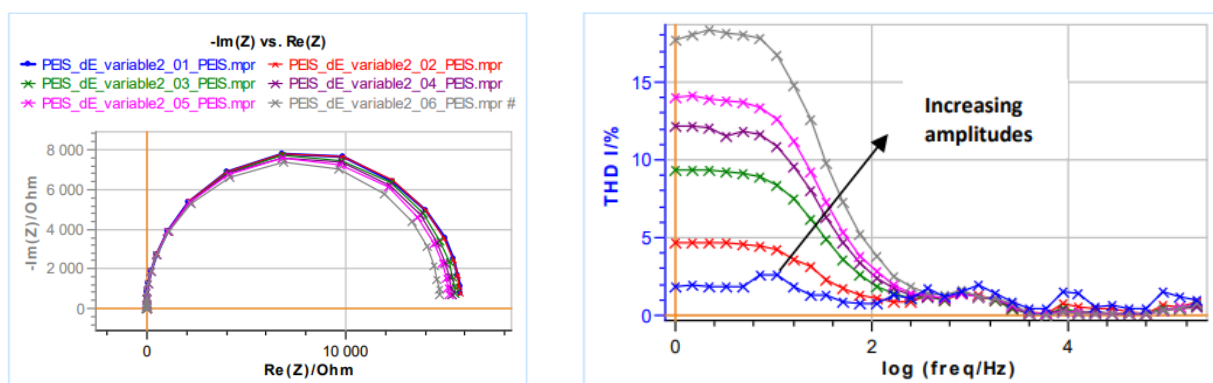


Figure 2. (left) Nyquist diagrams

Figure 3. (right) THD vs $\log(f)$ plots

Non-Stationary Distorsion (NSD)

It is important that the system and its response do not change with time during an impedance measurement. We can distinguish two causes for the nonstationarity of a system, either the response of the system has not reached its permanent regime or either the parameters defining the system are changing with time. The response of a non-stationary system will contain, in addition to the fundamental frequency, some adjacent frequencies. Hence the NSD indicator is defined as:

$$NSD_{\Delta f} = \frac{1}{|Y_f|} \sqrt{|Y_{f-\Delta f}|^2 + |Y_{f+\Delta f}|^2}$$

Where $|Y_f|$ is the amplitude of the signal at the fundamental frequency f (or first harmonic), $|Y_{f-\Delta f}|$ et $|Y_{f+\Delta f}|$ are the amplitudes of the peaks right next to the fundamental frequency and Δf is the frequency resolution. The NSD is expressed as a percentage and calculated on the potential and current. The drift correction in EC-Lab is based on the compensation of the adjacent frequencies.

Noise to signal ratio (NSR)

In an ideal measurement, all the signal energy is contained in the fundamental frequency, but because of various factors such as the accuracy and precision of the measuring device or external

perturbations, there might be some energy in other frequencies than the fundamental one, which is called noise.

Besides reducing the sources for noise it is useful to increase the amplitude of the signal.

The NSR quantifies the extent of noise in the measurement. It is expressed using the following formula:

$$NSR_f = \frac{1}{|Y_f|} \sqrt{\sum_k |Y_{k\Delta f}|^2}$$




With:

$$k\Delta f \notin \{f; 2f; 3f; 4f; 5f; 6f; 7f; f - \Delta f; f + \Delta f\}$$

It represents all the signal not contained in the fundamental frequency, the 6 harmonics used to calculate THD or the signal at frequencies adjacent to the fundamental frequency used to calculate NSD.

Conclusion

Getting a linear system and the corresponding low THD requires decreasing the amplitude but increasing the amplitude helps to get a better NSR. We can therefore see that tuning the settings of an experiment requires compromises and likely several tries.

Observation	Reason	Solution
High THD	Your system is not linear 	Decrease the perturbation amplitude of the input signal
High NSD	Your system is not yet stationary 	Increase the time of the rest period before the EIS measurement
High NSR	Your output signal is too small 	Increase the perturbation amplitude of the input signal

Batteries in SEM: in situ battery materials synthesis and electrical testing

O. Klvač^{a,b}, L. Novák^a, Petr Glajc^a, T. Kazda^b

^a Thermo Fisher Scientific Brno, Vlastimila Pecha 12, 627 00, Brno, Czech Republic

^b Department of Electrical and Electronic Technology, Faculty of Electrical Engineering and Communication, BUT, Technická 10, 616 00 Brno, Czech Republic

The aim of this paper is to show the possibilities of lithium-ion battery research using scanning electron microscopy (SEM). We present in-situ battery testing holders for SEM and FIB-SEM systems. Two types of in-situ holders were developed, which allow transfer of the battery sample in a protective environment (under inert gas or high vacuum), electrical testing, and heating. Heating can be combined with the injection of reactive gases for the synthesis of electroactive materials, subsequently used for battery preparation and in-situ investigation.

Introduction

Commercial secondary lithium-ion battery production began in 1991. Thanks to intensive development and research, their properties have improved significantly. Currently, they are the most widespread energy storage devices for portable electronics and electric vehicles. With such a massive expansion, it is necessary to look for new materials and continue with technology improvement focused mainly on price, performance, ecology, safety, and cycle life [1][2].

Electron microscopy is an essential part of battery development and brings a lot of valuable information. It enables the analysis of a wide range of processes during the synthesis of electrode materials as well as electrode aging processes such as deformation and delamination of electrodes, particle cracking, growth of films, clogging of pores, and elemental composition changes [3].

In most cases, the battery is discharged after cycling, disassembled, and the electrode surface or cross-section is scanned. However, certain phenomena such as lithium plating cannot be observed with an ex-situ approach **Chyba! Nenalezen zdroj odkazů.** Furthermore, a direct correlation between electrochemical characterization and grain level changes is missing. For these purposes, in-situ/in-operando SEM characterization can be helpful. In both cases, it is necessary to prevent material degradation caused by air exposure and electrolyte evaporation [2][3][4].

This work presents solutions for specific requirements during an investigation of battery materials using SEM. Air-sensitive samples can be transported using two different types of inert gas transfer modules. For in-situ investigation, the whole battery is created inside the SEM chamber. The materials are observed from the first soaking with the electrolyte and the presented method is universally applicable for various materials. Furthermore, used materials can be synthesized directly in the SEM chamber using our MEMS chip.

Instrumentation

For battery materials research purposes, a special shuttle (see Figure 1) was designed. It contains a stub for bulk material, from which the battery can be created by FIB, and the electrical

testing holder, electrically connected with a 15-pin CANON connector at the air side of the vacuum feedthrough installed on the SEM chamber. A MEMS chip designed for heating and biasing experiments [5] in Thermo Fisher Scientific tools [6] is placed in the electrical testing holder.

The heating pad on the MEMS chip allows to set and measure temperatures up to 1200 °C. A further option is a connection of a gas inlet apparatus with an aperture or penetrated membrane [7]. The gas pressure can be set up to several hundreds of Pascals. In this arrangement, the synthesis of materials can be observed during injection of reactive gases, which cannot be used in a standard environmental SEM due to safety reasons. This setup was used for in-operando observation of the LMNO (Lithium Manganese Nickel Oxide) and NMC (Nickel Manganese Cobalt Oxide) grains nucleation in pure oxygen or for the formation of WS₂ nanotubes in hydrogen sulfide.

Biasing contacts can be used for the measurement of electrical properties of a heated material or as current collectors of a microscopic battery. Figure 1 shows the preparation procedure of an electrical cell. A chunk of an electroactive material can be cut using the FIB-SEM system from bulk material on the stub. Material is then transferred and aligned with biasing pad by an EasyLift micromanipulator and contacted by FIB-assisted deposition of conductive material (Pt, W, C, ...) using MultiChem Gas Delivery System. It is also possible to use a modified micromanipulator as a current collector of a reference or examined electrode. This arrangement allows quick disassembling of the cell before further analysis.

The procedure was applied for the in-situ characterization of the lithium - lithium titanate (LTO) half-cell. The ionic liquid EMIM BF₄ in a mixture with LiBF₆ salt was used as the electrolyte. Very low vapor pressure of ionic liquids allow their usage in vacuum of the SEM chamber. Another advantage of this approach is that the ionic liquid can be moved along the surface of the MEMS chip with a FIB. During the experiment, it was possible to find a correlation between the results of electrochemical cycling and changes on the electrode surface [8].

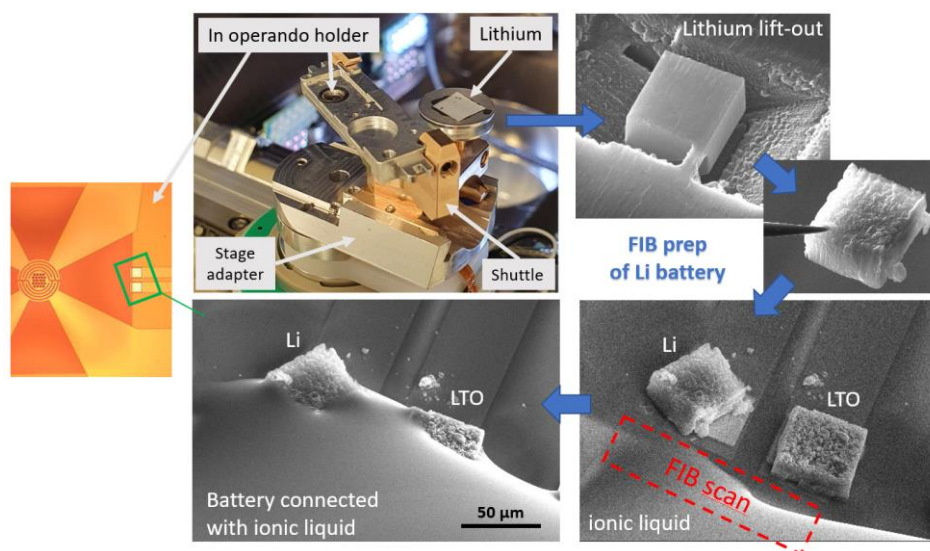


Figure 1. The battery testing holder with MEMS chip and sample stub; FIB preparation of battery system

Two types of transfer modules - CleanConnect device (Figure 2; left) and standalone transfer box (Figure 2; right) were designed for the transfer of electrical testing holder with air-sensitive samples between glovebox and SEM.



Figure 2. Clean Connect (left) and standalone box (right) inert gas transfer systems

In the case of the Clean Connect device, the sample is placed into a capsule with a mechanical shutter. Transport can take place in a vacuum or under the overpressure of an inert gas (i.e. argon). A special loading antechamber is located on the glovebox and the SEM chamber. After connecting the capsule with the sample, it is pumped down and filled up with inert gas several times. After that, the capsule shutter can be opened and the sample is loaded. The advantage is that pumping of the low volume enables fast loading [9].

The standalone transfer box allows sample transfer under vacuum only, because it is sealed by the overpressure of the surrounding air. Using the SEM stage, the entire box is parked in a holder inside the SEM chamber. During the pumping of the SEM chamber, the upper part is separated and the box is opened. After the experiment, the transfer box is closed and sealed again during chamber venting. The pressure inside the transfer box can be monitored through the MEMS heating pad (the heat conduction principle). The advantage is the simplicity of the system without the need for an antechamber.

Acknowledgments

This work was supported by the specific graduate research of the Brno University of Technology No. FEKT-S-20-6206.

References

1. G. E. Blomgren, *Journal of The Electrochemical Society*, 164, A5019-A5025 (2017)
2. D. Liu et al., *Advanced Materials*, 31 (2019)
3. T. Waldmann et al., *Journal of The Electrochemical Society*, 163, A2149-A2164 (2016)
4. Kovachev et al., *Batteries*, 5 (2019)
5. L. Mele et al., *Microscopy Research and Technique*, 79, 239-250 (2016)
6. L. Novak et al., *Microscopy and Microanalysis*, 22, 184-185 (2016)
7. L. Novak et al., *Microscopy and Microanalysis*, 26, 1144-1145 (2020)
8. O. Klvac et al., *ECS Transactions*, 105, 655-663 (2021)
9. K. K. Neelisetty et al., *Microscopy and Microanalysis*, 27, 2508-2509 (2021)

Characterization of Materials for Conversion and Energy Storage – Presentation of Pragolab Company

A. Kolouchová

Pragolab s.r.o., Jamborova 32/3181, 615 00 Brno – Židenice, Česká republika

The energy storage technology will play a key role in the trend toward renewable and sustainable industrial solutions involving electrification. Batteries consist of many different types of materials and their properties are crucial for the performance. Used materials could be described by different analytical techniques that will be introduced with application related examples.

Separators are an important component within a Li-ion battery that mechanically separates the anode and cathode while allowing maximum ionic conductivity of the Li-ion containing electrolyte. Its design and performance directly affect the capacity, cycle life, and safety performance of the battery. The separator must have sufficient porosity to hold liquid electrolyte, but excessive porosity hinders the ability of the pores to close which shuts down an overheated battery. The porosity of a separator, also called a diaphragm, is commonly measured directly by the mercury intrusion method.

Diffusion constants can be measured by dynamic vapor sorption technique and the surface energy contributions of a solid matter can be measured by inverse gas chromatography.

The humidity of the feed stream is vital to the performance of proton exchange membrane fuel cells. The surface energy is related to electro-osmotic drag, back diffusion of water, and water retention.

Both porosity and surface area are important electrode material properties measured usually by gas adsorption technique. The true density is a good indicator of purity and composition of the cathode which can be used to improve the overall performance of the battery. Battery slurries are produced from powders by mixing the binder and solvents. The powder rheometer offers comprehensive powder flow analysis, helps to optimize the electrode packing density and control slurry agglomerates and dispersibility.

Electrode coating slurries are complex systems, which contain a large percent of solid particles of different chemicals, sizes and shapes, dispersed in a highly viscous media. Cathode slurry contains active material, conductive agent, binder and solvent. However, these components can present various challenges. Static multiple light scattering consists of illuminating the sample with an infrared light source and acquiring backscattered and transmitted signals over the whole height of the sample. By repeating this measurement over time, the instrument enables to monitor physical stability of the slurry. When producing electrode slurries, the drying protocol must be optimized (time, temperature, thickness). The kinetics and understanding of the effect of temperature and humidity can be described by contactless brownian motion monitoring within thin layer under controlled conditions.

Different electrolytes providing high ionic conductivity are required, they also have to be chemically and thermally stable, for this reason different additives extending their cycle life, minimizing gassing and protectors against overcharging are required. An accurate determination of particle size and zeta-potential in these complex systems is required. Not only anisotropic particles can be described directly with a first commercial analyzer using the principle of depolarized dynamic light scattering. Advanced kinetics, molecular weight, gyration radius and concentration measurement are included too.

Techniques used to describe battery materials covered by the presentation:

- Mercury and gas porosimetry – porosity and surface area
- Helium pycnometry – true density
- Stoke's law – particle size of solids
- Powder rheology – static and dynamic powder properties
- Diffusing wave spectroscopy – thin layer formation
- Static multiple light scattering – stability studies
- Dynamic vapor sorption – the effect of humidity
- Inverse gas chromatography – surface energy
- Dynamic light scattering – particle size in suspensions
- Depolarized dynamic light scattering – particle size of (not only) anisotropic particles
- Laser Doppler electrophoresis – zeta-potential

This presentation was prepared using materials from: Thermo Fisher Scientific (Haake), Micromeritics, Freeman Technology, Formulaction and Cordouan Technologies. The company Pragolab is an authorized distributor providing a high-level support and service maintenance to the customers in Czech Republic and Slovakia since 1993. These uniquely valuable techniques deliver speed, accuracy, and characterization of properties critical to safety, energy density, and longer cycle life of different types of batteries.

Experimentally Based Modelling of Li-S Batteries

M. Mačák^a, K. Jaššo^a, P. Mezera^a, T. Kazda^a, P. Vyroubal^a

^aDepartment of Electrical and Electronic Technology, Brno University of Technology
Brno 616 00, Czech Republic

Physical processes in Li-S batteries are very complex and are difficult to describe in a way, which would be effective for the use in numerical simulations. As a result, it is convenient to build models, that are based on experimental measurements. The presented article describes a simple empirical 0D model of a Li-S battery, which is based on discharge characteristics and their subsequent curve fitting. The main advantage of this model is its simplicity and easy acquisition of the experimental data.

Introduction

As the overall energy demand increases due to continuous electrification of various areas such as transportation or energy storage, there is also a higher demand for sustainable energy systems with high energy density. Li-S batteries pose as one of the most interesting next generation battery technologies due to their high specific capacity ($1675 \text{ mA}\cdot\text{h}\cdot\text{g}^{-1}$) and theoretical energy density ($2600 \text{ W}\cdot\text{h}\cdot\text{kg}^{-1}$). Additionally, sulfur is common and environmentally friendly material, unlike general cathode materials used in Li-ion batteries (1).

Currently, the research in this area is mainly focused on finding optimal compositions of the batteries, which would be able to suppress negative properties of this technology. On the other, the research in numerical simulation is still relatively limited (2). While physics-based models should be the most precise, they contain many parameters, which are often very difficult to measure or even estimate precisely (3). The other common modelling approaches use equivalent electrical circuits. In this method, characteristics of a battery are described through a defined electrical circuit consisting of different circuit elements. The element values are obtained from experimental measurements such as electrochemical impedance spectroscopy or galvanostatic intermittent titration technique (4). This modelling approach is still very accurate despite its simplicity. The only disadvantage is that it is necessary to carry out additional measurements and find an appropriate circuit model, which can fit the experimental data.

This article presents an empirical model of a Li-S battery, which was based on a model originally designed for Li-Ion batteries (5). The model was simplified to a 0D case, in which it was not necessary to resolve the computational domain. The model is governed by curve fitting of discharge and charge characteristics, which are the most common experimental data. As a result, this model is very simple but still precise for the modelling of a battery cycling and can be easily extended to include additional effects.

Numerical Model

The presented model is based on a model described in the works of Kwon et al. (5) and Gu (6). This model (5, 6) uses a multi-scale multi-domain approach in which, the macroscopic description of electric potential distribution is defined by the Poisson equation. The electrochemical sub-model,

which is responsible for the modelling of battery behavior is based on a curve fitting of discharge/charge characteristics. These two scales are coupled through a current density source term in the macroscopic electric potential equations. As it is not always necessary to resolve spatial variations of electrode potentials, especially if the simulations are only focused on the battery cycling, this model can be significantly simplified into a 0D model defined by (6):

$$I = Y(\Phi - U) \quad [1]$$

Where I is the current, Φ is the battery voltage, Y is the apparent conductivity and U is the open circuit voltage.

The battery voltage is then defined as:

$$\Phi = U + I/Y \quad [2]$$

To obtain model parameters (Y and U), it is first necessary to generate polarization curves, which describe the relation of current and battery voltage at a defined depth of discharge (DoD). This was carried out by measuring discharge characteristics at current rates of 0.05 C, 0.2 C, 0.5 C and 1 C (shown in Fig. 1). Polarization curves for every 0.1 DoD are shown in Fig. 1 on the right. The DoD step for simulations was set to 0.01 to obtain detailed data points. The DoD dependences of Y and U parameters were obtained by fitting the data with the equation [1]. The parameter Y was defined as an inverse gradient of the curve, while U was defined as the intercept of the current voltage curve (6). To properly describe Li-S characteristic behavior, it was necessary to implement current dependency of the battery capacity (visible capacity decrease shown in Fig. 1).

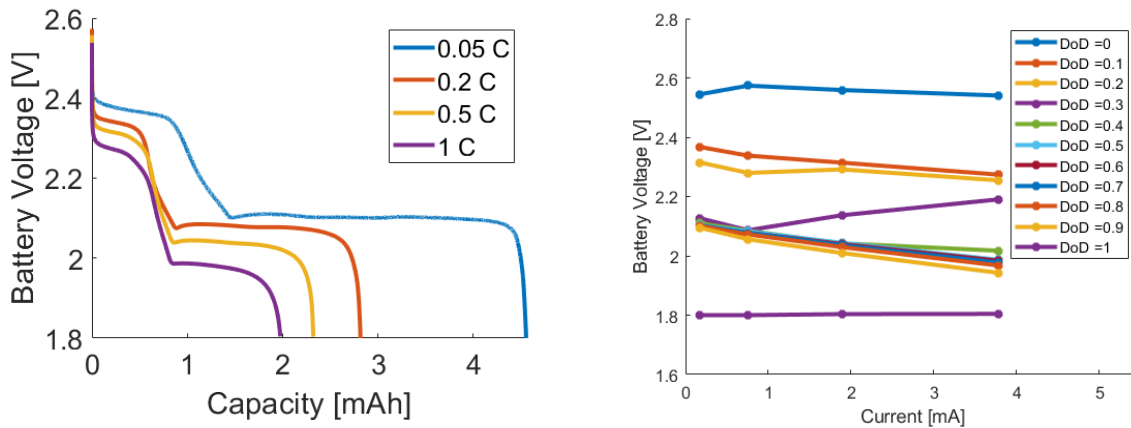


Figure 1. Experimentally measured discharge characteristics (left). Current-voltage characteristics at defined DoDs (right).

Results

Obtained numerical results (Fig. 2) show that the presented model can accurately describe Li-S characteristic properties such as two plateaus (higher around 2.35 V and lower around 2 V - 2.1 V) or the dip at the beginning of the lower plateau. Also, it was possible to model the influence of the current load on the battery overall capacity and the potential decrease of the plateaus. The main advantage of this model lies in its simplicity and low requirements for experimental data.

Additionally, it can be simply adjusted to consider the effects of long-term cycling or temperature effects.

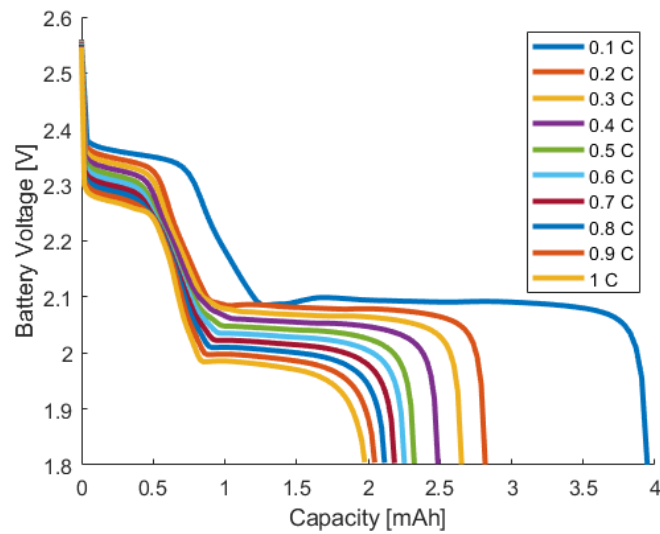


Figure 2. Discharge characteristics obtained from the numerical model.

Acknowledgments

This work was supported by the BUT specific research program (project No. FEKT-S-20-6206).

References

1. X. Qiu, Q. Hua, L. Zheng, and Z. Dai, *RSC Advances.*, **10**(9), pp. 5283-5293 (2020).
2. T. Kazda, D. Capková, K. Jaško, A. Fedorková Straková, E. Shembel, A. Markevich, and M. Sedlaříková, *Materials*, **14**(19) (2021).
3. K. Kumaresan, Y. Mikhaylik, and R. E. White, *Journal of The Electrochemical Society*, **155**(8) (2008).
4. A. Fotouhi, D. J. Auger, K. Propp, and S. Longo, *IET Power Electronics*, **10**(11), pp. 1289-1297 (2017).
5. K. H. Kwon, C. B. Shin, T. H. Kang, and C. -S. Kim, *Journal of Power Sources*, **163**(1), pp. 151-157 (2006).
6. H. Gu, *Journal of The Electrochemical Society*, **130** 1459 (1983).

Unconventional Hybrid Energy Systems Based on Innovative PV Modules and Electrochemical Batteries Provide High Energy Creator and Storage.

E. Shembel^a, K. Sukhyy^a, V. Redko^b, T. Pastushkin^b, Y. Pustovalov^c, J. Kaszuba^c, B. Kutnick^b,
V. Kyrychenko^d, D. Kaszuba^c, A. Fedorková^e, A. Markevich^a, Yu. Polishchuk^a,
I. Maksyuta^a, N. Zaderey^a

^a Scientific Research Laboratory of Chemical Power Sources of Ukrainian State University of Chemical Technology, Dnipro, 49005, Ukraine

^b Enerize Corporation, Coral Springs, FL, 33067, USA

^c INT sp z o.o., Ul Pilsudskiego 17/4, 34-074 Rzyszów, Polska.

^d Sunoil-Agro, Pavlograd, 51400, Ukraine

^e Pavol Jozef Safarik University, Košice, SK-04154, Slovak Republic

Hybrid energy storage systems are an important and critical factor for successful application in a wide range of renewable green solar, wind energy, and traditional energies, like nuclear power plants. Our article is presented the hybrid energy system, which is based on innovative photovoltaic modules for generating the energy, and Li or other batteries for storage of renewable solar energy.

Innovative Hybrid Systems Solar cells / Batteries for Electric Vehicle and Military Vehicles Such as Tanks.

Nano-Structured Transparent Polymers for Replace the Glass in Solar PV Modules

“More energy from the Sun hits the Earth in one hour than all of the energy consumed by humans in an entire year.” Mentioned the professor Nathan S. Lewis, California Institute of Technology. Let us in the business realizing this huge energy potential. Solar cells for PV modules and batteries for energy storage must have high energy and power, safety, use not-toxic materials, have a wide operating range of the temperature, low cost materials and technologies.

Enerize Corporation develop the single layer nano-structured transparent polymers (NSTP) enable solar PV modules, based on the Si and on non-Si materials, to be cheaper, lighter, & deliver higher efficiency via encapsulation - versus glass or multilayer polymer coating, benefit of using the NSTP includes: increasing the efficiency of solar cells by 20% relative, reducing price and weight by 30%; flexible design solution and long time durability.[1,2]

There is an important quote from the NATO Chief Jens Stoltenberg, who suggested battle tanks with solar panels as militaries go green: <https://www.thenationalnews.com/world/europe/nato-chief-suggests-battle-tanks-with-solar-panels-as-militaries-go-green-1.1160313> “NATO should do its part to look into how we can reduce emissions from military operations,” he told the Chatham House event. “We know that heavy battle tanks or fighter jets and naval ships consume a lot of fossil fuel and emit greenhouse gasses and therefore we have to look into how we can reduce those emissions by alternative fuels, solar panels or other ways of running our missions”.

Hybrid system of flexible PV modules and flexible Li batteries have the great market opportunity for the new use. Some examples are as follows: next generation of EV that will be using the solar cell on the roof of the car to power the EV. This high-tech, solar-powered car may be the future not only for traveling, but also for each day.

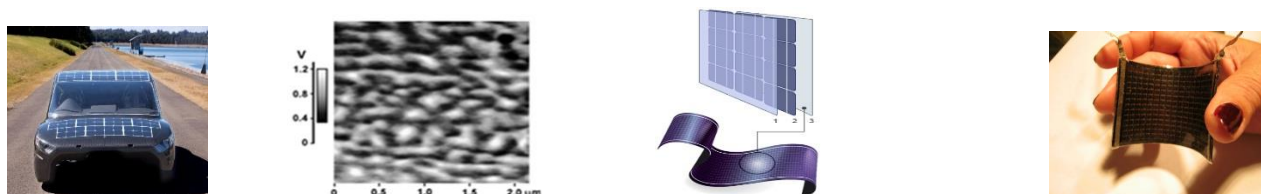


Figure 1. Design, which contacted Nano-structured transparent polymers for PV modules, which are developed by Enerize Corporation.

Other applications of Enerize Corporation single layer nano-structured transparent polymers include OLEDs, flexible displays, smart windows, etc.

Innovative Nanostructured Carbon-Based Materials for High Energy Flexible Batteries Using in Hybrid Energy Systems.

The goal is to modify the electrodes and solid electrolytes for producing the high energy flexible batteries, including Li-ion, Mg-ion, and Li-S batteries. Nanostructured carbon based powders are developed and are manufacturing by INT sp z o.o, Poland. [3]

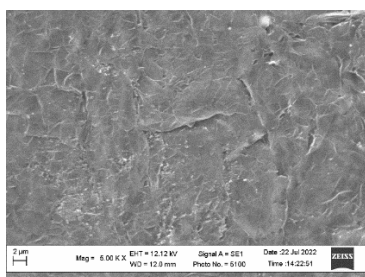


Figure 2

Figure 2. SEM of the plate, which has been made without binder from the nanostructured carbon based powders.

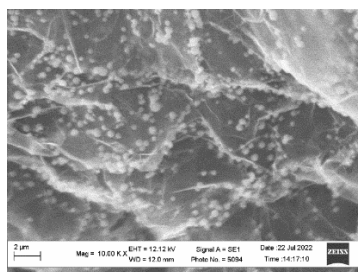


Figure 3

Figure 3. SEM of the nanostructured carbon powder.

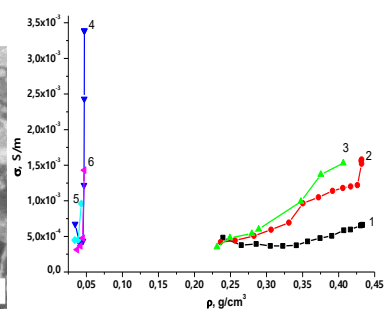


Figure 4

Figure 4. Dependence of conductivity / density of the powders at different frequencies of the magnetic field. 1, 2, 3: graphite powder, which is widely used in lithium batteries; 4,5,6: nanostructured carbon based powders. Magnetic field frequency in the MHz: 1,4- 20; 2,5- 54; 3,6-138. Conductivity of powder have been tested using the non-contact non-destructive electromagnetic method, which was developed by Enerize Corporation [4]

Melanin for Industries of Energy

Melanin is a biological organic polymer and has semiconductor properties. The structure of organic semiconductors - melanin determines the mechanism of their semiconductor nature, electrical and catalytic properties. Principal common structure of melanin is C₁₈H₁₀N₂O₄.

Molecular Weight 318 g/mol. Density: 1.6 to 1.8 g/cm³. Our investigations confirmed that melanin could successfully modify the electrodes of Li-ion and Li-S batteries. [5]. Our investigation and developed also confirmed that the Melanin cells can generate the energy and from this point of view the generate the energy is a serious competitor for the solar cells. We will present this information during the 23ST International Conference ABAF 23 and in a publication in the Journal of Physics

Conclusion and Acknowledgments

Innovative technologies and materials, which are developing and implementing for hybrid systems based on PV modules and high energy batteries, and presented in this article, are as follows:

1. Ukrainian State University of Chemical Technology (USUCT) develops Mg-ion batteries high energy and safe, and the Solid polymer electrolyte for Li-batteries with high operating temperature (from minus 30°C to plus 120°C);
2. Enerize Corporation develops the PV modules, which are encapsulated with single layer nanostructured transparent polymers instead of glass, and the non-destructive non-contact testing methods & devices for use during development and production of the PV modules and batteries;
3. Company INT sp z o.o, Poland, develops and produces of unique nanostructured carbon-based materials for modify the electrodes and the solid electrolytes for develop and produce high energy flexible lithium batteries, including Li-ion, Mg-ion, and Li-S batteries, etc;
4. Company Sunoil-Agro develops innovative technologies of production of various types of melanin for use in the new areas of energy based on hybrid systems;
5. USUCT, Ukraine; Pavol Jozef Safarik University, Slovak Republic; and Enerize Corporation, which is an industrial partner of this NATO project, together are realizing the NATO SPS 985148 project "Development of New Cathodes for Stable and Safer Lithium-Sulfur Batteries" / Science for Peace and Security Programme with the following progress of the Li-S batteries: using the modification the Li-S batteries with the unique nanostructured carbon-based materials, which is developed and produced by the Company INT sp z o.o, Poland.

References

1. E. Shembel, T. Pastushkin, V. Redko, etc. *Photovoltaic Module*. US Patent application No. 12/082,859
2. E. Shembel, V. Redko, T. Pastushkin, etc. *Nanostructured Transparent Polymer Provides Innovation Design for Solar Cells*. The ECS Transactions, 87 (1) 231-236 (2018)
3. Y. Pustovalov, E. Shembel, L. Vishnyakov, etc. Carbon material for electrodes of lithium-ion power sources and method of production thereof. US Patent application No. 10/898631
4. V. Redko, E. Shembel, T. Pastushkin, etc. Method and Device for Rapid Non - Destructive Quality Control of Powdered Materials. US Patent No. 8,102,181
5. E. Shembel, V. Kyrchenko, I. Maksyuta, V. Redko, N. Zaderey. Melanin as Semiconductor with Polymer Structure is Effective Modifier for Electrodes of High Energy Li - Ion Batteries. ECS Transactions. – 2020. – Vol. 99, № 1. – P.47-56

Electrochemical Investigation and Modeling of Ion- and Water Transport Through Polymer Membranes

L. Varain^a, G. Fafilek^a, M. Nelhiebel^b, S. Larisegger^b

^aTU Wien, Vienna/Austria;

^bKAI GmbH, Villach/Austria;

Ion exchange membranes are essential for energy applications such as fuel cells or redox flow batteries. Ion-mobility and -selectivity are the key features of such membranes. In interaction with aqueous electrolytes another important feature is the water/solvent transport. The determination of the describing coefficients for the ion permeability, transport number and water permeability is crucial to make systems comparable or to develop membranes with improved performance.

This work presents a measurement method for the simultaneous determination of coupled ion- and water permeability in polymer membranes. For this purpose, measurement methods for the determination of concentration-, volume- and membrane-potential changes are integrated into one miniaturized concentration cell.

A freestanding ion exchange membrane with largely known properties is then used to evaluate the new combined measurement setup. The membrane of choice is a Nafion 211 membrane, since Nafion is one of the most investigated PEM in literature and allows a comparison of the results with existing data.

For the general description of the coupled transport processes, a system of ordinary differential equations is developed.

Furthermore, a FEM model is developed in COMSOL Multiphysics®, which specifically simulates the ion distribution within the membrane and the resulting electrical fields.

Evaluation of ballistic resistance of thermoplastic and thermoset composite panels

J. Viliš^a, Z. Pokorný^a, J. Zouhar^b, R. Vitek^a, and J. Procházka^a

^a Department of Mechanical Engineering, Faculty of Military Technology, University of Defence, Brno 662 10, Czech Republic

^b Faculty of Mechanical Engineering, Brno University of Technology, Institute of Engineering Technology, 616 69 Brno, Czech Republic

In this study, the ballistic resistance of composite panels made of solid fabrics was investigated. In the experimental part, the materials Twaron CT 747 TH110 impregnated with thermoplastic resin and Twaron CT747 impregnated with thermoset resin were examined. The ballistic resistance of the composite panels was tested in the reduced version according to the NATO AEP-55 STANAG 4569 standard, protection level 1. The manufactured composite panels were tested by the rifle cartridges 7.62 x 51 mm FMJ M80. The high-speed camera was used to observe the impact of the missiles into the panel. As part of the evaluation of the experiment, the damage ranges of these panels were identified. The composite panel made of Twaron CT 747 TH110 impregnated with thermoplastic resin absorbed more energy of the impacting missiles than the panel made of Twaron CT 747 impregnated with thermoset resin. The results show that the panel made of Twaron CT 747 TH110 impregnated with thermoplastic resin, which was composed of 90 layers was not penetrated by the missile 7.62 mm M80 and complies with NATO AEP-55 STANAG 4569, protection level 1.

Mathematical and Physical Analysis of Character and Position of Shock Waves During Pumping of Vacuum Chambers

R. Bayer^a

^a Department of Electrical and Electronic Technology, Brno University of Technology, Technická 10, 616 00 Brno, Czech Republic

As part of the research in the field of pumping vacuum chambers in the Environmental Electron Microscope, research on supersonic flow through apertures is being carried out at the Department of Electrical and Electronic Technology of the Brno University of Technology in cooperation with the Institute of Scientific Instruments of the CAS. This paper deals with the nature and location of shock waves during the pumping of the vacuum chambers of the experimental chamber as a basis for a forthcoming experiment on mapping the resulting shock waves using the Schlieren optical method.

Introduction

At the Department of Electrical and Electronic Technology of Brno University of Technology, in cooperation with ISI Brno, research on supersonic flow at low pressures is underway (1, 2, 3). The results are used in the design of vacuum chambers of the Environmental Electron Microscope (4, 5, 6). During the planned studies, the shape and distribution of shock waves will be investigated when supersonic flow occurs behind a small aperture separating two chambers with different pressures.

Experimental chamber

The current Experimental Chamber consists of two chambers separated by a small opening that simulates the condition created by differential pumping in an electron microscope.

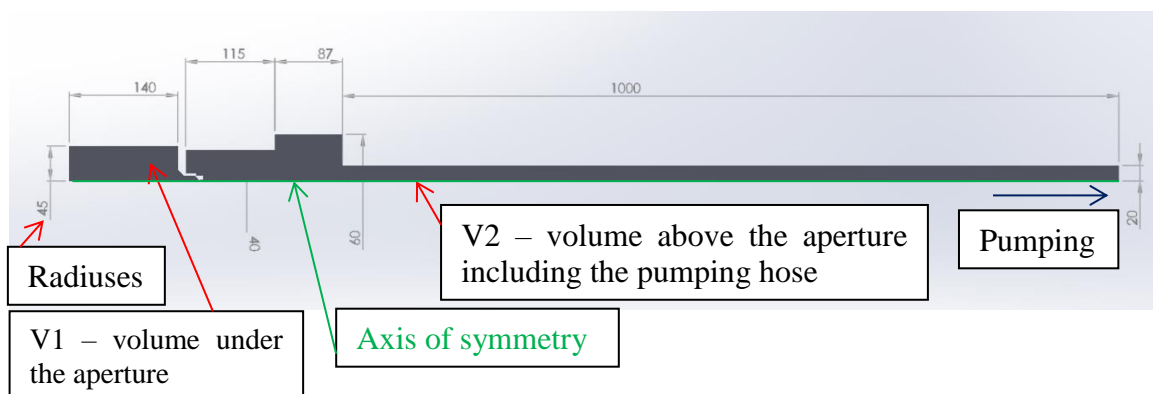


Figure 1. 2D axisymmetric model

Figure 1 shows a schematic of the given chambers P1 and P2 separated by the nozzle as it will be used for the calculation in Ansys Fluent. This calculation will be performed as 2D axisymmetric.

Chamber volume V1 = 2813743.82 mm³

Chamber volume V2 = 896023.41 mm³

Diameter of the aperture separating the two chambers d1 = 2 mm,

Initial temperature T₀ = 297.15 K

Initial pressure P₀ = 101325 Pa

Wall heat transfer convention = 25 W/m²K

PFEIFFER DUO 65 M rotary pump parameters were used for pumping:

Discharging velocity - V_p = 62 m³/hr.

Time-varying mathematical and physical analyses were performed to determine the pressure ratios in both chambers during the actual pumping.

The mathematical-physical model was designed as a 2D axisymmetric model of the pumping of the experimental chamber.

Results and Discussions

The results of Dr. Danilatos [7] were used for analysis of the location of the Mach disk under the given low pressure conditions:

$$z_M = 0.67D_{kr} \sqrt{\frac{P_0}{P_1}}. \quad [1]$$

Distance of the Mach disk is approximately 7,1 mm from the critical cross-section (tab. 1). Subsequent analysis of the ANSYS Fluent results showed the same Mach disk distance (Fig. 2). The Mach disk is located in front of the perpendicular shock wave.

TABLE I. Pressure ratios and Mach disk locations.

Time [s]	Pressure V1 [Pa]	Pressure V2 [Pa]	Zm [mm]
1.	49496	1782	7.06
2.	27210	939	7.2
3.	15878	561	7.1
4.	9538	342	7.01
5.	5950	210	7.1
6.	3433	121	7.1
7.	1843	65	7.1

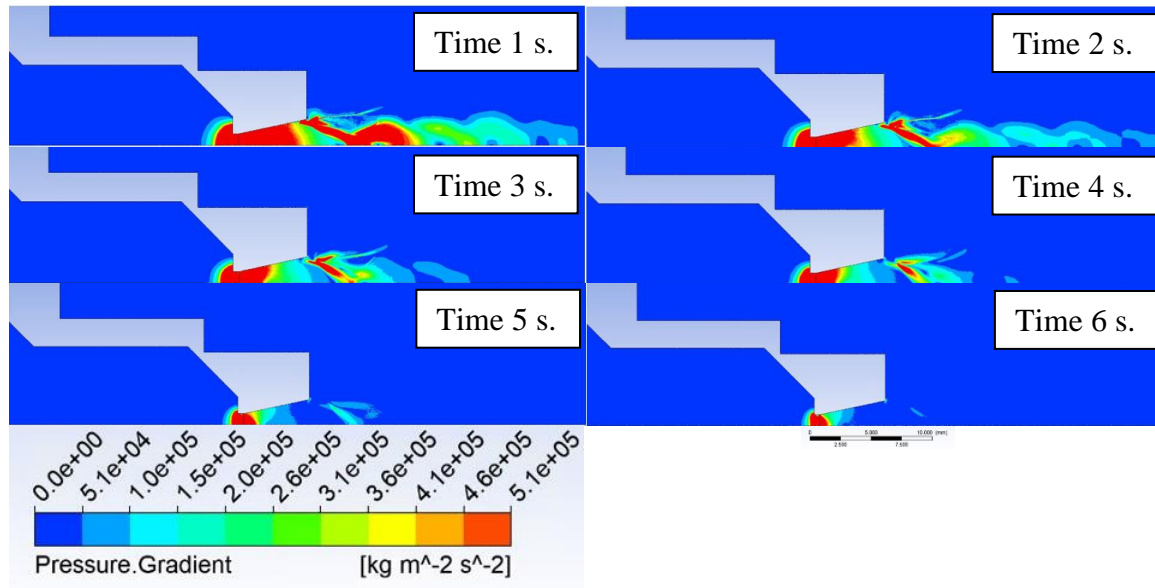


Figure 2. Location and intensity of shock waves during pumping of the experimental chamber.

The results will be used as a basis for a forthcoming experiment to map shock waves at low pressures using the Schlieren method.

Acknowledgments

This research was supported by Brno University of Technology specific research program: Materials and technology for electrotechnics IV, reg. no. FEKT-S-20-6206.

References

1. E. Tihlaříková, V. Neděla, and B. Dordevic, in In-situ preparation of plant samples in ESEM for energy dispersive x-ray microanalysis and repetitive observation in SEM and ESEM, *Scientific Reports*, 9(FEB), 2300. ISSN 2045-2322. doi: 10.1038/s41598-019-38835-w, (2019).
2. J. Maxa, V. Neděla, J. Jiráček, P. Vyroubal, and K. Hladká, in Analysis of gas flow in a secondary electron scintillation detector for ESEM with a new system of pressure limiting apertures, *Advances in Military Technology*, roč. 7, č. 2, s. 111-116. ISSN 1802-2308, (2012).
3. J. Maxa, M. Bílek, P. Hlavatá, P. Vyroubal, and K. Leptová, in Comparisons Using Methods of Continuum Mechanics and Monte Carlo at Differentially Pumped Chamber, *Advances in Military Technology*, **11**, n. 2, p. 143-150. ISSN: 1802-2308, (2016).
4. M. Bílek, J. Maxa, P. Hlavatá, and R. Bayer, in Modelling and simulation of a velocity field within supersonic flows in low-pressure areas, *ECS Transactions*, **81**(1), pp. 311–316, (2017).
5. P. Hlavatá, J. Maxa, M. Bílek, and V. Neděla, in Impact of the shape of the differentially pumped chamber on critical flow character, *ECS Transactions*, **81**(1), pp. 317–322, (2017).
6. P. Hlavatá, J. Maxa, M. Bílek, P. Vyroubal, and R. Bayer, in Influence of critical flow in the differentially pumped chamber AQUASEM, *Advances in Military Technology*, **12**(2), pp. 301–310, (2017).
7. Danilatos, G. D. Velocity and ejector-jet assisted differential pumping: Novel design stages for environmental SEM. *Micron* 2012, **43**, 600-611.
- 8.

Physics Informed Neural Network and RC model of Li-Ion Battery

R. Cipin^a, M. Toman^a, P. Prochazka^a, and I. Pazdera^a

^aDepartment of Power Electrical and Electronic Engineering, Brno University of Technology, Brno, Technicka 12, 6161 00, Czech Republic

This paper deals with simulation of Li-ion battery in the form of an equivalent RC circuit. Physics informed Neural network is used for time-dependent simulations. The article deals with the problems associated with this kind of simulation.

Introduction

Physics informed Neural network (PINN) is a class of machine learning model where the loss function of the neural network satisfies governing differential equations, i.e., ordinary differential equation (ODE), partial differential equation (PDE), and so on, with appropriate initial and boundary conditions. The architecture of PINN was firstly introduced in (1). Its use in describing many physical processes is currently the focus of many research teams. In our case, we use the PINN architecture to describe the battery behavior with only the knowledge of the actual time and current of the battery.

Mathematical Model of Li-Ion Battery

The first-order RC Li-ion battery model, see Figure 1 a), is almost the most widely used model of the simplest ones. It can predict the battery voltage waveform under dynamic conditions in very good agreement with measurements.

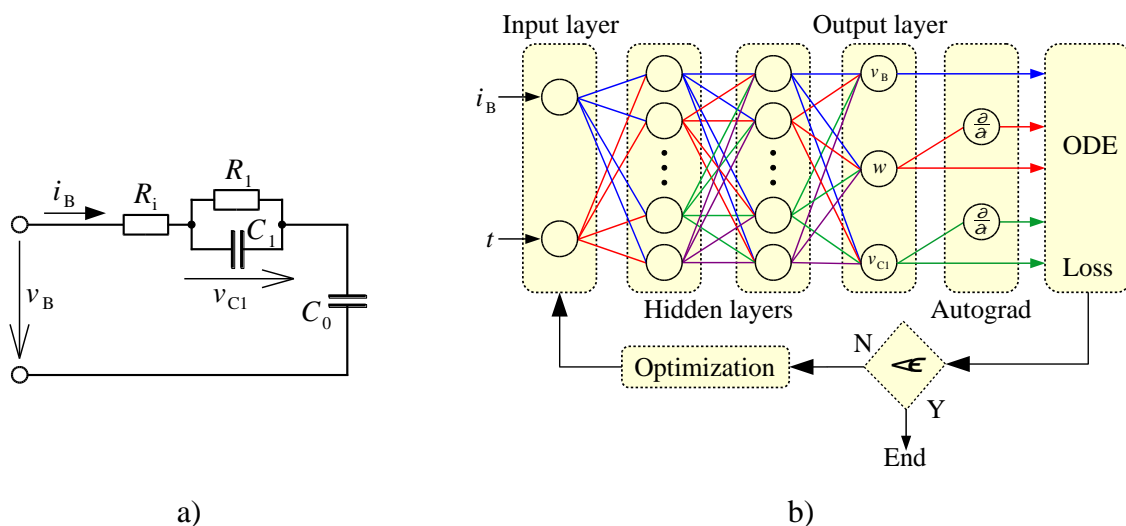


Figure 1. a) RC Li-ion battery model. b) Architecture of used neural network.

Voltage equations have the following form

$$v_B = \frac{1}{C_0} \int i_B dt + V_0 + R_i i_B + v_{C1}, \quad [1]$$

$$v_{C1} + R_1 C_1 \frac{dv_{C1}}{dt} = R_1 i_B, \quad [2]$$

where v_B is battery voltage, i_B is battery current, R_i is battery internal resistance, C_0 is battery equivalent capacitance. R_1 and C_1 are resistance and capacitance used to simulate short, or long-term battery dynamics, see (2). For the sake of simplicity in this article, the battery no-load voltage is modeled by capacitor C_0 . The parameters of the individual resistors and capacitors have such values to show the ability of the PINN to simulate the transient behavior of the RC circuit, but on the other hand, their values do not correspond to any real Li-ion battery. Values of individual used parameters are: $V_0 = 4 \text{ V}$, $R_i = 0.1 \Omega$, $R_1 = 0.1 \Omega$, $C_0 = 10 \text{ F}$, $C_1 = 1 \text{ F}$.

Physics Informed Neural Network

The structure of the neural network (NN) is shown in Figure 1 b). NN consists of two linear neurons in the input layer corresponding to battery current and time, twenty neurons in two hidden layers, and three linear neurons in the output layer corresponding to battery voltage, integral of battery current, and voltage on capacitor C_1 . The activation function of individual neurons in hidden layers is the hyperbolic tangent function (tanh). The used NN consists of total 963 trainable parameters.

The equations of Li-ion battery system f_1 , f_2 , and f_3 can be formulated from [1] and [2]

$$f_1 = v_{C1} + R_1 C_1 \frac{dv_{C1}}{dt} - R_1 \frac{dw}{dt}, \quad [3]$$

$$f_2 = \frac{dw}{dt} - i_B, \quad [4]$$

$$f_3 = \frac{1}{C_0} w + V_0 + R_i \frac{dw}{dt} + v_{C1} - v_B. \quad [5]$$

The equation [4] is introduced to eliminate the use of direct numerical integration of the battery current in [1] and [5], respectively. A similar approach to elimination using numerical integration is used in (3). The total loss function consists of the sum of the ODE system losses \mathcal{L}_{sys} and the initial boundary losses \mathcal{L}_{IC} , i.e., $\mathcal{L}_{\text{total}} = \mathcal{L}_{\text{sys}} + \mathcal{L}_{\text{IC}}$

$$\mathcal{L}_{\text{sys}} = \frac{1}{N} \sum_{i=1}^N (f_{1,i})^2 + \frac{1}{N} \sum_{i=1}^N (f_{2,i})^2 + \frac{1}{N} \sum_{i=1}^N (f_{3,i})^2, \quad [6]$$

$$\mathcal{L}_{\text{IC}} = [w(0) - w_{\text{IC}}]^2 + [v_{C1}(0) - v_{C1,\text{IC}}]^2. \quad [7]$$

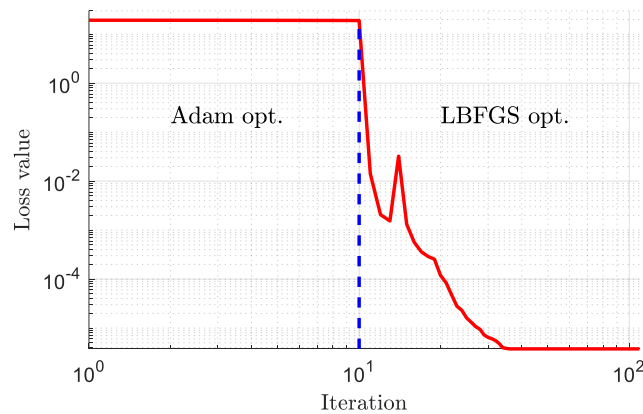


Figure 2. Dependence of the loss value ($\mathcal{L}_{\text{sys}} + \mathcal{L}_{\text{IC}}$) on training iteration.

The neural network used was trained using 100 training time and current samples, see Figure 3. The training was divided into two tasks, see figure 2. For the first optimization, the Adam algorithm with 10 iterations was used and for the second optimization, the LBFGS algorithm with 100 iterations was used. The total loss value after optimization was 3.8×10^{-6} .

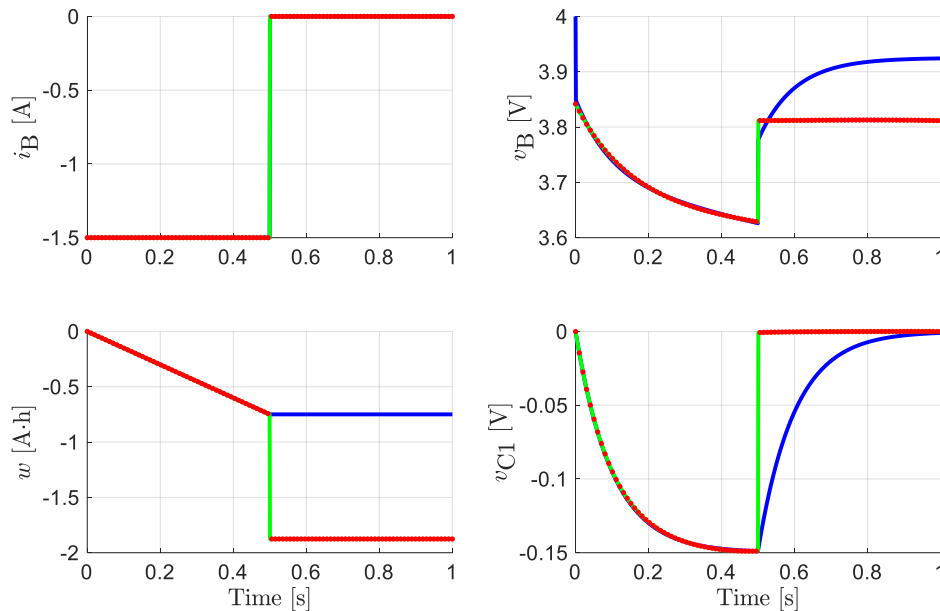


Figure 3. Time courses of battery current (i_B), voltage (v_B), integral of battery current (w), and voltage on capacitor C_1 (v_{C1}). Blue courses are ground truth values, red dots are values used for training of NN, and green curves are values used for validation of NN.

Conclusions

The paper presents a possibility to use the physics informed Neural network to simulate the transients of a equivalent RC circuit of a Li-ion battery.

Acknowledgments

This research work has been carried out in the Centre for Research and Utilization of Renewable Energy (CVVOZE). Authors gratefully acknowledge financial support from the Ministry of Education, Youth and Sports under institutional support and BUT specific research programme (project No. FEKT-S-20-6379).

References

1. M. Raissi, P. Perdikaris, and G.E. Karniadakis, *Journal of Computational Physics*, **378**, 686 (2019), DOI: 10.1016/j.jcp.2018.10.045.
2. R. Cipin, M. Toman, P. Prochazka, and I. Pazdera, 2019 International Conference on Electrical Drives & Power Electronics (EDPE), (2019), DOI: 10.1109/EDPE.2019.8883926.
3. Y. Lei, N. Yi-Qing, D. Xiang-Yun, and H. Shuo, *SSRN*, (2022), DOI: 10.2139/ssrn.4000235.

Preparation and analysis of carbon derived from biological materials for use in Li-S batteries

P. Čudek^a, and K. Jaško^a

^a Department of Electrical and Electronic Technology, Brno University of Technology, Technicka 10, 616 00 Brno, Czech Republic

Lithium-sulfur (Li-S) batteries offer high energy density at a very low cost. However, several issues such as low conductivity, volume changes during cycling and the shuttle effect need to be resolved before Li-S can be used in practice. One component of Li-S that can potentially affect its electrochemical properties is the use of a suitable carbon material incorporating sulfur as the active material of the positive electrode. One potential source of carbon for use in batteries is biological materials. This article focuses on the use of biological carbon from coffee grounds.

Introduction

Lithium-sulfur batteries have the potential to replace conventional Li-Ion batteries in some areas due to their properties. The main advantages of Li-S include the high theoretical energy density of sulfur (1672 mAh / g) and low cost of sulfur compared to other materials used for cathodes in Li-Ion batteries [1]. Sulfur is also more environmentally friendly compared to other materials used in batteries as it is non-toxic in its atomic state as well as in most compounds found in nature. One of the main disadvantages of sulfur with respect to its use in batteries is that sulfur is an insulator. Low electrical conductivity of sulfur impairs the transfer of electrons from the electrode material to the circuit and increases the internal impedance of the cell, thus reducing the available capacitance. This disadvantage is most often compensated for by the addition of a carbon, which has no positive effect other than to increase conductivity of the cathode material. However, this carbon component reduces the effective sulfur - loading of the electrode. Therefore, many research studies focus on 1D, 2D or 3D carbon nanostructures that would have other positive effects such as reducing the bulk expansion of sulfur, suppressing shuttle effect, etc. [2]

High-porosity carbon can provide high electrical conductivity, which can overcome the insulating nature of sulfur and in addition its pores provide enough space for sulfur to expand during cycling. Precisely because of their high availability and diverse microstructure, biological materials or carbon derived from them are remarkable for use in Li-S electrochemical power sources.

Unfortunately, the carbon mixture obtained directly from raw biomass has very poor electrochemical properties, low conductivity, contains a number of undesirable compounds and has a high oxygen content. It is the oxygen in this mixture that has a negative effect on the adsorption between the Li⁺ ions and the carbon matrix. For this reason, it is necessary to reduce the oxygen and all other elements in the resulting mixture as much as possible and to achieve the highest possible purity of carbon before further processing to enable use in Li-S cathode materials. [3]

Experiments

For the purpose of the experiments, organic carbon was prepared from coffee grounds. The coffee grounds was first dried and then elemental microanalysis was performed by energy dispersive spectroscopy (EDS). From the EDS results shown in TAB. I, it can be observed that the mixture contained 41.49 wt% of oxygen and less than 1 wt% of undesirable elements.

TABLE I. Results of elemental microanalysis of dried coffee grounds. Area of analysis: 415 μm . Accelerating voltage: 30kV.

Element	Weight concentration %	Atom concentration %
Carbon	57,60	64,65
Oxygen	41,49	34,96
Others (Mg, Si, S, K, Ca)	0,91	0,39

This was followed by experiments where the resulting mixture was heated under different conditions, and it was assumed that the unwanted elements would evaporate, and the oxygen content of the mixture would be reduced.

Incineration of dried coffee grounds in a tube furnace in a nitrogen atmosphere

The dried coffee mixture was placed in a tubular furnace and then nitrogen was fed into the furnace for 1 h to replace the original air. The mixture was then incinerated in furnace at 900 °C for 2 hours. The resulting mixture was subjected to EDS. According to the results shown in TAB. II., there was a significant reduction of oxygen in the mixture during combustion, but other elements were not eliminated.

TABLE II. Results of the elemental microanalysis of dried coffee grounds incinerated in tube furnace in nitrogen atmosphere. Area of analysis: 415 μm . Accelerating voltage: 30kV

Element	Weight concentration %	Atom concentration %
C	87,10	91,86
O	8,02	6,35
Mg	0,70	0,37
P	0,45	0,18
S	0,64	0,25
K	1,12	0,36
Ca	1,97	0,62

Hydrothermal carbonization

Since simple incineration failed to produce pure carbon for use in batteries, the remaining coffee grounds were subjected to hydrothermal carbonization (HC). The dried coffee grounds (18g) were drenched in 50 ml of 30 % H_2SO_4 and heated at 180 °C for 18h. The resulting mixture was then filtered with deionized water until the pH of the filtered liquid was neutral. The resulting mixture was dried, and then elemental microanalysis was performed by EDS, the results of which are shown in TAB. III. The hydrothermal carbonization successfully eliminated undesirable elements and reduced the oxygen content by half to 19.81 wt. %. However, the disadvantage of this method was that residual sulfur from the sulfuric acid remained in the mixture.

TABLE III. Results of the elemental microanalysis of dried coffee grounds after hydrothermal carbonization. Area of analysis: 415 μm . Accelerating voltage: 30 kV.

Element	Weight concentration %	Atom concentration %
Carbon	75,73	82,06
Oxygen	19,81	16,12
Sulfur	4,49	1,82

Incineration of HC carbon mixture in a tube furnace under nitrogen atmosphere

HC carbon was placed in a tube furnace and then nitrogen was supplied to the furnace for 1 hour. The mixture was then heated to 500 °C in the furnace for 2 h, as 500 °C should have been a sufficient temperature to evaporate the sulfur if it were in its atomic form. The resulting mixture was subjected to EDS and the results are shown in TAB. IV. This reduced the oxygen content of the mixture from the original 19.81 wt.% in HC carbon to 8.09 wt.%. However, the sulfur content decreased only slightly.

TABLE IV. Results of the elemental microanalysis of HC carbon mixture incinerated in tube furnace in nitrogen atmosphere for 2 hours with temperature of 500 °C. Area of analysis: 415 μm . Accelerating voltage: 30kV.

Element	Weight concentration %	Atom concentration %
Carbon	88,35	92,26
Oxygen	8,09	6,34
S	3,17	1,24
Si	0,40	0,18

In view of the results, the procedure was repeated, but this time at 900 °C again for two hours. The results shown in TAB. V. show a further slight decrease in sulfur in the mixture from 3.17 wt.% to 2.77 wt.% and a noticeable decrease in oxygen again from the 8.09 wt.% to 4.41 wt.%.

TABLE V. Results of the elemental microanalysis of HC carbon burned in tube furnace in nitrogen atmosphere for 2 hours with temperature of 900 °C. Area of analysis: 415 μm . Accelerating voltage: 30kV

Element	Weight concentration %	Atom concentration %
Carbon	92,33	95,30
Oxygen	4,41	3,42
S	2,77	1,07
Si	0,49	0,21

Conclusion

From the values measured so far, it can be concluded that the use of hydrothermal carbonization followed by incineration in a nitrogen atmosphere can significantly reduce the oxygen content as well as get rid of most of the undesirable elements in the biomass-derived carbon.

Acknowledgments

This work was supported by the specific graduate research of the Brno University of Technology No. FEKT-S-20-6206.

References

1. C. Kesy, D. Leistenschneider, S. Wang, H. Tanaka, S. Dörfler, K. Kaneko and Kaskel S. *Batteries & Supercaps*, **11**, 612 (2020)
2. K. Sun, C. A. Cama, J. Huang, Q. Zhang, S. Hwang, D. Su, A. C. Marschilok, K. J. Takeuchi, E. S. Takeuchi and Gan H. *Electrochimica Acta*, **12** (2017)
3. B. Li, M. Xie, G. Yia and Zhang C. *The Royal Society of Chemistry 2020*, **10** (2020);

Cooling Ability of Smooth and Dimpled Surfaces

L. Dobsakova^a and T.D. Nguyen

^a Department of Mechanical Engineering , University of Defence, Brno, Czech Republic

Reliable cooling of electronic components is an essential factor in electrical engineering. Every electronic device produces a certain amount of heat during its operation. This heat can cause overheating and a device can suffer damage. Therefore, the issue of cooling plays a significant role and is an important theme appropriate for continuously finding new improvements

The paper describes a quantification of the heat transfer coefficients between a body and a surrounding environment. Experimental research of the heat transfer by cooling is focused on the plane smooth and structured surfaces. Surface structures improving the heat transfer rate are of dimples. The cooling process was measured by using a thermal imaging camera to obtain a cooling curve – the change in temperature time course during air cooling. The analysis of the cooling curve gradient allows us to identify convective and radiant components of the heat transfer. The presented results in the form of diagrams include different cases of air flow around smooth and dimpled surfaces.

Introduction

The heat transfer is composed of two phenomena – the convective component and the thermal radiation component. A heat transfer calculation is often calculated only with the convective component, because its amount is a dominant part of the heat transfer, while the radiant component is neglected. This paper describes the identification and quantification of convective and radiant components of heat transfer for two types of surfaces – smooth and structured surfaces. The surface structure is made of simple dimples.

The data needed for calculation we obtained from measurement by using a thermal imaging camera for different cases of airflow conditions. Samples material is copper, often used for heatsink manufacturing because of its high thermal conductivity.

Measuring objects and measurement

Two types of surfaces were measured. Both samples were 10 mm thick copper square-shaped plates with a side 150 mm long. One sample was with a smooth surface, the second was with a dimpled surface. All 182 dimples had approximately the same size (a difference was given by the accuracy of a manufacturing machine). The surfaces of both plates were supplied by a special coat with precisely defined emissivity $\varepsilon = 0,96$. Both measured plates are shown in Figure 1 and their parameters are written in Table 1.

TABLE I. Parameters of copper plates.

Quantity	Smooth plate	Dimpled plate
Mass m [kg]	2,037	1,828
Specific heat capacity c [J·kg ⁻¹ ·K ⁻¹]	384,6	384,6
Surface Area A [m ²]	0,0225	0,0232

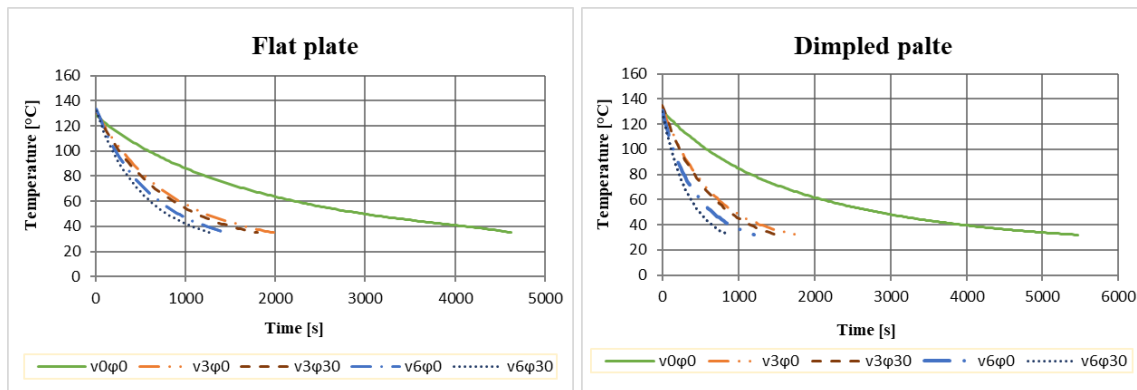
Measured plates were heated at the temperature of about 130°C and potted in the heat-insulating material bed from fiberglass, so only one plate surface had contact with the surrounding environment. The heat was transferred to the surrounding environment only from this exposed surface.

The measurement was performed for cases of natural convection, forced convection with the air speed $v = 3$ m/s and $v = 6$ m/s, and for cases of incidence angle between direction of airflow and the plate position $\varphi = 30^\circ$. Plates were positioned for all cases in a vertical position.

Experimental results and discussion

Measured cooling curves by using a thermal imaging camera are shown in figure 2 for all cases mentioned above. Cooling curves of the flat plate are on the left figure, and measured cooling curves of the dimpled plate are on the right figure.

By comparing graphs, the cooling curves of the dimpled plate for all cases are steeper than the cooling curves of the flat plate. So, the cooling process is faster at the beginning. A difference increases with a faster airflow v and a greater angle of incidence φ .

**Figure 2.** Cooling curves of both plates for all examined cases of convection

The heat transfer rate Q and its components (convective and radiation) depending on time are shown in Figure 3 for two flat plate cases – the natural convection case and the case with an airflow velocity of 6 meters per second.

For the natural convection case, the difference between convective and radiant heat transfer rates is small. For the forced convection case with $v = 6$ m/s, the convective heat transfer is dominant and the radiant component has almost neglecting size.

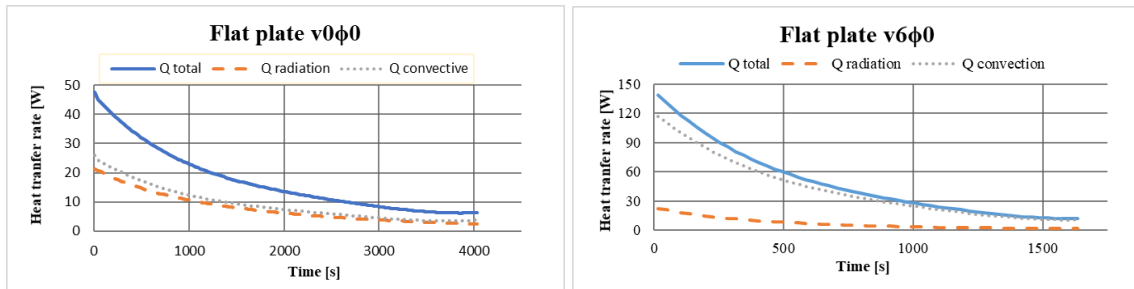


Figure 3. Heat transfer rates for the flat plate – the natural convection case on the left and the forced convection case $v = 6 \text{ m/s}$ on the right.

Conclusion

The presented results show that the heat transfer measurement by using a thermal imaging camera is a suitable method for a cooling process evaluation.

The cooling process measurement of the flat and the dimpled plate proved that the dimpled plate has steeper cooling curves in all measured cases. So the dimpled plate cooling process is faster, especially in higher temperatures.

The analysis of measured data pointed out that the radiant component of the heat transfer during the natural convection cooling process occupies a significant part of the total heat transfer rate. Neglecting the radiant component in a heat transfer calculation could bring out a large deviation.

The dimpled surface impact on the heat transfer process will continue by using CFD simulation.

Acknowledgments

The paper has been prepared thanks to the support of the project "VAROPS (DZRO FVT 3) Military autonomous and robotic systems" and Surface technology in applications special techniques SV20-216.

References

1. HORÁK, V. and KULISH, V. Thermodynamics. Brno: University of Defense, 2011, 102 p.

Environmentally friendly epoxy resin

L. Horák^a, J. Kazelle^a

^a Brno University of Technology, Faculty of Electrical Engineering and Communication, Department of Electrotechnology, Technická 10, 616 00 Brno, Czech Republic

This article deals with electro-insulating casting systems based on „green“ epoxy resin. The main points of the article are the EnviPOXY epoxy resin and the EnviDURIT epoxy system. It is an environmentally friendly epoxy system, where the basic component of this system is produced from renewable resources.

Introduction

The present time is more and more concerned with environmental protection. During production, it is necessary to reduce the carbon footprint, use as little energy as possible, reduce waste, use renewable resources, recycle, etc.

There are very few so-called „green“ epoxy resins on the world market. Products based on various natural oils began to appear, but after curing with standard hardeners, very poor properties are achieved. It would be ideal to use a similar epoxy resin, which is based on bisphenol A. In this direction, the Spolchemie company made great progress and started producing a range of epoxy resins under the name EnviPOXY, where glycerin is used for production as waste from the production of biodiesel. This resin guarantees a bio carbon content of 28 %. A very low proportion of crude oil is used for production. It is the world's first epoxy resin certified in the environmental EPD (LCA) system Environdec. The EPD (Environmental Product Declaration) transparently presents objective, comparable and third-party verified data on the environmental properties of products and services from the point of view of the life cycle LCA (Life Cycle Assessment). [1]

EnviPOXY

The Spolchemie company offers four types of „green“ epoxy resins. Basic Unmodified Liquid Epoxy Resins - EnviPOXY with the numerical designation 510, 520, 525 and 530. [2] The numerical designation agrees with the epoxy index (number of moles of epoxy groups per 100 g of sample). This is the so-called purity of the resin. A higher number equals a higher purity. Purer systems are characterized by a higher glass transition temperature, slightly better mechanical properties, lower viscosity and higher price. The purer resin crystallizes more, which can be an undesirable phenomenon from the point of view of subsequent application. The system can be re-liquefied by heating.

Basic low molecular weight epoxy resin is made from epichlorohydrin and bisphenol A. Epichlorohydrin is produced in two ways:

- from a limited fossil resource (propylene) – commonly used resin CHS-EPOXY 520
- from a renewable resource (glycerin) – „green“ epoxy resin EnviPOXY 520

In the case of EnviPOXY, the carbon footprint is up to 64 % lower than that of epoxy resins based on propylene epichlorohydrin (CHS-EPOXY). There is a reduction in other environmental

impacts (lower energy consumption, lower potential for eutrophication and acidification). EnviPOXY are the only epoxies produced in Europe containing at least 27 % traceable carbon from renewable resources. The use of renewable resources is a step towards independence from fossil resources. [3]

EnviDURIT

In cooperation with SYNPO a.s. Pardubice was designed a two-component epoxy casting system designed for indoor use with the trade name Envidurit 520-1667. Component A is a modified „green“ epoxy resin based on bisphenol A. The resin is made using glycerin as waste from biodiesel production. The resin has a bio carbon content of 28 %. It is the first chemical product with an EPD certificate in the Czech Republic and the worldwide first product with certification in the field of epoxies. Component A is filled with special fillers based on micro-ground silicon dioxide and calcium silicate (the amount of filler is 54.5 %). Liquid methyltetrahydrophthalic anhydride (MTHFA), which is not on the list of prohibited substances, is used as a hardener (component B). The hardener complies with authorization according to REACH. Component B is also filled with special fillers based on micro-ground silicon dioxide and calcium silicate (the amount of filler is 63.5 %).

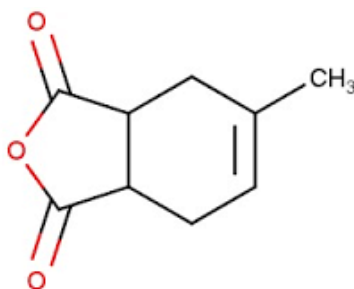


Figure 1. MTHFA

Acknowledgments

This work was supported by the specific graduate research of the Brno University of Technology No. FEKT-S-20-6206.

References

1. The EPD – Environmental Product Declarations [online]. [15.07.2022]. Available from: <https://www.environdec.com/all-about-epds/the-epd>
2. Basic Epoxy Resins – Spolchemie [online]. Copyright © 2021 Association for chemical and metallurgical production, joint-stock company [15.07.2022]. Available from: <https://www.spolchemie.cz/en/epoxidove-pryskyrice-zakladni/>
3. Environment & green Spolchemie – Spolchemie [online]. Copyright © 2021 Association for chemical and metallurgical production, joint-stock company [15.07.2022]. Available from: <https://www.spolchemie.cz/en/environment-protection-green-spolchemie/>

The Potential of Brownfields as a Suitable Locations for Solar Panel Instalation Based on Global Radiation Measurements

P. Houška^a, K. Caisová^b and J. Koutský^a

^a Faculty of Social and Economic Studies, J. E. Purkyne University in Ústí nad Labem, 400 01 Ústí nad Labem. Česká republika.

^b Faculty of Mechanical Engineering, J. E. Purkyne University in Ústí nad Labem, 400 01 Ústí nad Labem. Česká republika.

This research emphasizes on the effect of global radiation on solar panels output. Used panels represent one of the renewable energy sources installed within chosen locations (Ústí nad Labem, Brno). The main goal of this research is to evaluation the benefit of the photovoltaic panels installation within locations affected by lignite mining (i.e. brownfields) in order to increase the energy self-sufficiency of the Czech Republic. Therefore measured weather data are correlated with given solar panels output during a calendar year followed by analysis of the energy benefit for the Ústí Region. Introduction.

Introduction

Areas affected by lignite mining, (i.e. brownfields), being tranformed into photovoltaic parks is nowadays prevailing conception within the academic field [1]. This opinion is supported by the recommendation [2] of the Coal commission from 2020. According to this regulation, the Government of the Czech Republic has decided to expedite the transition from coal energy by the end of 2033. This decision increased the pressure to resolve the situation regarding brownfields and their potential as energy parks.

The aim of this research is to evaluate the benefit of installing solar panels in the Ústí Region according to the amount of global radiation typical for this area. Depending on the results, assess the overall energy benefit for the area.

Methodology of research

This research is focused on assessing the measured performance values of individual solar power plants depending on the amount of global radiation and temperature. Observed power plants are situated in Brno - Olešná with an installed capacity of 665 kWp and Ústí nad Labem with a capacity of 35 kWp. Meteorological data in the field of global radiation from the monitored areas was provided by the Czech Hydrometeorological Institute.

For the purposes of this research, a characteristic (R_{pot}) was introduced describing the ratio between the area under the curve (integral of the function calculated by the trapezoidal method) of the function describing the performance of the PV panel in the year, to the area under the curve determined by the global irradiance function. This characteristic will be denoted as R_{pot} and is determined by the following ratio:

$$R_{pot} = S_1/S_2 \quad [1]$$

where: S1 is the area under the curve given by the development of the PV panel performance in time (calendar year) and S2 is the area under the curve given by the global irradiance in the same period. This share is further multiplied by 100 to determine the percentage share.

Result and discussion

Average global radiation measured within chosen locations and measured PV panels output are presented in Tab.1. Output measurements were conducted via Sopray Solar 240 PV panels. Brno - Olešná location revealed 665 kWp within area of 20 000 m² and Ústí nad Labem 35 kWp per 500 m².

Table 1. Global solar radiation and PV output

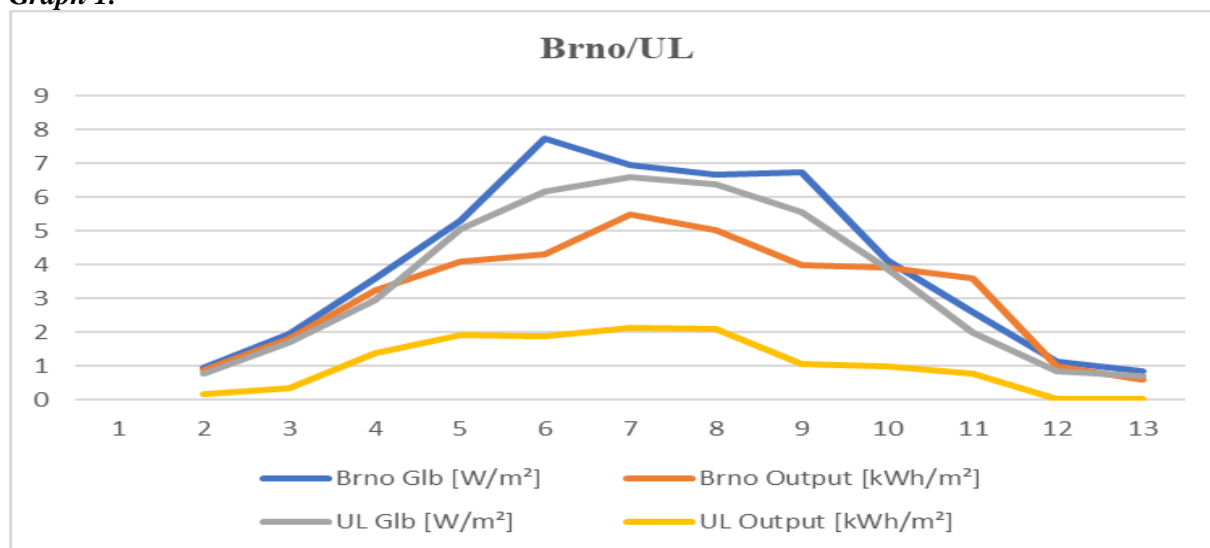
Month	BRNO		UL	
	Glb [W/m ²]	Output [kWh/m ²]	Glb [W/m ²]	Output [kWh/m ²]
1	0.94	0.89	0.76	0.15
2	1.94	1.79	1.7	0.33
3	3.6	3.23	2.95	1.39
4	5.32	4.11	5.07	1.91
5	7.74	4.31	6.17	1.88
6	6.96	5.5	6.6	2.13
7	6.68	5.03	6.39	2.1
8	6.76	4	5.58	1.05
9	4.12	3.92	3.89	0.99
10	2.6	3.6	1.99	0.76
11	1.12	0.99	0.83	0.01
12	0.83	0.59	0.7	0.03
Total	48.6	37.95	42.63	12.71

Glb – average global radiation value per month

Output – average monthly value of the PV output per m²

Compared measured data are graphically presented in Graph 1, where outputs of individual PV plants with global solar radiations can be observed throughout the calendar year. Values stated in the upper right corner are integral characteristics R_{pot} expressing percentage of the areas ration under presented values considered as continuous functions.

Graph 1.



The measured data together with presented graphs show that the characteristic describing the relationship between the solar panels outputs and global radiation acquires 78.0% value for Brno and 30.1% for Ústí nad Labem.

Energy potential of North Bohemia can be estimated based on solar panel output data in order to assess transformation of location affected by lignite mining. In North Bohemia, more than 400 km² of land is affected by mining. [3] The area affected by the heaviest mining activity occupies 140 km² [4]. With the total efficiency of the PV plant in Ústí nad Labem of 12.71 kWh/m² and the possibility of transform an area of 140,000 m² into PV power plant, the future energy potential of this region can be estimated to 1,779 MW.

Conclusion

This paper was focused on the effect of global radiation on PV output in chosen localities. The assessment consisted of radial potential (Rpot) integral characteristics evaluated by percentage of the areas ratio under presented values considered as continuous functions. These potentials acquired Rpot=78.0% for Brno and 30.1% for Ústí nad Labem. Another characteristics was estimating the PV efficiency being installed within locations affected by lignite mining, where the total area of 140,000 m² could after transformation into solar power plant can generate up to 1,779 MW and therefore vastly contribute to energy self-sufficiency of the Ústí region.

References

1. Vráblíková, J., Vráblíková, P., Wildová, E. and Blazková, M. (2017) *Future of Renewable Resources in an Area Burdened by Brown Coal Mining*. Natural Resources, 8, 757-766. doi: 10.4236/nr.2017.812046.
2. Uhelná komise; Doporučení Uhelné komise o konci hnědého uhlí v roce 2038. Dostupné z: <https://www.mpo.cz/cz/rozcestnik/pro-media/tiskove-zpravy/doporuceni-uhelne-komise-o-konci-hnedeho-uhli-v-roce-2038-projednala-vlada--261557/>
3. Pešout, P., Porteš, M., Pixová, K., Hendrychová, M., Kříž, P., Lacina, D., *Ekologická obnova hnědouhelných velkolomů*. Ochrana přírody 2/2021.

In-situ characterization of an electrochemical cell prepared in SEM

O. Klvač^{a,b}, T. Kazda^a, O. Čech^a, Y. Fam^b, L. Novák^b

^a Department of Electrical and Electronic Technology, Faculty of Electrical Engineering and Communication, BUT, Technická 10, 616 00 Brno, Czech Republic

^b Thermo Fisher Scientific Brno, Vlastimila Pecha 12, 627 00, Brno, Czech Republic

This work describes a universally applicable method for in-situ research of electrochemical cells inside the chamber of a scanning electron microscope (SEM). The tested cell consists of lithium metal, an ionic liquid, and lithium titanate (LTO). As a current collector of investigated LTO electrode micromanipulation needle is used. The first part describes experiment preparation using the FIB-SEM system, second part shows electrochemical testing results. The work is evolved in cooperation with Thermo Fisher Scientific Brno.

Introduction

Lithium-ion batteries (LIBs) are currently the most commonly used cells for high-performance applications. It is one of the fastest growing markets and large funds are invested in development [1][2][3].

During the research, it is important to understand the physical processes at the grain level of the active material, which can currently be derived mainly from electrochemical measurements. Other non-destructive techniques, such as X-ray and CT, usually do not achieve sufficient resolution. Electron microscopy together with energy dispersive spectroscopy and ion technologies may be the solution [4][5][6].

This work describes the design of an experimental setup for in-situ battery characterization inside the SEM chamber. The proposed arrangement consists of lithium metal, an ionic liquid, and the LTO sample as an investigated electrode. An SEM micromanipulator is used as a current collector of the investigated electrode which allows quick disassembling of the cell and observation of grain-level changes induced by cycling.

Experimental

Scios 2 DualBeam SEM (Thermo Fisher Scientific) with gallium FIB was used for the in-situ experiment. The experimental scheme is shown in Figure 1.

The experimental cell was assembled on a sample stub fixed in an insulating plate separating it from the SEM frame. The stub was electrically directly connected with the CANON connector at the air side of the vacuum feedthrough installed on the SEM chamber. Using double-sided carbon tape, a piece of lithium dripped with electrolyte was attached to the surface of the stub. As an electrolyte, 1-Ethyl-3-methylimidazolium tetrafluoroborate ionic-liquid (IL) in a mixture with LiBF₆ salt in 0.5M concentration was used.

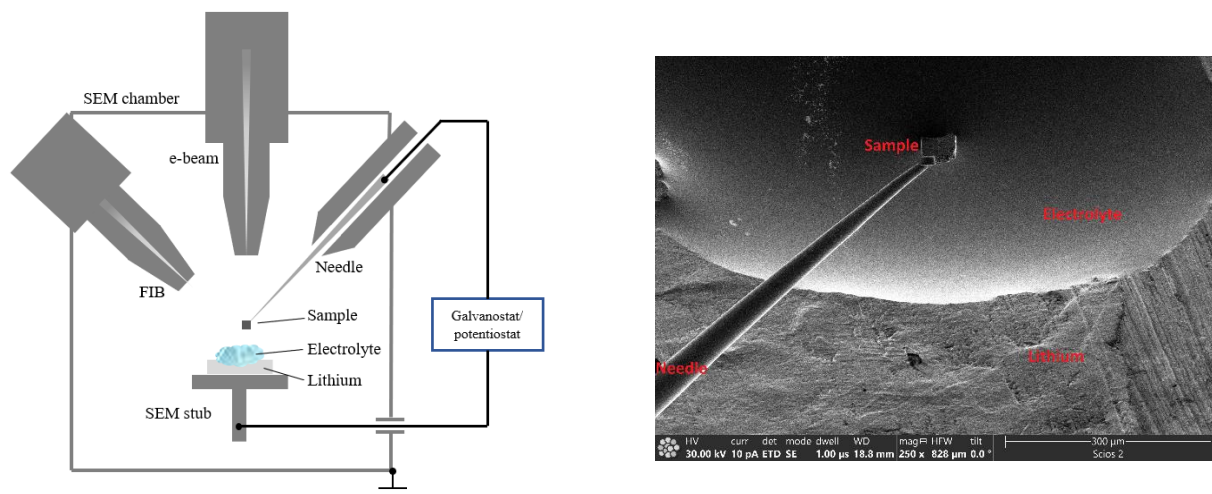


Figure 1. Experimental scheme of the performed experiment (left); SEM image of created half-cell (right)

A modified EasyLift micromanipulator was used as the current collector for the second electrode. A chunk of approx. $50 \times 50 \times 20 \mu\text{m}$ from a commercially available LTO electrode sheet was cut using the FIB system and attached to the micromanipulator by platinum deposition using MultiChem Gas Delivery System.

For measurements, BioLogic SP-150 galvanostat/potentiostat was connected with a shared reference electrode (RE) and the counter electrode (CE) to the stub with lithium, and the micromanipulator with LTO was on the working electrode (WE).

Results

A total of 7 complete cycles in different voltage ranges were performed (see detail in Table 1, Figure 2).

Table 1: Cycling conditions and achieved capacity

	Ewe [V]	Q_discharge [nAh]	Q_charge [nAh]
1. cycle	1.3 - 2.0	2.8	1.32
8 hod break			
2. cycle	1.2 - 2.1	6.14	3.33
3. cycle	1.2 - 2.1	4.09	2.34
4. cycle	1.2 - 2.1	0.34	0.22
5. cycle	1.2 - 2.1	0.5	0.29
6. cycle	1.2 - 2.1	0.2	0.12
CV			
7. cycle	1.3 - 2.0	2.03	1.07
discharging	up to 1.0	6.09	–

When the sample was immersed into electrolyte completely, the voltage stabilized at 2.21 V. Then the GCPL was set to a current of $\pm 5 \text{ nA}$. A maximum capacity of 6.14 nAh was reached after eight hours of relaxation in the second cycle. With each next cycle, the capacity decreased rapidly.

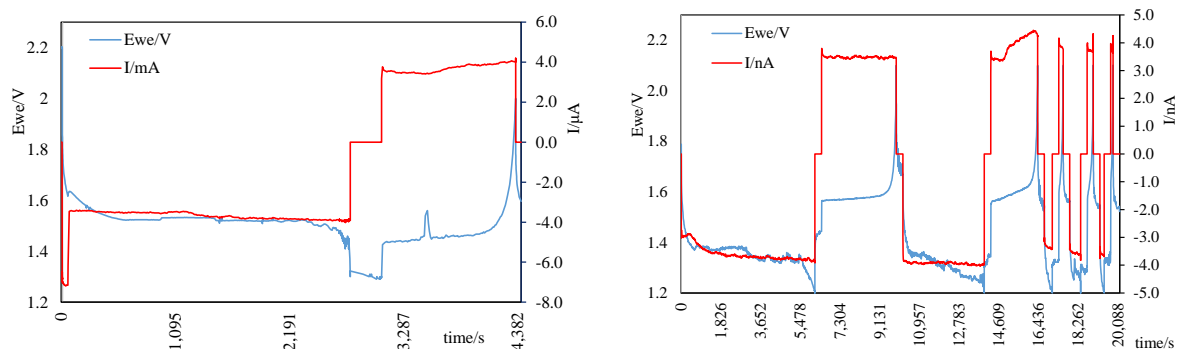


Figure 2. First performed cycle (left); next cycles after 8 hours of relaxation (right)

The CV characteristic showed the shift of the discharge plateau. In the voltage range of 1.3 V - 2.0 V, only the ramp of the reduction peak was visible, but not the maximum. It may be the result of an increase in internal resistance. The measurement results in a lower capacity because the cycle is completed before the battery is actually discharged. After modifying the voltage range, the cell was able to reach almost the original capacity again. Consequent analysis showed electrolyte side reactions with lithium.

Conclusion

The battery system consisting of metallic lithium, ionic liquid, and lithium titanate was assembled using the FIB-SEM system and in-situ tested. It was confirmed that it is possible to use the SEM micromanipulator as the current collector of the investigated electrode. Future plans include the usage of different types of electrolytes and electroactive materials.

Acknowledgments

This work was supported by the specific graduate research of the Brno University of Technology No. FEKT-S-20-6206. The work was developed in cooperation with Thermo Fisher Scientific Brno.

References

1. Y. Liang et al., *InfoMat*, 1, 6-32 (2019).
2. H. -J. Kim et al., *Electronics*, 9 (2020).
3. Grand View Research, Inc., 2020.
4. L. Li and X. Zhang, (I2MTC), p. 1-5, IEEE (2018)
5. P. Pietsch and V. Wood, *Annual Review of Materials Research*, 47, 451-479 (2017)
6. D. J. Miller et al., *Advanced Energy Materials*, 3, 1098-1103 (2013)

Evaluation of Ballistic Coefficient for .223 rem Projectiles

J. Maxa^a

^a Department of Electrical and Electronic Technology, Brno University of Technology, Technická 10, 616 00 Brno, Czech Republic

As part of the research in the field of vacuum chamber pumping in the Environmental Electron Microscope, research on supersonic flow through apertures is being carried out at the Department of Electrical and Electronic Technology of Brno University of Technology in cooperation with the Institute of Scientific Instruments of the CAS. This paper deals with the influence of reflected shock waves on the resulting flow in the pumped part of the Experimental Chamber.

Introduction

At the Department of Electrical and Electronic Technology of Brno University of Technology, in cooperation with Institute of Scientific Instruments of the CAS, research on supersonic flow at low pressures is being carried out (1, 2, 3). The results are used in the design of vacuum chambers of the Environmental Electron Microscope (4, 5, 6). Within the framework of research on supersonic flow, research on ballistics of supersonic projectiles is also underway. This paper deals with the determination of the ballistic coefficient for .223 rem caliber bullets for the AR 15 type V-AR self-loading rifle with a 22" barrel in preparation for further experimentation in the field of supersonic flight of projectiles.

Experimental equipment

The rifle used for the experiment was a .223 rem AR 15 V-AR with a 22" heavy barrel. 4 types of .223 Rem bullets from GGG Ammunition were used with different weights: 55 grs, 62 grs, 69 grs HPBT and 77 grs HPBT. The last two versions with a stabilizing cavity are Sierra bullets (Fig. 1).



Figure 1. Calibre .223 rem. with stabilizing hollow point on the right and without hollow point on the left

Caldwell Chronograph Premium electronic gates (Fig. 2) were used to measure the velocity of the projectiles, which measure with a resulting measurement error ($\pm 0.25\%$).



Figure 2. *Electronic gates*

Ballistic coefficient

The ballistic coefficient G was used, which is not only a characteristic of the shape and weight of the missile, but also reflects the instantaneous air resistance at a certain velocity.

$$G1 = \frac{0.0052834 \cdot x}{\sqrt{v_0} - \sqrt{v_x}} \quad [1]$$

v - velocity of the projectile at a given distance from the muzzle. The index of the velocity variable indicates the distance of the projectile from the barrel.

For the calculation of the ballistic coefficient, two velocities were measured. Measuring directly v_0 is difficult, so the velocity v_1 and $v_{48.7}$ were measured, which is the longest distance at the indoor range of SC Solutions Brno, where the measurement was performed. The measurements were made under the following conditions: Indoor range temperature 27 °C, Atmospheric pressure 102125 Pa. Relative humidity 41 %. Measurements were taken after the rifle barrel was heated to an approximate barrel temperature of 40 °C by approximately 20 shots.

Results and Discussions

Measurements of 10 shots were taken for each type of bullet and a statistical calculation of the average velocity at both distance v_1 , and $v_{48.7}$ was performed.

The ballistic coefficient is the value that, at a given projectile velocity, is directly proportional to the delay of the projectile due to air resistance. The higher the value, the greater the delay of the projectile as it moves through the atmosphere and the shorter the range (8). The higher $G1$ results than normally claimed by the manufacturer are due to the fact that the firing was carried out at a relatively higher atmospheric pressure.

TABLE I. Comparison of projectiles.

	Bullet 55 grs.	Bullet 62 grs.	Bullet 69 grs.	Bullet 77 grs.
v1	1009.6	982.4	882.4	825.2
v48.7	945.75	944.2	849.2	794.2
G1	0,246	0,41	0,45	0,46

These results are followed by mathematical and physical analyses in Ansys Fluent.

Acknowledgments

This research was supported by Brno University of Technology specific research program: Materials and technology for electrotechnics IV, reg. no. FEKT-S-20-6206.

References

1. E. Tihlaříková, V. Neděla, and B. Dordevic, in In-situ preparation of plant samples in ESEM for energy dispersive x-ray microanalysis and repetitive observation in SEM and ESEM, *Scientific Reports*, 9(FEB), 2300. ISSN 2045-2322. doi: 10.1038/s41598-019-38835-w, (2019).
2. J. Maxa, V. Neděla, J. Jiráček, P. Vyroubal, and K. Hladká, in Analysis of gas flow in a secondary electron scintillation detector for ESEM with a new system of pressure limiting apertures, *Advances in Military Technology*, roč. 7, č. 2, s. 111-116. ISSN 1802-2308, (2012).
3. J. Maxa, M. Bílek, P. Hlavatá, P. Vyroubal, and K. Lepřtová, in Comparisons Using Methods of Continuum Mechanics and Monte Carlo at Differentially Pumped Chamber, *Advances in Military Technology*, **11**, n. 2, p. 143-150. ISSN: 1802-2308, (2016).
4. M. Bílek, J. Maxa, P. Hlavatá, and R. Bayer, in Modelling and simulation of a velocity field within supersonic flows in low-pressure areas, *ECS Transactions*, **81**(1), pp. 311–316, (2017).
5. P. Hlavatá, J. Maxa, M. Bílek, and V. Neděla, in Impact of the shape of the differentially pumped chamber on critical flow character, *ECS Transactions*, **81**(1), pp. 317–322, (2017).
6. P. Hlavatá, J. Maxa, M. Bílek, P. Vyroubal, and R. Bayer, in Influence of critical flow in the differentially pumped chamber AQUASEM, *Advances in Military Technology*, **12**(2), pp. 301–310, (2017).
7. <https://www.sellier-bellot.cz/produkty/vypocet-balistickeho-koeficientu/>
8. Č. Jirsák, and P. Kodym, in *Vnější balistika a teorie střelby*, Naše vojsko ISBN: 978-80-206-1650-0, (2017)

Mathematical and Physical Analysis of Waste Heat Dissipation During Compression of Air Used as Energy Storage.

J. Maxa^a

^a Department of Electrical and Electronic Technology, Brno University of Technology, Technická 10, 616 00 Brno, Czech Republic

As part of the research in the field of pumping vacuum chambers in the Environmental Electron Microscope, research on supersonic flow through apertures is being carried out at the Department of Electrical and Electronic Technology of the Brno University of Technology in cooperation with the Institute of Scientific Instruments of the CAS. This paper deals with limiting the heating of compressed air when filling a storage tank as energy storage.

Introduction

At the Department of Electrical and Electronic Technology of Brno University of Technology, in cooperation with ISI Brno, research on supersonic flow at low pressures is underway (1, 2, 3). The results are used in the design of vacuum chambers of the Environmental Electron Microscope (4, 5, 6). Electricity consumption from the grid is not constant throughout the day or year. The best rating is achieved by compressed air energy storage technology. However, the disadvantage of this method of energy storage is the waste heat generated during the compression of the gas, which is subsequently released during the storage process and thus significantly reduces the efficiency of the whole cycle.

Mathematical and physical model

In this part of the research, the simulation of air pumping in ANSYS was carried out on a model example in which a bottle with the dimensions shown in Figure 1 was used as a reservoir instead of an underground storage tank. This is a 2D model of a bottle where the dimension b is the radius of the base. ANSYS Fluent simulation software was used to simulate the process of air compression into the container and subsequent cooling.

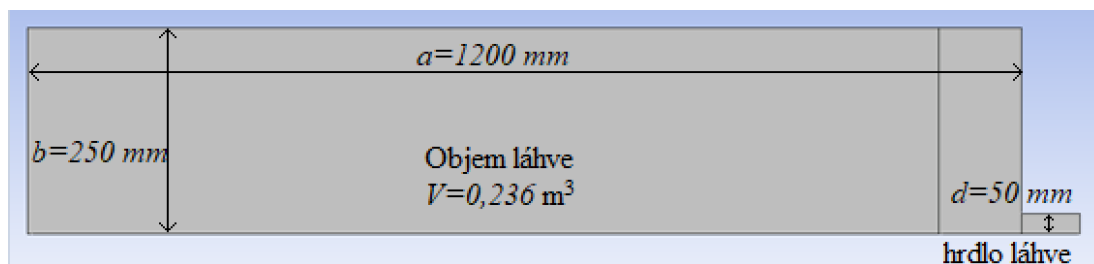


Figure 1. 2D axisymmetric model of the bottle

Air from the compressor was pumped into the neck of the bottle with a mass flow rate inlet of $Q_m = 0.007$ [kg/s]. Furthermore, the heat transfer coefficient $H = 25$ [W/m²·K] (7) was set on the walls of the bottle. The temperature of the air pumped into the bottle is the compressor outlet temperature and was set to 40 °C according to the given equations (7).

The pumping process was carried out for 209 s, increasing the pressure to 709 kPa and the temperature to 61.49 °C. The pumping was then stopped and the cylinder cooled freely until a time of 600 s, at which time it cooled to a temperature of 27,75 °C and the pressure dropped to 638 kPa.

This model example was used to investigate the behaviour of the air during pumping into the store, the heating of the air during pumping and the pressure drop during subsequent cooling.

Subsequently, several cases in which the air heating during pumping is minimised in different ways were designed and simulated. The bottle model was modified by adding rings (Fig. 2). The rings, based on the technology used, reduced the heating of the air during bottle pressurization:

Variant A - Only embedded heat absorbing rings.

Option B - Heat absorbing rings acting as a thermocouple

Option C - Refrigerator rings cooled to -10 °C for 72 s.

Option D - Rings pre-cooled to 10 °C before pumping begins. They were no longer cooled during pumping.

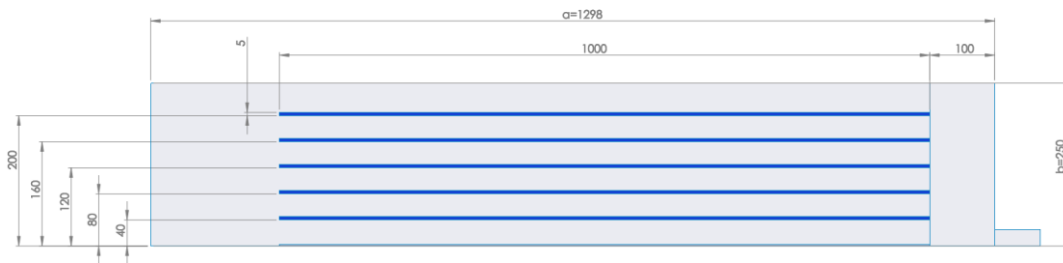


Figure 2. 2D axisymmetric model of a bottle with embedded cooling elements.

Results and Discussions

The results show that heat removal by any of the tested variants has an effect of reducing the pressure in the cylinder by up to 50 kPa. The rings themselves prevent rapid heating of the gas in the cylinder by their large surface area and mass, which removes the heat from the pressurized gas by convection and does not require any external power such as a refrigeration compressor. The thermocouple option demonstrates that there is a combination of the effect of the rings (added mass), and the energy extraction by the thermocouples, but only with a small difference. The option with cooled rings at -10 °C proves to be unnecessarily expensive. The pre-cooled to 10 °C option, which no longer requires external power to be supplied during pumping, shows better results than the previous options, due to the fact that it can keep the compressed gas at approximately room temperature. The pressure level of the compressed gas is not affected by temperature changes which cause it to expand further and ultimately shrink.

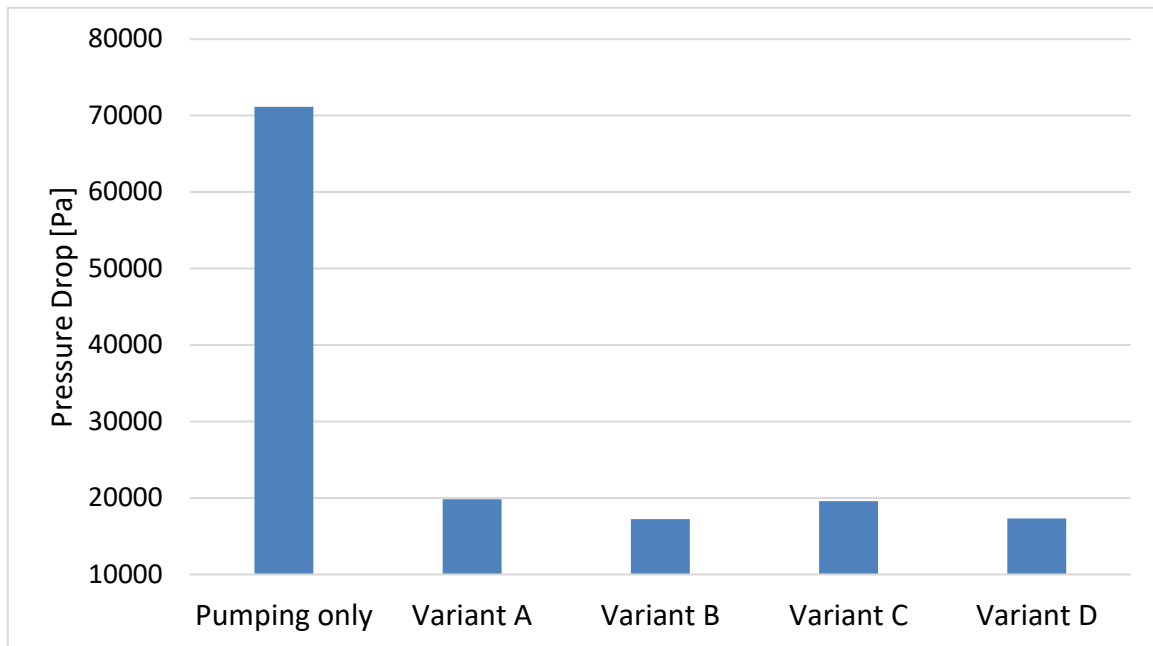


Figure 4. Comparison of pressure drop when using supplementary rings on the container

Acknowledgments

This research was supported by Brno University of Technology specific research program: Materials and technology for electrotechnics IV, reg. no. FEKT-S-20-6206.

References

1. E. Tihlaříková, V. Neděla, and B. Dordevic, in In-situ preparation of plant samples in ESEM for energy dispersive x-ray microanalysis and repetitive observation in SEM and ESEM, *Scientific Reports*, 9(FEB), 2300. ISSN 2045-2322. doi: 10.1038/s41598-019-38835-w, (2019).
2. J. Maxa, V. Neděla, J. Jiráček, P. Vyroubal, and K. Hladká, in Analysis of gas flow in a secondary electron scintillation detector for ESEM with a new system of pressure limiting apertures, *Advances in Military Technology*, roč. 7, č. 2, s. 111-116. ISSN 1802-2308, (2012).
3. J. Maxa, M. Bílek, P. Hlavatá, P. Vyroubal, and K. Leptová, in Comparisons Using Methods of Continuum Mechanics and Monte Carlo at Differentially Pumped Chamber, *Advances in Military Technology*, **11**, n. 2, p. 143-150. ISSN: 1802-2308, (2016).
4. M. Bílek, J. Maxa, P. Hlavatá, and R. Bayer, in Modelling and simulation of a velocity field within supersonic flows in low-pressure areas, *ECS Transactions*, **81**(1), pp. 311–316, (2017).
5. P. Hlavatá, J. Maxa, M. Bílek, and V. Neděla, in Impact of the shape of the differentially pumped chamber on critical flow character, *ECS Transactions*, **81**(1), pp. 317–322, (2017).
6. P. Hlavatá, J. Maxa, M. Bílek, P. Vyroubal, and R. Bayer, in Influence of critical flow in the differentially pumped chamber AQUASEM, *Advances in Military Technology*, **12**(2), pp. 301–310, (2017).
7. <http://www.jmccampbell.com/tip-of-the-month/2011/11/compressor-calculations-rigorous-using-equation-of-state-vs-shortcut-method/>

Innovative Non-Destructive Non-Contact Methods Testing to Solve for the Bridge the Gap Between Materials Limitation and Manufacturing. Answering the Requirements of High Energy Batteries

V. Redko^a, T. Pastushkin^a, E. Shembel^{a,b}, B. Kutnick^a, P. Novak^c, A. Fedorková^d, V. Khandetsky^a, N. Zaderey^b, S. Pukha^e, A. Redko^b.

^aEnerize Corporation, Coral Springs, FL, 33067, USA.

^bScientific Research Laboratory of Chemical Power Sources of Ukrainian State University of Chemical Technology, Dnipro, 49005, Ukraine

^cPeter Novak, Fort Lauderdale, FL, 33300, USA.

^dPavol Jozef Safarik University, Košice, SK-04154, Slovak Republic

^eSpecial Design Bureau “Shtorm”, Kyiv, Ukraine

Continuous application of appropriate non-destructive non-contact testing (NDT) procedures to materials and components before, during and after the manufacturing process is the most cost effective method to achieve the highest possible product quality and reliability. Areas of applications of Enerize Corporation are as followings: batteries, solar cells, supercapacitors, chemical and construction industries, petrochemistry, etc

Non-destructive Non-Contact Testing Technologies and Devices are Focusing on the Following Key Topics:

1. Examples of physical principles of non-destructive & non-contact methods for evaluation and testing of components Li batteries during production:

- -Initial materials, including nano-structured powders of electrode materials
- -Polymer and solid inorganic electrolytes
- -Properties of electrodes during coating, including the resistance of interface between current collectors and electrode mass
- -Multi-layered electrode structures, such as Jelly roll dry electrode structure
- -Final product of electrode structure

2. Design of equipment for non-destructive testing.

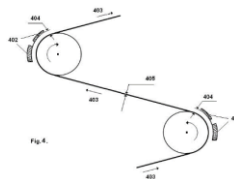
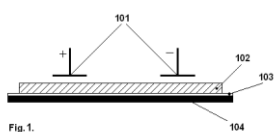
3. Examples of using non-destructive methods in Li batteries, super-capacitors, solar cells, chemical industry, and other industries (example –evaluating the properties of the cement)

4. Benchmarking and the market of application for non-destructive, non-contact testing.

Some Examples of Using the Non- Destructive Method and Device, which Developed by Enerize Corporation

1. Non-contact electromagnetic testing of interface resistance between current collector and electrode mass. Enerize US Patent No. 7,982,457. Method and eddy current system for non-contact determination of interface resistance.

The value of contact resistance between metallic current lead and electrode mass composite coating is one of the key parameters for determination of performance of energy storage devices, such as batteries, supercapacitors, etc. A method and an eddy current system developed for non-contact evaluation of the resistance between the current lead stripe and the coating during continuous fabrication of electrodes for the batteries and supercapacitors, and before assembly of electrode structure inside



2. Method of test powdered materials in chemical industry. US Patent No. 8.309,024. Methods and systems for non-destructive determination of fluorination of carbon powders.

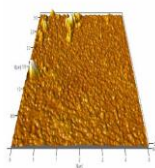
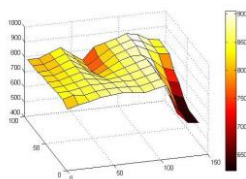
Electromagnetic non-destructive capacitance method for testing electromagnetic properties and chemical composition of Carbofluor (CF_x)_n. Synthesis: C + F₂ -----CF_x. Degree of fluorination influences on the CF_x conductivity and efficiency of CF_x based cathode.



3. Non-Destructive Non-Contact detection of hidden faults in batteries and ultracapacitors. Patent application is prepared.



4. Non-Destructive non-contact tests the conductivity of thin films of transparent conductive oxide for Dye-Sensitized Solar cells. Test spatial distribution of electrical conductivity using non – destructive electromagnetic method and AFM for thin conductive layer of Indium Tin Oxide on a plastic base



During our presentation on the International Conference ABAF 23 we will see which our Non-destructive Non-contact methods are important and interesting. Based on this we will prepare information for our publication in the Journal of Physics.

Below we presented the List of US granted Patents of Enerize Corporation in the area of Non-Destructive non-contact method and device.

Acknowledgments

Among the new projects, in which the Enerize Corporation participate for using the developed and in generating new innovating non-destructive non-contact test the method and device - it is the framework Enerize Corporation with NATO SPS 985148 project "Development of New Cathodes for Stable and Safer Lithium-Sulfur Batteries" / Science for Peace and Security Programme. Enerize Corporation, USA is an industrial partner under NATO SPS 985148 project. This investigations under NATO project have been carried out also in cooperation with the Enerize Corporation and Ukrainian State University of Chemical Technology, Scientific Research Laboratory of Chemical Power Sources.

References of Enerize Corporation Intellectual Property in the Area of Non-Destructive Non-Contact Testing are the Following

1. Method of Non-Contact Measuring Electrical Conductivity of Electrolytes with Using Primary Measuring Transformer. US Patent No. 7,071,684.
2. Method and Apparatus for Measuring Conductivity of Powder Materials Using Eddy Currents. US Patent No. 7,288,941.
3. Method and Apparatus For Eddy Current-Based Quality Inspection Of Dry Electrode Structure. US Patent No. 7,355,395.
4. Method of Nondestructive Tightness Testing Based on Gas Discharge Visualization. US Patent No. 7,498,817.
5. Integrated Non-destructive Method and Device for Electrochemical Energy System Diagnostics. US Patent No. 7,783,438.
6. Apparatus and Method for Determining Service Life of Chemical Energy Sources Using Combined Ultrasonic and Electromagnetic Testing. US Patent No. 7,845,232.
7. Holographic Interferometry for Non-destructive Testing of Power Sources. US Patent No. 7,911,618.
8. Method and Eddy Current System for Non-Contact Determination of Interface Resistance. US Patent No. 7,982,457.
9. Method and Device for Rapid Non-Destructive Quality Control of Powdered Materials. US Patent No. 8,102,181.
10. Method and Apparatus for Detecting and Inspection Through-Penetrating Defects in Foils and Films. US Patent No. 8,284,247.
11. Methods and Systems for Non-Destructive Determination of Fluorination of Carbon Powders. US Patent No. 8.309,024.

Overview of tribological properties of UHMW polyethylene under rotation

Z. Studeny^a, D. Dobrocky^a, J. Viliš^a, J. Adam^b

^a Department of Mechanical Engineering , University of Defence, Brno, Czech Republic

^b Department of Weapons and Ammunition, University of Defence, Brno, Czech Republic

Keywords:

UHMW polyethylene, tribological testing, coefficient of friction, Stellite 6, ZrO₂

The paper works with ultra-high molecular weight polyethylene (UHMW). This polyethylene is widely used in technology, in engineering or its applications are also in the field of medicine in prosthetics in the lining of joint replacements.

This wide use is mainly due to its properties. It is mainly its abrasion resistance and very low coefficient of friction (COF), so it has excellent sliding properties. It is these properties that are the subject of research on UHMW polyethylene. The investigation of these properties is always linked in tribological tests to the material in the friction pair, which consists of the material under test (UHMW) and the indenter. For the purpose of tribological testing, 6.35 mm diameter balls of ZrO₂ ceramic material and a cobalt-chromium alloy known as Stellite 6 were chosen as indentors.

The tribological tests were carried out under rotation on a Bruker UMT tribometer. Trace parameters were verified by profilometric analysis on a TalySurf CLI1000. The wear parameters of samples and balls were also documented and evaluated. The results of the tests are the load dependences on the wear of the UHMW polyethylene and the test specimens.

Clear dependencies of tribological properties of UHMW polyethylene and ceramics or cobalt-chromium alloy were found. Practical applications are the above mentioned fields of technology, engineering, etc.

Mathematical and Physical Analysis of Thermal Conductivity at Low Pressures

P. Šabacká^a

^a Department of Electrical and Electronic Technology, Brno University of Technology, Technická 10, 616 00 Brno, Czech Republic

As part of the research in the field of pumping vacuum chambers in the Environmental Electron Microscope, research on supersonic flow through apertures is being carried out at the Department of Electrical and Electronic Technology of the Brno University of Technology in cooperation with the Institute of Scientific Instruments of the CAS. This paper deals with the effect of low pressures on the thermal conductivity of gases that occurs when observing samples in the Environmental Electron Microscope.

Introduction

At the Department of Electrical and Electronic Technology of Brno University of Technology, in cooperation with ISI Brno, research on supersonic flow at low pressures is underway (1, 2, 3). The results are used in the design of vacuum chambers of the Environmental Electron Microscope (4, 5, 6). Within the framework of this research, an experimental chamber was created for research on supersonic flow at low pressures and for research on thermal conductivity of gases at low pressures in order to examine heated and cooled samples in an electron microscope.

Experimental chamber

The chamber in the configuration for measuring the thermal conductivity of gases is cylindrical with a base diameter of 80 mm and a height of 100 mm. A sample, also cylindrical in shape, with a base diameter of 2 mm and a height of 30 mm, is inserted into the chamber and placed exactly in the center of the chamber.

Mathematical-physical model

The thermal conductivity of a gas is relatively independent of pressure when the pressure is close to 1 atm. The thermal conductivity becomes dependent on the magnitude of the pressure only at higher or, on the other hand, at very low pressures.

Gases are composed of a large number of particles that behave like hard, spherical objects. These particles move in a straight line until they collide with another particle or the walls of the container. Thermal conductivity (the ability to conduct heat) is caused by the collision of molecules in a gas.

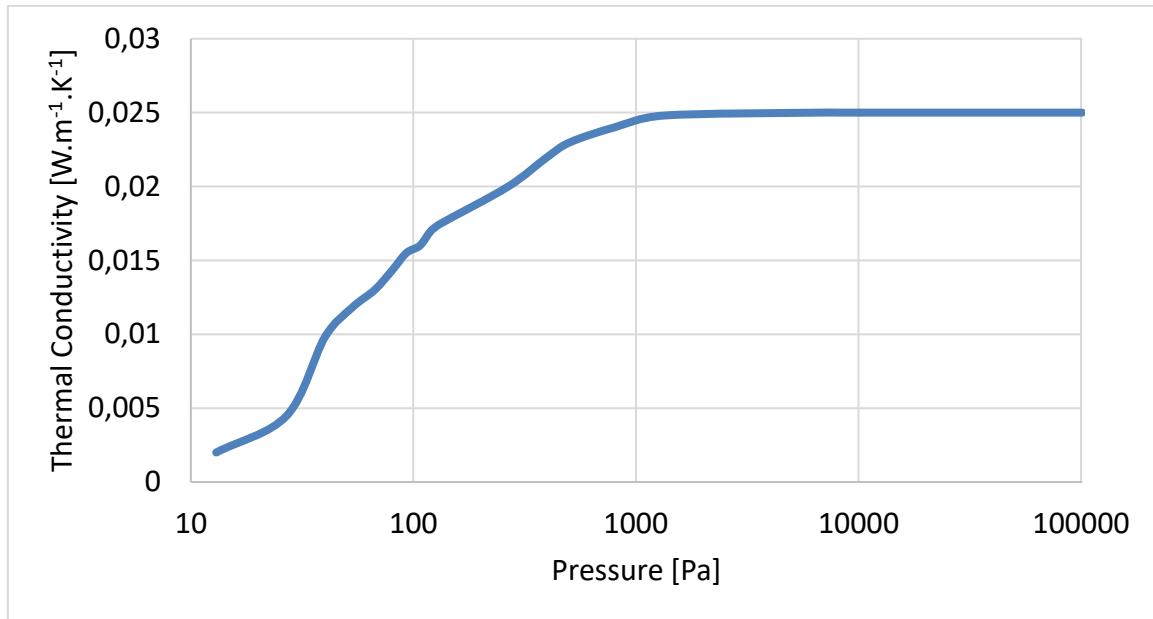


Figure 1. Dependence of thermal conductivity on pressure.

As the pressure of the gas increases, the number of collisions between the molecules and with the walls of the container increases. Thus, the thermal conductivity of a gas increases with gas pressure. This phenomenon occurs at higher pressures. The gas behaves similarly, but with the opposite effect, at low pressures, when the value of thermal conductivity decreases (Fig. 1).

Results and Discussions

In these simulations, the thermal conductivity of an aluminum sample placed in a chamber with atmospheric pressure was compared with a chamber depleted to a pressure of 5000 Pa, which is the upper limit in the Environmental Electron Microscope for observing samples, and a pressure of 267 Pa, which is the lower limit. The results are shown in Fig. 2.

The results show that at pressures above 5000 Pa, there is only a slight decrease in the thermal conductivity of the gas in the chamber compared to the conductivity at atmospheric pressure, but at pressures in the lower range of the ESEM operating conditions, a significant decrease should already be expected.

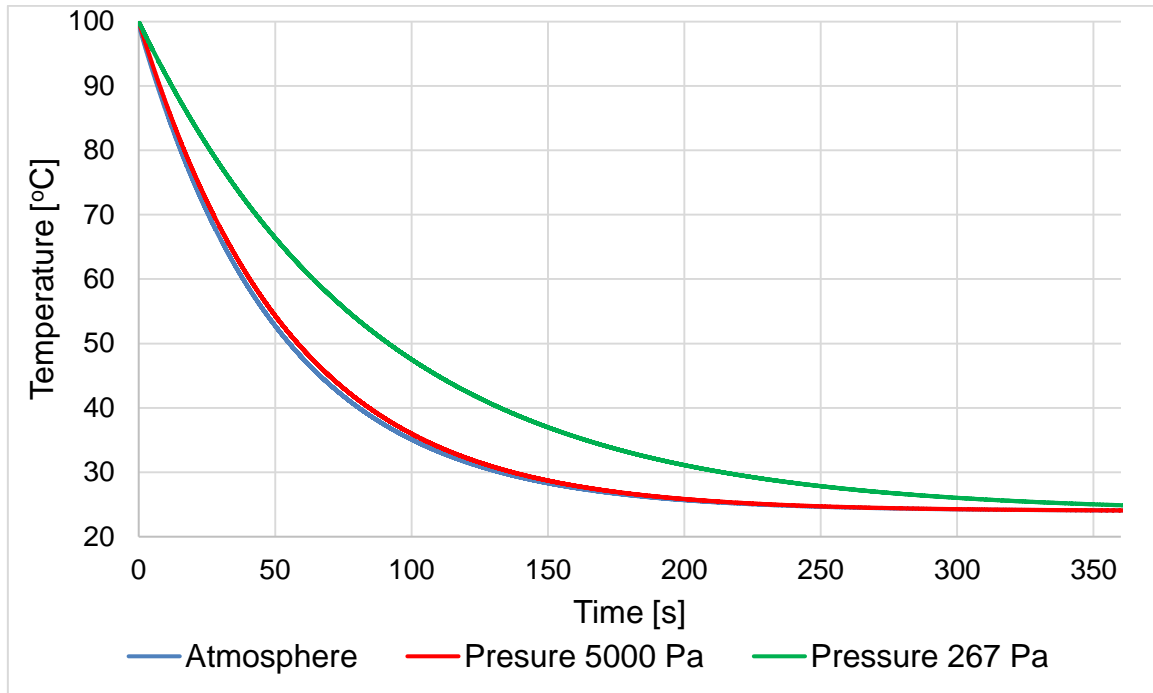


Figure 2. Dependence of thermal conductivity over time at specified pressure levels

Acknowledgments

This research was supported by Brno University of Technology specific research program: Materials and technology for electrotechnics IV, reg. no. FEKT-S-20-6206.

References

1. E. Tihlaříková, V. Neděla, and B. Dordevic, in In-situ preparation of plant samples in ESEM for energy dispersive x-ray microanalysis and repetitive observation in SEM and ESEM, *Scientific Reports*, 9(FEB), 2300. ISSN 2045-2322. doi: 10.1038/s41598-019-38835-w, (2019).
2. J. Maxa, V. Neděla, J. Jiráček, P. Vyroubal, and K. Hladká, in Analysis of gas flow in a secondary electron scintillation detector for ESEM with a new system of pressure limiting apertures, *Advances in Military Technology*, roč. 7, č. 2, s. 111-116. ISSN 1802-2308, (2012).
3. J. Maxa, M. Bílek, P. Hlavatá, P. Vyroubal, and K. Lepřtová, in Comparisons Using Methods of Continuum Mechanics and Monte Carlo at Differentially Pumped Chamber, *Advances in Military Technology*, **11**, n. 2, p. 143-150. ISSN: 1802-2308, (2016).
4. M. Bílek, J. Maxa, P. Hlavatá, and R. Bayer, in Modelling and simulation of a velocity field within supersonic flows in low-pressure areas, *ECS Transactions*, **81**(1), pp. 311–316, (2017).
5. P. Hlavatá, J. Maxa, M. Bílek, and V. Neděla, in Impact of the shape of the differentially pumped chamber on critical flow character, *ECS Transactions*, **81**(1), pp. 317–322, (2017).
6. P. Hlavatá, J. Maxa, M. Bílek, P. Vyroubal, and R. Bayer, in Influence of critical flow in the differentially pumped chamber AQUASEM, *Advances in Military Technology*, **12**(2), pp. 301–310, (2017).

Mobile system for power sources monitoring and diagnostics based on INA 219 module

M. Tkach, Yu. Polishchuk

Ukrainian State University of Chemical Technology, Dnipro, 49005, Ukraine

The paper shows the possibility of using a mobile system for monitoring and diagnosing current sources based on the INA219 module. A device has been developed that is configured for several operating modes, including express diagnostics. The device has a small size and weight while providing high measurement accuracy. The working temperature range is from -10 to +80°C. The operation of the device has been tested on AGM Logic Power 12V 7Ah LPM 12-7 gel lead-acid batteries.

Today, many countries provide state regulation in the field of chemical current sources, which includes supervision and control of compliance by manufacturers, sellers, and consumers with the requirements of technical documentation for storage, operation of batteries, and transfer of spent chemical current sources for disposal. In this case, there is a need for constant monitoring of production parameters directly during the production process and storage of finished products. Battery manufacturers take safety issues so seriously that they use artificial intelligence (AI) to do this. For example, Comau uses Machine Inspection Recognition Archetypes (MI.RA) and machine vision system Thermography to optimize battery design and assembly. The company's website states that MI.RA/Thermography artificial intelligence (AI) is a non-invasive, automated assessment of battery weld inspection. In [1], it is proposed to apply an optimized machine learning (ML) technique to assess the possibilities of the technology for the production of lithium-ion batteries for electric vehicles. Another option for using AI in the production of lithium-ion batteries could be the use of a recurrent neural network for temperature estimation [2].

However, most battery users require simple, portable, mobile rapid diagnostic devices. The use of AI tools is not available to an ordinary consumer. Existing traditional diagnostic methods take a lot of time. It is necessary to carry out a full charge-discharge cycle, as well as to check the ability to generate a current of a certain amount for a given time. The standard charge current for a battery is 1/10 C. The discharge current depends on the type of battery and the load being consumed. General testing time is 11-12 hours.

This work shows the possibility of using a portable measuring device tested on lead-acid batteries. It is equipped and configured for the following modes of operation:

1. Determination of the nominal battery capacity. The device can work in three ranges of the measured capacity: range I - from 1 to 4.5 Ah; range II - from 4.5 to 12 Ah and range III - from 12 to 55 Ah. Voltage is 6 and 12 V.

2. Internal monitoring of own power supply. The device is designed for two modes: operation from an AC network 85 - 240 Hz, and a built-in battery. The device provides the ability to apply energy-saving modes (temporary shutdown of the screen, switching to energy-saving mode). This allows you to increase the battery life of the device from 8 to 16 hours.

3. Battery quality express test mode. To do this, charge and discharge curves are recorded, which determine the internal resistance, and capacity (approximate). In this case, the user determines the mode of operation: express or full test.

To work in express mode, you must first take a series of calibration curves that will form the base. In this case, the charge-discharge characteristics of the tested battery are compared with the calibration ones, on the basis of which it is possible to draw a qualitative conclusion about the state of the battery. Under certain modifications, a full battery test and rejection in case of non-compliance with operating parameters can be scheduled.

The measuring module is based on the INA219 microcircuit (Fig. 1). It is equipped with a current and voltage meter with zero drift, and has a small size and weight while providing high measurement accuracy. The working temperature range is from -10 to + 80°C.

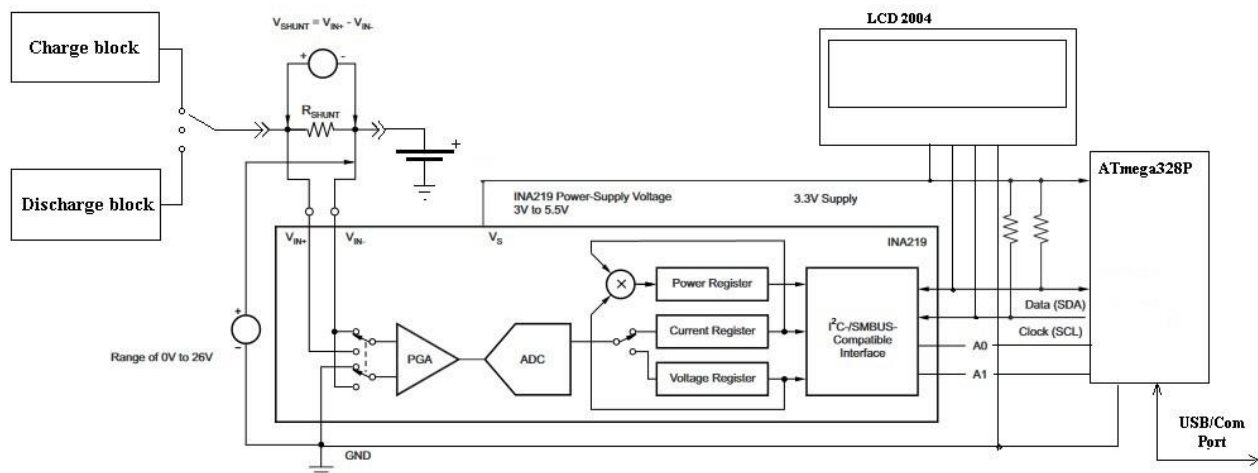


Figure 1. Current and voltage measurement based on the INA219 module

The microcircuit measures the parameters of the current flow in any direction with automatic switching of the measurement polarity. The module can be used in systems that control the process of charging/discharging batteries, and in power sources with control of voltage and consumed current load. The design of the INA219 microcircuit allows connecting up to 4 such devices to one bus. To increase the accuracy of measurements, a calibration register is provided. The device can be connected to an LCD display or a PC through the USB port; it is equipped with a memory card comport and a port for connecting a thermal printer.

References

1. M.A. Hannan, M.S. Hossain Lipu, Aini Hussain, Pin Jern Ker, T.M.I. Mahlia, M. Mansor, A. Ayob, M.H. Saad, and Z.Y. Dong. *Scientific Reports*, **10**, 4687 (2020).
2. Y. Jiang, Y. Yu, J. Huang, et al. *Sci. China Technol. Sci.* **64**, 1335–1344 (2021).

Numerical Modeling of Li-Ion Battery Gassing

P. Vyroubal^a, M. Mačák^a, T. Kazda^a

^a Department of Electrical and Electronic Technology, Brno University of Technology, Technická 10, 616 00 Brno, Czech Republic

This paper deals with the numerical modeling of conjugate heat transfer combined with a CFD model for combustion during thermal abuse of a li-ion battery. In terms of complexity, the model is presented as a 2D transient problem. The results are compared with images from a thermal camera and show a very good agreement between the model and reality.

Introduction

Thermal Runaway (TR) is a chain reaction in a battery/cell that is caused by the temperature inside the battery/cell reaching a critical point where exothermic chemical reactions occur that produce even more heat than is supplied. With TR, the temperature inside rises incredibly fast, in milliseconds, and the energy stored in the battery is suddenly released. The result is extremely high temperatures, from 400 °C and above, and these temperatures cause gassing of the battery, accompanied by an explosion and subsequent fire, which is almost impossible to extinguish.

It is therefore clear that the size of the subsequent exothermic reaction is directly proportional to the charge level (SoC - State of Charge) of the battery/cell.

TR is a major safety concern for lithium-ion batteries. The subsequent phenomenon that accompanies this phenomenon is a fire, which is difficult to put out in terms of methodology. Predicting possible undesirable states of a lithium-ion system, e.g. the entire storage, is a good way to prevent these potential problems. These predictions can be realized in several ways.

A new type in the field of simulations are the so-called digital twins, where it is possible to check and predict the state of the entire system based on heuristic algorithms and the use of modern machine learning (ML) and artificial intelligence (AI).

Real tests are a logically necessary addition, so that we can declare the numerical model to be approximately correct, because from the principle of numerical methods, the result of modeling is an approximate result. However, real tests are financially expensive and dangerous in terms of safety and human health [1] and [2].

Abuse Mechanisms

The mechanisms that lead to TR can be of mechanical, electrical or thermal type. The consequence of these factors is an internal short circuit in the battery and the creation of subsequent exothermic chain reactions that lead to decomposition reactions of the materials that make up the battery.

Mechanical initiation

Destructive deformation or displacement of the structure under the action of force are two common features of the mechanical type of damage. Collision and subsequent crushing, or penetration of a foreign body into the battery are typical factors. If the battery is deformed, the separator may rupture, and thus an internal short circuit, or the electrolyte may leak, causing a subsequent fire. During penetration, a foreign body penetrates into the battery structure (e.g. during an accident) and in the case of a conductive body, the internal structure of the battery is short-circuited. [3]

Electrical initiation

In the case of electrical initiation, it is mainly a short conductive connection of the battery electrodes, so we are talking about an external short circuit. Furthermore, overcharging of the battery, for example due to the failure of the BMS, which has the task of checking and stopping the charging process. This is then accompanied by gasification and heat generation (Joule heat and heat generated by electrochemical reactions). Another factor could be excessive battery discharge (BMS failure). [4]

Dendritic growth in the entire structure can then lead to an internal short circuit and mechanical damage to the internal structure, when the dendrites "grow" through the separator, thus creating a direct short circuit between the anode and the cathode.

Thermal initiation

Local overheating of the battery can be caused by both mechanical and electrical initiation or poor Thermal Management (TM) of the entire system, when the battery is excessively heated by its surroundings. Overheating is then associated with an internal short circuit in the battery and the collapse of the separator and the onset of spontaneous exothermic reactions. [5]

Experimental

First, it was necessary to measure the charge and discharge curves of one cell (it was an LG battery size 18650, capacity 3200 mAh, 3.7V) and implement them together with geometry and boundary conditions in ANSYS Fluent [6]. Here the calculation took place and temperature maps and curves were obtained to compare reality and the numerical model. A model was then set up to calculate the temperature generated for TR. Here it was necessary to apply heating to the battery and monitor the temperature progress in the time domain (see Figure 1a).

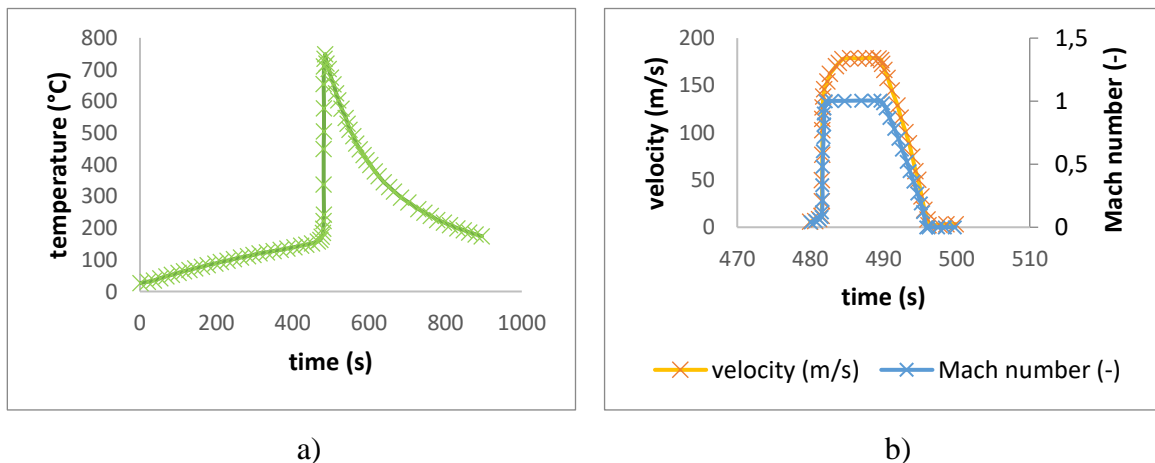


Figure 1. a) Dependence of the temperature inside the cell on time during the Thermal runaway phenomenon b) Course of gas velocity and Mach number over time.

It can be seen from the picture that at a certain moment the external heating of the flashlight ceases to play a role and exothermic reactions start. The time at which this happens depends on the material parameters of the battery.

As it is clear that gassing and burning of the battery will occur during this event, the course of the speed and Mach number in the model was monitored (see Figure 1b). The course of the Mach number, which describes the supersonic gas flow, is interesting. From this course, it can be concluded that the cell will explode and then burn. The explosion is accompanied by a sound effect, which is evidenced by the passage of the Mach number over the value 1, when a shock wave occurs.

Results and discussions

In the following figure (see Figure 2), it is possible to see the gradual development of gas and heat from the 18650 battery. In the first few time frames, the "start-up" phase is visible, and from time approx. 4 it is pure burning.

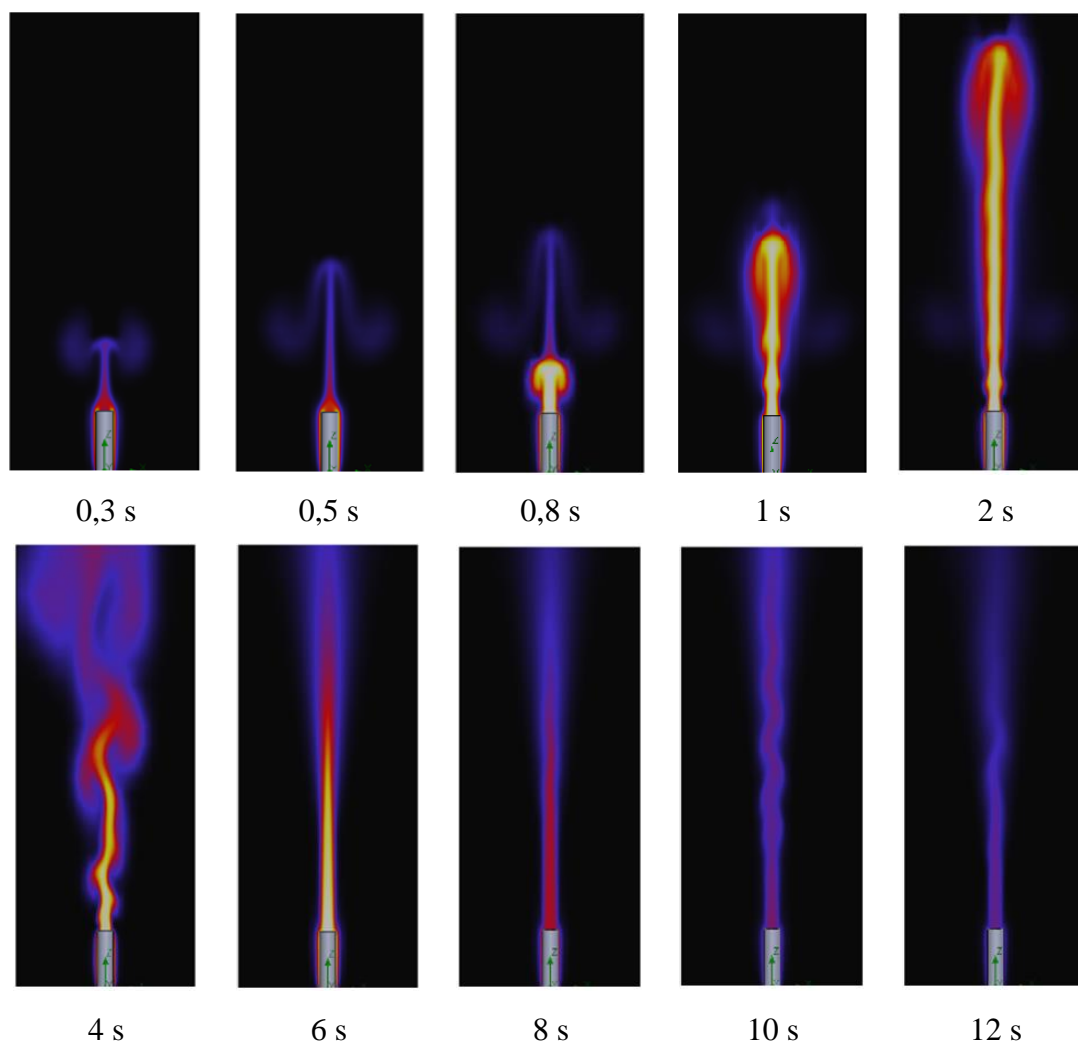


Figure 2. Simulation of temperature distribution at TR on an 18650 cell.

Conclusion

The numerical model shows the possibility of modeling the TR phenomenon in combination with combustion (see Figure 2). The model respects the gassing of the battery at elevated temperature and the change in pressure ratios throughout the model.

Acknowledgments

This work was supported by the specific graduate research of the Brno University of Technology No. FEKT-S-20-6206.

References

1. X. Feng, et al., Energy Storage Materials, **10**, (2018).
2. G-H. Kim, A. Peraran, R. Spotnitz, Journal of Power Sources. 170 (2), (2007).
3. A. A. Andreev et al., Procedia Engineering, 129, (2015).
4. D. Linden and T. B. Reddy, Handbook of Batteries, McGraw-Hill, Michigan (2002).
5. N. Nitta, F. Wu, J. T. Lee, G. Yushin, Materials Today, 18 (2015).
6. ANSYS, Inc. ANSYS Fluent Advanced Add-On Modules. 18.0. Canonsburg, PA 15317, (2015).

Failure Mechanism in The Pearlite Structure

J. Zimakova^a, T. Binar^a, P. Šafl^a, P. Čudek^a

^a Brno University of Technology, Technická 10, 616 00 Brno, Czech Republic

This article describes a change of the failure mechanism in the material of an engine, where the material structure consists of fine pearlite layers with lamellar graphite equivalent to grey cast iron. To assess the failure mechanism in the material, a fractographic analysis of the fracture areas was performed after the impact test. The range of test temperatures at which the impact test was performed on the test specimens with notch ranged from -80°C to +180°C. The occurrence of brittle fracture was detected at the low temperatures by cleavage along and over the planar layers of the lamellar graphite. The brittle fracture initiation at the higher temperatures was observed by cleavage in the basic layer of the perlite. Depending on the failure mechanism of the test specimens fracture area, critical temperatures were determined. Regression of temperature dependence of notch toughness allows very precise quantification of this decrease.

Introduction

There are a number of factors which influence the failure mechanism of materials from which the combustion engine cylinder insert, in which the piston moves, is made. One of the significant factors that can cause degradation processes in the material due to external stress is the ambient temperature or temperature generated during the engine operation [1, 2]. Determining the critical temperatures that initiate a failure mechanism in the material allows us to determine, for instance, the optimal operating temperature of the engine. Due to the material composition of the engine cylinder insert, which is the basic phase of a fine pearlite with lamellar graphite, a brittle fracture appears to be the most dangerous. Because of its nature and consequences, the brittle fracture represents the most serious and the most dangerous material failure which is the cause of failures of machine parts and structures. Based on this fact, extensive research has been carried out to define the underlying causes and process of brittle fracture formation and to assess the impact of external and internal factors involved in this degradation process [3, 4]. The early results of these studies, continuing to date, have enabled us to understand the causes and mechanism of the brittle fracture. Knowledge has been gained to identify the different types of sources from which fragile fractures occurs. From the results was also evaluated the role of internal stresses and the influence of thermal effects. From a macroscopic point of view, the brittle fracture can be characterized as a failure of cohesion during which did not occur macroscopic deformation in the fracture area.

Experimental material

To prepare the test specimens for the impact bending test, an electro-erosion wire cutting method was used, which produces only a slight heat-affected area and does not require any further treatment of the samples. The test specimens were sized to 7.0 x 7.5 x 55 mm, with a V-notch of 2 mm depth of 45° angle, and a notch base radius $R = 0.25$ mm, surface roughness 3.2. Using optical emission spectrometry, a chemical analysis of the engine cylinder material was carried out

by bulk analysis - "BULK" on the LECO SA-2000 spectrometer at a laboratory temperature of 25 °C. A total of 300 samples were produced and tested. In this work, illustrative examples of representative samples are given. The numbers for each sample correspond to the numbering in the test set.

Analysis of the microstructure of the material under investigation

The Neophot 32 microscope and the Olympus C-5050 digital camera were used for metallographic analysis of the base material. From the notch toughness specimens, cross-sections were removed from both halves of the test pieces at distance about 7 mm from the fracture and, after being pressed into a plastic, the samples were polished in a standard way. The microstructure was developed with 2 % nitaletch. The microstructure consists of a mixture of evenly distributed lamellar graphite [5] (ČSN 42 0464) and fine perlite with numerous clusters with a phosphide eutectic (steatite) (Chyba! Nenalezen zdroj odkazů.) which is formed at a phosphorus content of about 0.3 %. In Chyba! Nenalezen zdroj odkazů. small areas of the excluded ferrite in the area of the lamellar graphite are visible.

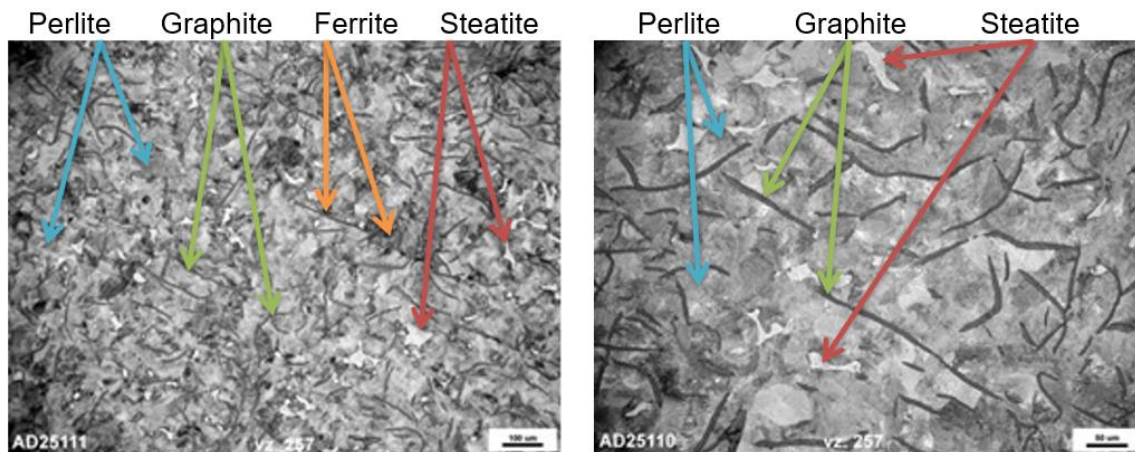


Figure 1. Microstructure of cast iron sample 257 after impact test at 22 °C

Conclusion

The effect of the test temperature on the mechanism of failure sustained during an impact bending test in the material with a fine pearlite structure, where ferrite clusters were formed in the area of the lamellar graphite, was investigated. In the investigated microstructure, structures of steatite have been identified, which are extremely fragile and hard. In the region of low test temperatures of -80 °C to 0 °C, a failure mechanism was observed on the fracture surfaces with transcrystalline cleavage regions (zones). The nucleation of the failure mechanism occurs by splitting the laminated graphite and then passes through the grains of the basic metal matrix. The most critical test temperature for assessing the effect of temperature on the rating of the resistance properties of the material against brittle fracture was determined to be -80 °C.

In the temperature range of above-zero test temperatures from +25 °C to +180 °C, a linear increase in the notched toughness characteristic was observed, and the failure mechanism was transcrystalline and longitudinally spreading at the facets of graphite. In the temperature range of +120 °C and +140 °C, the morphology of the fracture is composed of a mixed fracture, a proportion of the transcrystalline disruption and a sign of plasticity, and in that temperature interval

a reduced measured notch toughness was observed compared to +100 °C and +160 °C. In the above-zero temperature range, a brittle fracture failure mechanism occurred in a matrix consisting of fine perlite and graphite facets cleavage.

Various bent planes of lamellar graphite observed in the fractographic analysis of the fracture were probably caused by greater overheating of the melt and its rapid cooling.

The transient temperature of the studied material determined on the basis of the temperature-dependence of the notch toughness regression is 80 °C. This is relatively high value, however, this comes into play only during engine start-up and the time when the engine is warmed up, which is fairly short time. The notch toughness decrease at temperatures of 120 and 140 °C of nearly 13 J cm⁻² is explained by a change in the failure mechanism.

Acknowledgments

The publication was created as part of a specific research project at BUT (No. FEKT-S-20-6206).

References

1. J. Sukáč, T. Binar, T. Kazda and K. Šilinger, *ECS Transactions*, 70(1) p. 167-175. doi:10.1149/07001.0167ecst, (2015)
2. T. Binar, J. Kadlec, M. Rejzek, M. Vlkovsky, and V. Hruby, *Strength of Materials*, 43(5), p. 537–542, (2011)
3. J. Sukáč, T. Binar, M. Sedlaříková and K. Šilinger, *ECS Transactions*, 70(1), p. 177–185, (2015)
4. T. Binar, I. Dvořák, J. Kadlec, S. Rolc, and J. Křest'an, *Advances in Military Technology*, 9(2), p. 33–39, (2014)
5. ČSN EN ISO 643 Steels - Micrographic determination of the apparent grain size

Evaluation of Cold Kinetic Deposition Technology

P. Šafář^a, J. Zimaková^a, T. Binar^a, P. Čudek^a

^a Brno University of Technology, Technická 10, 616 00 Brno, Czech Republic

This article deals with the possibility of using cold spray technology. For the basic sample, an aluminum plate was used as a substrate, on which a layer of copper was subsequently formed. The samples were equipped with an acoustic emission measurement sensor and were placed in a condensation chamber, where the formation of corrosion was evaluated. Corrosion testing took place in a condensation chamber under steady conditions at a temperature of 50 °C and relative humidity 100%. The samples were exposed to the internal environment of the chamber for a given time, while continuous acoustic emission measurements were performed on them. A metallographic test was performed on the individual samples after the end of the given time cycle of the test

Introduction

The formation of coatings and surfaces using Cold spray is most often used to create a layer resistant to high temperatures in combination with abrasiveness or chemical resistance to halide elements, generally against high-temperature corrosion. The process of forming and applying surfaces takes place via elastic collisions without reaching the melting or melting temperatures of these particles. Unlike pure thermal spray processes. Size applied of particles ranges in the order of a maximum of tens of micrometers. According to various sources, several possible mechanisms are described. We can talk about two main bindings mechanisms. The first of these is compaction of the deposited layer and the second is metallurgical bonding to a significant fraction of the particle-particle interface. [1] The formation of an undesirable bond due to the compaction of individual dust particles manifests itself as an unsatisfactory porosity of the applied surface. Bad or imperfect formation of the metal bond affects the strength of the connection between the applied layer and the substrate. Comprehensive studies, e.g. [2], state that when creating a layer by the Cold spray process, it is extremely important to pay attention to the so-called critical speed. The critical speed is mechanical property of the applied material. The applied particles must not exceed the critical speed, because if it is exceeded, the desired flexible shift will not occur with the surface and the formation of a layer, but to the erosion of the substrate. Determining the critical speed is problematic. From the experiments and studies carried out, it can be claimed that the critical speed can be estimated according to the formula [3]: $Vc = 667 - 14 \cdot \rho + 0.08 \cdot Tm + 0.1 \cdot \rho u - 0.4 \cdot Ti$. Where ρ is the volume density of the particle, Tm is the melting temperature of the material used, ρu is the total strength of the dust particle and Ti is the temperature of the particle upon impact on the substrate. [4]

Substrate and applied material

An aluminum sheet with dimensions of 120 x 100 mm and a thickness of 3 mm was used as a substrate for copper deposition. The selected copper powder for Cold spray was from the supplier Safina. Purity according to the specification, copper is 99.9%. The PSD (Particle Size Distribution)

parameter of the used powder is in the range of 15 – 53 μm . The equipment for the Cold Spray process is the type Impact Cold Spray System 5/11 from the manufacturer Impact Innovations GmbH. This device operates at a temperature of up to 1,100 $^{\circ}\text{C}$ and a pressure of up to 50 bar. The heating output is 40 kW. Nitrogen was chosen as the working gas. With regard to the selected deposited material, i.e. copper and carrier gas nitrogen, the parameters of the Cold spray process were also set. Required temperature 450 $^{\circ}\text{C}$, working pressure 25 bar. The distance of the Laval nozzle from the substrate was 30 mm. At the same time, the parameters were set in such a way as to achieve the required speed for the deposition of copper on aluminum.

Measurements and tests carried out in the corrosion chamber

The prepared plates were fitted with an acoustic emission sensor and inserted into the condensation chamber in a vertical position. Individual samples were placed in the condensation chamber for the selected time frame. The acoustic emission was continuously measured, and then the occurrence of corrosion in the surface of the applied copper material was evaluated. Using acoustic emission, the extent and rate of corrosion was determined in the course of the experiment as a function of time inside the condensation chamber. For each sample, it was after removal a metallographic test was carried out from the condensation chamber with the aim of evaluating the formed corrosion cracks towards the surface of the copper towards the aluminum substrate and at the edges.



Figure 1. view of condensation chamber and sample detail

The test environment in the condensation chamber was at a constant temperature of 50 $^{\circ}\text{C}$ with a permitted fluctuation of ± 5 $^{\circ}\text{C}$ at 100% relative humidity. The water bath inside the condensation chamber was made up of distilled water with a conductivity less than or equal to that 20 $\mu\text{S}/\text{cm}$. Clean samples were placed in the chamber from a laboratory temperature of 20 $^{\circ}\text{C} \pm 2$ $^{\circ}\text{C}$ and a relative humidity of 65% $\pm 5\%$ after settling for at least one hour in accordance with ČSN 038131-Corrosion test in a condensation chamber.

Conclusion

The most obvious corrosion progress was always at the edge of the sample, when the structure was broken by splitting the original sample, despite the fact that the samples were prepared using a water jet. On the edges, the progress of corrosion was already visible after 168 hours. However, it can be stated that the oxidic layers of corrosion always formed at the edge of the

sample and did not proceed deeper into the sample at the interface between the substrate and the copper layer. Delamination was always observed protective layers from the sample, with the exception of the sample that had edges treated with an anti-corrosion coating. The obtained results were compared with other researches. However, the tests carried out were specific and had a different character than the available research. However, it can be stated that he was not found a contradiction between the conclusions of this work and the conclusions of other researches. It has been confirmed that the protective copper layer created by Cold spray has good corrosion resistance. The samples in the experimental measurement were not surface modified in any way after the application of copper. The conclusions of other studies show that surface roughness has a significant effect on corrosion endurance. When compared to other experiments, their samples achieved approximately half the surface roughness. This is caused by the parameters of the Cold spray process, especially the temperature and pressure of the propellant gas. He did not have the type of propellant for the roughness of the surface significant influence. The distance of the nozzle from the substrate can also have an effect on the surface roughness. However, this is only an assumption, since this statement is not supported by any literature support or disprove. If the literature focuses on the setting of the Cold spray process, the temperature and pressure, or the type of gas, are always addressed. The nozzle distance was always constant.

Acknowledgments

The publication was created as part of a specific research project at BUT (No. FEKT-S-20-6206).

References

1. Heimann, B., 1996, Plasma Spray Coating, VCH Publishers, New York, Chapter 3
2. Frank J. Hermanek, Thermal Spray Terminology and Company Origins, First Printing, 2001, ASM International, Materials Park, OH
3. F. Raletz, Ph.D. thesis, Université de Limoges, Limoges, France, 2005
4. T. Schmidt, F. Gartner, H. Kreye, C. Borchers, T. Stoltenhoff, H. Kreye, H. Assadi, in: B.R. Marple, C. Moreau (Eds.), Thermal Spray 2003: Advancing the Science and Applying the Technology, May 5–8 2003, vol. 1, ASM International, Orlando, FL, 2003, p. 1.

Evaluation of The Use of Non-destructive Methods of Acoustic Emission on Materials

T. Binar^a, J. Zimakova^a, P. Šafl^a

^a Brno University of Technology, Technická 10, 616 00 Brno, Czech Republic

This article describes acoustic emission as a nondestructive method of testing materials. There are different types of metal materials corrosion. The experimental part is focused on samples preparing and measuring the acoustic emission signals during continual corrosion process of grey cast iron in condensational corrosion chamber. These results are supported and completed with metallographic analysis.

Introduction

Nowadays, manufacturing companies face increasingly demanding requirements for the quality of their products. In addition to implementing methods that control the course of production and its reliability and improve production processes, companies are also looking for new design and production procedures. The quality of individual products and constructions is monitored not only during their production, but also often throughout their lifetime [1]. The loading of materials by internal or external forces causes dynamic processes that are manifested by elastic undulations inside the given material. Acoustic emission (AE) as a modern method of non-destructive testing of materials enables the monitoring of the course of plastic deformation and possible cumulative damage to the material, including the formation and propagation of cracks. AE can be used to examine various defects inside the material as well as its phase transformations and corrosion processes. It is also possible to use this method in the overall quality assessment, especially in welding, but also, for example, to monitor the flow of liquids [1]. However, this is not a completely universal method. With this non-destructive method, compared to others, the influence of the type of construction, the given material, the measurement regime, the type of operation, operating conditions and load is more pronounced. It follows from the above that any signal interference will have a great influence on the results of each measurement [2]. Other ČSN standards dealing with acoustic emission include ČSN EN 13477-1 for the description of devices, ČSN EN 13477-2 for verification of working characteristics and ČSN EN 13554 for general principles [2]

Experiment

For the corrosion test, a compact Liebisch Constanco condensation chamber designed for small laboratories was used, which, among other things, is supplied by Labimex CZ. It is a table chamber with a volume of 300 liters. It is suitable for tests either in a clean condensing atmosphere or for tests using sulfur dioxide (so-called Kesternich tests), in the temperature range from - 50 °C to + 70 °C. At the same time, it is also suitable for salt tests at temperatures up to 50 °C. The corrosion effect on the samples took place continuously in this chamber, both for unprotected samples and for samples with a protective coating. A constant relative humidity of 100%, created with distilled water, and a constant temperature of 50°C were maintained in the chamber. Throughout this test, acoustic emission data was recorded thanks to sensors attached to the samples. [43]. First, samples without corrosion protection were exposed to corrosion effects, and then

samples with corrosion protection in the form of a selected coating with corrosion inhibitors under the designation VpCI- 368D from Cortec Corporation. The VpCI-368D version is a factory-diluted previous variant of the above-mentioned coating (the letter D after the numerical designation is derived from the English term "diluted"), suitable especially for spraying. [3].

Metallography

The samples that were exposed to corrosion in the condensation chamber were further submitted for metallographic analysis. For the purposes of this analysis, two groups of samples were available, completely uncoated and with a protective coating. Furthermore, a group of reference samples was subjected to analysis. For metallographic analysis, all samples were further modified as needed. The cylindrical part (side) of the sample was machined relatively smoothly by turning, the cut surfaces (faces) were, on the other hand, relatively rough with visible grooves after cutting with a band saw. For the corrosion test, the samples were fixed in a special fixture, where one side of the surface (front) was exposed to condensation, and the acoustic emission sensor was attached to the other side.

Sample preparation

Specimens for metallographic analysis were cut in approximately half of the circular area, perpendicular to the rough grooves after cutting, and one half of the cut was always used for evaluation. An oxide layer formed on the surface of the samples not protected by the coating, which made it impossible to press the samples well. The oxide layer crumbled and caused polishing wetting agents to come out of the gaps after peeling, so it had to be desalted first. For this, a solution containing 3.5 g of hexamethylenetetramine powder (or also urotropin or hexamine), 500 ml of hydrochloric acid and 500 ml of water was mixed, while the pickling time was about 2 minutes. After that, it was possible to press the samples into plastic material and grind and polish them as standard.

Metallographic analysis

During the metallographic analysis, the depth of corrosion attack of the samples was also measured by the counting module at 200x magnification. The measurement results were statistically processed using the STADAT software, where mutually comparable sample parameters were compared using a pairwise test (F-test for variances and T-test for mean values). A Neophot 32 metallographic microscope and a Canon EOS 4000D digital camera were used for observation and photo documentation. The above-mentioned types of cutting surfaces were evaluated separately. The surface evaluation is carried out both for reference samples and for samples exposed to corrosion, both completely unprotected and provided with a protective coating.

Conclusion

For unprotected samples, the AE signals showed a gradual increase in corrosion from the initial stage. The number of AE events was in the order of tens of thousands, which means a sharp increase in the corrosion layer after the first week and in the final part of the experiment. In the second week, relatively constant values were recorded, which may indicate a certain passivation of the material before the development of further corrosion. For the protected samples, the acoustic

emission values are only in the order of thousands with a slight linear increase after the first week of the corrosion test. The second stage is again relatively constant as in the previous case. In the final stage of the test, the course differs quite significantly - compared to the previous measurement, it shows a slightly increasing character. Acoustic emission revealed corrosion activity in the protected samples already in phase 1 (ie 2), while metallography showed corrosion only in the third phase. This means that corrosion could penetrate under the protected surface at the point of its weakening and subsequently spread under this surface. However, acoustic emission also revealed significant changes in protected and unprotected samples in favor of those with corrosion protection.

Acknowledgments

The publication was created as part of a specific research project at BUT (No. FEKT-S-20-6206).

References

1. Production and technology – Trends / Measurement: Diagnostics by acoustic emission method. MM Industrial spectrum [online]. Prague, 12 June 2002, (6) [cit. 2021-4-27]. ISSN 1212-2572
2. KOPEC, Bernard. Non-destructive testing of materials and structures: (material science IV). Brno: Academic Publishing House CERM, 2008. ISBN 978-80-7204-591-4
3. Highly effective VpCI coatings: VpCI-368, 368D. Cortec Corporation: Minnesota (USA) [prospectus]. Brno - Černovice: TART, s.r.o. [feeling. 2022-05-14].

Resistivity and polarization resistance of special grounding materials

P. Šteffan¹, V. Novák²

¹Department of Microelectronics, Faculty of Electrical Engineering and Communication, BUT, Technická 10, 616 00 Brno, Czech Republic

²Department of Electrical and Electronic Technology, Faculty of Electrical Engineering and Communication, BUT, Technická 10, 616 00 Brno, Czech Republic

The article describes the methods of determining the parameters of resistivity and polarization resistance for the developed set of special grounding materials. They are characterized by the ability to conduct electric current and thus prevent the occurrence of overvoltage in building structures or they can be part of a lightning protection system. We use two basic measurement methods, namely determination of resistivity and polarization resistance.

For resistivity measurement we produced samples of each carbon-based conductive admixture were made from the prepared mixture. Voltage electrodes are placed in the samples during production. Resistivity was measured on three randomly selected samples after a period of 28 days. The sample was then adjusted in the measuring fixture to ensure good contact between the current electrodes and the mixture. The measurement took place at two test frequencies of 1 kHz and 100 kHz, at an ambient temperature of 24 °C.

Polarization resistance was again measured on dry samples. Due to the excellent electron conductivity of the sample and polarization events of an ionic nature, a part without conductive additives was inserted between the measured sample and the graphite plate. The ionic conductivity of this part was increased by moistening with distilled water. The entire assembly was adjusted to ensure good contact between the electrodes and the measured sample.

Polarization resistance was determined based on polarization curves obtained using the potentiodynamic polarization resistance method according to ASTM G59-97 in a three-electrode connection. A graphite plate was used as an auxiliary (active) electrode, the reference electrode was Cu/CuSO₄. The polarization resistance was determined as a tangent to the polarization curve at the point $i=0$, i.e. according to the relation

$$R_p = \left(\frac{\partial \Delta E}{\partial i} \right)_{i \rightarrow 0, \partial E / \partial t \rightarrow 0}$$

where R_p is the polarization resistance [$\Omega \cdot \text{m}^2$], E is the voltage [V] and also the current density [A/m^2], the area of the copper electrode is 7.54 cm^2 . If necessary, the measured characteristics were smoothed with a fast Fourier transform and the polarization resistance values were determined using linear regression. As we can see

Acknowledgement:

This paper has been worked out with the financial support from the Czech Science Foundation under the project with registration No. 20-09072J and name ‘Structure formation of advanced silicate composites with reduced impedance’.

References

1. Standard Test Method for Field Measurement of Soil Resistivity Using the Wenner Four-Electrod Method, Designation G57-06
2. Standard Test Method for Conducting Potentiodynamic Polarization Resistance Measurements, designation G 59-97

Battery Powered City-Bike Light with an Optimized Step-up Converter

P. Vorel^a, J. Martis^a

^a Department of Power Electrical and Electronic Engineering, Brno University of Technology, Brno 61600, Czech Republic

Introduction

Current environmental demands include a wider usage of bicycle transportation in cities. A city-bike is a specific bicycle. Its design is not as aggressive as that of modern sport bikes, it is more traditional and elegant. Also the seat and ride comfort is accented. Lighting is an essential part of city-bike accessories. Currently light-emitting diodes (LEDs) are the most efficient electric light sources. Their luminous efficacy can achieve even 200 lm/W for cool-white LEDs or ca. 180 lm/W for warm-white LEDs (light similar to a tungsten lamp). The tungsten lamp luminous efficacy is more than 10 times lower. Li-ion batteries are an obvious choice for an energy source because of their high volume energy density.

A powerful retro-lantern was constructed. High-power LEDs (above 5W) usually contain many chips in series. Therefore the operating voltage is often several tens of volts. Further the LED should be supplied from a current source (not voltage source) because of its V-A characteristics. These facts result in a requirement of a DC/DC converter between the battery and LED. It is advantageous to use a battery block with all cells in parallel to avoid the necessity of a cell balancing. This is why a step-up converter is required, producing the output voltage of tens of volts from a low input voltage (3 V to 4.2 V).

Many variants of step-up converters can be used. Generally the variants without transformer have low efficiency when the ratio between output and input voltage is as high as in our application. However classical converters with transformer like fly-back or forward are more complex and problems of transistor and rectifier diode voltage spikes have to be solved. An alternative step-up converter was constructed as a compromise between the mentioned variants. A pulse generator for an electromagnetic bell is included in the construction as old-fashion stylish accessories.

Retro-lantern design

The view of the lantern is in Figure 1. A power LED of type BXRE-27E1000-B-83 from Bridgelux was used (1). Its luminous efficacy is ca. 154 lm/W and color temperature 2700 K (old-fashioned warm color).



Figure 1. View of the constructed lantern.

The maximum input of 9 W was chosen (although a higher value is allowed). The LED is placed on a copper base through which the heat is transferred to the copper heatsink with ribs placed in the inner space behind the parabolic reflector. The LED is placed in the reflector focal point and it illuminates only the upper half-space (see the yellow LED chip in the left photo in Figure 1). This way the appropriate radiation pattern of the lantern is achieved. A stray light shield (glazed aluminum disk) is placed in the front side to suppress the dazzling of drivers. The electromagnet constructed for the bell can be seen together with the lantern parts in the right photo of Figure 1.

Battery dimensioning

The battery contains 4 cells type NCR18650A from Panasonic connected in parallel. The used minimum voltage is 3.1 V, maximum is 4.1 V. So not the full available capacity is used but a higher lifetime is expected. The whole battery capacity is ca. 12 Ah (40 Wh). The maximum input from the battery is ca. 10 W (at the approximate converter efficiency of 90 % and full LED electric input 9 W). It means the maximum duration of full power light is ca. 4 hours. If a lower power of ca. 2 W or 0.5 W is used (user switch) which is enough for common lighting then its operation time is ca. 20 hours or 80 hours.

Converter topology and operation

The power circuit of the proposed converter is in Figure 2. It is based on a simple step-up converter without transformer (boost converter) but instead of a single coil there is an autotransformer with two windings of the same number of turns and with a good coupling, performing as a choke coil with two windings.

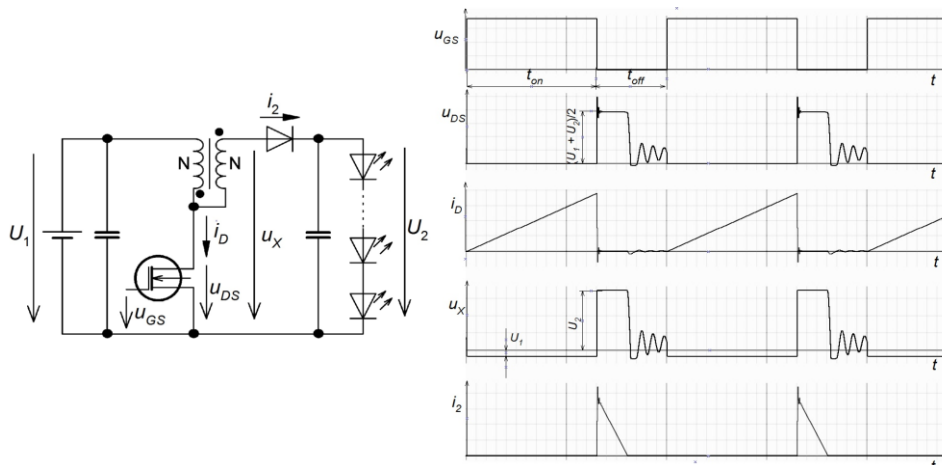


Figure 2. Power circuit of the converter and its important waveforms.

In the simple step-up with a single coil (2) the turned-off transistor is stressed with the full output voltage. In the proposed converter the maximum drain-source voltage is lower. Then a transistor with lower breakdown voltage can be used which has lower on-state resistance R_{DSon} resulting in lower conducting losses. As the transistor switching losses are proportional to both on-state current and off-state voltage, the decreasing of the off-state voltage also decreases the switching losses. This way the efficiency is significantly increased in comparison to the simple step-up converter.

The important waveforms can be seen in right side of Figure 2. While the transistor is turned on the input voltage U_1 is on the primary winding and therefore the same voltage is on the secondary winding. This is why the voltage u_x equals $-U_1$ and the output diode is closed. The input current flows through the transistor and increases linearly because this current corresponds to the time integral of the constant voltage U_1 present on the primary inductance. Only the output capacitor supplies the LED during this time. When the transistor is turned off the primary current cannot continue to flow to the transistor but it will continue to flow through the series connected primary and secondary winding and opened diode to the output. As the current suddenly starts to flow through $2N$ instead of N (number of turns), the current must instantaneously drop to a half of the value in the instant of turning-off to keep the same ampere-turns. During the turn-off duration the current decreases linearly because the inductor consisting of the two identical windings is now connected to a constant voltage equal to a difference between the input and output voltage and the voltage direction is opposite compared to the turn-on state of the transistor. Because of this voltage distribution it is obvious that the voltage in the node between the two winding to the ground (so the drain-source transistor voltage) is now equal to $(U_1+U_2)/2$. This is the explanation of the above mentioned advantage of this converter that not the full U_2 appears on the turned-off transistor.

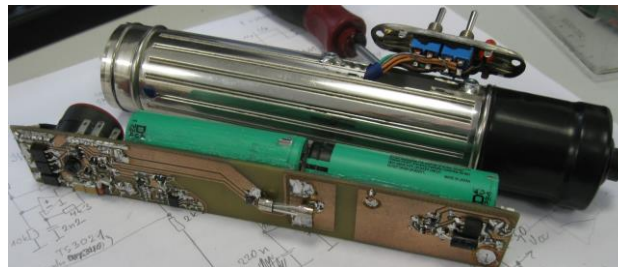


Figure 3. Converter and battery packaging.

Conclusion

Li-ion battery powered LED lights for bicycles are standard nowadays. However a retro-design was performed and a non-traditional converter topology was used to achieve a good efficiency although a simple circuit is used. The practical tests show a good reliability of the solution.

Acknowledgment

This research work has been carried out in the Centre for Research and Utilization of Renewable Energy (CVVOZE). Authors gratefully acknowledge financial support from the Ministry of Education, Youth and Sports under institutional support.

References

1. Bridgelux Gen 8 V10 Array Series [online]. Fremont: Bridgelux Inc., 2021. https://bridgelux.com/sites/default/files/resource_media/Bridgelux%20DS412%20V10%20Gen%208%20Array%20Data%20Sheet%2020200622%20Rev%20A.pdf
2. Y. Lu, D. Czarkowski and W. E. Bury, "High efficiency adaptive boost converter for LED drivers," 2011 7th International Conference-Workshop Compatibility and Power Electronics (CPE), 2011, pp. 315-318.

High Current Battery Charger with a Resonant Converter

J. Martis^a, P. Vorel^a

^a Department of Power Electrical and Electronic Engineering, Brno University of Technology, Brno 61600, Czech Republic

Introduction

High power battery chargers are becoming a necessity in today's world. Chargers with switch-mode converters have almost completely taken over the classic mains transformer approach. A standard design for high-current, low-voltage chargers is a forward converter with an output LC-filter. The problems of this topology are hard switching (losses, electromagnetic interference) and the requirement of two large magnetic components – transformer and output inductor. Recent designs often use a resonant LLC converter (1). This approach requires only one magnetic component (transformer with integrated leakage inductance), but is relatively complex to control with variable frequency, requires burst mode for low load and puts stress on the output filtering capacitor.

This contribution presents a low-complexity battery charger derived from the LLC converter, but with a classic simple fixed frequency PWM control. The problem of output capacitor stress is solved by using modern solid polymer electrolytic capacitors which have become widely available for a good price (2). The converter also uses a synchronous rectifier with control signals identical to the primary transistors.

Basic parameters of the charger are summed in Table 1.

TABLE I. Basic parameters of the battery charger.

Input Voltage	230 V, 50 Hz
Output Voltage	9 – 12.5 V
Output Current	0 – 40 A
External Dimensions	85 x 140 x 150 mm (PC power supply enclosure)

The charger is intended to be used with a Li-Ion battery pack for use with an electric boat, see Figure 1. The pack uses a 3-series 64-parallel combination of 18650 cells.

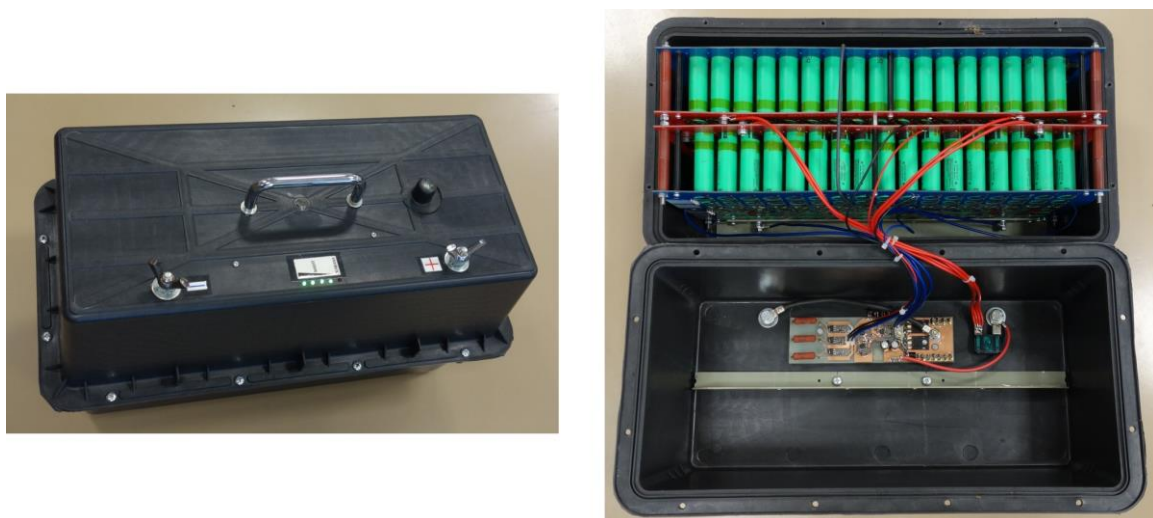


Figure 1. Battery pack for an electric boat.

Power Part of Charger

Schematic of the charger power part is shown in Figure 2. Because of personal use of the charger, there is no power factor correction, however a standard PFC front-end can be added without problems. Capacitors C3 and C6 together with the transformer TR2 leakage inductance form the resonant circuit. Moreover, capacitors C3 and C6 double as a bypass capacitance for the transistor half-bridge. CT1 is a current transformer, measuring the transformer primary winding current. There is a great advantage compared to forward converter, because the current transformer output can be, after rectification and low-pass filtering, used as a very close approximation of the DC output current. This is not possible with the forward converter where a shunt resistor on the secondary side must be used, with associated problems of noise and power loss.

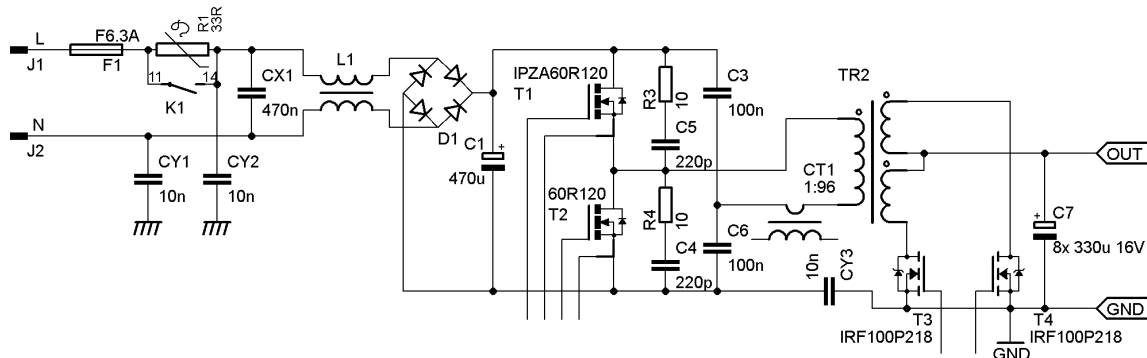


Figure 2. Power part schematic of the battery charger.

Transformer TR2 has an ETD49 core with primary and secondary windings placed next to each other, as opposed to classic layered construction. This geometry deliberately increases the leakage inductance of the transformer which is required for proper operation of the converter. The secondary winding is center-tapped and a push-pull synchronous rectifier with transistors T3 and T4 is used. These transistors are controlled with the same signals as the primary half-bridge transistors T1 and T2.

A filter consisting of 8 parallel solid polymer capacitors (C7) is used. These capacitors are only 8 mm in diameter, however each can take over 4 A rms current. A photo of the output rectifier together with the filtering capacitors is in Figure 3. Also an inrush current limiting inductor can be seen which limits the peak charging current of the filtering capacitance after connecting a battery. The inductor has a solid iron core in order to introduce HF losses and damp unwanted oscillations, however DC losses are very low.



Figure 3. Output synchronous rectifier, filtering capacitors, inrush limiting inductor (top).

Construction

The whole charger is built onto a single printed circuit board which fits inside a standard personal computer power supply enclosure, see Figure 4. Forced air cooling with controlled airflow (holes under the secondary power part) is used, which also allows using a higher current density for transformer winding and PCB traces. The current carrying capability of the PCB traces on the secondary part is further strengthened by a copper foil soldered onto the traces. There are three status LEDs – charging (constant current mode), almost charged (constant voltage mode, current above 1/10 of maximum) and fully charged (current below 1/10 of maximum).

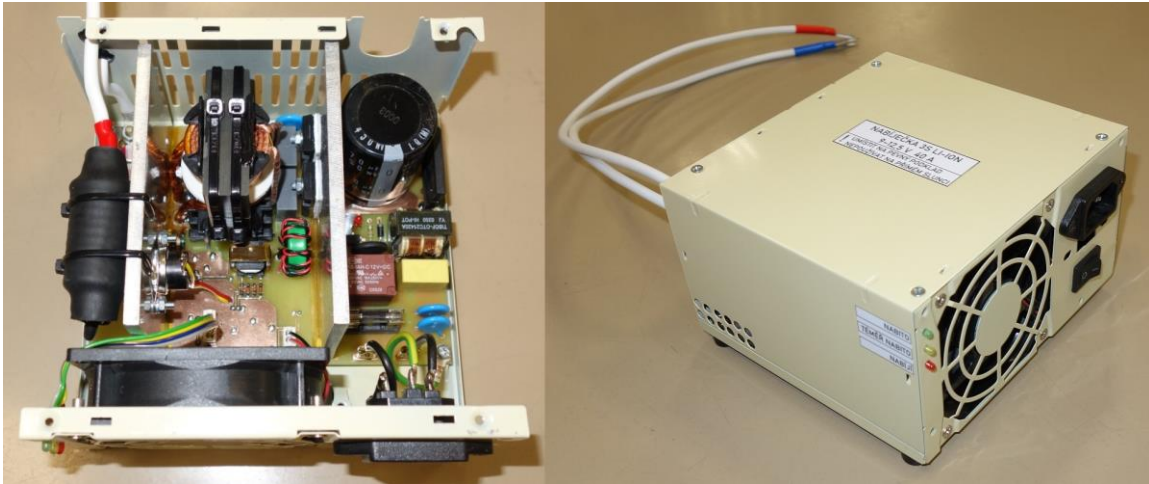


Figure 4. Charger without cover (left), SMD components are on the bottom of PCB. Overall view of finished charger (right).

Conclusion

A more detailed description of the converter including control scheme and measured waveforms will be included in the full contribution. The charger has been tested and operates reliably with only a little heating.

Acknowledgment

This research work has been carried out in the Centre for Research and Utilization of Renewable Energy (CVVOZE). Authors gratefully acknowledge financial support from the Ministry of Education, Youth and Sports under institutional support.

References

1. Y. S. Dow, H. I. Son and H. -D. Lee, "A study on Half bridge LLC resonant converter for battery charger on board," *8th International Conference on Power Electronics - ECCE Asia* (2011).
2. D. Butnicu and A. Lazar, "Why Choose Polymer Electrolytic Output Capacitors for Maximum Ripple Capability and Reliability Performance within eGaN based POL Converters," *2020 International Conference and Exposition on Electrical And Power Engineering (EPE)* (2020)

Comparison of the Diffusion Coefficient of Li-Ions by Methods of PITT and Network Thermodynamics for Fe-Sulfides of Li-Battery

Markevych O.V., Apostolova R.D., Shembel E.M.

Ukrainian State University of Chemical Technology, Dnipro, 49005, Ukraine

Solving the problems of efficient conversion of Li-battery systems is associated with the problems of heterogeneous kinetics of multistage electrode processes with phase transitions at the interface, diffusion, and other reasons. The most important parameter of diffusion kinetics in a Li-battery is the diffusion coefficient of Li-ions D_{Li} . A number of methods are proposed with their characteristic boundary conditions, assumptions, and shortcomings to determine D_{Li} : different methods were used to determine D_{Li} in V_2O_5 [1].

In this study, we compared the values of the effective diffusion coefficient of Li-ions obtained by the method of pulsed potentiostatic titration (PITT) and the method of network thermodynamics for electrochemically synthesized iron sulfides of Li-battery. Fe-sulfide-electrode was obtained with an active mass of 1.5-1.8 mg/cm² on the aluminum substrate by the method [3]. The conversion of the active electrode material in the electrochemical reaction with lithium took place in a three-electrode cell with electrolyte (ethylene carbonate, dimethyl carbonate Merck), 1M LiClO₄ (Iodobrome), Li-counter electrode and Li/Li⁺-reference electrode. Recordings of (I, current–t, time) – curves were performed using an analytical radiometer VoltaLab PJZ 301.

Theoretical aspects of PITT method and the obtained results

Using the approximation to the response of the electrode to the low-amplitude electrical signal, we can determine the diffusion time constant for the lithiation process of the electrode material [2] (1):

$$\tau = \left[Q_m \Delta x / \pi^{1/2} I t^{1/2} \right]^2 = \left[Q_m \left(\frac{\Delta x}{\Delta E} / (\pi^{1/2} I t^{1/2} / \Delta E) \right) \right]^2 = \left[C_{dif} / \pi^{1/2} I t^{1/2} / \Delta E \right]^2, t \ll \tau \quad (1)$$

where Q_m – the charge passing through the electrode after the imposition of an electrical signal, c/g; X – the degree of lithiation of the electrode material; $I t^{1/2}$ – Cottrell slope, determined from the linear section of the curve I (current) – t (time), $A \cdot s^{-1/2}/cm^2$; C_{dif} – differential intercalation capacity, c/g V. Effective coefficient (D_{Li}) can be determined as (2):

$$D = L^2 / \tau, \tau \ll t, \tau \ll t \quad (2)$$

where L is the characteristic diffusion length.

Based on the experimental PITT research, D_{Li} of the order of 10^{-11} cm²/s) was determined in the Fe_xS_y-electrode. The calculations took $L = (3.0-4.5) \times 10^{-4}$ cm, based on the size of the aggregate particles, which are formed in turn from submicron units determined by electron microscopy of electrolytically obtained Fe-sulfides [4]. If we take $L = (0.30-0.45) \times 10^{-5}$ cm into account the size of the spherical submicron particle, which consists of micro aggregates of the electrode material, the value of D_{Li} is obtained 2 orders of magnitude lower (10^{-13} cm²/s). However, only the conditional effective value of D_{Li} was obtained in the electrode material with a porosity of 18% [3], the pores of which are filled with electrolyte. The value of D_{Li} (if $L = 3 \times 10^{-5}$ cm) varies with the potential in the 1.40–1.56 V potential interval of the second stage of recovery of Fe_xS_y-electrode as a result of curve analysis in Figure 1. The order of D_{Li} values is set to (4.3×10^{-13} ; 3.0×10^{-13} ; 1.0×10^{-13} ; 4.5×10^{-13}) in the E-range of (1.42; 1.44 ; 1.50; 1.56 V, respectively) when $L=3 \times 10^{-5}$ cm.

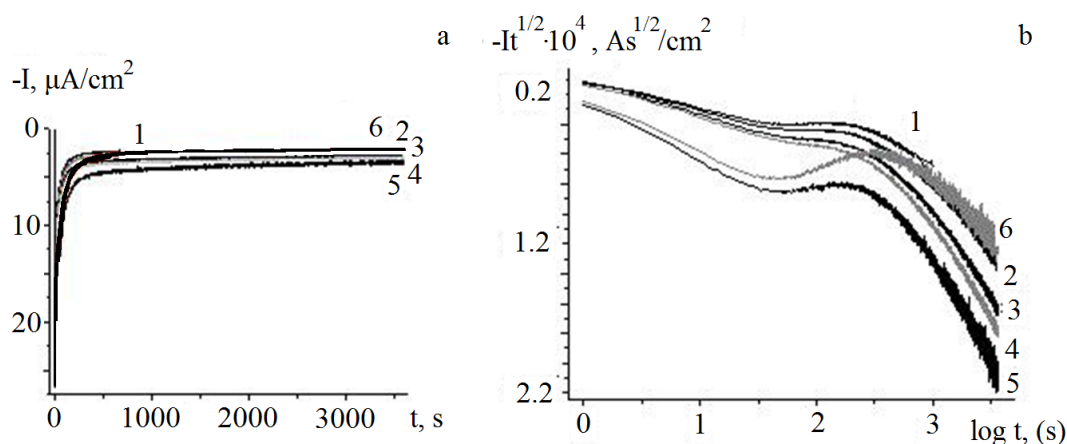


Figure 1. PITT response of Fe_xS_y - electrode depending on the E , V
 In $I - t$ coordinates, b) in $it^{1/2} - \log t$ coordinates. E , B: 1) 1.419, 2) 1.449, 3) 1.479,
 4) 1.554, 5) 1.499, 6) 1.514.

D_{Li} values are determined ($D1-5.76 \times 10^{-11}$; $D2-5.15 \times 10^{-11}$; $D3-2.01 \times 10^{-11}$; $D4-6.13 \times 10^{-11}$) when $L=3,0 \times 10^{-4} \text{ cm}^2/\text{s}$ at potentials ($E1-1.64$; $E2-1.66$; $E3-1.68$; $E4-1.71 \text{ V}$).

Theoretical aspects of network thermodynamics method and the obtained results

The possibility of using network thermodynamics in electrochemistry is consistent with work [5, 6]. The method of network thermodynamics was used to determine the effective coefficient of diffusion of Li^+ in V_2O_5 in an aprotic medium [1], as well as in MoO_3 oxide [7].

The method of the network thermodynamics is based on the mathematical model of diffusion of the Li^+ in electrode material using the diffusion equation for a one-dimensional system:

$$\frac{\partial c}{\partial t} = D \cdot \frac{\partial^2 c}{\partial x^2} \quad (3)$$

Equation (3), according to principles based on the network thermodynamics, may be transformed to the equation (4) [3]:

$$Z(t) = A1 \cdot \left\{ A0 \cdot t - 2 \cdot \sum_{k=1}^{\infty} \frac{1}{k^2} \exp[k^2 \cdot A0 \cdot t] \right\} + A2 \quad (4)$$

where

$$A0 = \frac{\pi^2 \cdot D_{Li^+}}{\delta^2} \quad (5)$$

$$A1 = \frac{RT \cdot \delta}{(nF)^2 \cdot c \cdot D_{Li^+} \cdot \pi^2} \quad (6)$$

$$A2 = R_f + A1 \cdot \frac{\pi^2}{3} \quad (7)$$

k – quantity of the exponents in the equation (4); t – relaxation time, s; δ – thickness of the electrochemical active layer, cm; D_{Li} – diffusion coefficient of the Li^+ in the electrode structure, (cm^2/s); R – gas constant, 8.31 J/mole·K; T – temperature, K; n - number of electrons in the electrochemical process; R_f – resistance of the electrode, $\Omega \cdot \text{cm}^2$.

Equation (4) was used for the approximation of the relaxation curves.

The description of research methods:

1. Method of current relaxation and transformation of this curve to relaxation of impedance during the time.
2. Approximation of the relaxation curves according to the equation obtained on the basis of principles of the network thermodynamics. The goal of this approximation is determination of the variable factors (A0, A1 and A2) in the equation (4).
3. Calculation of the D_{Li} coefficient into Fe_xSy electrode according to the equation (5).

The discharge curve of synthesized Fe_xSy sulfide in the range of $E=2.8-1.1$ V is carried out in two stages: 1—with a maximum near 1.68–1.71 V, 2—in the range of 1.40–1.1V. To determine D_{Li} in this study, stage 1 was analyzed with a final discharge voltage of 1.6 V. Figure 2 shows an example of close agreement between the experimental and approximated data used to determine D_{Li} at $E = 1.71$ V.

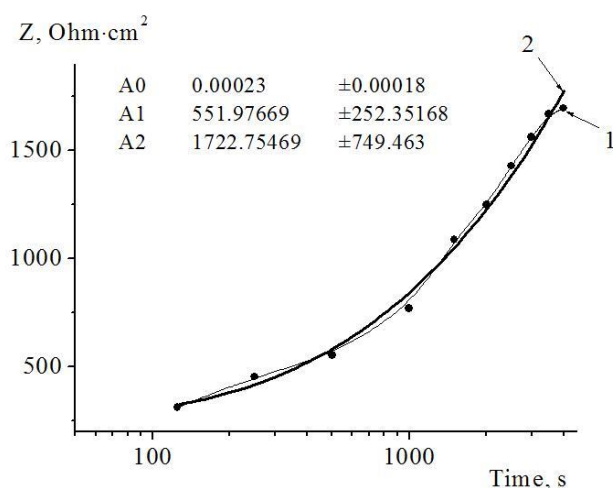


Figure 2. Experimental (curve 1) and approximated (curve 2) data at $E=1.71$ V for $A0=0.00023$.

The resulting D_{Li} value is equal to 2.3×10^{-11} cm^2/s when $L = 3.0 \times 10^{-4}$ cm and to 2.3×10^{-13} cm^2/s when $L = 3.0 \times 10^{-5}$ cm at $E=1.71$ V.

In the range of the discharge curve of 2.80–1.85 V, it is not possible to determine D_{Li} , neither by the PITT method [2], nor by the method of network thermodynamics, since the semiconductor Fe -sulfide has a high ohmic resistance.

The value of D_{Li} , corrected for the voltage drop across the high resistance of Fe_xSy , and the slow charge transfer in [8], exceeds that of D_{Li} in this study using the PITT method by an order of magnitude. Obviously, in the future, it is necessary to improve the method of network thermodynamics to determine the correct D_{Li} , taking into account non-diffusion electrode processes.

References

1. Apostolova R.D., Tsyachny V.P., Markevich A.V., Ksenjek O.S., Shembel E.M., Markovsky B., Aurbach D. *Voprosi khimii i khimicheskoy tekhnologii*. №2 (2014) 4.
2. Wen C.J., Boukamp B.A., Huggins R.A. *J. Electrochem. Soc.* 126 (1979) 2258.
3. Shembel E.M., Apostolova R.D., Nagirnij V.M., Baskevich A.S., Lytvin P.M. *Electrochemistry*.40 (2004) 843. (In Russian).
4. Apostolova R.D., Shembel E.M. Thin-layer electrolytically synthesized sulfides and oxides of transition metals for Li-current sources. Monograph. Dnipro: LIRA. 2019. 264 p.
5. Ksenzhek O.S., Petrova S.A. *Electrochemistry*. 32 (1996) 1477.
6. Ksenzhek O.S., Petrova S.A. *Advances in mathematical modeling and simulation of electrochemical process and oxygen depolarized cathodes* / Ed. by Van Zee and T. Fuller. "Electrochem. Soc. Inc. (1998) 132.
7. Markevich A.V., Ksenzhek O.S., Shembel E.M. *Voprosi khimii i khimicheskoy tekhnologii*. №3 (2005) 164.
8. Apostolova R.D., Kolomoyets O.V., Shembel E.M. *Proceedings of the XII International conference fundamental problems of energy conversion in lithium electrochemical systems, Krasnodar, Russia, October 1–6, 2012.*

Changes of the Impedance of Li-ion Cell During Discharge

Petr Křivík¹, Petr Bača¹, Jiří Kazelle¹

¹ Department of Electrotechnology, Faculty of Electrical Engineering and Communication, Brno University of Technology, Technická 10, 616 00 Brno, Czech Republic

The paper deals with the measurement of the cell impedance parameters during discharging of the Li-ion NCR18650B cell. Re (Z) and Im (Z) of the battery were measured by PEIS method. Results of the impedance changes during discharging and charging were plot to Nyquist diagrams. Important values R_s , R_{sei} , R_{ct} , C_{sei} , C_{dl} and σ were found during discharging of the Li-ion cell.

Introduction

Lithium ion cells are currently among the common products of a number of renowned companies (SAFT, VARTA, Sony, Duracell, etc.). The charged cell of the usual design has an open circuit voltage of 2.4 - 3.7 V and its energy density ranges from 80 to 260 Wh/kg. Self-discharge is about 5 – 10 % of the capacity per month. The cell has a long cycle life and after 500 of cycles capacity of LI-ion cell decreases by 10 – 20 %. The electrodes of these cells are very thin (around 200 μm) and are made of intercalating compounds (compounds that can accept an atom or molecule into their crystal lattice).

The active material of the positive electrode are metal compounds, the 6 most common types of Li-ion batteries include Lithium Cobalt Oxide (LiCoO_2) - LCO (ICR), Lithium Manganese Oxide (LiMn_2O_4) - LMO (IMR), Lithium Nickel Manganese Cobalt Oxide (LiNiMnCoO_2) - NMC (INR), Lithium Iron Phosphate (LiFePO_4) - LFP, Lithium Nickel Cobalt Aluminum Oxide (LiNiCoAlO_2) - NCA (NCR) and Lithium Titanate (Li_2TiO_3) - LTO. The negative electrode is carbon (graphite). These substances must be sufficiently porous. The matrix must very well receive (intercalate) lithium ions and again easily release them. The collectors of the negative electrodes are usually made of copper foil, the positive electrodes are aluminum foil. Active electrode materials are applied to the collectors. The separators are usually made of a very thin porous film made of polyethylene or polypropylene or a microporous polymer film. The electrolyte is a lithium salt (LiPF_6 , LiBF_4 , or LiClO_4) and an organic solvent (ether, various mixtures of ethylene-, propylene-, dimethyl- or diethyl carbonate, etc.). The liquid electrolyte is conductive for lithium ions, which travel between the electrodes during discharging and charging [4].

The chemical process in the cell consists only in the transport of lithium ions. During charging, positively charged lithium ions travel to the negative electrode, where they are deposited in free spaces in the carbon structure. When discharging, the opposite process takes place - lithium ions travel to the positive electrode, where they are deposited in free spaces in the crystal lattice of the positive active material. During the discharge, the impedance of the Li-ion cell is changing, including ohmic resistance R_s , resistance and capacitance of SEI layer (R_{sei} , C_{sei}), charge transfer resistance R_{ct} , double layer capacity C_{dl} and Warburg impedance Z_w . Electrochemical impedance spectroscopy (EIS) is a suitable method for determining these parameters. This method is suitable for monitoring the impedance of a Li-ion cell over a wide range of frequencies. Results are displayed by the impedance diagrams [2].

The electrochemical impedance of a battery Z is a complex number, frequency-dependent, described either by its real and imaginary parts Re (Z) and Im (Z), or by its modulus $|Z|$ and phase

angle φ . Different frequencies reflect different parameters of the Li-ion cell, from ohmic resistance through resistance and capacitance of the SEI layer, charge transfer resistance at the electrodes, diffusion double layer capacity to Warburg impedance related to ion diffusion in the electrolyte and electrode pores. The SEI layer is a passivation layer formed on the surface of the negative electrode materials of lithium-ion batteries.

The general shape of the Nyquist diagram of the complex electrochemical impedance of the battery is shown in Fig. 1. This diagram starts at the highest frequencies around 5 kHz below the x-axis, where the circuit inductance and skin effect predominate. At frequencies around 1 kHz, the ohmic resistance of the RS cell is presented in the range of mΩ, the imaginary part of the impedance is close to zero. The ohmic resistance includes the resistance of the interconnection, the separator, the electrolyte and the both electrodes. The first arc appears at frequencies in the hundreds of Hz. Here, the phenomena in the SEI layer are applied, which represents the resistance and capacity of the SEI layer. The resistance of the SEI layer indicates the size of the first arc. The second arc appears at frequencies in tens of Hz. Here, the charge transfer resistance at the electrodes Rct and the capacitance of the double layer Cdl caused by the distribution of the space charge in the electrochemical double layers are presented. The charge transfer resistance indicates the size of the second arc. At the lowest frequencies, the Warburg impedance is presented due to the diffusion of ions in the electrolyte and in the electrodes. All of these parameters can be represented by an equivalent circuit [1-3].

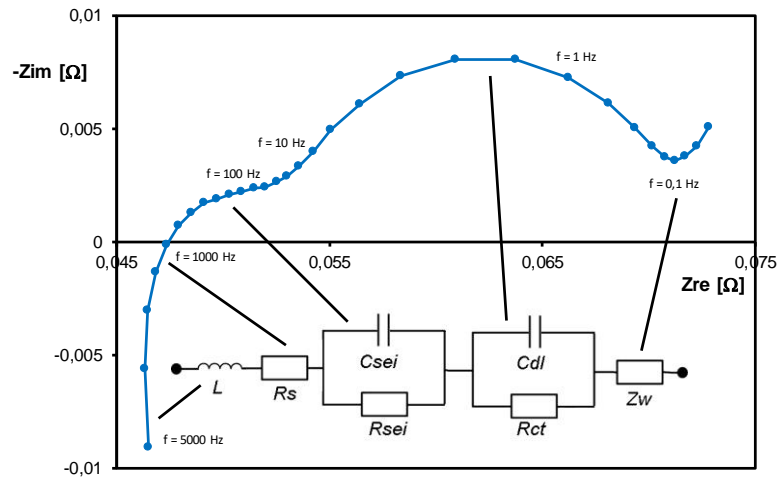


Figure 1. Nyquist impedance diagram and equivalent Li-ion cell circuit.

The cell impedance is equal to:

$$Z = R_S + \frac{1}{j\omega C_{sei} + \frac{1}{R_{sei}}} + \frac{1}{j\omega C_{dl} + \frac{1}{R_{ct}}} + Z_w, \text{ where } Z_w = \frac{\sigma}{\sqrt{\omega}} - j \frac{\sigma}{\sqrt{\omega}} \quad (1)$$

Z_w is the Warburg impedance, σ the Warburg coefficient [$\Omega s^{-1/2}$] and ω the angular frequency [s^{-1}].

From the measured values of the cell impedance at different frequencies, individual parameters of the measured impedance can be found by fitting.

Experiment

A Li-ion cell NCR18650B with a nominal capacity of 3350 mAh, a nominal voltage of 3.6 V, an energy density: 676 Wh/l, 243 Wh/kg was used to measure the impedance changes. The positive electrode is composed of LiNiCoAlO_2 , the negative electrode of graphite, electrolyte: ethylene carbonate, diethyl carbonate, salt: lithium hexafluorophosphate. The cell was placed in a temperature chamber with a temperature of 34.4 °C and subjected to intermittent discharging with a current of 0.4 A for 1 hour, followed by current off period for 2 hours. The voltage limitation at the end of discharging was 2.5 V. Impedance changes were measured by EIS during the experiment. The voltage amplitude at EIS was set at 5 mV, frequency from 6 kHz to 50 mHz, 6 measurements per decade.

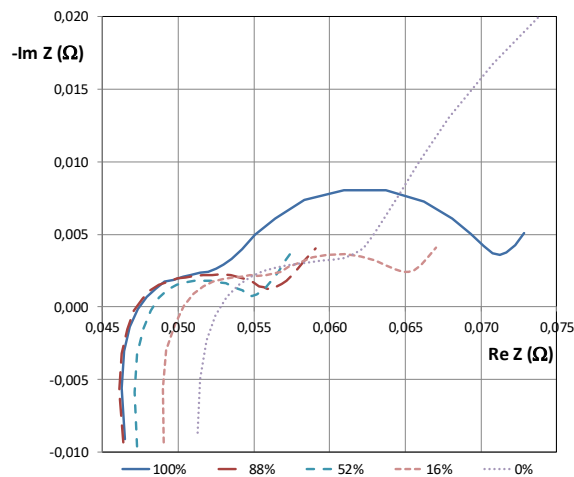


Figure 2. Nyquist diagram of Li-ion cell during intermittent discharge (SoC = 100% - 0%).

Fig. 2 are Nyquist diagrams during intermittent discharge of a Li-ion cell. From individual Nyquist diagrams we can obtain the changes in the impedance parameters of the Li-ion cell during discharging by fitting, see Fig. 3.

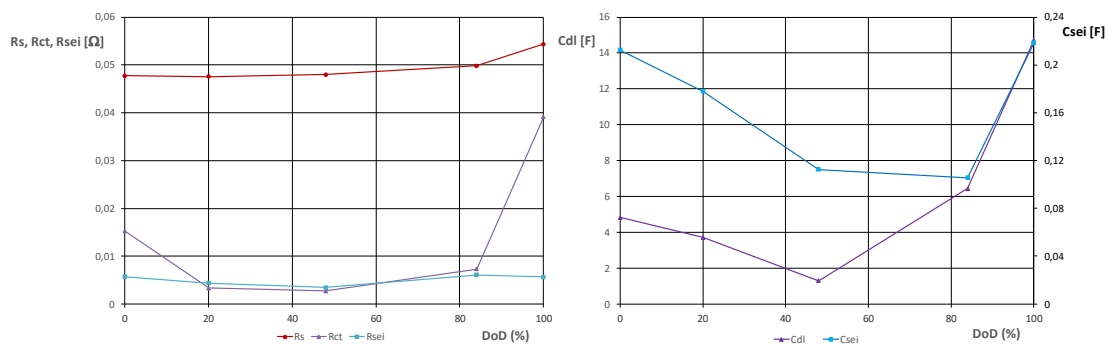


Figure 3. Dependence of R_s , R_{ct} and R_{sei} (left), C_{dl} and C_{sei} (right) of the battery during intermittent discharging (DoD = 0% - 100%).

It can be seen that the ohmic resistance R_s during discharge gradually increases, the most at the end of discharge. Lithium atoms intercalate into the structure of the positive electrode and increase its resistance. The charge transfer resistance R_{ct} decreases up to about 50 % DoD. At the end of discharge, on the other hand, it rises sharply. It is obvious that at the end of the discharge, lithium is added to the active mass of the positive electrode, and fills the remaining free spaces in the structure

of the electrode, and this is reflected in the increase of the charge transfer resistance. The resistance R_{sei} of the SEI layer does not change much during discharge, its magnitude is around 0.05Ω , comparable to the value of R_{ct} between 20 - 80% of discharge. The capacity of the Cdl double layer during discharge decreases to about 50 % DoD and at the end of discharging it increases sharply. The capacity C_{sei} of the SEI layer has a similar course as the capacity of the Cdl double layer. Compared to Cdl, capacity of C_{sei} is much lower by 1 to 2 orders of magnitude.

Conclusions

Nyquist diagrams of the Li-ion cell during discharge were measured. Important parameters of the battery equivalent circuit were found from the diagrams. These parameters indicate the changes of the impedance of the Li-ion cell in different states of discharge.

Acknowledgements

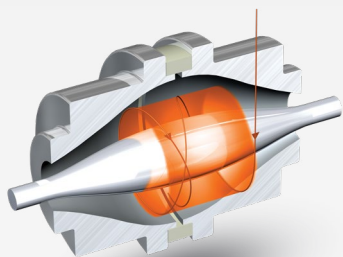
This work was supported by the specific research of the BUT No. FEKT-S-20-6206.

References

1. Yun Bao, Yuansheng Chen, Lithium-Ion Battery Real-Time Diagnosis with Direct Current, *Energies* 2021, 14, 4396, <https://doi.org/10.3390/en14154396>
2. Aramis Pérez, Matías Benavides, Heraldo Rozas, Sebastián Seria, Marcos Orchard, Guidelines for the Characterization of the Internal Impedance of Lithium-Ion Batteries in PHM Algorithms, *International Journal of Prognostics and Health Management*, ISSN 2153-2648, 2018, 015.
3. Uwe Westerhoff, Kerstin Kurbach, Frank Lienesch, Michael Kurrat, Analysis of Lithium-Ion Battery Models Based on Electrochemical Impedance Spectroscopy, *Energy Technology*, 2016,4, 1620–1630.
4. <https://batteryuniversity.com/article/bu-205-types-of-lithium-ion>

Pragolab

Špičkové služby a přístroje z oboru analytické chemie,
mikroskopie, materiálografie a fyzikálního
měření pro český a slovenský trh.
Již více než 30 let.



**ORGANICKÁ ANALÝZA
A SEPARAČNÍ
TECHNIKY**



**MIKROSKOPIE
A PŘÍPRAVA VZORKŮ
PRO METALOGRAFII**



**FYZIKÁLNÍ
A MATERIÁLOVÉ
ANALÝZY**

plynová chromatografie ICP-OES příprava vzorku elementární analýza elektrochemie testery akumulátorů EIS SEA analýza povrchů separační techniky DVS reologie atomová spektroskopie GC temperace kapalinová chromatografie UV-VIS spektrometrie GC-MS lyofilizátory konfokální B.E.T. lims mikroskopie materiálografie metalografie technická čistota optická mikroskopie elektronová mikroskopie koncentrátory CHNSO analýza AAS analýza částic HPLC hmotnostní spektrometrie centrifugy extruze ICP-MS servis AIR monitoring XPS widefield textura spotřební materiál NMR DLS automatické dávkování iGC TOC analýza RVC stopped-flow cirkulární dichroismus XRF XRD

Title: Advanced Batteries Accumulators and Fuel Cells – 23rd ABAF
Edited: Marie Sedlaříková
Vítězslav Novák
Tomáš Kazda
Petr Bača
Publishing Office: Marie Sedlaříková
Vítězslav Novák
Tomáš Kazda
Petr Bača
Deadline: July 31th 2022
Publisher: Brno University of Technology
Faculty of Electrical Engineering and Communication
Department of Electrical and Electronic Technology
Year: 2022

The authors are fully responsible for the content and language of their contribution

ISBN 978-80-214-6088-1